

FRICION STIR WELDING TECHNOLOGY FOR ADVANCED MANUFACTURING OF AIRCRAFT STRUCTURES

EGOITZ ALDANONDO BEGUIRISTAIN

Thesis supervisor:

Dr. Iñaki Hurtado Hurtado

Thesis co-supervisor:

Dr. Pedro Álvarez Moro



Thesis directed to the obtention of the title of
Doctor in “Applied Engineering” from Mondragon Unibertsitatea
Mechanical and Manufacturing Department
Mondragon Unibertsitatea

October 2022

ORIGINALITY STATEMENT

DECLARACIÓN DE ORIGINALIDAD

I declare through this document that this thesis and the work presented in it with its results were made entirely by me, in the Joining Technology Research Group of Lortek Technological Centre, in coordination with Mondragon Unibertsitatea.

Declaro a través de este documento que esta tesis y el trabajo presentado en ella con sus resultados fueron hechos totalmente por mí, en el Grupo de Investigación en Tecnologías de Unión del Centro Tecnológico Lortek, en coordinación con Mondragón Unibertsitatea.

Nire ama Lourdes,

Nire aita Joakin,

Eñaut,

Gainontzeko familia

RESUMEN

Uno de los principales retos en el sector aeronáutico es la reducción del consumo energético con el fin de incrementar la eficiencia, reducir emisiones, así como reducir costes operacionales de los aviones. Con el fin de abordar este reto, son necesarias estructuras cada vez más ligeras para poder diseñar sistemas de transporte aéreo más eficientes y respetuosos con el medioambiente. Por lo tanto, actividades de investigación y desarrollo en nuevos materiales y procesos de fabricación que permitan desarrollar estructuras aligeradas y económicamente eficientes despiertan un gran interés para la industria aeronáutica.

El desarrollo de paneles integrales reforzados y soldados ofrecen nuevas oportunidades para la fabricación de estructuras aligeradas y económicamente eficientes. Sin embargo, estas aplicaciones presentan importantes retos que se deben superar para una implementación exitosa debido a alta complejidad y el enfoque multidisciplinar necesario para el diseño, fabricación, mantenimiento y procesos de fin de vida útil de dichas estructuras.

Desde el punto de vista de los procesos de fabricación, la soldadura por fricción-agitación o “Friction Stir Welding” (FSW) es una innovadora tecnología de unión con potencial para reemplazar la tecnología de remachado empleada tradicionalmente para la fabricación de estructuras aeronáuticas. Desde el punto de vista de materiales, el desarrollo de aleaciones de aluminio-litio de tercera generación ha generado nuevas oportunidades para la introducción de aleaciones de aluminio de baja densidad y altas prestaciones. La exitosa implementación de ambas innovaciones, es decir, la tecnología de soldadura FSW y aleaciones de aluminio de tercera generación abre nuevas perspectivas para el desarrollo de estructuras avanzadas para aeronaves. Sin embargo, es necesario desarrollar las apropiadas condiciones de proceso de soldadura FSW con el fin de maximizar la calidad de las uniones y estructuras para que cumplan con los exigentes requisitos del sector aeronáutico.

Esta tesis se centra en el desarrollo del proceso de soldadura FSW para su implementación en la fabricación de paneles reforzados integrales caracterizados por uniones tipo larguero-piel empleando aleaciones de aluminio-litio de tercera generación. Aunque se han investigado varias aleaciones de este tipo, el trabajo está principalmente centrado en las aleaciones AA2060-T8E30 y AA2099-T83. Se investigan factores críticos para el desarrollo del proceso de soldadura FSW tales como diseños de herramientas, parámetros de soldadura y efectos introducidos por técnicas innovadoras de protección contra la corrosión (tratamientos superficiales libres de Cr, sellantes). El impacto de estos factores en la calidad de las uniones soldadas mediante FSW se investiga mediante examen metalográfico y ensayos mecánicos incluyendo microscopía óptica y electrónica, ensayos estáticos de arrancamiento, tracción y ensayos de fatiga. Como resultado del trabajo realizado, se han definido condiciones de soldadura FSW optimizadas incluyendo un diseño de herramienta alternativo capaz de producir uniones soldadas mediante FSW de gran calidad en configuraciones de junta a solape.

La tesis se ha desarrollado en el marco del proyecto ecoTECH, que es un proyecto europeo entre socios esenciales de la iniciativa “Clean Sky 2” para la investigación y desarrollo de nuevas tecnologías para futuras aeronaves. Se ha realizado un excelente trabajo colaborativo entre los socios del proyecto y el desarrollo de demostradores de paneles-fuselaje innovadores se encuentra en curso en el momento en el que se deposita la tesis. Las conclusiones obtenidas en la tesis se están aplicando en la

fabricación mediante soldadura FSW de los demostradores de fuselaje con el objetivo de incrementar el nivel de madurez tecnológica de este tipo de estructuras. Los trabajos de investigación de esta tesis junto con las pruebas de validación de los demostradores, en caso de ser exitosas, permitirían introducir la soldadura FSW como tecnología habilitadora para la fabricación avanzada de estructuras aeronáuticas mostrando beneficios tales como la reducción de peso, la reducción de consumo energético, la reducción de tiempos y costes de fabricación, así como avances hacia una fabricación más automatizada y digitalizada.

Con el fin de presentar el trabajo de la forma más clara posible, la tesis menciona 11 artículos presentados de forma cronológica que representan el trabajo realizado en el desarrollo de la tecnología de soldadura FSW para distintos tipos de aleaciones aluminio y uniones en configuraciones de juntas a solape. En cualquier caso, los artículos esenciales que llevan a completar la tesis son los artículos 9, 10 y 11. Estos son los artículos que cumplen con los requisitos académicos y deben ser considerados como compendio de publicaciones en sustitución de la memoria de tesis tradicional.

ABSTRACT

One of the current challenges in the aeronautic sector is the reduction of fuel consumption aiming at energy efficiency, reduction of emissions as well as reductions in operational costs of the aircraft. In order to face this challenge, increasingly lighter structures are required for more efficient and environmental-friendly airframe systems. Therefore, research and development in new materials and manufacturing processes leading to innovative lightweight and cost-effective structures is of great interest for the aeronautic industry.

The development of welded integral reinforced panels offers new opportunities for lightweight and cost-effective structure manufacturing. However, these applications present important challenges that must be overcome for a successful implementation due to the highly complex and multi-disciplinary approach required for the design, manufacturing, maintenance and disposal of such structures.

From the manufacturing process point of view, Friction Stir Welding (FSW) is an innovative joining technology with potential to substitute the traditionally used riveting for aircraft structure manufacturing. From the material point of view, the development of Third-Generation aluminium-lithium alloys have created opportunities for the introduction of low density and high-performance aluminium alloys. The successful implementation of both innovations, i.e., FSW technology and Third-Generation aluminium-lithium alloys opens new perspectives for the development of advanced aircraft structures. However, it is necessary to develop appropriate FSW process conditions in order to maximize the quality of the joints and structures that comply with the stringent requirements of the aeronautic sector.

This thesis is mainly focused on the FSW process development for its implementation in the integral reinforced panel manufacturing characterised by stringer-skin type joints, using Third-Generation aluminium-lithium alloys. Although several alloys of this type have been investigated, the work is mainly focused on the AA2060-T8E30 and AA2099-T83 alloys. Critical factors for FSW process development such as tool designs, welding parameters and effects introduced by innovative corrosion protection techniques (Cr-free surface treatments, sealants) are investigated. The impact of all these factors in the quality of FSW joints is investigated by metallographic examination and mechanical tests

including optical and electron microscopy, static pull-out, static tensile and fatigue tests. As a result of the work, optimized FSW process conditions are defined including a new FSW tool design capable to produce high-quality FSW joints for overlap joint configurations.

The thesis has been developed in the framework of the project ecoTECH, which is a core-partner project of the Clean Sky 2 initiative for research and development of new technologies for future aircraft. An excellent collaborative work has been carried out among project partners and the development of innovative fuselage panel demonstrators is in progress at the time when this thesis is being deposited. The conclusions obtained in the thesis are being applied to the FSW manufacturing of the fuselage demonstrators with the aim of increasing the TRL level of this type of advanced structures. This could permit to introduce FSW as an enabling technology for the advanced manufacturing of aircraft structures showing benefits such as weight savings, reduction of energy consumption, reduction in the manufacturing time and costs, as well as advances towards a more automatic and digital manufacturing.

In order to present the work in the clearest way possible, the thesis mentions 11 articles presented in a chronological way that represent the work performed in the FSW technology development for different types of aluminium alloys and overlap joint configurations. The contributions of each article are explained in each corresponding chapter. Nevertheless, the core articles that led to the completion of this thesis are articles 9, 10 and 11. These are the relevant articles that comply with the academic requirements and must be considered as a compendium of publications in substitution of the traditional PhD dissertation.

LABURPENA

Sektore aeronautikoaren erronka nagusienetako bat erregaien kontsumoa murriztea da, efizientzia energetikoa, emisioen murrizketa edota hegazkinen operazioetako kostuen murrizketa bilatze aldera. Erronka honi aurre egiteko, eranginkorrakoak eta ingurumenarekiko errespetagarriak diren sistema aeronautikoentzat gero eta estuktura arinagoak beharrezkoak dira. Beraz, arinak eta ekonomikoki eranginkorrek diren estrukturen garapenerako material eta fabrikazio prozesu berrien ikerketa eta garapenerako aktibitateak interes handikoak dira industria aeronautikoan.

Soldatutako panel integral errefortzatuen garapenak aukera berriak eskeintzen ditu estuktura arin eta ekonomikoki eranginkorren fabrikazioan. Hala ere, aplikazio hauek erronka garrantzitsuak aurkezten dituzte, konplexutasun eta disziplina anitzeko hurreratzea eskatzen baitute beraien diseinua, fabrikazioa, mantentzea eta erretiratze prozesuak kontutan izanda.

Fabrikazio prozesuen ikuspuntutik, marruskadura-astintze soldadura edo "Friction Stir Welding" (FSW) estuktura aeronautikoen fabrikazioa betidanik erabili izan den errematxeen teknologia ordezkatzeko potentziala duen lotura teknologia berritzaile bat da. Materialeen ikuspuntutik, hirugarren belaunaldiko aluminio-litiozko aleazioen garapenak dentsitate baxuko eta erresistentzia handiko aluminiozko aleazioen erabilerarako aukera berriak zabaldu ditu. Bi berrikuntza hauen inplementazio arrakastatsuak ate berriak irekitzen ditu aeronautikarako estuktura aurreratuen fabrikazioan. Hala ere, sektore aeronautikoko eskaera zorrotzak beteko dituzten kalitate handiko soldadurak gauzatzeko ezinbestekoak diren FSW soldadura baldintzak garatzea beharrezkoa da.

Tesi hau hirugarren belaunaldiko aluminio-litiozko aleazioak erabiliz, langa-azal moduko FSW soldadurez osaturiko panel errefortzatu integralen fabrikaziorako beharrezkoa den FSW soldadura prozesuaren garapenean murgiltzen da. Gisa honetako hainbat aleazio aztertu diren arren, egindako lanak bereziki AA2060-T8E30 eta AA2099-T83 aleazioetan du ardatza. FSW soldadura prozesuaren garapenerako kritikoak diren faktoreak ikertu dira, nola hala, erreminten diseinua, soldadura parametroak eta korrosioaren aurkako babesa eskeintzen dute teknika berritzaileen efektuak (Cr-rik gabeko gainazalen tratamenduak, zigitzaileak). Faktore hauek FSW bidez eginiko soldaduren kalitatean duten eragina azterketa metalografiko eta entseiu mekanikoen bidez ikertu da, mikroskopia optiko eta elektronikoa, deserrotze eta trakzio entseiu estatikoak eta neke entseiuak barne. Eginiko lanaren emaitza bezala, FSW soldadura prozesuaren baldintza optimizatuak definitu dira, gainjarritako loturetan kalitate handiko FSW soldadurak egiteko aukera ematen duen erreminta diseinu berri bat barne.

Tesia ecoTECH proiektuaren barnean garatu da, etorkizuneko hegazkinen teknologia berrien ikerketa eta garapenerako "Clean Sky 2" inziatibaren barneko ezinbesteko bazkideen proiektu mota izanik. Proiektuko bazkideen artean oso elkarlan aberasgarria egin da eta fuselaia panel berritzaileen estruktura erakusleen fabrikazioa martxan da tesi hau aurkeztu den unean. Tesian lortutako ondorioak fabrikazio honetan aplikatzen ari dira garatutako FSW teknologia aplikatuz, non estruktura berritzaile hauen heldutasun teknologikoa igotzea den helburu. Helburu hau gauzatzeak, FSW soldadura teknologia estruktura aeronautikoen fabrikazio aurreraturako teknologia giltzarri bezala kokatzea ekarriko luke. Honen onurak pisu murrizketa, energia kontsumoaren murrizketa, fabrikazio kostu zein denboren murrizketa eta fabrikazio automatikoago eta digitalago baterako aurrerapenak izango lirateke.

Egindako lana ahalik eta modu argienean aurkezteko asmoz, tesian 11 artikulua aipatzen dira kronologikoki aurkeztuta, zeintzuk FSW soldadura teknologiarekin gainjarritako loturetan eta aluminiozko aleazioekin egindako garapen lan guztiaren erakusle diren. Dena dela, tesiaren garapena bideratu duten ezinbesteko artikulua 9, 10 eta 11 artikulua dira. Hauek dira baldintza akademikoak betetzen dituzten artikulua eta publikazioen konpendiorako kontutan izan beharrekoak, tesi tradizionalen memoria ordezkatzuz.

LIST OF FIGURES

Figure 1: The Clean Sky 2 Programme Setup [2].	2
Figure 2: Structural parts of an aircraft fuselage at different levels, [4] [5].	3
Figure 3: Use of materials in aircraft structures [5].	4
Figure 4: Use of materials in the structure of the Airbus A380 [6].	4
Figure 5: Aluminium alloy developments for the aeronautic sector [8].	5
Figure 6: Evolution of aluminium and lithium concentration in Third-Generation Al-Li alloys [11].	5
Figure 7: Differential and Integral reinforced panel concepts [17].	6
Figure 8: LBW facility at Airbus [15].	6
Figure 9: Detail of stringers joined to skin by FSW and FSW tool [18].	7
Figure 10: FSW equipment and clamping jigs for reinforced panel manufacturing [23].	7
Figure 11: Reinforced panel manufactured by FSW stringer-skin lap joints and skin-skin butt joints [22].	7
Figure 12: Basic principle of FSW [41].	10
Figure 13: Schematic drawing of FSW [38].	10
Figure 14: Schematic drawing of the FSW tool [38].	11
Figure 15: Whorl type probe design variations [39], [45].	11
Figure 16: Material flow pattern during FSSW for threaded probes and different rotational speeds [43] [44].	12
Figure 17: Joint configurations used in FSW: Butt (left); Lap (middle); T-joint (right) [40].	12
Figure 18: Transversal section of a Al-Mg-Sc FSW joint showing the typical microstructural zones in FSW [33].	12
Figure 19: Different machine types for FSW: Aero system – courtesy of Eclipse Aviation Corporation (top-left); Process Development System (PDS) – courtesy of MTS Systems Corporation (top-right); RoboStir™ – courtesy of Friction Stirlink (bottom-left); Marine Aluminium FSW – courtesy of ESAB (bottom-right), [33].	13
Figure 20: Clamping systems for FSW: Z-stringer clamping – courtesy of MTS (left); Vacuum clamping fixture – Courtesy of Airbus-Bremen (right), [33].	13

Figure 21: FSW applications for different industry sectors: FSW module for “Finnmarken” at Marine Aluminium (top-left); FSW in a Falcon 9 tank of SpaceX (top-middle); FSW side panels made by Sapa and used by Bombardier (bottom-left); FSW taylor welded blank for BMW and Land Rover (bottom-middle); Lower fuselage reinforced panel made by stringer-skin FSW at Eclipse Aviation (right), [33].	14
Figure 22: Representation of the hook imperfection in ISO25239-5 [41].	15
Figure 23: Principal FSW lap joint features [48].	15
Figure 24: Schematic representation of typical FSW lap joint characteristics.	15
Figure 25: Advancing loading (a) and retreating loading (b) cases and the shear strength comparison in FSLW AA2198-T4 aluminium alloys [50].	16
Figure 26: Tool designs, metallographic properties and proposed material flow model for FSLW of Alclad 2024-T4 alloy [55].	17
Figure 27: Hook and sheet thinning defects as functions of the weld-pitch [51].	17
Figure 28: Effects of double-pass and tool rotation in the joint strength [51].	18
Figure 29: Stringer-skin joint configuration (left) and joint macrostructures showing defects [56].	18
Figure 30: Schematic of typical surface treatments applied in aluminium parts to protect against corrosion in aeronautic structures.	19
Figure 31: Reduction in joint strength depending on the applied surface treatments and aluminium oxide entrapments in the crack opening region [58].	19
Figure 32: Effect of sealant application on FSLW joint strength [59].	20
Figure 33: Static and fatigue strength results of Swept FSSW joints with sealants and several surface treatments [61].	20
Figure 34: Schematic of T-joints by FSW (left) and macrographs of the T-joints produced with 2024 and 2098 alloys [63].	21
Figure 35: Joint design solutions for T-joints produced by FSW [5] [64].	21
Figure 36: T-joints produced by the Corner SSFSW technique [65].	22
Figure 37: Li and Cu concentrations in some Third-Generation Al-Li alloys (left) [66], (right) [67].	24
Figure 38: Material property improvements for AA2198-T8 sheet (left) and AA2196-T8511 extrusions (right) over current solution AA2024-T3511 for fuselage and wing applications [67].	24
Figure 39: Threaded and non-threaded FSW tool-probe designs (left) and macrosections of FSLW joints produced using the same welding parameters but different tool-probe designs (right) [70].	151

Figure 40: Macrosections and FSW tool-probes used for FSLW tests; cylindrical threaded tool-probe (top) and tool-probe with three flats and mixed thread (bottom) [71].	151
Figure 41: Macrosections of FSLW joints produced by the 2 different tool-probe designs and welding parameters with AA7075-T6 aluminium sheets [72].	152
Figure 42: Macrosections of FSLW joints produced by the 2 different tool-probe designs and welding parameters with AA2198-T8 aluminium sheets [73].	152
Figure 43: Graphic representation of the hook size measured in FSLW joints produced by 2 different tool-probe designs and welding parameters with AA7075-T6 (left) [72] and AA2198-T8 (right) [73].	152
Figure 44: Hook and cold lap defect details (left); and EST and BIW representation (right) in FSLW joints performed by several probe designs and welding parameters [75].	153
Figure 45: Robotic FSW system at LORTEK used for FSLW tests (left) and a FSLW joint (right) made with AA7050-T7651 extrusion (stringer) and AlcladAA7475-T761 sheet (skin) [74].	154
Figure 46: Macrosections of FSLW joints made with AA7050-T7651 extrusion on top of an AA2024-T3 sheet (top) or AlcladAA7475-T761 sheet (bottom) [74].	154
Figure 47: Pull-out strength test (left) and strength results (right) with stringer-skin FSLW joints produced by different tool-probe designs, alloy combinations and loading conditions [74].	155
Figure 48: Selected Third-Generation Al-Li alloy materials and clamping arrangements developed for FSLW tests.	156
Figure 49: FSW tool-probe design with “mixed threads + three flat” concept.	156
Figure 50: i-STIR PDS 4 FSW machine used for FSW manufacturing tests (left); clamping configuration developed to produce the FSW coupons using AA2099-T83 extrusions on top of AA2060-T8E30 sheets (right).	157
Figure 51: (a) FSLW joint produced using AA2099-T83 and AA2060-T8E30 alloys; (b) conventional tool; (c) new tool proposed for lap joints; (d) sketch with details of the new three flat + mixed thread tool.	158
Figure 52: Cross-section of FSLW joint produced at 1200 rpm and 250 mm/min using a conventional threaded tool.	158
Figure 53: Cross-section of FSLW joint produced at 1200 rpm and 250 mm/min using a three flat + mixed thread tool.	158
Figure 54: Representation of the hook size measured in FSLW joints produced using different welding parameters (weld pitch) and tool designs.	159
Figure 55: Cross-section showing the characteristic features of FSLW joints; (a) effective lap with (ELW); (b) hook at the advancing side (D1); (c) cold lap defect and hook at the retreating side (D2).	160

Figure 56: Representation of the (a) hook height in the advancing side; and (b) hook height in the retreating side; in FSLW joints produced using different welding parameters and tool designs.....	160
Figure 57: Representation of the ELW in FSLW joints produced using different welding parameters and tool designs.....	161
Figure 58: Pull-out strength and failure mode of FSLW joints produced using different tools and welding parameters.	161
Figure 59: Sealant preparation and application in AA2060-T8E30 sheet without any surface treatment (left); and surface treated base materials (right).	162
Figure 60: (a) Setup for the FSW process manufacturing; and (b) Examples of FSLW joint-coupons produced using base materials with different surface conditions and sealant.....	163
Figure 61: (a) Torque and (b) tool penetration average values obtained during the FSW process for C1-C6 coupons.	164
Figure 62: (a) Cross-section of FSLW joint C1 and (b) SEM image and EDS analysis of region A in Figure 62a.....	165
Figure 63: (a) Cross-section of FSLW joint C2 and (b) details of the SZ interface by optical microscopy, SEM and EDS analysis of the fragment remnants.	165
Figure 64: (a) Cross-section and detail magnification of FSLW joint C6 and (b) SEM image and EDS analysis of region A in Figure 64a.	166
Figure 65: Examples of the specimens (C1-left; C2-middle) used for the static pull-out tests (right).....	166
Figure 66: Representation of the progress in pull-out tests. (a) Initiation; (b) before failure; and (c) after failure.....	167
Figure 67: (a) Representation of maximum pull-out force values for FSLW joint-coupons C1-C6; and (b) examples of stringer failure in specimens obtained from FSW coupons C2, C4 and C6.....	167
Figure 68: Sketch of the specimens machined from the FSLW joint-coupons C1-C6 for the static tensile and fatigue tests under hoop-stress loading conditions.	168
Figure 69: Specimens machined from coupons C3 (left); C6 (right); and the setup for the static tensile tests (middle).....	169
Figure 70: Setup for the fatigue tests monitored by IR thermographic cameras.	169
Figure 71: (a) Cross-section of a specimen cut from FSLW joint C01; (b) microhardness scan measurements in the A-B line shown in Figure 71a.....	169
Figure 72: (a) Yield strength and ultimate tensile strength values obtained for the FSLW joints C01-C06 in static tensile tests; and (b) metallographic cross-section of a fractured C01 specimen showing the fracture initiation at the HAZ.	170

Figure 73: S-N curves of FSLW joints showing a comparison between FSW specimens produced using bare aluminium alloys (C01) and surface treated alloys without sealant (C02 and C03).	171
Figure 74: S-N curves of FSLW joints showing a comparison between FSW specimens produced using bare aluminium alloys without sealant (C01) and with sealant (C04).	171
Figure 75: S-N curves of FSLW joints showing a comparison between FSW specimens produced using bare aluminium alloys without sealant (C01) and surface treated aluminium alloys with sealant (C05 and C06).....	172
Figure 76: S-N data of FSLW joints showing different fracture modes in high and low stress loading conditions.....	172
Figure 77: IR thermographic images showing the instant of the fracture in fatigue tests; (a) fracture out of the FSLW joint at high n ^o of cycles (specimen C05_A in Figure 76); and (b) fracture at the HAZ of the FSLW joint at low n ^o of cycles (specimen C05_B in Figure 76).	173
Figure 78: Cross-sections of FSLW joints showing different fracture modes; (a) fracture out of the FSLW joint (specimen from coupon C05 tested at a 30% of the YS); and (b) fracture at the HAZ of the FSLW joint (specimen from coupon C05 tested at a 70% of the YS).....	173
Figure 79: Fracture surface analysis of specimen C05_A (indicated in Figure 76) showing the fracture out of the FSLW joint; (a) general view of fractured specimen; and (b) perpendicular view of the fracture surface.....	174
Figure 80: SEM image and EDS analysis of the zone A1 indicated in Figure 79.	174
Figure 81: SEM observations of the fracture surface of specimen C05_A shown in Figure 79b; (a) point A2; (b) point B1; and (c) point C1.	175
Figure 82: Fracture surface analysis of specimen C05_B (indicated in Figure 76) showing the fracture in the HAZ of the FSLW joint; (a) general view of fractured specimen; and (b) perpendicular view of the fracture surface.	175
Figure 83: SEM observations of the fracture surface of specimen C05_B shown in Figure 82b; (a) point D1; (b) point E1; and (c) point E1.	176
Figure 84: Disposition of the FSLW joint-coupons in the NSS chamber during the ASTM-B117 NSS corrosion test (left); FSLW joint-coupon 4 after NSS exposure (middle); and specimens cut from FSLW joint-coupons ready for static pull-out tests (right).....	178
Figure 85: Results of static pull-out tests of FSLW joints produced and corrosion tested according to the conditions shown in Table 6.....	178
Figure 86: FSLW joint-coupon manufactured using a AA2198-T8 sheet/skin and a AA2196-T8511 extrusion/stringer.....	179

Figure 87: Cross-sections of FSLW joints produced with AA2198-T8 sheet and AA2196-T8511 extrusion at 800 rpm and 250 mm/min (left) and 1200 rpm and 150 mm/min (right).	179
Figure 88: FSLW joint-coupons manufactured using pocketed AA2198-T8 sheet/skins (left), specimens for static tensile and fatigue testing machined from the coupons (top-right) and detail of a machined specimen showing the pocketed region (bottom-right).	180
Figure 89: S-N curves of FSLW joints produced using pocketed AA2198-T8 sheet/skins and AA2196-T8511 extrusion/stringers.	180
Figure 90: S-N curves of FSLW joints showing a comparison between pocketed and non-pocketed FSW specimens produced using AA2060-T8E30 and AA2099-T83 alloys.	181
Figure 91: Robotic FSW system used for FSLW tests using AA2198-T8 sheets of small thicknesses.	182
Figure 92: Cross-section of a FSLW joint produced using a 1.3 mm thick AA2198-T8 sheet on top of a 2.3 mm thick AA2198-T8 sheet.	182
Figure 93: Cross-section of a FSLW joint produced using a 1 mm thick AA2198-T8 sheet on top of a 2.3 mm thick AA2198-T8 sheet.	182
Figure 94: Static tensile test results of FSLW joints produced using AA2198-T8 sheets of different thicknesses.	183
Figure 95: General design of fuselage panel demonstrator to be manufactured by FSLW and details of the design of stringers and frames.	184
Figure 96: Initial fuselage panel demonstrator manufactured in the robotic FSW system at LORTEK.	184

LIST OF TABLES

Table 1: Partner institutions and developed technologies for metallic materials in ecoTECH.....	9
Table 2: Compositions of selected Second-Generation Aluminium-Lithium Alloys (wt%) [10].	23
Table 3: Chemical Composition of some Third-Generation Al-Li alloys (wt%) [10].	23
Table 4: Summary of the work performed and published in each article.....	149
Table 5: Chemical compositions of base materials, wt.%.	157
Table 6: Friction stir welded coupon identification with the applied surface treatments and sealant.	163
Table 7: FSLW joint-coupon description and test plan.	177

LIST OF ACRONYMS

ACARE: Advisory Council for the Aviation Research and Innovation in Europe

ATM: Air Traffic Management

BIW: Bonded Interface Width

BM: Base material

EST: Effective Sheet Thickness

ELW: Effective Lap Width

FP6 / FP7: Framework Programme 6 / Framework Programme 7

FSLW: Friction Stir Lap Welding

FSSW: Friction Stir Spot Welding

FSW: Friction Stir Welding

HAI: Hellenic Aerospace Industries

HAZ: Heat Affected Zone

IAI: Israel Aerospace Industry

IR: Infra Red

ISO: International Organization for Standardization

ITD: Integrated Technology Demonstrator

LBW: Laser Beam Welding

MRL: Manufacturing Readiness Level

NDT: Non-Destructive Testing

NLR: Netherlands Aerospace Centre

NSS: Neutral Salt Spray

PDS: Process Development System

RFSSW: Refill Friction Stir Spot Welding

SEM: Scanning Electron Microscopy

SESAR: Single European Sky ATM Research

SSFWS: Stationary Shoulder Friction Stir Welding

SZ: Stir Zone

TMAZ: Thermo-Mechanically Affected Zone

TRL: Technology Readiness Level

TWI: The Welding Institute

UK: United Kingdom

UTS: Ultimate Tensile Strength

XWB: Xtra Wide Body

YS: Yield Strength

LIST OF SYMBOLS

ω : Rotational Speed of the FSW tool given in rpm (revolutions per minute)

v_w : Welding speed of the FSW tool given in mm/min (millimetres per minute)

0.- CONTENTS

0.- CONTENTS.....	i
1.- INTRODUCTION	1
1.1.- RESEARCH IN THE AERONAUTIC INDUSTRY	1
1.2.- TECHNOLOGICAL FRAMEWORK	2
1.2.1.- Innovative lightweight structural concepts.....	2
1.2.2.- The project ecoTECH	8
2.- BACKGROUND AND STATE OF THE ART	10
2.1.- FRICTION STIR WELDING: BASIC PRINCIPLES	10
2.2.- FSW JOINTS FOR REINFORCED PANEL MANUFACTURING	15
2.3.- NEW ALUMINIUM-LITHIUM ALLOYS FOR INNOVATIVE AIRCRAFT STRUCTURES.....	22
3.- OBJECTIVES, HYPOTHESIS AND METHODOLOGY	25
3.1.- OBJECTIVES.....	25
3.2.- HYPOTHESIS.....	25
3.3.- METHODOLOGY.....	26
3.3.1.- Performed work	26
4.- ARTICLE 1: FRICTION STIR WELDING OF LAP JOINTS: PROCESS PARAMETERS AND JOINT PROPERTIES.....	29
5.- ARTICLE 2: MECHANICAL AND MICROSTRUCTURAL PROPERTIES OF FSW LAP JOINTS	33
6.- ARTICLE 3: THE ROLE OF THE TOOL DESIGN IN PROPERTIES OF FRICTION STIR WELDED LAP JOINTS	43
7.- ARTICLE 4: MICROSTRUCTURAL FEATURES IN FRICTION STIR WELDED LAP JOINTS.....	54
8.- ARTICLE 5: FRICTION STIR WELD LAP JOINT PROPERTIES IN AERONAUTIC ALUMINIUM ALLOYS.....	59
9.- ARTICLE 6: DEVELOPMENTS IN STRINGER-SKIN LAP JOINTS BY FSW.....	68

10.- ARTICLE 7: INFLUENCE OF PIN IMPERFECTIONS ON THE TENSILE AND FATIGUE BEHAVIOUR OF AA7075-T6 FRICTION STIR LAP WELDS.....	80
11.- ARTICLE 8: FRICTION STIR WELDING OF LAP JOINTS USING NEW AL-LI ALLOYS FOR STRINGER-SKIN JOINTS.....	92
12.- ARTICLE 9: EFFECT OF TOOL GEOMETRY AND WELDING PARAMETERS ON FRICTION STIR WELDED LAP JOINT FORMATION WITH AA2099-T83 AND AA2060-T8E30 ALUMINIUM ALLOYS	105
13.- ARTICLE 10: FRICTION STIR WELDING OF AA2099-T83 AND AA2060T8E30 ALUMINIUM ALLOYS WITH NEW CR-FREE SURFACE TREATMENTS AND SEALANT APPLICATION.....	118
14.- ARTICLE 11: FRETTING FATIGUE AS A LIMITING FACTOR ON THE DURABILITY OF FRICTION STIR WELDED LAP JOINTS USING AA2099-T83 AND AA2060-T8E30 ALUMINIUM ALLOYS.....	133
15.- SUMMARY OF RESULTS, CONCLUSIONS AND FUTURE LINES	149
15.1.- SUMMARY OF RESULTS.....	149
15.1.1.- Initial results.....	150
15.1.2.- Main results	156
15.2.- CONCLUSIONS.....	185
15.3.- FUTURE LINES	187

1.- INTRODUCTION

1.1.- RESEARCH IN THE AERONAUTIC INDUSTRY

During the last 60 years the aviation industry has evolved significantly. In the last 20 years the air traffic has increased enormously reducing distances between remote geographical places for people and goods. According to the Advisory Council for the Aviation Research and Innovation in Europe (ACARE) and its Strategic Research and Innovation Agenda [1] this air traffic will continue growing and the number of passengers is expected to double in the next 20 years. Globally speaking the worldwide fleet is estimated in 25000 aircrafts and the growth expectations forecast a need of 32000 new units for the next two decades for additions and replacements [2].

The European aeronautic industry is one of the most important sector as it is reflected in the numbers produced by its activity. Approximately 450 airlines operate in nearly 700 airports throughout the European geography. In 2010 606 million passengers were transported and this number has continued increasing in the last years. The European aeronautic industry provides nearly 12 million jobs directly and indirectly, and generates about 700 billion Euros for the European economy. Due to the huge impact and the expected future growth of the European aeronautic sector, the investment in research and development is also very important. Thus, approximately 7 billion Euros are invested every year for research and development activities in the commercial aeronautic sector in Europe.

The aeronautic industry is continuously looking for innovations and advances in different systems that form the overall structure of the aircrafts. Prove of these continuous innovation actions are the latest research programmes launched by the European aeronautic industry such as the already completed European Community's Framework programmes FP6 and FP7, the Clean Sky 1 Joint Undertaking or the ongoing Horizon 2020, SESAR Joint Undertaking [3] and the Clean Sky 2 Joint Undertaking [2]. In line with the Flightpath 2050 strategic goals established by the European Commission, one of the main goals of these research and innovation programmes is to achieve a more efficient air transportation system with a lower ecological footprint. Thus, currently SESAR focuses on developing technical and operational solutions to modernise Europe's air traffic management system, while Clean Sky 2 fosters the development of new technologies that will make tomorrow's aircraft greener and more efficient for the commercial aviation.

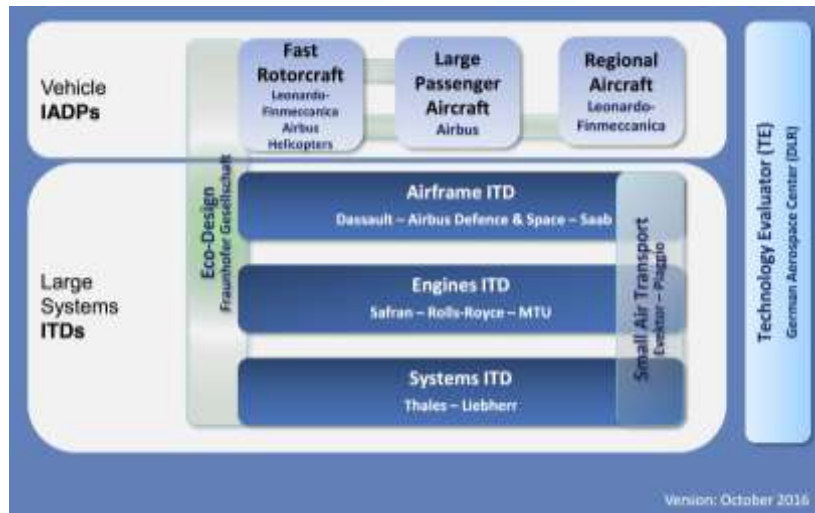


Figure 1: The Clean Sky 2 Programme Setup [2].

The Clean Sky 2 Joint Undertaking [2] is the largest European research programme for the development of new technologies with the aim to reduce CO₂ (by 50%) and NO_x (by 80%) emissions as well as noise levels (by up to 50%). Research and activities within the Clean Sky 2 framework are divided into different themes and aircraft concepts as shown in Figure 1. Thus, a large number of technologies, materials and manufacturing processes with potential for enabling the achievement of the mentioned goals are under development for different aircraft types and their sub-systems. For example, the Airframe ITD within Clean Sky 2, among other innovation activities, is directed to the development of advanced fuselage, wing and other structures in order to address the challenges of weight, cost, life-cycle impact and durability.

1.2.- TECHNOLOGICAL FRAMEWORK

1.2.1.- Innovative lightweight structural concepts

An evident approach towards the compliance with the fuel consumption and emission reduction goals is the research and development of new lightweight structural concepts for future aircrafts. The structural weight of an aircraft is an important part of the total weight. Therefore, weight savings in the structures that form the overall structure of an aircraft can contribute in a large extent to the achievement of fuel consumption and emissions reduction goals stated by the aeronautic industry. For example, Figure 2 shows the structural parts at different levels that from the fuselage of an aircraft [4], [5]. The development of new lightweight materials such as high strength and low density aluminium alloys, along with new manufacturing processes with potential to reduce the weight of sub-structures by substituting hundreds of rivets in structural fuselage parts, can result in lightweight structures with lower manufacturing cost, time and environmental footprint among other benefits. Obviously, these innovative structures have to equal or exceed the performance of current sub-structures in terms of mechanical strength, corrosion resistance, end of life operations, etc.

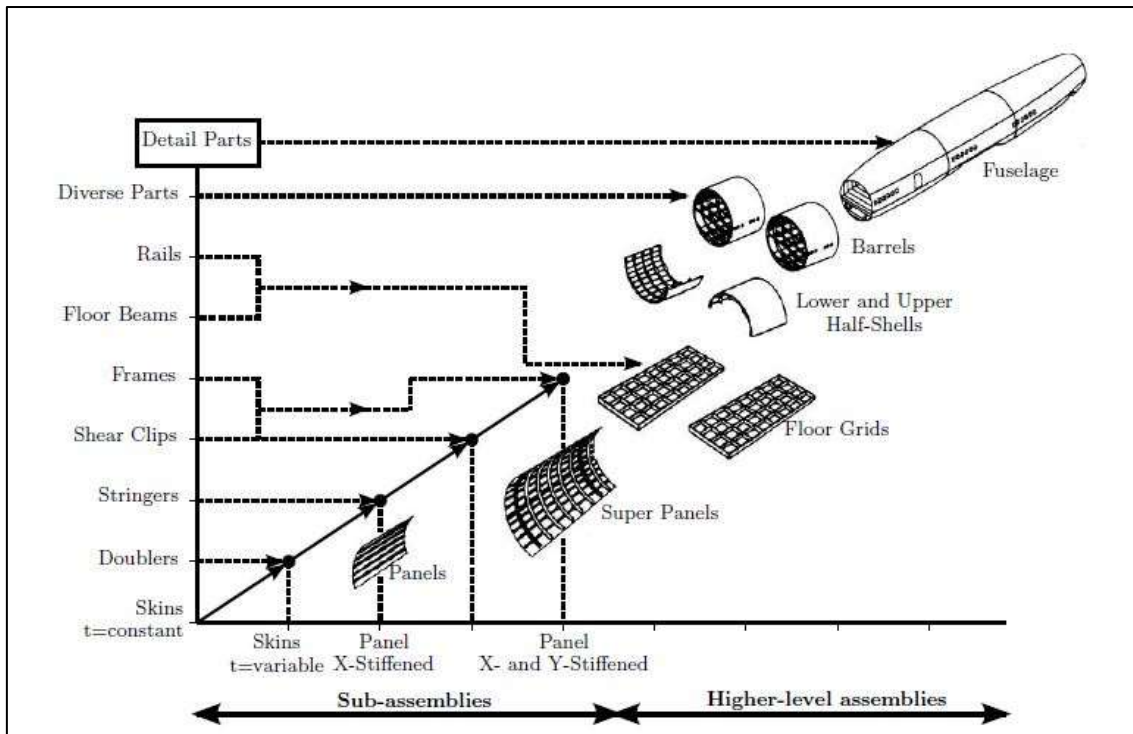


Figure 2: Structural parts of an aircraft fuselage at different levels, [4] [5].

Materials typically used to manufacture aircraft structures are mostly aluminium alloys, fibre reinforced composites, fibre metal laminates and or titanium alloys as shown in Figure 3 and Figure 4. Traditionally aluminium alloys have been the prevalent material for airframe construction due to their good strength-to-weight ratio and reasonable cost. However, fostered by their superior lightweighting potential, fibre reinforced composite materials have increased their usage in the latest aircraft models developed by the main aircraft producers Boeing and Airbus [5], [6]. Thus, aluminium alloys represented the 65,5% of the materials used in the Airbus A320, while this number decreased to a 61% in the Airbus A380 and to a 20% in the Airbus A350 XWD. The Boeing 787 also presents 20% of aluminium alloys. This reduction of aluminium use is mainly due to the extended use of composite materials that goes from the 12,5% in the Airbus A320 to the 52% in the Airbus A350 XWD. However, material choice for aircraft structures is not consensual as composite materials also present disadvantages such as high material costs, higher production costs, limited knowledge of material properties during the life cycle or difficulties to establish feasible end of life procedures such as recycling and material disposal. In addition to these issues, the introduction of new aluminium alloys and tempers opens new possibilities for extended aluminium use in future aircrafts. Prove of that is the use of 20 different alloys and tempers in the Airbus A380 in comparison with the 6 used in the Airbus A320 [6].

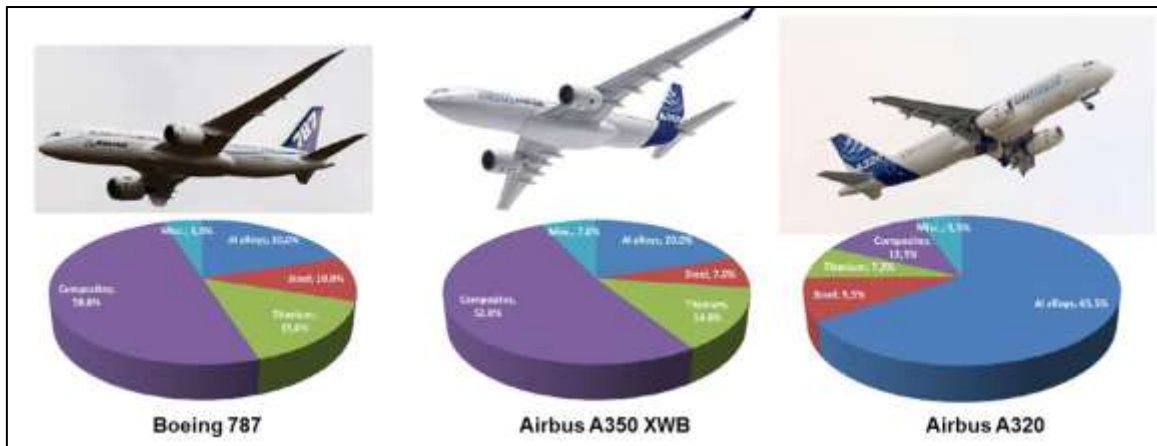


Figure 3: Use of materials in aircraft structures [5].

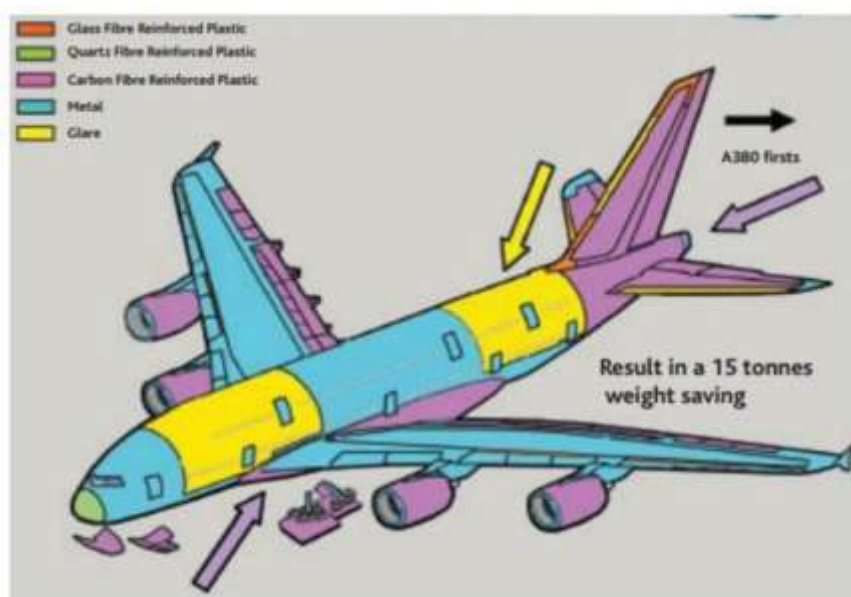


Figure 4: Use of materials in the structure of the Airbus A380 [6].

Aluminium producers have invested in research and development of new aluminium alloys for the aeronautic sector in the last years [7] [8], as shown in Figure 5. The main goal has been the development of alloys with higher mechanical performance, lower density as well as better processing capabilities for innovative manufacturing processes such as welding. Thus, a new family of aluminium alloys was developed for the Airbus A380 by an Alcan-Airbus integrated project team including several alloys for wing (7040, 7449-T7651, 2027, 7056, 2050) and fuselage (7040, 6156) structures, including weldable alloy grades by LBW [9]. One of the main outcomes of these developments was the maturation and launch of the third generation of aluminium-lithium alloys. The problems encountered in the previous generations of such alloys (reduced thermal stability, reduced ductility and fracture toughness in the short-transverse direction) were solved by improvements in the chemical compositions (Figure 6) and developing optimized thermo-mechanical treatments [10]. Therefore, Third-Generation Al-Li alloys were ready to be implemented and next developments focused on improving properties and processing options (welding, casting...) with the final goals of producing cost and weight savings in aircraft structures.

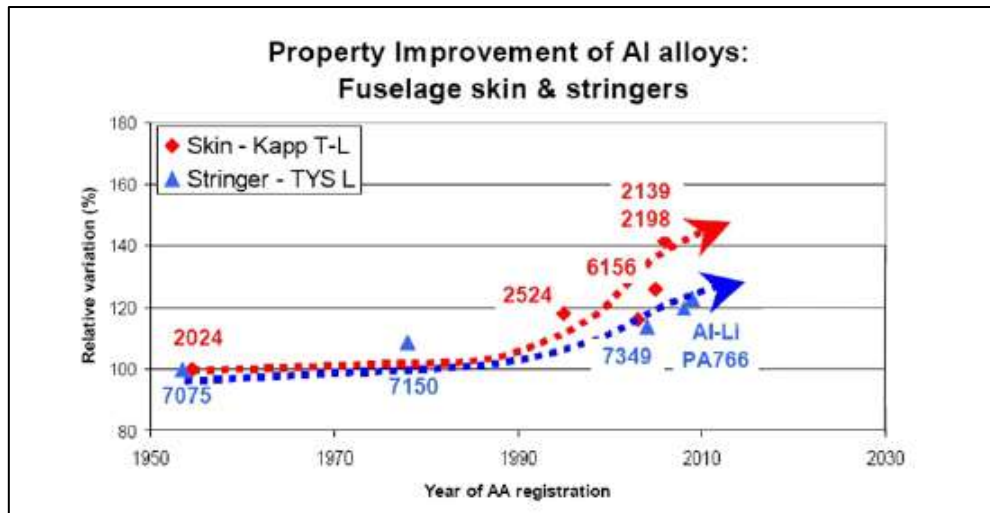


Figure 5: Aluminium alloy developments for the aeronautic sector [8].

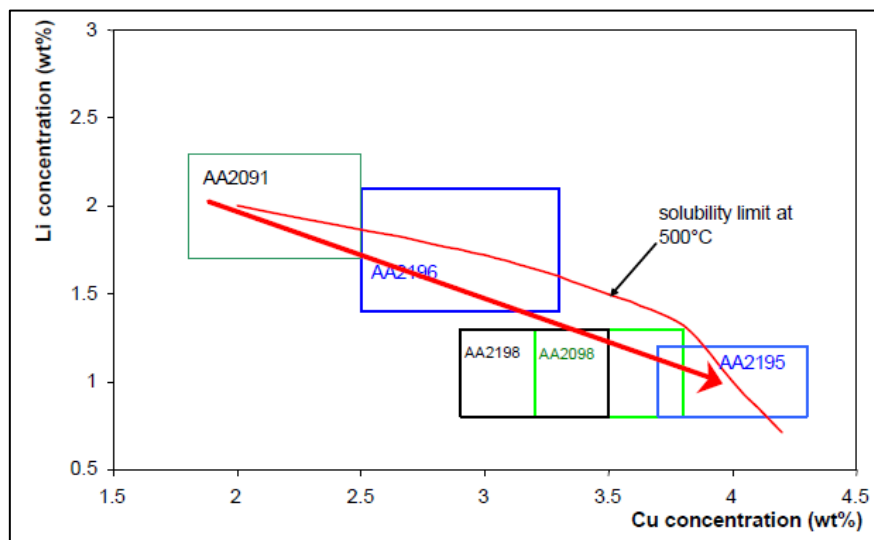


Figure 6: Evolution of aluminium and lithium concentration in Third-Generation Al-Li alloys [11].

The development of new aluminium alloys with enhanced weldability over traditional 2XXX and 7XXX alloys, opened new possibilities for the manufacturing of welded integral reinforced panels as an alternative for riveted differential reinforced panels (Figure 7). Riveting has been the dominant joining technology for reinforced panel manufacturing for aircraft structures. However, there are some disadvantages in the riveting processes such as low productivity and lack of potential for weight reduction [12] [13]. Welded integral structures represent benefits such as reductions in the number of necessary parts, enhanced weight saving as well as significant reductions in manufacturing times and costs. These integral reinforced panels have aroused the interest of the aircraft manufacturers so that innovative welding technologies and aluminium alloys have been extensively investigated [14] [15] [16]. The main welding technologies investigated have been LBW and FSW so that some reinforced panel applications have been applied in different aircraft models. For example, Airbus implemented LBW technology for the manufacturing of lower fuselage panels in the Airbus A318 (1 panel) and in the Airbus A380 (8 panels) [15]. Figure 8 shows the LBW facility and the reinforced panel manufactured by LBW of stringers on skin. However, due to the extremely low weldability

of traditional aerospace grade aluminium alloys, new aluminium alloys with improved weldability had to be developed.

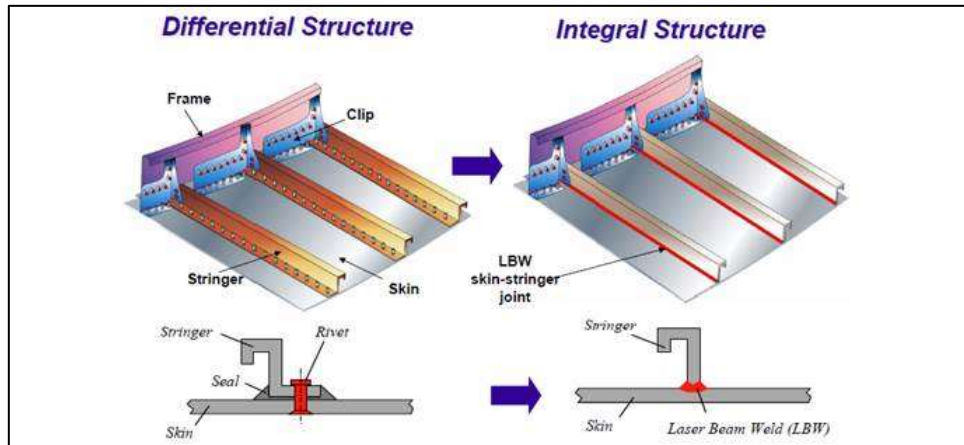


Figure 7: Differential and Integral reinforced panel concepts [17].



Figure 8: LBW facility at Airbus [15].

FSW is another technology that has been implemented for the manufacturing of reinforced panels of aluminium for primary aircraft structures [18] [19] [20] [21] [22]. The solid-state nature of this technology allows avoiding the main weldability issues such as hot cracking or porosity presented by other fusion-solidification based welding technologies. Material strength reductions in the HAZ of the welds when precipitation-hardening aluminium alloys are welded, is also lower in FSW due to the low processing temperatures and heat inputs, resulting in a higher joint strength efficiency. Thus, practically all aluminium alloys are weldable by FSW, including the high strength precipitation hardening aerospace grade 2XXX and 7XXX aluminium alloys. In fact, the Eclipse 500, which is a six-person twin-engine business jet and the first airplane to implement FSW technology for the manufacturing of its primary structure, was manufactured using 2XXX and 7XXX aluminium alloys.

One Aviation (the former Eclipse Aviation and Eclipse Aerospace) delivered the first Eclipse 550 in 2013, an improved model of the Eclipse 500 which is also intensive in FSW implementation [19] [20] [23]. Both models apply FSW technology instead of riveting for stringer-skin lap joining for the manufacturing of structures in the cabin,

fuselage, wings and engine mounts, as shown in Figure 9 [18]. The FSW equipment used for panel production can be observed in Figure 10 [23]. The result was a lighter and stronger structure that saved in the range of 50lbs eliminating 65% of the previously riveted joints that supposed about 30.000 rivets. In addition to that, 1600 man hours were achieved [21] and production times were reduced by 40% due to the faster joining operations, which allowed saving between \$50.000-\$100.000 per plane [14]. However, other technical challenges such as corrosion protection, distortion control and the understanding of joint properties for the designing phase had to be overcome and details of how this was achieved are not well known.



Figure 9: Detail of stringers joined to skin by FSW and FSW tool [18].

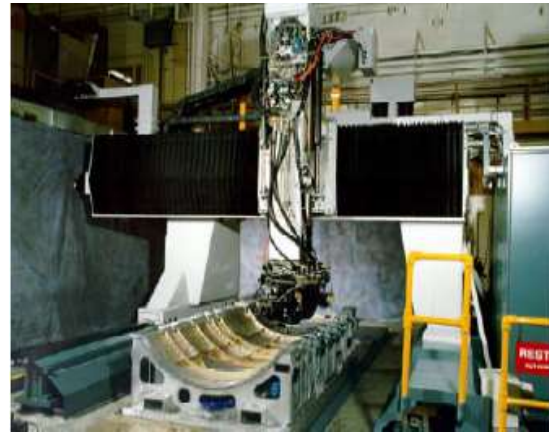


Figure 10: FSW equipment and clamping jigs for reinforced panel manufacturing [23].

Embraer also announced the implementation of FSW in the manufacturing of integral reinforced panels for fuselage structures in the mid-size aircrafts Legacy 450 and 500 [22]. In this case, butt joints performed by FSW were also used for joining skin sheet materials, in addition to the similar stringer-skin lap joints as developed by One Aviation for the Eclipse 500 and 550. The reinforced panel structure can be observed in Figure 11. Critical details about the application of FSW technology such as welding parameters, FSW tool designs... were not disclosed.



Figure 11: Reinforced panel manufactured by FSW stringer-skin lap joints and skin-skin butt joints [22].

Other companies and researchers involved in developments for the aerospace sector have also proposed FSW welding technology as an alternative joining technology to

riveting for lap joints in stringer to skin and other similar applications [5] [16] [24] [25] [26] [27] [28] [29] [30] [31] [32]. Some of the proposed developments resulted in real industrial applications such as the Boeing C-17 cargo ramp, the Boeing 747 freighter barrier beams [31] or the cargo floor of the Airbus A400M military aircraft [27]. Some other FSW applications such as structures for fuselage and wings have been matured and demonstrated but did not reach to the final production floor due to issues not related to technical stoppers such as the increased adoption of composite materials in some of the latest aircraft models [33]. In any case, the potential to develop lightweight and cost effective aluminium structures by the implementation of new alloys and FSW technology is huge. However, the FSW process conditions for new alloys (especially dissimilar combinations of aluminium alloys) have to be developed firstly and their effects on joint properties have to be well understood for a successful implementation of the technology.

The topic of the thesis is based on the research of the FSW process and its implementation for the manufacturing of integral reinforced panels for aircraft structures. The main focus is the development of stringer-skin lap joints by FSW using Third-Generation Al-Li alloys. Thus, the research and development activities are directed to the FSW joint preparation, joint characterisation and the understanding of the relationships between FSW conditions and joint properties. All the activities are carried out with the final goal to define appropriate FSW conditions to produce lightweight and cost effective structures that comply with the stringent requirements of the aeronautic sector, investigating the static strength, fatigue strength and techniques to improve the corrosion resistance of the FSW joints.

1.2.2.- The project ecoTECH

The work carried out in this thesis is aligned with part of the activity that LORTEK has performed in the project ecoTECH [34], which is a core-partner project in the frame of the Clean Sky 2 initiative for research and development of new technologies for future aircraft. ecoTECH is titled “Development of innovative and ECO-friendly airframe TECHNOLOGIES from design to manufacturing to improve aircraft life cycle environmental footprint” and its activity is included in the Airframe ITD under the contract “JTI-CS2-2015-CPW02-AIR-01-03”. The activity is divided in 4 principal technology streams:

- Technologies for thermoplastic composite materials
- Technologies for thermoset composite materials
- Technologies for metallic materials
- Technologies for biomaterials

This thesis is aligned with the activities for the development of technologies for metallic materials, where different partner institutions of ecoTECH have developed new technologies for joining, surface treatment and other manufacturing technologies for advanced airframe structures based on Third-Generation Al-Li alloys. The Table 1 shows the main partner institutions that have interacted with the activities of this thesis and their role in ecoTECH.

Table 1: Partner institutions and developed technologies for metallic materials in ecoTECH.

Partner institution	Role in ecoTECH – related technologies
LORTEK	Development of innovative joining technologies for integral reinforced panels, mainly FSW and LBW. Design and manufacturing of demonstrators.
HAI	Development of innovative surface treatments, mainly TFSA and Sol-Gel. Design and manufacturing of demonstrators.
AKZONOBEL	Development of innovative primer and top-coat formulations.
NLR	Corrosion testing of innovative Al-Li alloys and structures, mainly integral reinforced panels (including welded parts)
IAI	Project coordinator. Development of manufacturing technologies for Al-Li alloys. Design and manufacturing of demonstrators.

The main goal of the partners involved in the technology stream for metallic materials in ecoTECH is the development of innovative metallic structures that will reduce the environmental impact. The work is focused on lightweight reinforced panels incorporating welded parts, eco-friendly surface treatments, primers and top-coats. The interactions between the involved technologies are under investigation, for example, the effects of surface treatments in welded components. So far, the aluminium alloys selected for these activities are the Third-Generation Al-Li alloys as shown in Table 3. Therefore, the activity of ecoTECH aligned with this thesis is focused on the effects of surface treatments such as TFSA and sol-gel in FSLW process implementation and the resulting joint properties for the following stringer-skin alloy combinations:

- AA2060-T8E30 skin sheet – AA2099-T83 stringer extrusion
- AA2198-T8 skin sheet – AA2196-T8511 stringer extrusion

2.- BACKGROUND AND STATE OF THE ART

This thesis is focused on the development of the FSW technology for aeronautic reinforced panels made using Third-Generation Al-Li alloys, primarily by stringer-skin lap joints. Therefore, it is necessary to introduce the state of the art of the relevant technologies, which is covered in the following sections.

2.1.- FRICTION STIR WELDING: BASIC PRINCIPLES

Friction Stir Welding (FSW) is a solid-state continuous joining technology where a non-consumable rotating tool plunges in the materials to be joined and creates the weld by softening and mixing those materials. The heat produced by the friction and the plastic deformation softens the materials while the rotation and traverse motion of the tool produces the stirring and the consolidation of the weld in the solid state (Figure 12, Figure 13). An important feature of the FSW process is its non-symmetric nature resulting in the advancing and retreating side in the weld microstructure as represented in Figure 13. In the advancing side the tool rotation direction and the travel direction are the same while in the retreating side they are opposite. This has important effects in the resulting FSW joint properties as reflected later in this report, especially in FSW lap joints.

The process was invented at The Welding Institute (TWI) in UK in 1991 [35] [36] and it has seen an extensive development and expansion since then, especially in applications where aluminium joining is required. Many industrial applications and technological advances have been developed and reported in the literature during the last two decades [37] [38] [39] [33] [40]. The increasing number of applications and industrial implementations resulted in the development of the ISO standard for FSW manufacturing for aluminium alloys in 2011 [41], which is currently under revision.

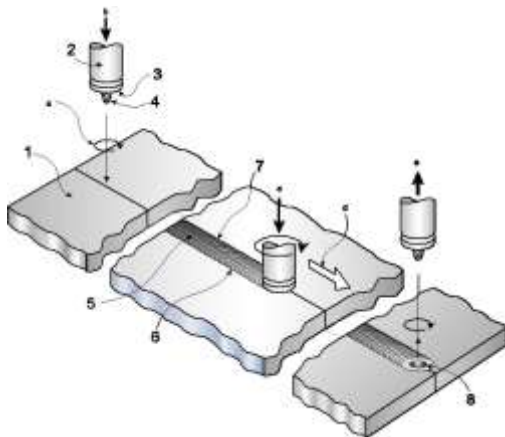


Figure 12: Basic principle of FSW [41].

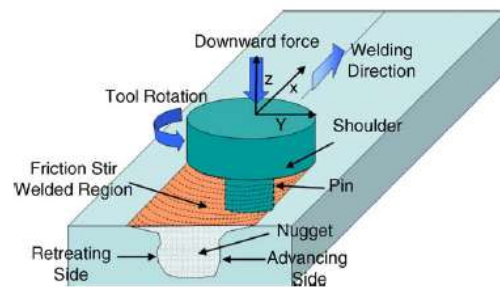


Figure 13: Schematic drawing of FSW [38].

Extensive details on the critical aspects of FSW technology such as FSW tool characteristics, joint configurations, typical joint properties, process variants, FSW machines and clamping systems, as well as industrial applications can be found in the literature.

The FSW tool design is one of the most critical factors for the successful implementation of the FSW process. It is typically formed by a shoulder, that travels in contact with the surface of the material, and a pin or probe, which is plunged and travels immersed in the plasticised material. The mission of the FSW tool includes many functions such as heat

generation, material stirring and mixing, joint line breaking, oxide layer dispersion, plasticised material containment and joint consolidation, etc. The FSW tool have to show a good balance of hardness and toughness in order to present a sufficient wear resistance without fracture at the operating conditions, which involve high temperatures and high process loads. Some other important characteristics of FSW tools are explained in the literature [38] [39] [40].

Probes and shoulders of FSW tools with different features and designs can be used for FSW processes as shown in Figure 14 and Figure 15. Depending on those designs, the plasticised material flow induced by the FSW tool can be modified and the properties of the resulting joints can differ considerably. The material flow induced by conventional threaded probe was investigated by the authors [42] [43] [44], showing an important downwards-upwards vertical flow dependant on the thread's characteristics and FSW parameters (Figure 16). The introduction of design features such as flats or different thread characteristics have been shown to modify the material flow, impacting directly in FSW process conditions and the properties of the resulting joints. Thus, Thomas et. al. found that probes featuring flats or flutes produced benefits such as FSW process force reduction, improvements in welding speed and joint properties [45] [46].

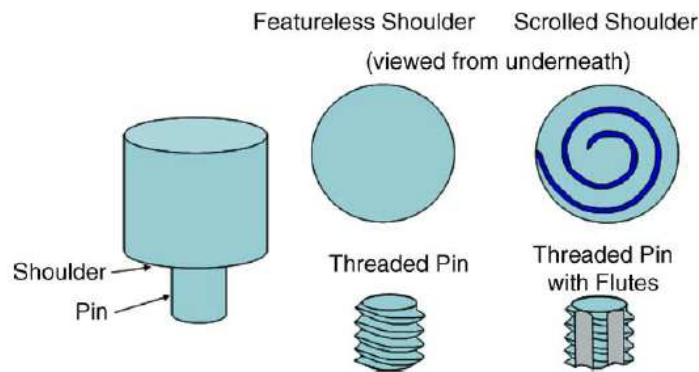


Figure 14: Schematic drawing of the FSW tool [38].

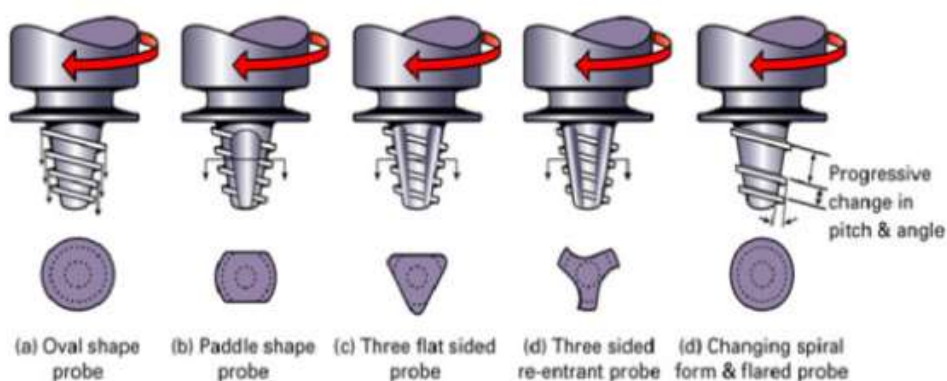


Figure 15: Whorl type probe design variations [39], [45].



Figure 16: Material flow pattern during FSSW for threaded probes and different rotational speeds [43] [44].

FSW can be applied to a wide variety of joint configurations although the most typical ones are butt joints, lap joints and T-joints as shown in Figure 17. Other relevant joint configurations are also shown in part 2 of the ISO25239 standard, which is referred to the design of FSW joints [41]. It is important to remark that a good selection of tool design and FSW parameters is critical to obtain the desired material flow and resulting joint properties, which is highly dependent on the joint configuration for each application. Therefore, tool designs that are appropriate for butt joints may not be so for other joint configurations such as lap joints or T-joints, as demonstrated by researchers [45] [46].

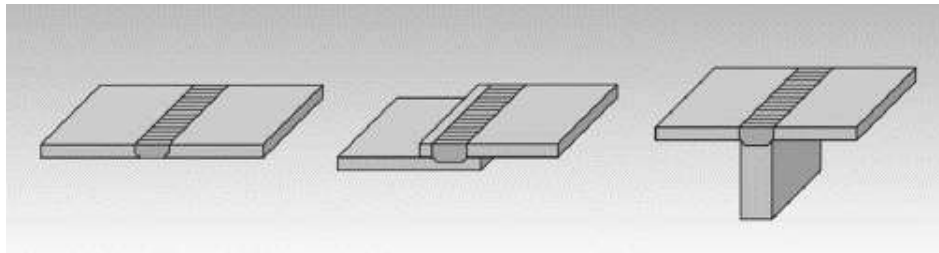


Figure 17: Joint configurations used in FSW: Butt (left); Lap (middle); T-joint (right) [40].

The solid-state nature of the FSW process results in substantially different microstructural characteristics of the welds in comparison with other fusion-solidification welding technics. FSW was classified as a hot metalworking process in the solid state similar to an extrusion process [47] [48] and the resulting microstructures are a direct consequence of such a process. The typical microstructural zones that are present in FSW joints are shown in Figure 18 and their characteristics are well explained in the literature [39]:



Figure 18: Transversal section of a Al-Mg-Sc FSW joint showing the typical microstructural zones in FSW [33].

- Base material (BM): Includes material far enough from the weld that has not suffered any deformation nor microstructural and mechanical property variation derived from the thermal cycle of the FSW process.

- Heat Affected Zone (HAZ): In this region, which is confined between the BM and the TMAZ, the material does not suffer any plastic deformation but its properties are affected by the thermal cycle of the FSW process.
- Thermo-Mechanically Affected Zone (TMAZ): The material in this region located between the HAZ and the SZ suffers plastic deformation induced by the FSW tool as well as microstructural and mechanical property variation due to the heat created in the FSW process. Grains oriented in the preferential plasticised material flow direction and presenting large strains are typical in this zone.
- Stir Zone (SZ): Also called Weld Nugget, corresponds with the material located in the zone previously occupied by the probe. The material suffers full recrystallization and newly formed small grains can be found typically in this zone.

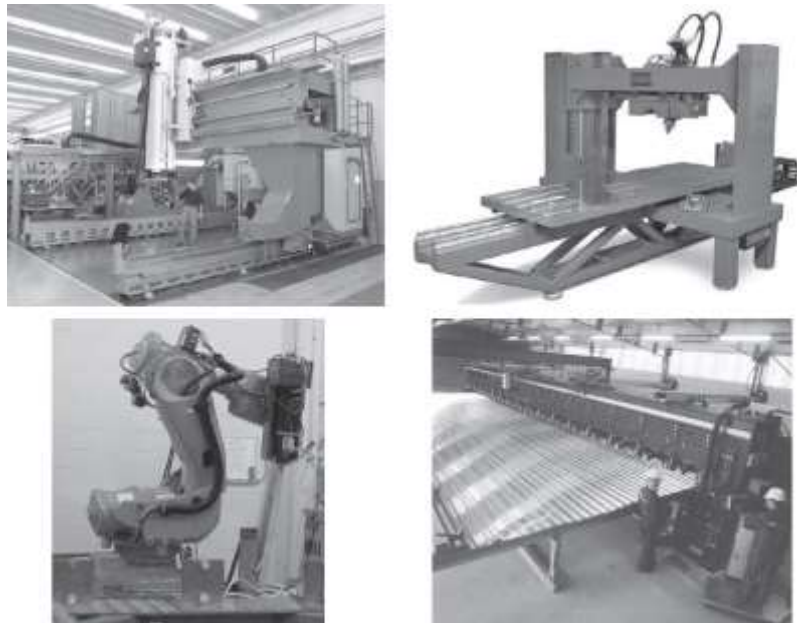


Figure 19: Different machine types for FSW: Aero system – courtesy of Eclipse Aviation Corporation (top-left); Process Development System (PDS) – courtesy of MTS Systems Corporation (top-right); RoboStir™ – courtesy of Friction Stirlink (bottom-left); Marine Aluminium FSW – courtesy of ESAB (bottom-right), [33].



Figure 20: Clamping systems for FSW: Z-stringer clamping – courtesy of MTS (left); Vacuum clamping fixture – Courtesy of Airbus-Bremen (right), [33].

Another important factor for the FSW technology is the type of machine used for the process. There are a number of different machines or equipment solutions for FSW implementation (Figure 19) that present particular technical and economic characteristics. The best option for FSW development and production is typically based on technical factors as well as the required capital investment. Each application

(material, thickness...) dictates the basic technical factors that have to be met by the FSW machine in terms of process forces, stiffness, process control and data management, heat management, rotational and welding speed, etc. The equipment solution that meets with the technical requirements and supposes the lowest capital investment is generally the most suitable choice for each FSW application. Thus, different FSW equipment solutions such as custom-built FSW machines, FSW process development systems, robotic arms or milling machines adapted for FSW have been implemented for research and production purposes during the last 2 decades of FSW development.

In addition to the FSW machine, the clamping system used to position and fix the parts in place in the working area of the machine is a critical factor in order to get a stable FSW process and high quality FSW joints. Figure 20 shows an example of a clamping system for stringer-skin FSW joints (left), as well as a vacuum clamping system as a backing solution developed for skin placement and clamping (right).



Figure 21: FSW applications for different industry sectors: FSW module for “Finnmarken” at Marine Aluminium (top-left); FSW in a Falcon 9 tank of SpaceX (top-middle); FSW side panels made by Sapa and used by Bombardier (bottom-left); FSW taylor welded blank for BMW and Land Rover (bottom-middle); Lower fuselage reinforced panel made by stringer-skin FSW at Eclipse Aviation (right), [33].

Since its invention in the 90-s, many FSW applications have been implemented in different industrial sectors such as marine-shipbuilding, railway, automotive, aerospace and aeronautic, as shown in Figure 21. The advanced manufacturing of aluminium based lightweight structures for transport vehicles is the common characteristic of all these industrial implementations. However, the employed aluminium alloys, joint configurations, in-service requirements and other characteristics are application specific and the appropriate FSW process-technology has to be developed for each case, including FSW tools, process parameters, clamping systems, etc. FSW practitioners keep all this technological knowledge carefully and critical FSW factors are not revealed generally. Therefore, it is necessary to generate the technological knowledge that brings together base materials and joint configurations, FSW process conditions and the properties of the resulting FSW joints for each case-application. This is the aim of this thesis, with the main focus on the development of FSW lap joints using innovative aluminium alloys for the advanced manufacturing of aircraft structures based on integral reinforced panels.

2.2.- FSW JOINTS FOR REINFORCED PANEL MANUFACTURING

One of the most outstanding FSW applications implemented in industry is the production of reinforced panels for aircraft structures as shown in Figure 9, Figure 10 and Figure 21 (right). This is achieved by performing high quality stringer-skin FSW lap joints, which are able to comply with the stringent requirements demanded by the aeronautic sector. This means that the FSW joints and structures at least must show a sufficiently high mechanical strength (static and fatigue), corrosion resistance and durability, among other requirements. Therefore, it is critical to understand the joint formation mechanisms in FSW lap joints in order to define the FSW process conditions that could produce the high-quality joints required for the aeronautic structures.

Lap joints present particular characteristics for FSW implementation in comparison with the more typically used butt joints as the joint interface is horizontally oriented while this interface is vertical in butt joints. This has important implications in the joint formation mechanisms resulting in specific imperfections or defects that are associated to FSW in the lap joint configuration as reported by Arbegast et.al. [48]. The main characteristics found in FSW lap joints are:

- Hook imperfection, which is covered in the ISO25239 standard [41], and the associated sheet thinning defect (see Figure 22 and Figure 23). The direct consequence of the hook and the sheet thinning defect is the reduction of the Effective Sheet Thickness (EST) of the welded parts. This generally reduces the joint strength.
- Col lap defect as shown in Figure 23. The origin of this defect is the non-effective Al_2O_3 surface layer disruption and oxide dispersion in the SZ of the FSW joint. A larger cold lap defect reduces the Bonded Interface Width (BIW) reducing the joint strength.

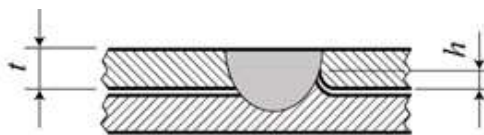


Figure 22: Representation of the hook imperfection in ISO25239-5 [41].

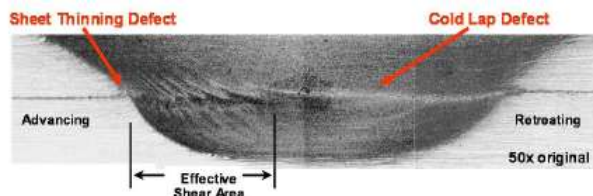


Figure 23: Principal FSW lap joint features [48].

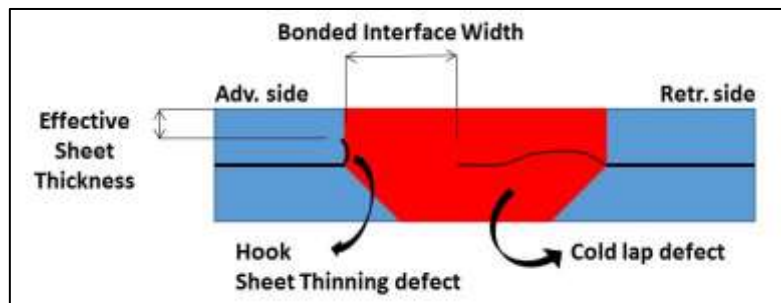


Figure 24: Schematic representation of typical FSW lap joint characteristics.

Figure 24 shows the main defects and characteristics typically observed in Friction Stir Lap Welding (FSLW). Hook imperfections can occur in the advancing and the retreating side, although the severity in the advancing side is generally higher. The hooks cause

sheet thinning defects reducing the EST and the strength of the joints. In addition to that, cold lap defects are also typical in FSLW reducing the BIW and the strength of the joints. Therefore, it is very important to avoid or minimize the hook and cold lap defects, i.e. large EST and BIW) in order to produce FSW joints with high strength.

A number of researchers have reported developments and investigations carried out in FSLW [46] [49] [50] [51] [52] [53] [54] [55]. The main goal of these works was to optimize FSW process conditions in order to improve weld quality and optimize the joint strength. Thomas et.al. introduced especial features in FSW tools such as non-concentric probes, flutes and other features in order to induce a favorable material flow and increase the joint interface [46]. With the same purpose, Cederqvist et.al. used a double pass strategy combining advancing-retreating side positions in order to minimize hook and cold lap defect formation in FSLW with 2024 and 7075 alloys [49]. Advancing or retreating side loading cases in FSLW of 2198-T4 alloy were also investigated by Buffa et.al. [50], concluding the advancing side loading case presented better joint strength as shown in Figure 25. This was associated to the better metallurgical bonding at the advancing side and the presence of a cold lap defect at the retreating side using cylindrical, conical and cylindrical-conical FSW tool designs. Costa et.al. also used cylindrical and conical probe designs for FSLW of 5XXX and 6XXX series alloys in similar and dissimilar combinations [52] [53]. They concluded that unthreaded conical probes presented the better joint strength. Ji et.al. investigated FSLW of Alclad 2024-T4 alloy using different probe designs and probe lengths [54] [55]. Especial thread features provided better shear strength results generally and the conical partially threaded probe tip design gave the best results. In the study performed with conical-threaded probes of different lengths, they concluded that a probe tip penetration of approximately 0,2 mm showed best joint strength. Too short penetrations provided insufficient material mixing and too large penetrations resulted in important hook formation due to the material flow pattern induced by the tool (Figure 26).

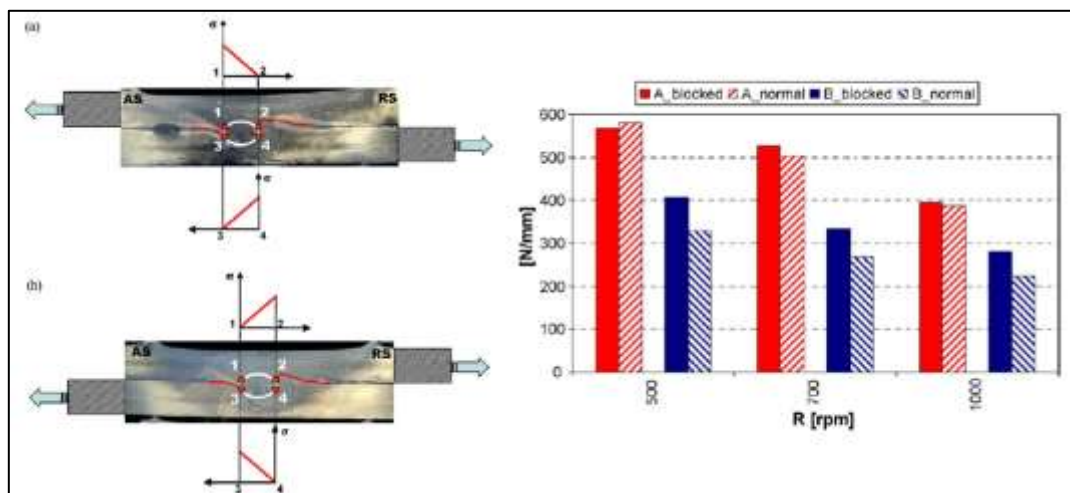


Figure 25: Advancing loading (a) and retreating loading (b) cases and the shear strength comparison in FSLW AA2198-T4 aluminium alloys [50].

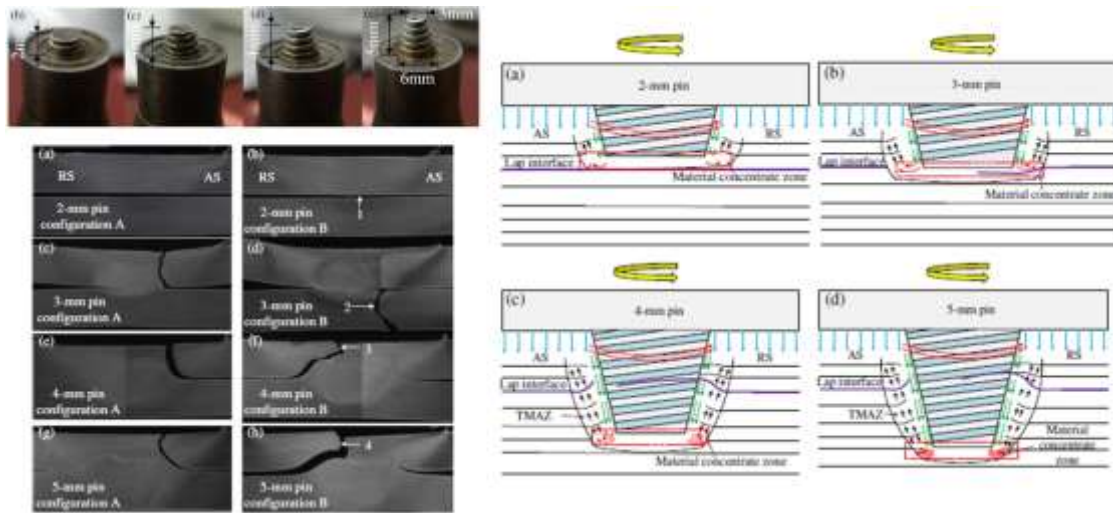


Figure 26: Tool designs, metallographic properties and proposed material flow model for FSLW of Alclad 2024-T4 alloy [55].

All the above-mentioned works were based on FSLW using aluminium sheet materials to produce sheet-sheet type joints. However, other researchers have investigated extrusion-sheet material combinations [51] [56], which are more representative for stringer-skin joints.

Dubourg et.al. found that hook formation was reduced by low rotational speeds (ω) and high welding speeds (v_w), i.e. by large weld-pitch values, using conventional cylindrical threaded tools not optimized for FSLW (Figure 27). The weld-pitch, also called feed ratio, was defined as the relation of ω and v_w and indicates the distance travelled by the FSW tool for each revolution, which is indicative of the heat input applied on the weld. They also concluded that double-pass strategies overlapping the advancing sides as well as using counter-clockwise rotations for modifying the material flow were effective strategies to limit joint imperfections and increase joint strength as shown in Figure 28. Even the fatigue resistance of FSLW joints performed under optimum conditions exceeded the fatigue resistance of conventional riveted joints. From these results, it can be concluded that FSW tool designs and material flows that are appropriate for butt joints, are not directly usable for lap joints. Hence, it is necessary to adapt the material flow in order to limit joint imperfections and optimize the joint strength in FSLW.

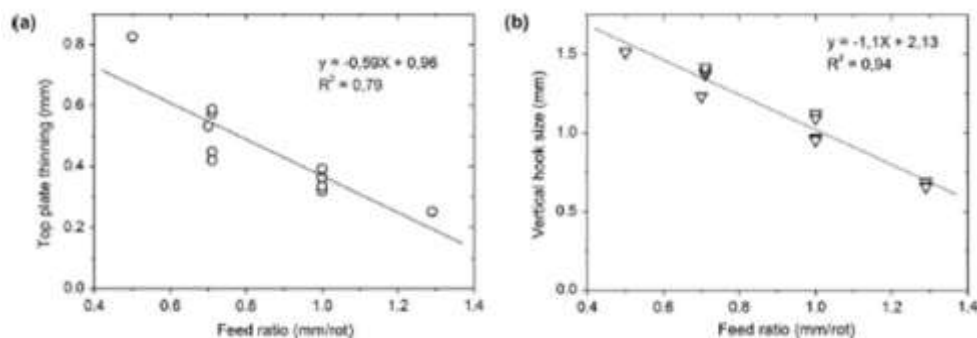


Figure 27: Hook and sheet thinning defects as functions of the weld-pitch [51].

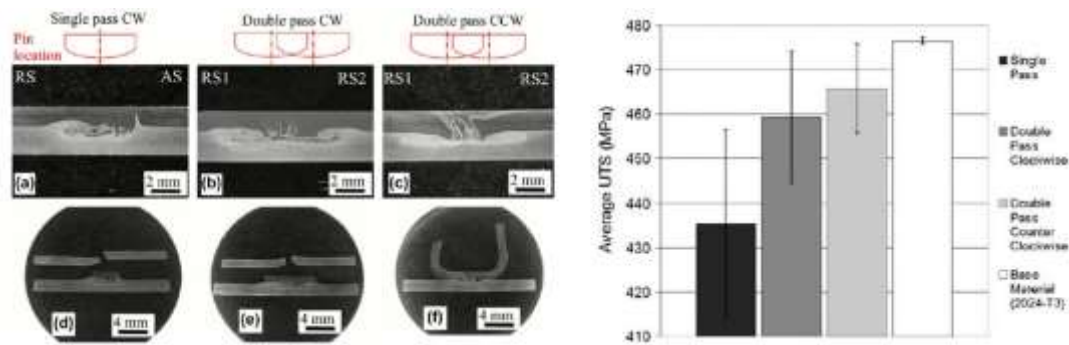


Figure 28: Effects of double-pass and tool rotation in the joint strength [51].

Huang et.al. also investigated stringer-skin type FSW joints using innovative Al-Li based materials such as AA2099—T83 extrusions and AA2060-T8 sheets [56]. They used a taper-screwed tool-probe not optimized for FSLW and consequently they reported difficulties to avoid defects such as hook, cold lap and cavities as shown in Figure 29. However, the effect of FSW parameters, i.e. ω and v_w , on the defect size was found to be consistent with the results presented by Dubourg et.al. [51].

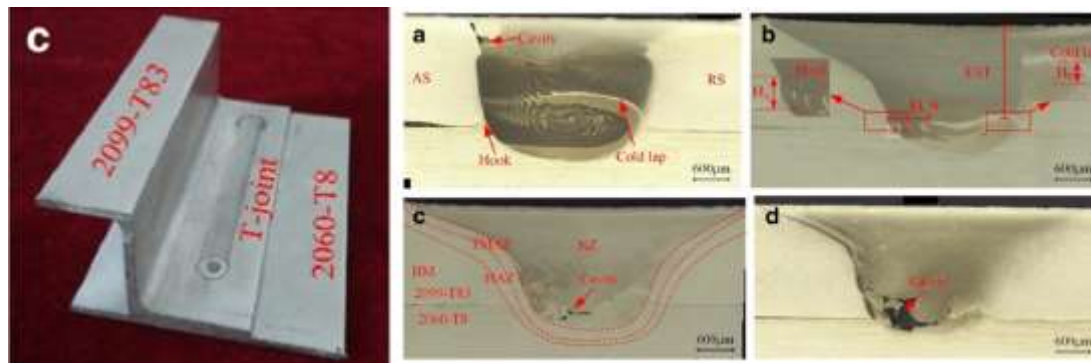


Figure 29: Stringer-skin joint configuration (left) and joint macrostructures showing defects [56].

From all the investigations and results analyzed, it is clear that tool design and welding parameters play a critical role in material flow and joint properties in FSLW. Appropriate tool designs for lap joints have to be developed and welding parameters identified in order to avoid or minimize defects and maximize joint strength. This was also the main outcome from discussions held with Gil Sylva [57], who suggested the use of flats and mixed thread orientations in probe designs in order to produce improved lap joint properties. This probe design would avoid a preferential vertical material flow limiting the hook formation, while providing good oxide layer disruption at the interface with good material mixing between the top and bottom parts. Therefore, one of the challenges of the proposed work is to develop appropriate FSW tools for FSLW and investigate the properties of the joints produced by them.

CHALLENGE 1: Develop FSW tool designs appropriate for lap joints and evaluate FSLW joint properties.

In order to improve the durability and corrosion resistance, aeronautic structures of aluminium are typically subjected to several surface treatments as shown in Figure 30. Anodizing processes such as Chromic Acid Anodizing (CAA) have been widely applied although currently other anodizing technics such as Thin Film Sulfuric Anodizing (TFSA) or even Sol-Gel procedures are under development. The main goal of these new surface

treatments is the elimination of Cr and develop more environmental friendly processes. The main purpose of the anodizing processes is to generate a porous oxide layer at the surface to improve the attachment and adhesion of the primers and top-coats. Furthermore, stringer-skin lap joints are unfavorable locations where corrosion mechanisms can easily occur due to the crevices formed between stringers and skins. In order to prevent these corrosion issues at the crevices, polymeric sealants are typically applied at stringer-skin interfaces.

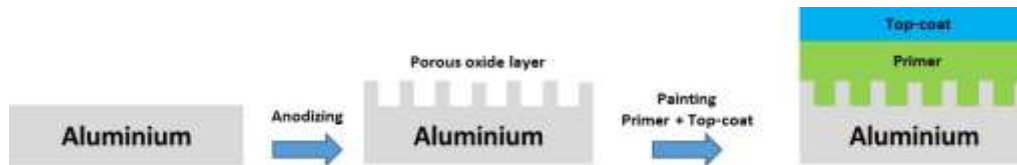


Figure 30: Schematic of typical surface treatments applied in aluminium parts to protect against corrosion in aeronautical structures.

In order to produce stringer-skin FSLW joints that comply with the stringent requirements demanded for the aeronautical structures, corrosion protection of the joints has to be considered. Thus, it is necessary to combine strategies such as anodizing, sol-gel and sealant application on aluminium components and lap joint interfaces with the FSLW process. The effects of several surface treatments on the properties of Refill Friction Stir Welded (RFSSW) joints were investigated by Fukada et.al. [58]. They observed that joint strength was reduced to some extent in comparison with joints performed with untreated aluminium, as shown in Figure 31. The reduction in strength was highly dependent on the surface treatment applied.

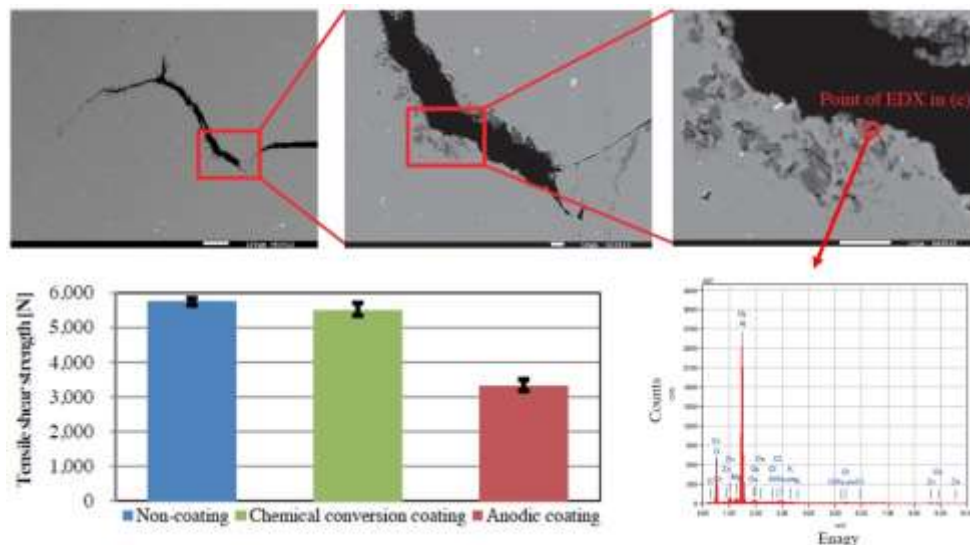


Figure 31: Reduction in joint strength depending on the applied surface treatments and aluminium oxide entrapments in the crack opening region [58].

Gibson et.al. investigated the effects of sealant application in the overlapped interface of 2198-T8 Al-Li alloy sheets and subsequent FSLW process application [59]. Although some inconsistencies in fracture modes were observed, they concluded that the reduction in joint strength referred to the sealant application was minor (Figure 32), claiming for the suitability of applying FSLW combined with sealant application. Doering et.al. also investigated the FSLW joint mechanical properties incorporating sealants in the interfaces of joints [60]. They concluded that the effects in tensile strength and fatigue properties were negligible if the selection of the applied sealant was correct.

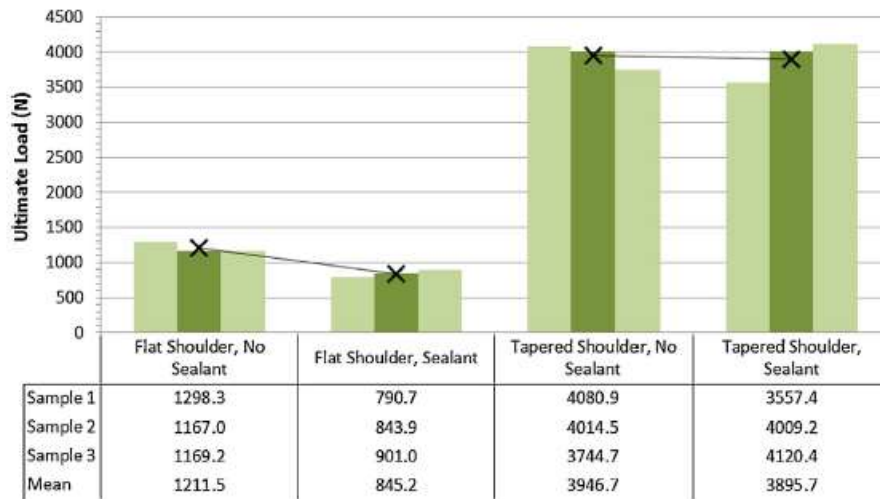


Figure 32: Effect of sealant application on FSLW joint strength [59].

Brown et.al. investigated the effects of sealants and several surface treatments on the properties of joint performed by Swept FSSW [61]. They concluded that sealants could be successfully applied in combination with the Swept FSSW process. The sealants produced a small reduction in the joint strength of each individual spot weld under static and fatigue loads, as shown in Figure 33. The effects of the surface treatments were found to be more important resulting in more severe joint strength reductions.

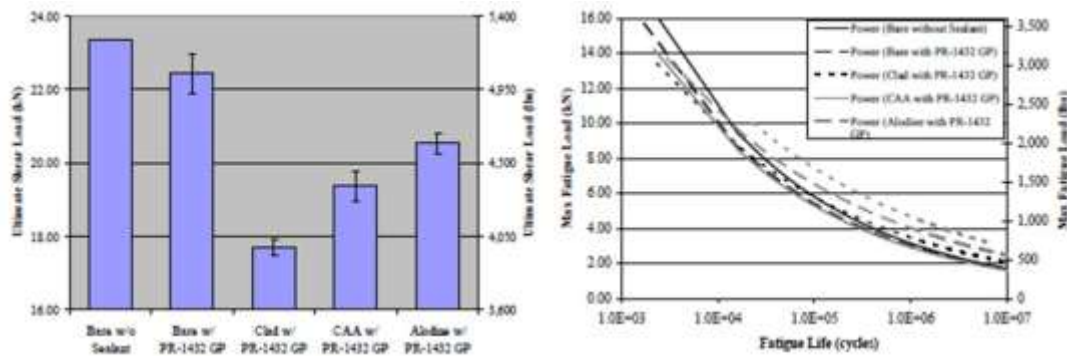


Figure 33: Static and fatigue strength results of Swept FSSW joints with sealants and several surface treatments [61].

From the discussion of these results, it can be concluded that the application of sealants and surface treatments can be successfully combined with the FSLW process with the main goal of increasing the corrosion resistance of the lap joints and the overall aluminium reinforced structures. However, it is critical to understand the effects of sealants and surface treatments on the resulting FSLW joint properties. Therefore, the study of FSLW combined with sealants and surface treatment application (focusing on Cr-free innovative treatments such as TFSA or sol-gel coatings) will be another challenge of this work.

CHALLENGE 2: Investigate the effects of sealant and surface treatments combined with the FSLW process and properties of the resulting joints.

One of the disadvantages of the lap joint configuration is the presence of the crevices that can be critical zones acting as corrosion initiation points. In addition to that, particular

joint imperfections of FSLW joints are difficult to avoid completely. Thus, other joint configurations such as T-joints [62] [63] [5] [64] and corner joints [65] have been proposed with the potential for application in stringer-skin joining for reinforced panel manufacturing of aeronautic structures.

Biallas et.al. investigated the feasibility of T-joints produced by FSW for stringer-skin type joints using 2024 and 2098 aluminium alloys [63]. They showed the feasibility of the process to produce such joints successfully even producing a 2mm radius in the fillet region of the welds as shown in Figure 34. Specific FSW tool designs and welding parameters had to be developed to optimize the weld quality for each alloy combination, which were substantially different from T-joints performed in 6XXX alloy skins [62]. In any case, an inherent notch effect was observed in the fillet region for T-joints produced with this joint configuration (Figure 34 – left).

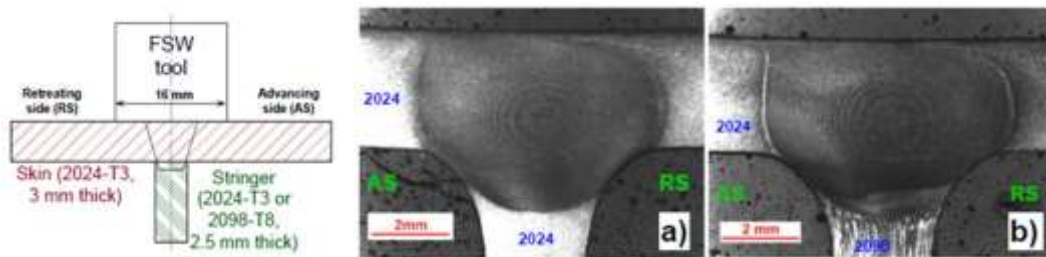


Figure 34: Schematic of T-joints by FSW (left) and macrographs of the T-joints produced with 2024 and 2098 alloys [63].

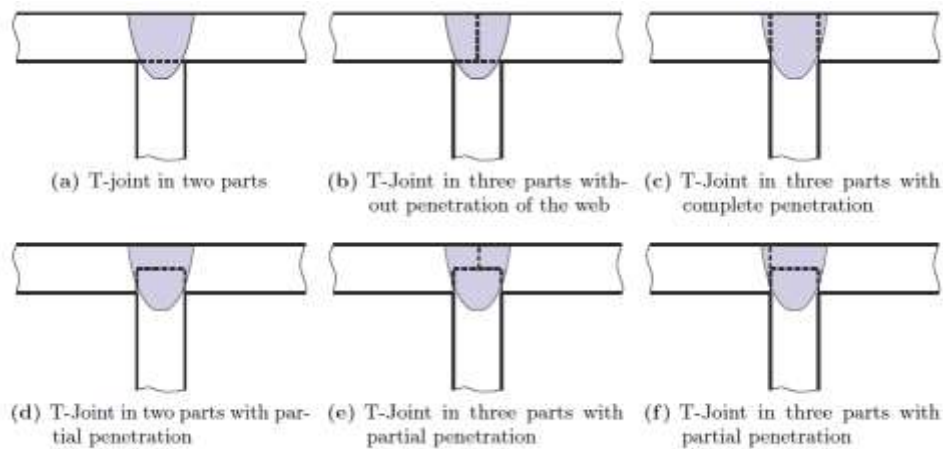


Figure 35: Joint design solutions for T-joints produced by FSW [5] [64].

Tavares et.al. also investigated T-joints by FSW using AA7075-T6 aluminium alloy sheets [5]. They proposed different types of joint configurations for T-joint production as shown in Figure 35. They concluded that using the case (c) joint configuration it was possible to avoid the notch effects at the corner region and produce defect free welds. However, FSW tool design, welding parameters and a careful FSW process control had to be developed in order to avoid defects at the corner region produced by a lack of penetration.

Another FSW process alternative for T-joint production was presented by Martin et.al [65]. This alternative was the Corner Stationary Shoulder FSW (SSFSW) technique that consisted of a rotating probe located in a non-rotating shoulder shaped to the internal corner of the plates to be welded, as shown in Figure 36 – left. They concluded that it

was possible to achieve an excellent weld quality and components with low distortion in T-joints produced using a combination of 8 mm thick AA7075-T6 and AA2014-T6 aluminium alloys. However, the feasibility of the process for thinner aluminium materials was not demonstrated and it is a major challenge.

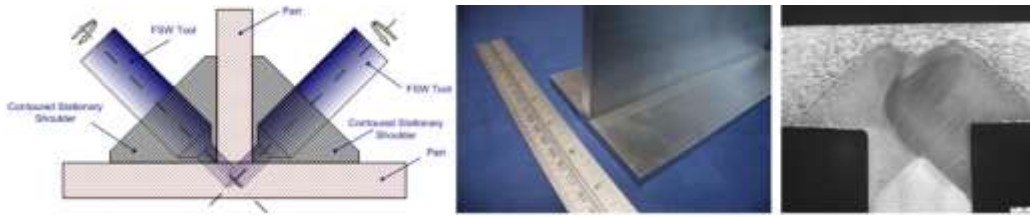


Figure 36: T-joints produced by the Corner SSFSW technique [65].

Parts manufactured by introducing T-joints or corner joints present obvious advantages over lap joints in terms of corrosion resistance. The absence of the crevices reduces the risks of corrosion initiation regions considerably, facilitates the application of anodizing or similar surface treatment processes and eliminates the need of any sealant application. However, the FSW process implementation is more complex in T-joints and corner joints than in lap joints. It is not clear which joint configuration is the best option for reinforced panel manufacturing by FSW implementation and all considered options have to be investigated in order to evaluate each case. Therefore, this work will investigate the feasibility of T-joints or corner joints produced by FSW in addition to the previously discussed lap joints.

2.3.- NEW ALUMINIUM-LITHIUM ALLOYS FOR INNOVATIVE AIRCRAFT STRUCTURES

Aluminium alloys have been the dominant materials for the manufacturing of structural parts of aircrafts for more than 80 years. Although composite materials have been introduced in large commercial aircraft structures in the last decade, aluminium alloys remain important in airframe construction. Important advances have been achieved in aluminium alloy development so they can compete with composite materials. The low manufacturing and maintenance costs are the main advantages of aluminium alloys over composite materials and the latest developments in aluminium alloys have focused on weight reduction as well as mechanical and corrosion property improvements. Thus, one of the most important advances in modern aluminium alloys has been the development of new aluminium-lithium (Al-Li) alloy families [10] [66] [67].

Al-Li alloys are attractive for aerospace applications due to their reduced density and higher modulus than conventional aluminium alloys used in aerospace. Each weight percent of lithium lowers the density of aluminium by approximately 3% and increases the modulus by approximately 6% [10] [68]. Early developments resulted in the First-Generation and Second-Generation Al-Li alloys, which contained relatively large Li, Cu and other alloying element quantities, as shown in Table 2. This led to a complex precipitate structure during ageing of Al-Cu-Li-X alloy families that resulted in undesirable mechanical performance of the First-Generation and Second-Generation Al-Li alloys and their usage in airframe structures was consequently limited. The major problems associated to Second-Generation Al-Li alloys were high anisotropy of mechanical properties that was related to sharp crystallographic textures, low short transverse properties, crack deviations and delamination problems during manufacture of parts. Low ductility and fracture toughness produced by strain localization issues was one of

the problems that had to be addressed for the development of Third-Generation Al-Li alloys.

Table 2: Compositions of selected Second-Generation Aluminium-Lithium Alloys (wt%) [10].

Alloy	Li	Cu	Mg	Si	Fe	Zr	Specific Gravity
2090	1.9-2.6	2.4-3.0	0.25	0.10	0.12	0.08-0.15	2.60
2091	1.7-2.3	1.8-2.5	1.1-1.9	0.20	0.30	0.04-0.10	2.58
8090	2.1-2.7	1.0-1.6	0.6-1.3	0.20	0.30	0.04-0.16	2.53
8091	2.4-2.8	1.8-2.2	0.5-1.2	0.30	0.5	0.08-0.16	2.54
8092	2.1-2.7	0.5-0.8	0.9-1.4	0.10	0.15	0.08-0.15	2.53
8192	2.3-2.9	0.4-0.7	0.9-1.4	0.10	0.15	0.08-0.15	2.51

Table 3: Chemical Composition of some Third-Generation Al-Li alloys (wt%) [10].

Alloy	Li	Cu	Mg	Ag	Zr	Mn	Zn
2060	0.75	3.95	0.85	0.25	0.11	0.3	0.4
2099	1.8	2.7	0.3	-	0.09	0.3	0.7
2198	1.0	3.2	0.5	0.4	0.11	0.5 max	0.35 max
2196	1.75	2.9	0.5	0.4	0.11	0.35 max	0.35 max

The large content of Li (~2%) and low content of Cu of the Second-Generation Al-Li alloys was very interesting as the resulting density was in the range 2.51-2.60 g/cm³, approximately 8-10% less than conventional 2XXX and 7XXX alloys. Unfortunately, lithium contents above 2% resulted in technical problems such as anisotropy, low toughness, poor corrosion resistance and manufacturing issues (hole cracking and delamination during drilling). In Third-Generation Al-Li alloys Li concentrations were reduced to 0.75-1.8% (Table 3) resulting in densities in the range of 2.63-2.72 g/cm³, approximately 2-8% less than conventional alloys. Although density reductions are more limited than in Second-Generation Al-Li alloys, the problems shown by these were overcome by the Third-Generation Al-Li alloys. The higher Cu/Li ratio and the reduced Li content (Figure 37) led to a more controlled precipitate and phase distribution in the microstructure, which results in improved mechanical and corrosion resistance properties. Thus, the Third-Generation Al-Li alloys represent a well-balanced, lightweight and high-performance aluminium alloy family, which has found a wider application in airframe structures. A clear proof of the success in the development of Third-Generation Al-Li alloys is the launch by the aluminium producers of alloy families specific for the aerospace market such as the Airware ® family by Constellium [67].

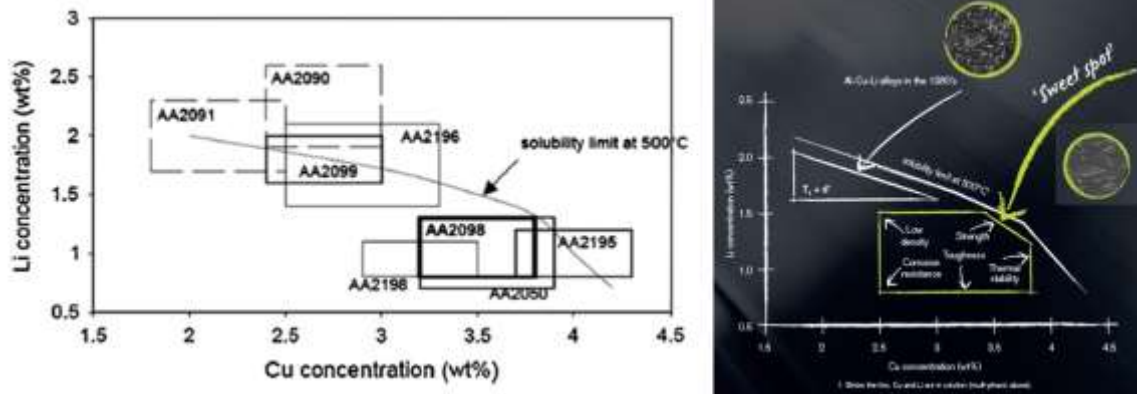


Figure 37: Li and Cu concentrations in some Third-Generation Al-Li alloys (left) [66], (right) [67].

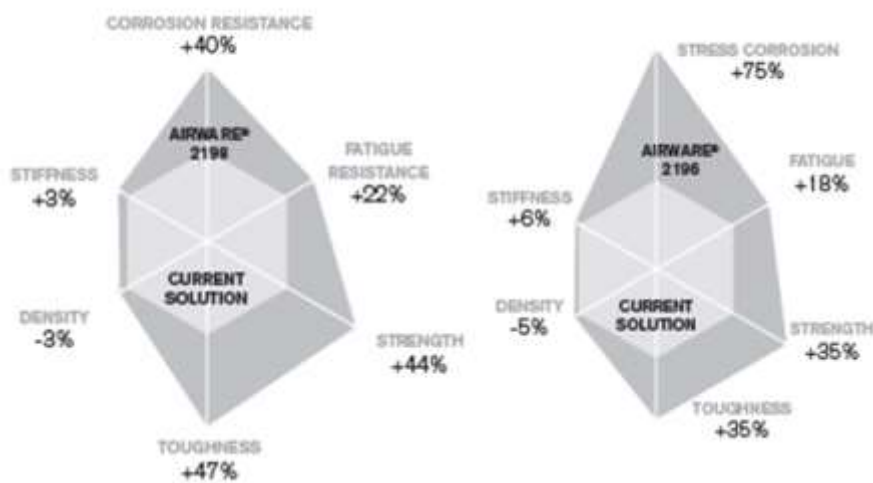


Figure 38: Material property improvements for AA2198-T8 sheet (left) and AA2196-T8511 extrusions (right) over current solution AA2024-T3511 for fuselage and wing applications [67].

Figure 38 shows the improvements in the properties of the AA2198-T8 Al-Li developed for fuselage or wing skin sheets as well as the AA2196-T8511 extrusions developed for fuselage or wing stringers by Constellium. Similar materials have been developed also by Alcoa-Arconic such as the AA2060-T8E30 skin sheet and the AA2099-T83 stringer extrusions. These materials represent new opportunities for reinforced panel manufacturing in the aeronautic sector, along with innovative joining technologies such as LBW and FSW, which have been identified as promising alternative joining technologies to riveting for Al-Li alloys [10] [66]. Therefore, this work will focus on achieving the successful implementation of the FSLW process in stringer-kin joints with the selected alloys as shown in Table 3.

CHALLENGE 3: FSLW process developments for AA2060, AA2198, AA2099, AA2196 aluminium alloy sheets and extrusions.

3.- OBJECTIVES, HYPOTHESIS AND METHODOLOGY

3.1.- OBJECTIVES

The main objective of the work carried out in this thesis was to investigate the potential of FSW technology to be implemented in the manufacturing of integral reinforced panels for aircraft structures made of Third-Generation Al-Li alloys, by testing the static and fatigue properties of representative FSW joints produced under relevant manufacturing conditions to ensure high corrosion resistance.

In order to accomplish this main objective, the following specific objectives were established:

1. Develop FSW tools with improved design to avoid or minimize characteristic imperfections that can be found in lap joints.
2. Perform FSW tests and create stringer-skin joints with the selected AA2060-T8E30, AA2099-T83, AA2198-T8 and AA2196-T851 Al-Li alloys.
3. Perform FSW tests and create stringer-skin joints with the above-mentioned alloys including sealant at the stringer-skin interface; and with surface treated aluminium alloys.
4. Perform an extensive FSW joint characterisation including microstructural examination, static and fatigue strength analysis.
5. Investigate the effects of FSW tool design, welding parameters, sealants and surface treatments on joint formation mechanisms, joint imperfections and the resulting joint properties.
6. Conclude on the potential of FSW technology for the manufacturing of advanced aircraft structures and define required manufacturing conditions.

3.2.- HYPOTHESIS

The following hypothesis were raised and checked by the work carried out in this thesis:

Hypothesis 1: FSW tool probes featuring mixed thread orientations and flats produce smaller hook sizes than conventional threaded probes in lap joint configurations and this is beneficial for the mechanical performance of FSW joints.

Hypothesis 2: FSLW over anodized and sol-gel treated components is possible obtaining consistent strength values. However, the mechanical performance can be reduced due to a non-effective dispersion of remnants from these surface treatments.

Hypothesis 3: FSW using sealants is possible obtaining consistent strength values. However, the mechanical performance can be lower due to the generation of defects caused by these organic compounds.

Hypothesis 4: FSW of anodized and sol-gel treated components using sealants in critical areas (crevices, matching surfaces) is an effective solution for corrosion protection of FSW aircraft structures.

Hypothesis 5: Aircraft structures manufactured by Third-Generation Al-Li alloys and FSW technology can effectively reduce their weight resulting in reductions in fuel consumption, dangerous emissions and manufacturing costs.

3.3.- METHODOLOGY

3.3.1.- Performed work

Once established the general objectives and hypothesis of the proposed research work, this chapter outlines the methodology followed and the work carried out for the completion of the thesis. The work was divided in 4 main phases with associated tasks, which are detailed next:

Phase 1. FSW tests in lap joint configuration by several tool-probe designs

The initial phase was focused on performing FSW tests in lap joint configuration using different tool-probes designed to provide desired joint characteristics after welding. The main approach was based on tool-probes featuring different thread-flat designs that were expected to improve joint properties by controlling vertical material flow. The used base materials were mainly the AA2060 or AA2198 aluminium alloys for sheet material and AA2099 or AA2196 aluminium alloys as extruded materials.

The following tasks were defined for the completion of this phase:

Task 1.1. Definition and manufacturing of FSW tool-probe designs: Different tool-probe designs were proposed and manufactured. These tool-probes were used in the subsequent FSW tests.

Task 1.2. Definition of FSW test plan: FSW test plans were defined in order to produce FSW joints under different processing conditions. These conditions included different tool-probe designs according to Task 1.1 as well as different FSW parameters such as rotational speed and welding speed.

Task 1.3. Execution of the FSW test plan: The test plans defined in the previous Task 1.2 were executed. As a result, FSW joints produced under different processing conditions and conclusions regarding the manufacturing of selected alloys by FSW were obtained. In parallel, the FSW joints were characterised as described in Task 4.1.

Phase 2. FSW tests in lap joint configuration with anodized or sol-gel treated components

In this phase, the base materials used in FSW tests (AA2060, AA2198, AA2099 and AA2196 aluminium alloys) were surface treated previously in order to improve their corrosion resistance and weld them in the conventional delivery state for aeronautic applications. The applied surface treatments were innovative Cr-free anodizing techniques (TFSA) as well as alternative sol-gel based surface treatments. Their effects on the manufacturing of the materials by FSW were investigated.

For the completion of this phase, the following tasks were carried out:

Task 2.1. Surface treatment + FSW test plan definition: A test plan for surface treatments of materials and FSW tests to be performed with them was created. The specific surface treatments that were applied, which were based on innovative anodizing and sol-gel technics, were selected. The FSW processing conditions were selected by choosing the best conditions identified in Task 1.3 and Task 4.1.

Task 2.2. Anodizing and sol-gel treatments of the aluminium components: The aluminium sheet and extrusion materials were subjected to the selected surface treatments (Cr-free anodizing and sol-gel treatments). These activities were supported by mainly two partners within the project ecoTECH, HAI and AKZONOBEL. As a result, surface treated materials were prepared for subsequent FSW tests.

Task 2.3. Execution of the FSW test plan: The test plan defined in Task 2.1 was executed with the materials prepared in Task 2.2. Thus, components manufactured by FSW using surface treated materials were produced as a result of this task. The effects of surface treatments on FSW manufacturing were investigated and surface treated + FSW components were obtained for their characterisation in Task 4.2.

Phase 3. FSW tests in lap joint configuration with sealants

The activities of this phase were conducted to the realisation of FSW tests and joints using the base materials mentioned before (AA2060, AA2198, AA2099, AA2196) and placing a sealant layer in the overlapped joint. The purpose of placing this interlayer was to improve the corrosion protection of the lap joints although it could result in damage of joint properties. Thus, the effects of the sealant application on the FSW joint properties was investigated in this phase.

For the completion of this phase, the following tasks were carried out:

Task 3.1. Selection of sealants: A survey of sealant types with potential for application in lap joints in combination with FSW processing was made and the most promising sealants were selected.

Task 3.2. Execution of FSW tests with sealant application: FSW tests were performed with the aluminium materials and placing the sealants selected in Task 3.1 in the interface between the extrusions and the sheets. Thus, components produced by FSW having a sealant in the interface were obtained for their characterisation in Task 4.3. In addition to that, the feasibility of using sealants combined with FSW processing was investigated.

Phase 4. Characterisation of FSW joints

The activities within this phase were directed to the characterisation of the FSW joints produced using extrusions and sheets of the selected aluminium alloys, which were AA2060 and AA2198 rolled sheet materials as well as AA2099 and AA2196 extrusion materials. The characterisation was carried out by several laboratory tests including metallographic examination, mechanical testing and corrosion tests.

For the completion of this phase, the following tasks were carried out:

Task 4.1. Characterisation of FSW joints performed using several tool designs:

The properties of FSW joints produced in Task 1.3 using different tool-probes and welding parameters were investigated. The characterisation included microstructural examination tests as well as mechanical strength tests (static and dynamic) in the as welded condition and after corrosion testing too. SEM characterisation of specific joint characteristics and fracture surfaces were carried out. The analysis and conclusions obtained upon the completion of this characterisation activity resulted in a selection of favourable FSW processing conditions that were used for later FSW tests. In addition to that, design values for FSW joints were obtained.

Task 4.2. Characterisation of FSW joints with anodized or sol-gel treated components:

Similar characterisation tests as in Task 4.1 were performed with FSW joints produced in Task 2.3 in order to investigate their properties. The obtained results served as point of comparison with results obtained in Task 4.1. Thus, the influence of surface treatments on FSW joint properties was investigated and design values for FSW joints made with surface treated materials were obtained.

Task 4.3. Characterisation of FSW joints with sealants:

The FSW joint properties of the components obtained in Task 3.2 was characterised. The characterisation tests were equivalent to those used in Task 4.1 and 4.2 so that a comparative analysis of joint properties was performed. As a result, the design values of FSW joints combined with sealant application were obtained.

4.- ARTICLE 1: FRICTION STIR WELDING OF LAP JOINTS: PROCESS PARAMETERS AND JOINT PROPERTIES

[69] E. Aldanondo, E. Arruti, P. Alvarez and A. Echeverria, "Friction Stir Welding of lap joints: Process parameters and joint properties," in *2nd International Conference on Technical Advances in Friction Stir Welding and Processing - FSWP2012*, Saint Etienne (France), 2012.

This was the first work carried out by us with FSW technology applied to lap joint configurations. The work was performed using the AA6082-T6 aluminium alloy and several tool designs and welding parameters were employed to produce the welds. The main objective of the work was to investigate the effects of these parameters on mechanical properties and to correlate them with microstructural features of the welds. We concluded that the properties of FSLW joints were significantly influenced by the tool design and the welding parameters.

The work was presented in the 2nd International Conference on Technical Advances in Friction Stir Welding and Processing - FSWP2012 in Saint Etienne (France) and it was published in the conference book as an extended abstract.

FSW of lap joints: process parameters and joint properties

Egoitz Aldanondo, Ekaitz Arruti, Pedro Alvarez, Alberto Echeverria

LORTEK -IK4
Barrio La Granja S/N
20240 Ordizia (Spain)

Abstract

The present study investigates the effect of several joining parameters on the microstructural and mechanical properties of FSW joints produced in overlap configuration of 6082-T6 aluminium alloy. The influence of different pin geometries and other process parameters such as rotational speed and weld speed has been studied. Mechanical performance of the joints has been evaluated by shear testing and the microstructural characteristics have been analysed by optical microscopy.

The results indicate there is a strong influence of process parameters and pin geometries on the flow of plasticised material around the rotating tool. Those flow patterns result in different joint formations that directly influence the mechanical properties of the joints. Thus, features such as hooking and sheet thinning have been identified to strongly impact the strength of the joints. Processing conditions to minimize those problems have been defined in order to produce joints with optimized properties.

Keywords

Friction stir welding, overlap configuration, hooking, sheet thinning.

1 Experimental procedure and results

1,5 mm thick 6082-T6 aluminium alloy sheets were friction stir welded in overlap configuration under different processing conditions. A modular tool concept was used allowing to set different pin lengths as well as to change pin geometries (Figure 1). Thus three different pin lengths (1,5; 2; 2,5 mm) and two

different pin geometries (threaded and flat) were used to produce the welds. Two different rotational speed (750; 1500 rpm) and weld speed (152 mm/min; 305 mm/min) values were used to produce the joints.

The welded samples were shear tested in order to assess their strength. The plot in Figure 2 shows the shear strength of the joints produced under different welding conditions. As a general trend the welds produced with the flat pin have shown higher strength values compared to the welds made with the threaded pin.

The microstructures of the produced joints were studied by optical microscopy after a metallographic preparation (Figure 3). This study has revealed the different joint features that are responsible for the mechanical performance of the joints. Hooking and sheet thinning effects have been identified as the most important features that influence joint strength. It has been shown the material flow caused by the threaded pin is responsible to promote the hooking and sheet thinning effects. On the contrary, material flow caused by the flat pin has minimized the hooking and sheet thinning features resulting in higher shear strengths of the joints.

The mechanical performance of the joints was reflected in the fracture mode of the tested samples as different fracture modes have been identified for different welding conditions.

2 Figures



Figure 1: Modular tool used for FSW.

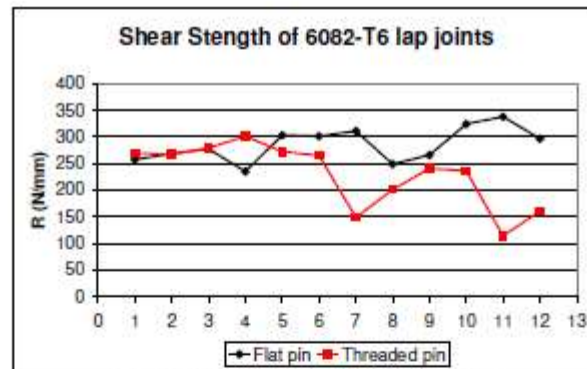


Figure 2: Shear strength of lap joints.

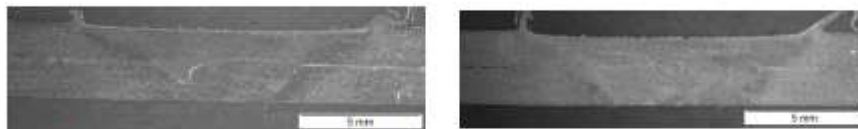


Figure 3: Cross sections of FSW lap joints produced under same welding parameters but different pin geometries (left-flat pin; right-threaded pin).

3 Conclusions

The metallurgical and mechanical properties of lap joints produced by FSW strongly depend on welding tool geometry and processing parameters. The material flow caused by the pin under certain welding conditions promote the formation of hooking and sheet thinning features resulting in poor joint properties. This investigation has revealed the formation mechanism of such features and remarks important issues in FSW of lap joints.

References

- [1] Cederquist L. et al, Factors affecting the properties of friction stir welded aluminium lap joints, *Weld J Res Suppl* 80, (2001), 281.
- [2] Kovacevic R. et al, Investigation of the friction stir lap welding of aluminium alloys AA5182 and AA6022, *J Mat Eng Perf*, 16 (4), (2007), 477.
- [3] Jung S.B. et al, Lap joint properties of FSWed dissimilar formed AA 5052 and AA 6061 Al alloys with different thickness, *J Mat Sci* 43, (2008), 3296.
- [4] Chen Z.W. et al, Effects of friction stir lap welding parameters on weld features on advancing side and fracture strength of AA6060-T5 welds, *J Mat Sci*, published online (2011).

5.- ARTICLE 2: MECHANICAL AND MICROSTRUCTURAL PROPERTIES OF FSW LAP JOINTS

[70] E. Aldanondo, E. Arruti, P. Alvarez and A. Echeverria, "Mechanical and microstructural properties of FSW lap joints," in *142nd Annual Meeting & Exhibition TMS2013 - Friction Stir Welding and Processing VII*, San Antonio (USA), 2013.

The mechanical and macrostructural properties of FSLW joints were investigated in this work. FSLW joints were produced using different welding parameters and FSW tool designs. The mechanical strength of the welds was studied using the AA6082-T6 alloy, while the dissimilar combination using AA6082-T6 and AA5754-H22 was employed to analyse the plasticised material flow and joint formation mechanisms. The selection of different aluminium alloys was particularly helpful to understand the flow of the plasticised material during FSLW. We concluded that it was possible to change the properties of the FSLW joints using specific welding parameters and especially FSW tool designs. We learnt that typical tool designs used for butt joint configurations were not appropriate for lap joint configurations.

The work was presented in the 142nd Annual Meeting & Exhibition TMS2013 - Friction Stir Welding and Processing VII in San Antonio (USA) and the article was published in the conference book.

MECHANICAL AND MICROSTRUCTURAL PROPERTIES OF FSW LAP JOINTS

Egoitz Aldanondo¹, Ekaitz Aruti¹, Pedro Alvarez¹, Alberto Echeverria¹

¹ IK4-LORTEK Centro de Investigación en Tecnologías de Unión
Arranomendia kalea 4A, Ordizia, 20240, Spain

Keywords: Aluminum, hook, un-welded interface, sheet thinning

Abstract

The properties of lap joints performed by FSW have been studied in this investigation. Similar and dissimilar combinations have been studied using AA6082-T6 and AA5754-H22 aluminum alloys. The effect of several joining variables on the mechanical and microstructural properties of the joints have been analyzed using different tool designs and welding parameters such as rotational speed and weld speed. The influence of welding parameters and probe design have been found to produce a very strong impact on effects such as hook feature formation and effective sheet thickness of the joints which greatly influence the properties of the joints. It has been concluded that using appropriate tool designs and welding conditions, the flow of the plasticized material can be driven to avoid the formation of undesired joint features and maximize the strength of the joints.

Introduction

Since it was invented [1], FSW has experienced a large research activity and many applications have been developed especially in products produced by FSW of aluminum alloys [2]. This research and development activity has been conducted primarily to butt joint configurations. However lap joint configurations are highly interesting too, as they are widely used for the manufacturing of structures in different transportation industries. The great potential of FSW to produce lap joints with aluminum alloy materials makes it a very interesting technology to replace other similar joining technologies that are applied currently for the manufacturing of components such as structural panels strengthened by stringers. Therefore it is very important to understand the basics of the joint formation in FSW lap joints in order to realize a high quality manufacturing of FSW lap joints.

There have been a number of studies conducted on FSW lap joints [3-10]. These studies have described the joint formation mechanisms, mechanical properties, as well as the importance of the tool design in the properties of the joints. According to some authors [3, 4, 5, 9], the pull-up or pull-down effects produced by the FSW tool have been identified as the main factors governing the joint formation and subsequent properties of the joints. The study of the mechanical properties of the joints [3-7] revealed that presence of defects such as hook features or un-welded interfaces are largely detrimental for the joint strength. It has been shown that conventional tool designs used for FSW of butt joints are not the best option for lap configurations and some attempts have been made in order to improve the tool design for FSW of lap joints [8-11]. The main goal is to avoid pull-up or pull-down effects on the advancing and retreating sides of the joints resulting in hook features or un-welded interfaces, while generating

sufficient welded area to allow a good transmission of the stresses from the top sheet to the bottom sheet of a lap joint.

The study reported in this document was focused on the investigation of the influence of different welding conditions on the microstructural and mechanical properties of FSW lap joints using 1,5 mm thick AA6082-T6 aluminum alloys. Different probe designs (length and geometry) were used under different welding conditions focusing on the microstructural features produced for each tool/parameter combination. Mechanical properties of the joints were analyzed by tensile shear testing paying attention to the fracture type produced in each case. From these data relationships have been established among tool design, welding parameters, microstructural features, mechanical properties and fracture types of the FSW lap joints.

Experimental Procedure

Materials

FSW lap joints were performed at IK4-LORTEK Research Centre (Ordizia, Spain) using similar and dissimilar aluminum alloy combinations. 1,5 mm thick AA6082-T6 aluminum alloy sheets were used to produce similar FSW lap joints. These joints were used to study the mechanical strength as well as the microstructural properties of the joints. In addition to these, dissimilar joints were produced using 1,5 mm thick AA6082-T6 and AA5754-H22 aluminum alloy sheets in order to analyze the material flow behavior and joint formation mechanisms. For this material combination AA6082-T6 alloy was placed on top of the overlap configuration. In all tests, both top and bottom sheets were 180 mm long and 100 mm wide while the overlap distance was 40 mm.

Welding Procedure

FSW experiments were conducted in a MTS ISTIR-PDS FSW machine in position control. A constant penetration depth, which was set to be the same as the pin length used in each case, was used for all welding tests. FSW lap joints were produced under different welding conditions as listed in Table I. Two different welding conditions were studied from a welding heat input viewpoint, considering that high rotational speed (RS) and low welding speed (WS) combinations correspond to high welding heat input in comparison with low RS and high WS. Therefore, high heat input joints were performed using a RS of 1500 rpm and a WS of 150 mm/min. On the other hand low heat input joints were produced at values of RS and WS of 750 rpm and 300 mm/min respectively. These two different welding conditions are referred to as “hot welds” (welds produced at 1500 rpm – 150 mm/min) or “cold welds” (welds produced at 750 rpm – 300 mm/min) hereafter.

An adjustable probe concept tool was used for the welding experiments, allowing the change of the probe or the adjustment of the probe length while using the same shoulder. Thus two different probe designs were used for the tests, one comprising a cylindrical threaded probe and the other one featuring a cylindrical non-threaded probe. FSW lap joints were produced by setting both probe designs to three different probe lengths with values of 1,5 mm, 2 mm and 2,5 mm. This means that at a pin length of 1,5 mm the tip of the probe travelled just in the interface of the bottom sheet while at pin lengths of 2 mm and 2,5 mm the probe penetrated the bottom sheet by 0,5 and 1 mm respectively. The tool had a shoulder diameter of 12 mm for all probe design and probe length combinations and the tilt angle was fixed at 1,5 deg.

Table I: Welding Parameters

Weld N°	Probe Design	Probe Length	Welding Parameters (RS-WS)
1	Threaded	1,5 mm	“Cold Weld” 750 rpm – 300 mm/min
2	Threaded	1,5 mm	“Hot Weld” 1500 rpm – 150 mm/min
3	Threaded	2 mm	“Cold Weld” 750 rpm – 300 mm/min
4	Threaded	2 mm	“Hot Weld” 1500 rpm – 150 mm/min
5	Threaded	2,5 mm	“Cold Weld” 750 rpm – 300 mm/min
6	Threaded	2,5 mm	“Hot Weld” 1500 rpm – 150 mm/min
7	Non-threaded	1,5 mm	“Cold Weld” 750 rpm – 300 mm/min
8	Non-threaded	1,5 mm	“Hot Weld” 1500 rpm – 150 mm/min
9	Non-threaded	2 mm	“Cold Weld” 750 rpm – 300 mm/min
10	Non-threaded	2 mm	“Hot Weld” 1500 rpm – 150 mm/min
11	Non-threaded	2,5 mm	“Cold Weld” 750 rpm – 300 mm/min
12	Non-threaded	2,5 mm	“Hot Weld” 1500 rpm – 150 mm/min

Mechanical Testing and Macro/Microstructural Characterization

Tensile shear tests were performed for evaluating the mechanical strength of the FSW lap joints. 25 mm wide test specimens were machined perpendicular to the welding direction and tested using a tensile testing machine Zwick Roell Z100 (100 kN load capacity). Three specimens were tested for each welding condition. Shims of the same material and thickness as the test specimens were used when clamping the samples in order to induce pure shear and avoid initial realignments. Fracture strength (R) defined as the maximum failure load divided by the width of the specimens (N/mm) has been used as the term for evaluating the strength of the FSW lap joints. In addition to this, fracture type of each condition has been studied too. Loading condition in lap joints can be different as either the advancing side or the retreating side of the joint can be loaded on the top sheet. In this study the condition of loading on the advancing side on the top sheet was used for all welded specimens.

For microstructural characterization, the specimens were carefully prepared following standard metallographic procedures comprising cross-sectioning, mounting and polishing. Similar FSW lap joint specimens produced with AA6082-T6 alloy were etched using a reagent based on a NaOH solution while Kroll's reagent was used for dissimilar AA6082-T6/AA5754-H22 FSW lap joint specimens. An Olympus GX51 light optical microscope was used to investigate the microstructural properties and the defect formation of the FSW lap joints.

Results and Discussion

Mechanical testing

The R of FSW lap joints produced with a threaded probe tool is shown in Figure 1. It is shown that for a probe length of 1,5 mm, where the probe does not penetrate the bottom sheet, “cold welds” and “hot welds” present similar R values of approximately ≈ 278 N/mm. However a very different R value can be observed for “cold welds” and “hot welds” when there is penetration of the probe in the bottom sheet (probe lengths of 2 and 2,5 mm). In this situation “cold welds” show a higher R compared to “hot welds”, which present a very pronounced decrease in the R values. Generally, the use of a larger probe length reduces the R value of the FSW lap joints, but this effect is much more prominent in “hot welds” than in “cold welds”.

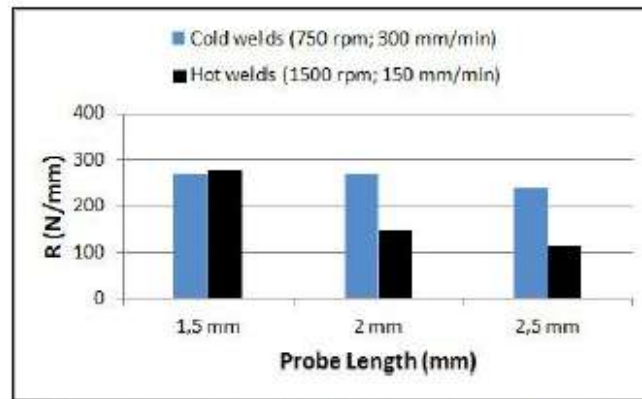


Figure 1: Fracture strength (R) of FSW lap joints performed using a threaded probe tool.

In Figure 2, the R values of the FSW lap joints performed by using a non-threaded probe tool are plotted. Similar R values have been observed for “cold welds” and “hot welds” corresponding to equal probe lengths although “hot welds” present slightly higher R values. Regarding the effects produced by the probe length, it can be clearly seen that the use of larger probe lengths produces an increment of the R values for both “cold welds” and “hot welds”. Therefore the use of a probe that penetrates the bottom sheet produces FSW lap joints that present higher R values, for the non-threaded probe tool case.

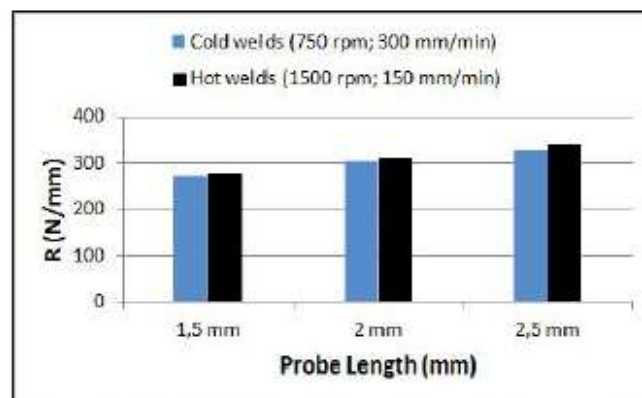


Figure 2: Fracture strength (R) of FSW lap joints performed using a non-threaded probe tool.

From comparison of data that are shown in Figure 1 and Figure 2, it is clear that the use of different tool designs produce radically different results in the mechanical properties of FSW lap joints. Large probes that penetrate the bottom sheet operated at “hot weld” conditions produce higher R values when using a non-threaded probe tool, while the exactly opposite effect is achieved when using a threaded tool at those same conditions. Thus maximum R values of ≈ 338 N/mm have been achieved with the non-threaded 2,5 mm long probe tool operated at “hot weld” conditions, while minimum R values of ≈ 114 N/mm have been observed for the threaded probe at the same welding conditions.

Fracture types

The fracture type of all tested FSW lap joints has been studied. Three different fracture types have been observed as shown in Figure 3. Figure 3-A shows a type 1 fracture, which is a shear fracture through the interface between the top and the bottom sheet. This is the most common fracture type that has been observed as all samples welded at “cold weld” conditions have shown this fracture type. Figure 3-B shows a type 2 fracture, which has been observed in FSW lap joints produced by the threaded probe operated at “hot weld” conditions and penetrating the bottom sheet significantly. Type 2 fractures are characterized by a fracture initiation on a hook feature that is present in the advancing side of the joint as it will be explained in detail later. FSW lap joints showing this type of fracture have presented low R values. Figure 3-C shows a type 3 fracture, which is a tensile fracture through the HAZ of the advancing side. Type 3 fractures occur outside the joint due to the softening of the HAZ in the advancing side, which is the loaded side of the FSW lap joints on the top sheet. Type 3 fracture has been observed for the weld N° 12 only, which was produced by a non-threaded 2,5 mm long probe tool operated at “hot weld” conditions, and has presented the highest R value of ≈ 338 N/mm.

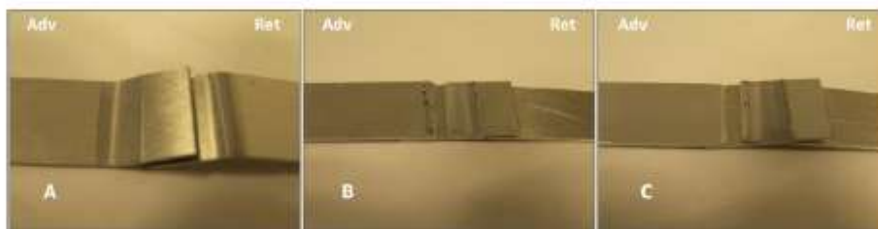


Figure 3: Fracture types in tensile shear strength specimens. (A) Type 1, shear fracture through the interface. (B) Type 2, tensile fracture through the hook feature. (C) Type 3, tensile fracture through HAZ.

Macro/Microstructural Characterization

Some representative cross sectional views of FSW lap joints produced under different welding conditions are shown in Figure 4. In FSW lap joints performed with a probe length that equals the top sheet thickness (Figure 4-A and Figure 4-B) a continuous un-welded interface remains where the original faying surfaces were located. This interface is formed as a result of a non-efficient elimination of the oxides present in the faying surfaces before welding. The use of a threaded probe promotes a slightly higher deformation in the un-welded interface due to a higher stirring action of the tool (Figure 4-B).

FSW lap joints carried out with probe penetration in the bottom sheet and “cold weld” conditions (Figure 4-C and Figure 4-D) feature a similar un-welded interface as FSW lap joints represented

in Figure 4-A and Figure 4-B. However, a more prominent deformation and bonding effect has been observed, primarily in the interface located in the advancing side.

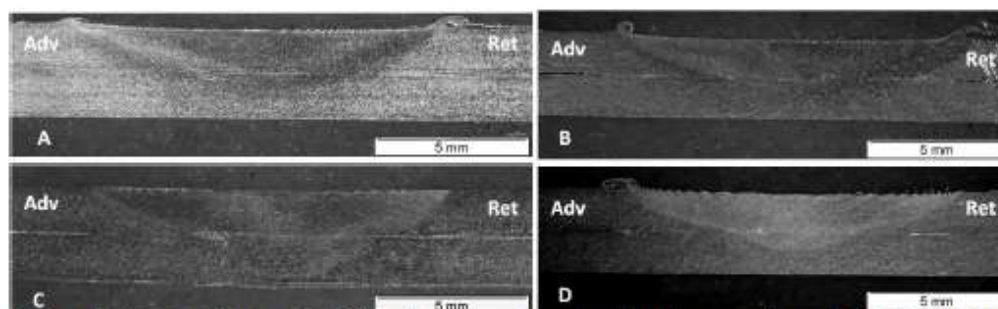


Figure 4: Cross-sections of FSW lap joints performed with (A) a non-threaded - 1,5 mm long probe tool at 1500 rpm – 150 mm/min; (B) a threaded - 1,5 mm long probe tool at 1500 rpm – 150 mm/min; (C) a non-threaded - 2 mm long probe tool at 750 rpm – 300 mm/min; and (D) a threaded - 2 mm long probe tool at 750 rpm – 300 mm/min.

Figure 5 shows a cross-section of a FSW lap joint produced at “hot weld” conditions by a threaded 2,5 mm long probe tool. It can be seen that an interface pull-up effect is produced in both advancing and retreating sides of the FSW lap joint (see details in Figure 5-A and Figure 5-C). These pull-up effects result in a hook feature formation in the advancing side and an extended un-welded interface in the retreating side. The hook feature and extended un-welded interface produce an effective sheet thickness reduction on the top sheet which is reflected into the reduced R values of FSW lap joints produced at these welding conditions.

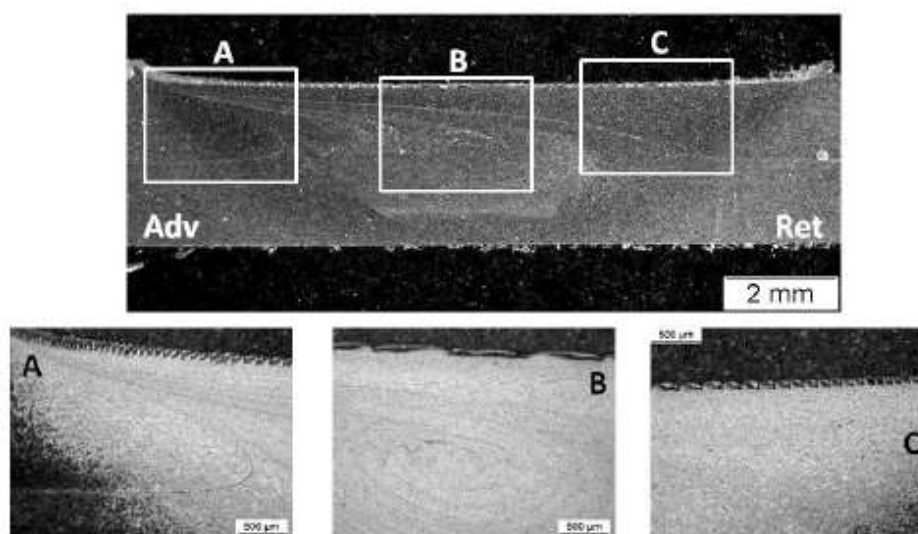


Figure 5: Cross-section of FSW lap joint performed with a threaded - 2,5 mm long probe tool at 1500 rpm - 150 mm/min.

A completely different joint microstructure has been observed in the study of the FSW lap joint cross section produced by using a non-threaded 2,5 mm long probe tool operated at “hot weld” conditions (Figure 6). Even though the only change in the welding conditions compared to the

sample represented in Figure 5 is the design of the probe (threaded/non-threaded), a very different defect formation has been observed. A pull-down effect takes place in the advancing side resulting in a hook feature formation towards the bottom sheet (Figure 6-A). This hook feature produces a reduction in the effective sheet thickness of the bottom sheet but the thickness of the top sheet remains the same in the advancing side. On the other hand, a very small pull-up effect has been observed in the retreating side having practically no influence on the effective sheet thickness of the top and bottom sheets. However an un-welded interface extension continuing the top and bottom sheet interface towards the stir zone has been observed in the retreating side (Figure 6-B). This un-welded interface crosses the stir zone and turns down towards the bottom sheet in the proximities of the hook feature observed in the advancing side (Figure 6-A).

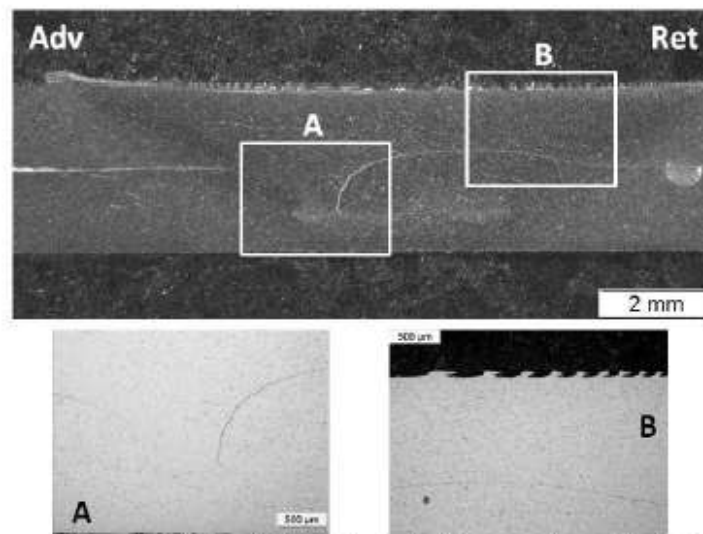


Figure 6: Cross-section of FSW lap joint performed with a non-threaded - 2,5 mm long probe tool at 1500 rpm - 150 mm/min.

Figure 5 and Figure 6 show the great influence of the probe design in the microstructural properties of FSW lap joints produced at certain welding conditions. In order to gain a better understanding of the material flow and joint formation mechanisms, cross sections of dissimilar FSW lap joints produced at “hot weld” conditions and using 2,5 mm long probes are shown in Figure 7. One can observe that there is no upward vertical flow of bottom sheet material while some of the top sheet material is driven downwards into the bottom sheet when a non-threaded probe is used (Figure 7-A). On the contrary, vertical flow of bottom sheet material towards the top sheet is promoted by the thread in case that a threaded probe is used (Figure 7-B). This vertical flow is responsible for the development of hook features in the advancing side and extended un-welded interfaces in the retreating side, resulting in a reduction of the effective sheet thickness of the top sheet.

As a summary, it can be stated that FSW lap joints produced under conditions that do not promote vertical flow of the bottom sheet material (Figure 4) show no effective sheet thickness reduction of the top sheet. FSW lap joints produced in these conditions show a reasonably high R values (270-300 N/mm) and present an interfacial type 1 fracture as they contain un-welded interfaces in the original faying surfaces. On the other hand, FSW lap joints produced under conditions that promote upward vertical flow of bottom sheet material develop defects such as

hook features in the advancing side reducing the effective sheet thickness of the top sheet (Figure 5). When these joints are loaded in the advancing side, they present a type 2 fracture at very low R values (≈ 114 N/mm). On the contrary, when conditions that promote downward vertical flow of top sheet material are used, there is no reduction of the effective sheet thickness of the top sheet and hook features as well as the un-welded interfaces are driven towards the bottom sheet (Figure 6). When these FSW lap joints are loaded in the advancing side of the top sheet, the absence of defects in the areas where the stresses are transmitted from the top to the bottom sheet produces a type 3 fracture in the HAZ at the highest recorded value of ≈ 338 N/mm.

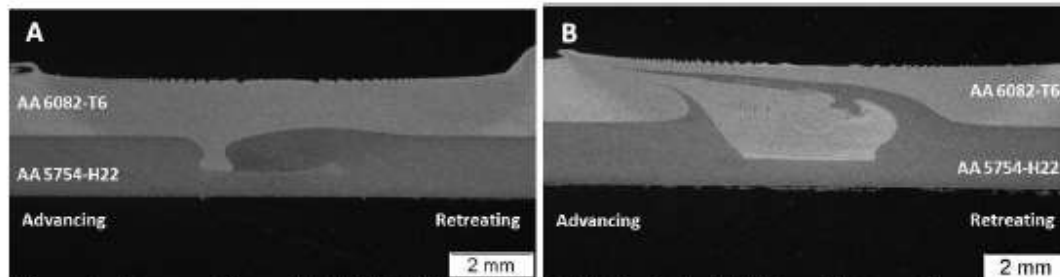


Figure 7: Cross-sections of AA6082-T6/AA5754-H22 dissimilar FSW lap joints performed with (A) a non-threaded - 2,5 mm long probe tool at 1500 rpm – 150 mm/min; and (B) a threaded - 2,5 mm long probe tool at 1500 rpm – 150 mm/min.

Conclusions

Mechanical and microstructural properties of FSW lap joints have been investigated using different probe designs and welding parameters. The following conclusions can be presented:

1. In cases where the probe length equals the top sheet thickness, i.e. it does not penetrate the bottom sheet, no significant differences have been found in R values of the joints for different probe designs and other welding conditions (“hot welds” or “cold welds”). In these cases an interfacial failure occurs due to the presence of un-welded interfaces in the original faying surfaces between the overlapping sheets.
2. In cases where the probe penetrates the bottom sheet, non-threaded probe tools have produced FSW lap joints with superior R values than those obtained with threaded probes. This effect has been more pronounced when “hot weld” conditions are employed.
3. Non-threaded probes have shown best results welding with large probe lengths and “hot weld” conditions. The absence of defects in the advancing side of the top sheet and a reduced un-welded interface have allowed an optimum stress transition between the top and the bottom sheets. Thus the highest R values of ≈ 338 N/mm have been obtained with a 2,5 mm long probe operated at 1500 rpm and 150 mm/min, presenting a fracture in the HAZ in advancing loading conditions.
4. Using these same conditions to perform FSW lap joints with a threaded probe has produced the lowest R values of ≈ 114 N/mm. The formation of a hook feature in the advancing side reduced the effective sheet thickness of the top sheet. Thus under advancing loading conditions a fracture through the hook feature occurs at a very low R value.
5. Different probe designs promote different flow of plasticized material during FSW of lap joints resulting in different defect formation. It is possible to optimize the strength of the FSW lap joints by using the appropriate probe design and welding conditions depending on the loading requirements of the joint.

References

1. W. M. Thomas et al., European Patent Specification EP 0 615 480 B1.
2. Threadgill et al., "Friction Stir Welding of Aluminium Alloys", *Int. Mat. Rev.*, Vol159 N°2 49-93 (2009).
3. L. Cederquist, A. P. Reynolds, "Factors affecting the properties of friction stir welded aluminum lap joints", *Weld J Res Suppl* 80, 281, (2001).
4. S. B. Jung et al, "Lap joint properties of FSWed dissimilar formed AA 5052 and AA 6061 Al alloys with different thickness", *J Mat Sci* 43, 3296, (2008).
5. S. Yazdaniyan, Z. W. Chen, G. Littlefair, "Effects of friction stir lap welding parameters on weld features on advancing side and fracture strength of AA6060-T5 welds", *J. Mater. Sci.*, Published online (2011).
6. M. Ericsson, L. Jin, R. Sandström, *Int. Jour. Fatigue* 29-57, (2007).
7. M. K. Kulekci, A. Sik, E. Kaluç, "Effects of tool rotation and pin diameter on fatigue properties of friction stir welded lap joints", *Int. J. Adv. Manuf. Technol.* 36: 877-882 (2008).
8. R. Kovacevic et al, "Investigation of the friction stir lap welding of aluminium alloys AA5182 and AA6022", *J Mat Eng Perf*, 16 (4), 477, (2007).
9. G. M. D. Cantin et el., "Friction Skew-stir welding of lap joints in 5083-O aluminium", *Sci. Tech. Weld. Join.*, Vol10 N°3 268-280 (2005).
10. M. J. Brooker et al., "Applying Friction Stir Welding to the Ariane 5 Main Motor Thrust Frame", *Proceedings of the Second International Symposium on FSW*, Gothenburg, (2000).
11. C. Fuller, M. Mahoney, W. Bingel, "Friction Stir Weld Tool and Method", U.S. Patent N° US2005/0121497A1.

6.- ARTICLE 3: THE ROLE OF THE TOOL DESIGN IN PROPERTIES OF FRICTION STIR WELDED LAP JOINTS

[71] E. Arruti, J. Sarasa, E. Aldanondo and A. Echeverria, "The role of the tool design in properties of friction stir welded lap joints," in *11th International Symposium on FSW*, Cambridge (UK), 2016.

In this work, we investigated the properties of FSLW joints produced using a dissimilar combination of aluminium alloys, a AA6063-T5 extrusion on top of a AA2024-T3 rolled sheet. It was the first approach to the concept of manufacturing reinforced structures using high strength aluminium alloys typically used in the aeronautic sector. A robotic FSW system was used for the first time with capabilities for the manufacturing of real aircraft structures with curved shapes and non-linear welding tracks. Similar to the previous works, it was concluded that the joint properties were largely influenced by the FSW tool design and welding parameters. The new FSW tool design proposed for the manufacturing of FSLW joints was introduced for the first time, having three flats and a mixed thread.

The work was presented in the 11th International Symposium on FSW in Cambridge (UK) and the article was published in the conference proceedings.

THE ROLE OF THE TOOL DESIGN IN PROPERTIES OF FRICTION STIR WELDED LAP JOINTS

Ekaitz Arruti, Julen Sarasa, Egoitz Aldanondo, Alberto Echeverria,
IK4 LORTEK, Ordizia (Gipuzkoa), Spain

SYNOPSIS

The Friction Stir Welding (FSW) process has shown a great potential for the manufacturing of structural parts in aluminium alloys due to the advantages offered by the technology. Most of the research works and applications developed over the past decades have focused in butt joint configuration although some other configurations such as lap joints are highly interesting too, as they are widely used for the manufacturing of structures in different transportation industries. FSW of lap joints with aluminium alloy materials has a great potential for stiffened panel construction in sectors such as aeronautic or automotive. However the technology issues are significantly different when dealing with lap joints from those related to butt joints. Therefore it is very important to understand the basics of the joint formation mechanism in order to perform high quality FSW lap joints. Thus the implications regarding the tool design, welding parameters, etc. need to be considered as shown in previous works [1, 2].

KEYWORDS

Lap joints; aluminium alloys; tool design; hooking; sheet thinning; un-welded interface.

INTRODUCTION

In this paper the influence of several joining variables on the mechanical and microstructural properties of joints performed by FSW has been analysed, using different tool designs and other process parameters such as rotational speed and weld speed. Dissimilar combinations of aluminium alloys have been friction stir welded in overlap configuration, positioning AA6063-T5 L shape stringers over AA2024-T3 sheets. Three different tool probe geometries have been used for the tests: a cylindrical threaded probe, a triflute threaded probe and a tool with three flats probe with a mixed thread (a mixture of left-handed, right-handed and neutral threads). The weld quality has been evaluated by means of microstructural analysis and mechanical testing. Metallographic sections of joints made under different welding conditions have been studied by optical microscopy. Moreover, the mechanical properties of the joints have been evaluated in terms of microhardness measurements and tensile testing, paying attention to the fracture mode of each case. The influence of welding parameters and probe design have been found to produce a very strong impact on effects such as hook feature formation (pull-up effect), un-welded interfaces and effective sheet thickness of the joints which greatly govern the joint formation and subsequent properties of the joints.

There have been a number of studies conducted on FSW lap joints [3-10]. These studies have described the joint formation mechanisms, mechanical properties, as well as the importance of the tool design in the properties of the joints. According to some authors [3, 4, 5, 9], the pull-up or pull-down effects produced by the FSW tool have been identified as the main factors governing the joint formation and subsequent properties of the joints. The study of the mechanical properties of the joints [3-7] revealed that presence of defects such as hook features or un-welded interfaces are largely detrimental for the joint strength. It has been shown that conventional tool designs used for FSW of butt joints, such as threaded pin

design, are not the best option for lap configurations and some attempts have been made in order to improve the tool design for FSW of lap joints [8-10]. The main goal was to avoid pull-up or pull-down effects on the advancing and retreating sides of the joints resulting in hook features or un-welded interfaces, while generating sufficient welded area to allow a good transmission of the stresses from the top sheet to the bottom sheet of a lap joint.

Taking into account how is loaded the FSW lap joint in terms of mechanical stresses, apart from the process parameters (rotational speed, welding speed...), it is very important to consider some design concepts to avoid or minimize defects and aspects such as where to locate the advancing/retreating sides, how much penetrate the probe in the bottom sheet (tool probe length), the effects of probe features (cylindrical/threaded/three flats, with a mixed thread...) have a vital importance. As it has been reflected in Figure 1, it is necessary to avoid pull-up or pull-down effects on the advancing and retreating sides of the joints resulting in hook features or un-welded interfaces, while generating sufficient welded area to allow a good transmission of the stresses from the top sheet to the bottom sheet of a lap joint:

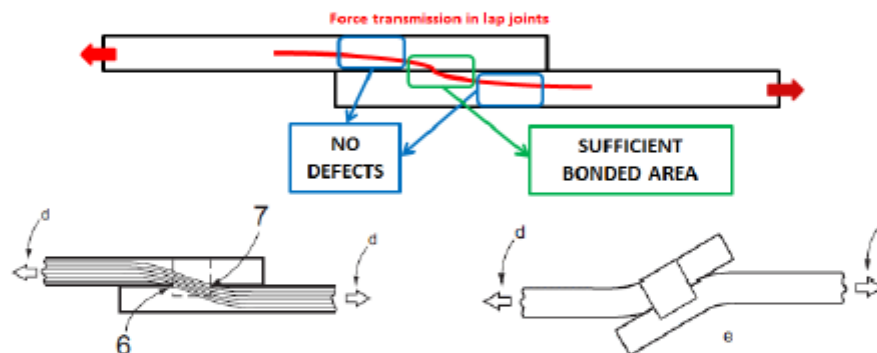


Figure 1: The importance of different FSW joint formation aspects in lap joints [11].

In this study it has been shown that using appropriate tool designs and welding conditions, the flow of the plasticized material around the rotating tool can be driven to minimize the formation of undesired joint features and maximize the strength of the joints.

EXPERIMENTAL PROCEDURE

2mm thick AA6063-T5 aluminum alloy L shape stringers were friction stir welded in overlap configuration positioned over 3mm thick AA2024-T3 sheets under different processing conditions. On the other hand, three different tool designs were used for the tests (Figure 2). Two of them with the same shoulder design (flat shoulder of 10 mm diameter), but different probe geometries: a cylindrical threaded probe (M4 probe) - tool F101; and a tool with three flats probe and a mixed thread (a mixture of left-handed, right-handed and neutral threads), ($\varnothing_{\text{probe}} = 4 \text{ mm}$) - tool F103. The third tool design consisted on a 15 mm diameter flat shoulder and a triflute threaded pin ($\varnothing_{\text{probe}} = 4 \text{ mm}$) - tool F49. The three tool probes had a 2.5 mm length, so that during welding the probe penetrated approximately 0.5 mm in the bottom sheet.



Figure 2: employed welding tools; a) F101, b) F103 and c) F049.

FSW lap joints performed with F101 and F103 tools were carried out in a MTS ISTIR-PDS 4 FSW specific machine, while the lap joints performed with the tool F049 were carried out with a KUKA robotic arm equipped with a FSW spindle; both of them available at IK4 LORTEK facilities. The specific FSW equipment allows a precise control of the main FSW process parameters, while the robotic arm allows FSW process automation and flexibility in terms of welding trajectories. The lap joints performed in the specific FSW equipment were conducted in position control, while the lap joints performed in the robotic arm were conducted in force control.

Two different welding conditions were studied for each welding tool, from a welding heat input viewpoint (see Table 1); considering that high rotational speed (RS) and low welding speed (WS) combination corresponds to a high welding heat input, while low RS and high WS combination corresponds to a low welding heat input. Therefore, high heat input joints were performed using a RS of 1500 rpm and a WS of 150 mm/min and the low heat input joints were produced at values of RS and WS of 1000 rpm and 300 mm/min respectively. These two different welding conditions are referred to as "hot welds" (welds produced at 1500 rpm – 150 mm/min) or "cold welds" (welds produced at 1000 rpm – 300 mm/min).

Table 1: Studied welding conditions.

Weld number	Welding tool / Probe design	FSW equipment Process control	Main welding parameters
n° 1	F101 ($\varnothing_{\text{shoulder}} = 10 \text{ mm}$)	FSW specific machine Position control	"Cold Weld" 1000 rpm – 300 mm/min
n° 2	Cylindrical threaded probe		"Hot Weld" 1500 rpm – 150 mm/min
n° 3	F103 ($\varnothing_{\text{shoulder}} = 10 \text{ mm}$)		"Cold Weld" 1000 rpm – 300 mm/min
n° 4	Three flats probe with a mixed thread		"Hot Weld" 1500 rpm – 150 mm/min
n° 5	F049 ($\varnothing_{\text{shoulder}} = 15 \text{ mm}$)	FSW robotic arm	"Cold Weld" 1000 rpm – 300 mm/min
n° 6	Triflute threaded probe	Force control	"Hot Weld" 1500 rpm – 150 mm/min

For microstructural characterization, the specimens were carefully prepared following standard metallographic procedures and etched using a Keller reagent, with the aim of revealing the microstructural features present at the specimens. An Olympus GX51 light optical microscope was used to investigate the microstructural properties and the defect formation of the FSW lap joints.

On the other hand, the mechanical properties of the lap joints were evaluated in terms of microhardness measurements and tensile testing (pulling the bottom sheet), paying attention to the fracture mode of each welding condition. This mechanical study was conducted only for lap joints made with F049 welding tool (welds n°5 and n°6). As shown below in Figure 3, each welding start and ends were discarded from welds n°5 and n°6, while two metallographic specimens and four tensile samples were obtained from each weld.

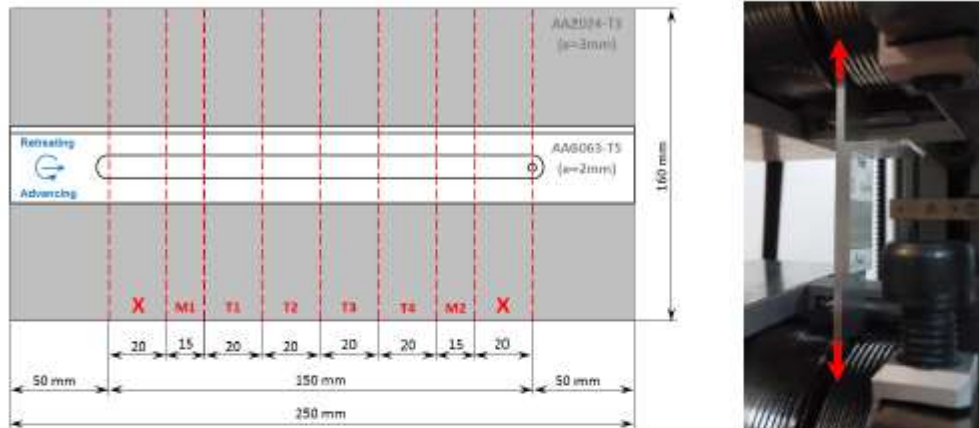


Figure 3: Sample obtainment and tensile test execution sketches, for welds made with F049 welding tool.

The microhardness measurements were conducted in metallographic specimens, performing HV0.5 microhardness scans. These scans were performed from side to side of the joints, in order to cover all FSW microstructural zones (base material, HAZ, TMAZ and stir zone), to a distance of 0.5 mm below from the overlap interface (in the bottom AA2024-T3 sheet).

RESULTS

A microstructural characterization of the welded specimens was carried out as shown in Table 2. As it can be seen, the material flow of the probe influenced area (nugget) was different, both for each welding condition and for each employed welding tool. Same volumetric defects called "worm-holes" were found in the cross sectional views in cold welds conducted with F101 and F103 welding tools, while no volumetric defects were detected in the cold weld conducted with F049 welding tool; neither in any weld performed in hot welding conditions, suggesting a good combination of welding parameters to obtain sound welds. It is important to note that the welds made with F101 and F103 welding tools were performed in position control, while the welds made with F049 tool were performed in force control.

Table 2: Microstructural characterization of the welded specimens.







Welding tool	Welding parameters	
	Cold Welds - 1000 rpm / 300 mm/min	Hot Welds - 1500 rpm / 150 mm/min
F101 Cylindrical threaded probe		
F103 Three flats probe with a mixed thread		
F049 Triflute threaded probe		

Figure 4 shows in more detail a cross-section of a FSW lap joint produced at "hot weld" conditions by a cylindrical threaded probe tool – F101. It can be seen that an interface pull-up effect was produced in both advancing and retreating sides of the FSW lap joint (see details from Figure 4-A to Figure 4-F). These pull-up effects resulted in a hook feature formation in the advancing side and an extended un-welded interface in the retreating side. This interface was formed as a result of a non-efficient elimination of the oxides present in the faying surfaces before welding. The hook feature and extended un-welded interface produced an effective sheet thickness reduction on the top sheet which affects directly to the mechanical properties of FSW lap joints produced at these welding conditions [1]. In the same way, a cross-section of a joint produced at "hot weld" conditions by a three flats and a mixed thread probe tool – F103, is shown in Figure 5. Similar metallurgical features were appreciated, with apparently same influence in mechanical properties of the joints.

Although the material flow features in the nugget zone were similar in these two cases, the heights of both advancing and retreating side hooks were different (see measurements in Figure 4 and Figure 5). The hook height affects directly to the top sheet effective thickness and thus to the mechanical properties of the joint. The higher the height of the hook, lower is the effective thickness of the top sheet, so that the joint strength will be also worse [1]. In this particular case, lower hooking feature heights were obtained with tool F103, which had a three flats probe and a mixed thread ($F103 \rightarrow 0.45 - 0.66 \text{ mm}$ VS $F101 \rightarrow 1.27 - 0.84 \text{ mm}$).

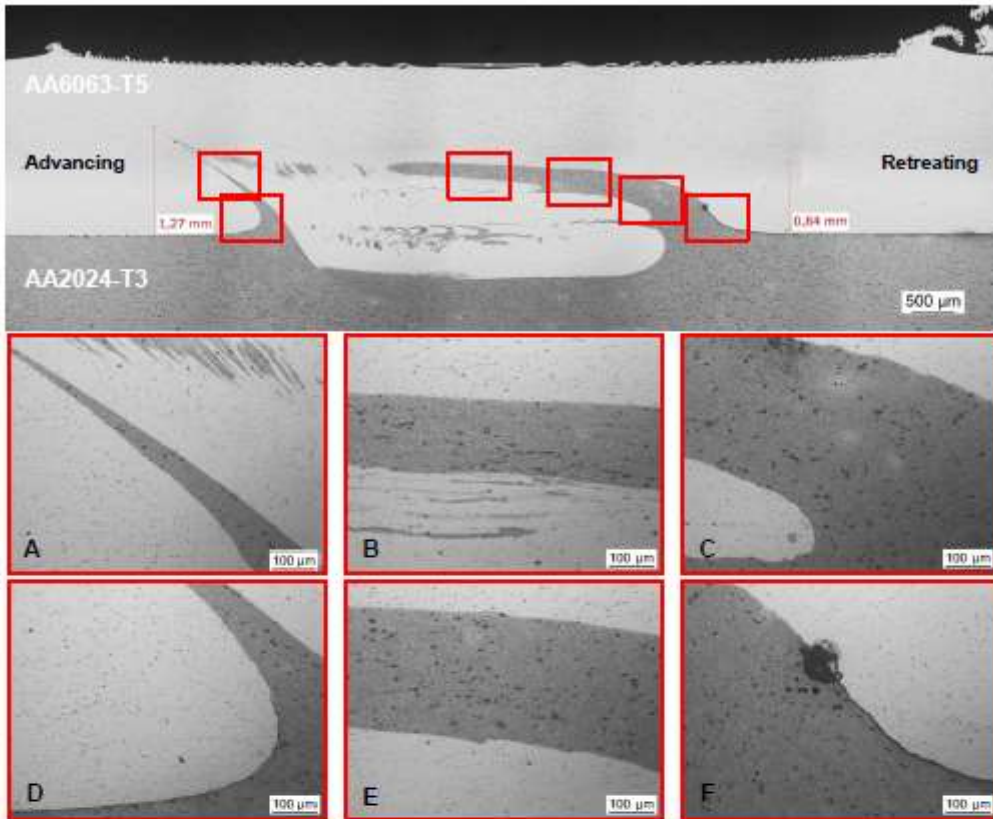


Figure 4: Cross-section of a FSW lap joint produced at "hot weld" conditions by F101 welding tool.

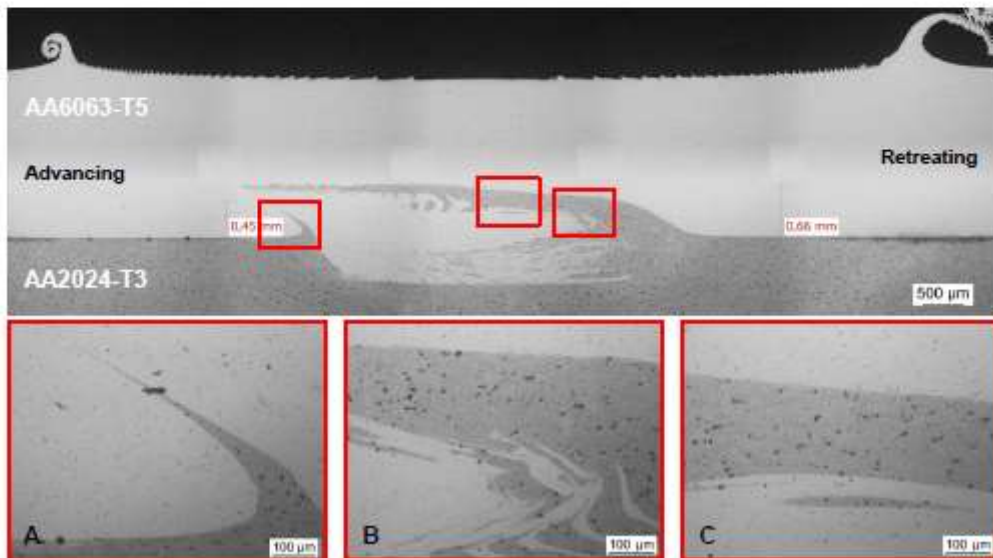
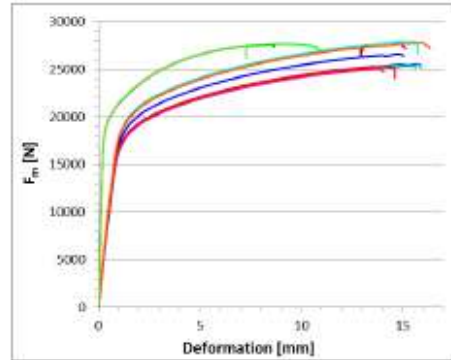


Figure 5: Cross-section of a FSW lap joint produced at "hot weld" conditions by F103 welding tool.

In order to quantify the loss of mechanical properties that had supposed each FSW lap weld in both hot and cold welding conditions, some tensile tests were performed pulling from the bottom sheet in welded samples (see Figure 3), as well as testing normalized samples obtained from the base material. The results of this mechanical study conducted only for FSW lap joints made by F049 welding tool, are summarized below:

Table 3: Tensile tests results, conducted on welds n°5 & n°6; lap welds performed by F049 welding tool.

Sample identification	Welding condition	Legend	S_0	F_m	R_{10}	R_m
			mm ²	N	MPa	average MPa
Weld n° 5_T1	Cold weld		57,38	25404,40	442,72	441,38
Weld n° 5_T2			60,45	26614,20	440,27	
Weld n° 5_T3			63,28	27907,30	441,03	
Weld n° 5_T4			57,89	25558,54	441,48	
Weld n° 6_T1	Hot weld		57,90	25319,24	437,29	439,69
Weld n° 6_T1			57,45	25052,72	436,08	
Weld n° 6_T1			62,86	27726,59	441,10	
Weld n° 6_T1			62,63	27822,30	444,27	
AA2024_BM_T1	Base Material		60,56	27610,13	455,91	454,82
AA2024_BM_T2			60,89	27707,55	455,01	
AA2024_BM_T3			60,41	27398,98	453,55	



Thus, it was possible to quantify the percentage of loss of properties respect to the base material. Regarding the maximum resistance (R_m), it could be concluded that the tensile strength of the bottom sheet was barely affected by the carrying out of the FSW lap joints; both in cold welding condition (loss of $\approx 2.96\%$) and in hot condition (loss of $\approx 3.33\%$).

Analysing the fracture modes of the tensile samples FSW lap welded in both welding conditions and already tensile tested, there was a clear difference between the distances from the weld center to the fracture surfaces, as it is shown in Figure 6. In the samples welded in cold welding condition, this distance (D) was considerably larger than in the ones welded in hot conditions (d).

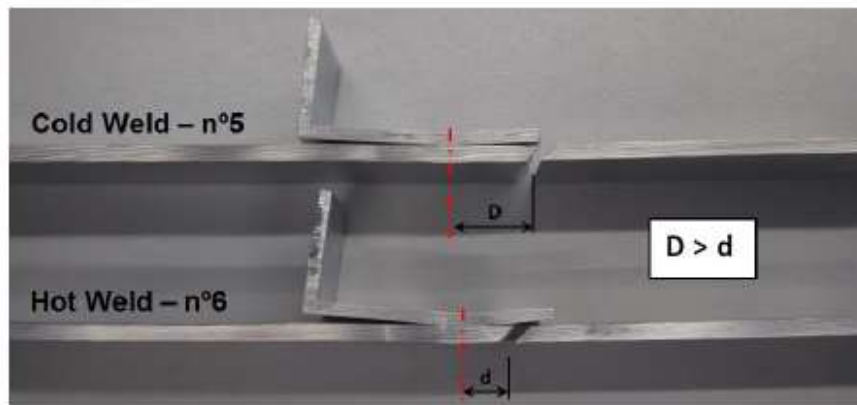


Figure 6: Fracture modes in each welding conditions.

This difference between the distances from the welding center to the fracture surfaces can be related to the amount of heat input contributed during the welding process. As the name implies, in the hot condition the heat input contributed was larger than in the cold condition.

In order to clarify the possible reasons why these fracture modes had occurred, microhardness measurements were conducted in metallographic specimens, performing HV0.5 microhardness scans from side to side of both specimens (see Figure 7).

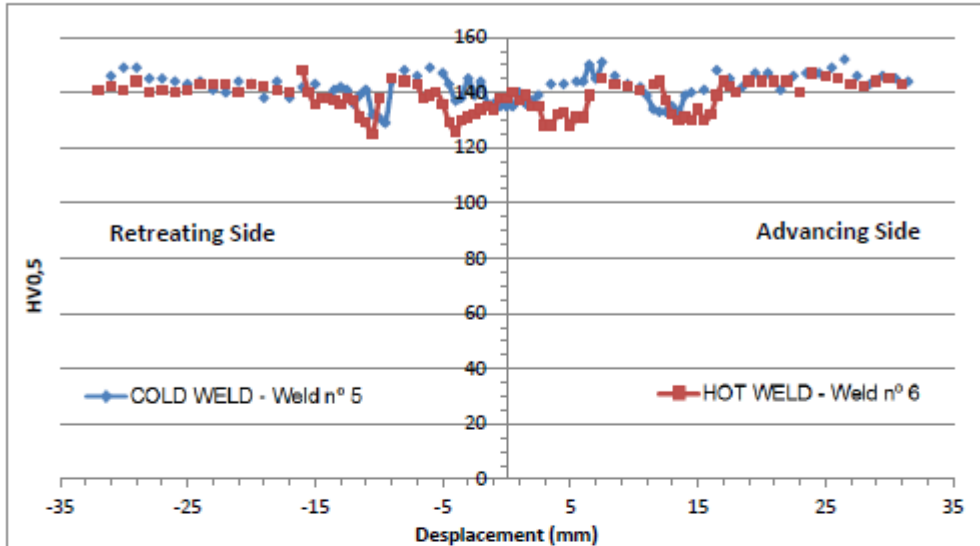


Figure 7: Microhardness scans conducted on the welded specimens.

In these microhardness scans it was possible to appreciate how in the hot welding condition, the loss of hardness of the bottom sheet in the HAZ zone (minimum value of 125HV0,5) was a little larger greater than in the welding performed in cold condition (minimum value of 138HV0,5). On the one hand, it is necessary to emphasize that the hot weld HAZ, was wider than at the cold weld, a fact that could be seen on the drop of microhardness values. Furthermore, another drop in hardness occurred in the bottom sheet welded in hot condition, below the zone influenced by the tool probe, both in the advancing and in the retreating sides. All this is represented in Figure 8.

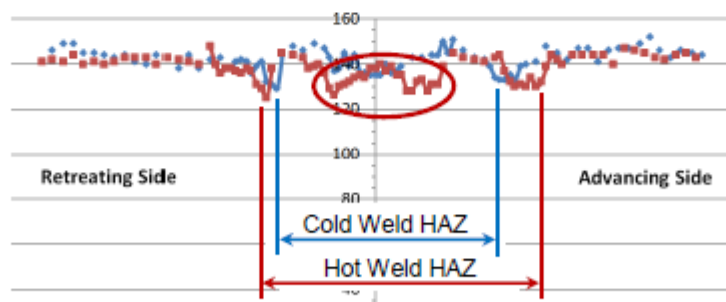


Figure 8: Microhardness values comparative in the zone influenced by the welding tool.

Watching the tensile specimen fracture modes, it could be concluded that the samples welded in cold condition had broken through the HAZ (tool shoulder influenced area), while the samples welded in hot condition had broken through the area influenced by the tool probe pin of the bottom sheet.

As mentioned in the experimental procedure, the lap joints performed with F101 and F103 welding tools were carried out in the specific FSW machine in position control, while the ones performed with the F049 tool were carried out in a robotic arm, in force control. The specific FSW equipment allows a precise control of the main FSW process parameters and good stability of the tool during welding process (good rigidity), while the control of the KUKA robot is not as robust (Figure 10). By the fact that the shoulder of the welding tool F049 had larger diameter comparing with tools F101 and F103 ($\varnothing_{F049}=15\text{mm}$ VS $\varnothing_{F101-F103}=10\text{ mm}$), there were no stability problems in this case, when welding by the robot using this welding tool.

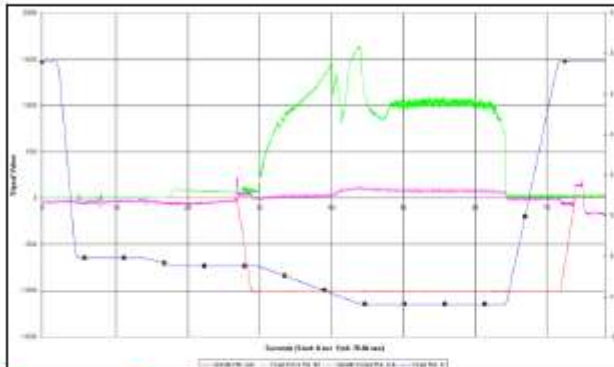


Figure 9: Main welding parameter measurements; weld n° 1, conducted in the specific FSW machine with F101 welding tool.

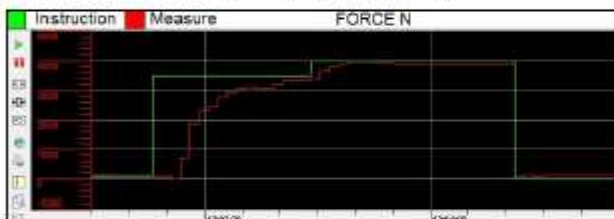


Figure 10: Force signal of weld n° 5, conducted in the robotic arm with F049 welding tool; force instruction & measurement.

SUMMARY AND CONCLUSIONS

Microstructural and mechanical properties of FSW lap joints have been investigated using different probe designs and welding parameters. The following conclusions can be presented:

1. Different probe designs promote different flow of plasticized material during FSW of lap joints resulting in different defect formation. It is possible to avoid the volumetric defects appearance and to optimize the strength of the FSW lap joints by using the appropriate probe design and welding conditions depending on the loading requirements of the joint.
2. An interface pull-up effect was produced in both advancing and retreating sides of all FSW lap joints welded in hot condition, resulting in a hook feature formation in the advancing side and an extended un-welded interface in the retreating side, producing an effective sheet thickness reduction on the top sheet which affects directly to a strength of FSW lap joints. The higher the height of the hook, lower is the effective thickness of the top sheet, so that the joint strength will be also worse.
3. Regarding the loss of mechanical properties of the bottom sheet that had supposed each FSW lap welds conducted with the F049 tool in both hot and cold welding conditions, the tensile strength of the bottom sheet was barely affected by the execution of the FSW lap joints.

4. Two different fracture locations had been obtained in the tensile samples, depending on the welding conditions. A clear difference between the distances from the welding center to the fracture surfaces was observed: in cold welds, this distance was considerably greater than in hot ones, related to the amount of heat input contributed during the welding process.
5. The microhardness scans had shown how in the hot welding condition, the loss of hardness of the bottom sheet in the HAZ zone, was a little larger than in cold condition. The hot welding condition HAZ was wider than the cold one. Another drop in hardness occurred in the bottom sheet welded in hot condition, below the zone influenced by the tool probe, suggesting that the samples welded in cold condition had broken through the HAZ (tool shoulder influenced area), while the samples welded in hot condition had broken through the area influenced by the tool probe pin of the bottom sheet.
6. Finally, and regarding to the process control and welding tool stability during welding process, the specific FSW equipment had allowed a precise control of the main FSW process parameters and good stability of the tool, while the control of the KUKA robot was not as robust.

REFERENCES

- [1] Aldanondo et al., "Mechanical and microstructural properties of FSW lap joints", 142nd Annual Meeting & Exhibition TMS2013 – Friction Stir Welding and Processing VII, San Antonio, USA, 3-7 March 2013.
- [2] Buffa et al., "Friction stir welding of lap joints: Influence of process parameters on the metallurgical and mechanical properties", *Materials Science and Engineering* (2009).
- [3] L. Cederquist, A. P. Reynolds, "Factors affecting the properties of friction stir welded aluminum lap joints", *Weld J Res Suppl* 80, 281, (2001).
- [4] S. B. Jung et al., "Lap joint properties of FSWed dissimilar formed AA 5052 and AA 6061 Al alloys with different thickness", *J Mat Sci* 43, 3296, (2008).
- [5] S. Yazdaniyan, Z. W. Chen, G. Littlefair, "Effects of friction stir lap welding parameters on weld features on advancing side and fracture strength of AA6060-T5 welds", *J. Mater. Sci.*, Published online (2011).
- [6] M. Ericsson, L. Jin, R. Sandström, *Int. Jour. Fatigue* 29-57, (2007).
- [7] M. K. Kulekci, A. Sik, E. Kaluç, "Effects of tool rotation and pin diameter on fatigue properties of friction stir welded lap joints", *Int. J. Adv. Manuf. Technol.* 36: 877-882 (2008).
- [8] R. Kovacevic et al., "Investigation of the friction stir lap welding of aluminium alloys AA5182 and AA6022", *J Mat Eng Perf*, 16 (4), 477, (2007).
- [9] G. M. D. Cantin et al., "Friction Skew-stir welding of lap joints in 5083-O aluminium", *Sci. Tech. Weld. Join.*, Vol10 N°3 268-280 (2005).
- [10] M. J. Brooker et al., "Applying Friction Stir Welding to the Ariane 5 Main Motor Thrust Frame", *Proceedings of the Second International Symposium on FSW*, Gothenburg, (2000).
- [11] ISO 25239-2; Friction Stir Welding – Aluminium. Part 2: Design of weld joints.

7.- ARTICLE 4: MICROSTRUCTURAL FEATURES IN FRICTION STIR WELDED LAP JOINTS

[72] E. Aldanondo, E. Arruti, J. Sarasa and A. Echeverria, "Microstructural features in Friction Stir Welded lap joints," in *10th International Conference on Trends in Welding Research and 9th International Welding Symposium of Japan Welding Society*, Tokyo (Japan), 2016.

In this work, further investigation was carried out on FSLW joint manufacturing using high strength aluminium alloys typically used in the aeronautic sector. In this occasion, the AA7075-T6 alloy was employed to produce the welds and a direct comparison between welds produced with a standard tool and the new design proposed for lap joints was carried out. We concluded that the new tool design proposed by us was able to minimize defects typically found in FSLW joints such as hooks and cold lap defects.

The work was presented in the 10th International Conference on Trends in Welding Research and 9th International Welding Symposium of Japan Welding Society in Tokyo (Japan) and the article was published in the proceedings of the symposium.

MICROSTRUCTURAL FEATURES IN FRICTION STIR WELDED LAP JOINTS

Egoitz Aldanondo, Ekaitz Arruti, Julen Sarasa, Alberto Echeverria
IK4 LORTEK, Ordizia, Spain
Egoitz@lortek.es, +34 943 882303

Abstract

Friction Stir Welding of aluminium alloys in lap joint configuration has shown a great potential for lightweight structure manufacturing but it is very important to consider specific issues relative to lap joint formation that are different from the more commonly used butt joint configuration. Typical features such as the hook formation at the advancing side or the cold lap defect or joint uplifting at the retreating side are the most characteristic defects in the lap joint configuration. The formation of such defects is mostly influenced by the FSW tool design and welding parameters. It is very important to identify appropriate processing conditions that avoid or minimize these defects in order to create welds with good properties that can be applied in final products.

The effect of several FSW variables on the formation of lap joint features is presented in this work. FSW joints in lap joint configuration were performed using an AA7075-T6 aluminium alloy and different welding conditions including tool designs and main welding parameters. The microstructural characteristics of lap joints were analysed by metallographic examination and the formation of the characteristic features was evaluated. Thus the influences of FSW variables such as welding tool design, rotational speed and welding speed on the formation of hook features or joint uplifting was established.

Introduction

Although the majority of applications based on FSW technology manufacturing have been focused in butt joint configurations, the lap joint configuration is highly interesting too representing a number of applications or potential developments [1, 2]. Therefore many research works have been conducted with the main objective of understanding the joint formation mechanisms, microstructural features and the joint strength of FSW lap joints [3-6]. According to those works, there are a number of factors that influence the joint properties such as tool design, welding parameters or number of passes. Depending on those factors typical characteristics of FSW lap joints have been defined as hook features, cold lap defects or the joint uplifting. These characteristics are the main factors that determine the joint strength and microstructural properties, and are largely influenced by the tool design used to perform FSW lap joints as shown in Figure 1. Therefore it is very important to optimize the tool design, as well as other welding parameters, in order to produce FSW lap joints without unwanted features that could reduce the joint strength.

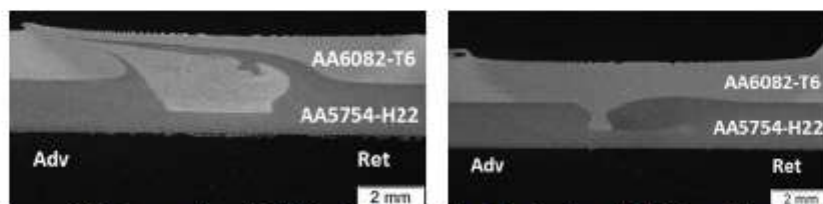


Figure 1: Macrographs of FSW lap joints produced by tools with different designs [4].

Experimental details

FSW lap joints were performed between a 2 mm thick AA7075-T6 aluminium alloy on top of a 3 mm sheet of the same alloy. FSW tests were performed in a I-STIR PDS4 machine using two different tool designs and two different welding conditions. Thus a cylindrical threaded tool and a tool containing three flats were used both having a shoulder diameter of 10 mm and a pin length of 2,5 mm. Different welding conditions were represented from a heat input point of view, using 1200 rpm and 152 mm/min as high heat input conditions; while 800 rpm and 254 mm/min were used as low heat input welding conditions. FSW tests were conducted initially in position control in order to identify the appropriate axial or Z force and torque for each welding condition and FSW tool as

shown in Figure 2. It can be observed that high heat input conditions require lower Z force and torque values than lower heat input conditions for both FSW tool designs used for the tests. Final FSW samples used for the metallographic examination were produced in force controlled FSW tests applying the appropriate Z force for each tool and welding condition.

For metallographic examination cross section specimens were obtained from the FSW lap joints and carefully prepared following standard metallographic procedures comprising cross-sectioning, mounting, polishing and etching. Keller's reagent was used as etchant and the specimens were submerged for 5 seconds, rinsed in water and dried in a warm airflow. An Olympus GX51 light optical microscope was used to investigate the microstructural properties and defects of the FSW lap joints.

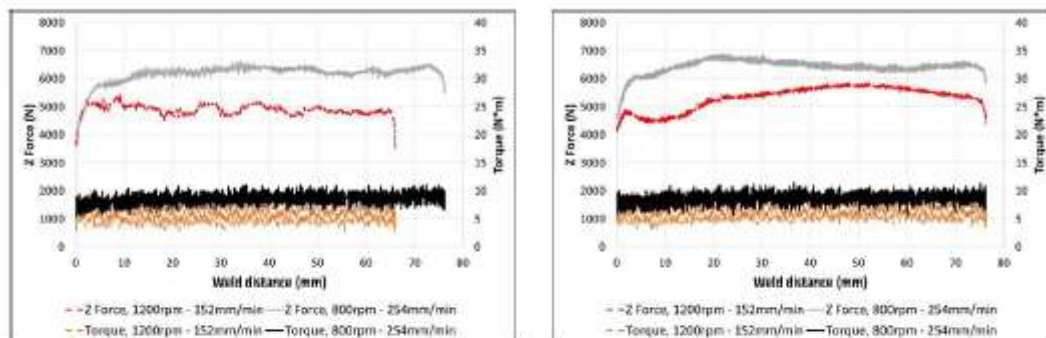


Figure 2: Z force and Torque values registered in FSW tests performed in position control with a cylindrical threaded tool (left) and a 3 flat tool (right).

Results and discussion

Cross sections of FSW lap joints produced by the two different tools and the two different welding conditions are shown in Figure 3. Obvious volumetric defect free joints were obtained except for the cylindrical threaded tool operated at high heat input welding conditions (1200 rpm, 152 mm/min). A continuous wormhole was identified in that sample at the advancing side suggesting an insufficient material flow and consolidation at these welding conditions. Larger stirred zones and TMAZ extensions were observed in the joints produced by the 3 flat tool in comparison with the joints produced by the cylindrical threaded tool at equivalent welding conditions (images "c" and "d" vs "a" and "b" at Figure 3). The same effect was seen by using low heat input conditions vs the high heat input conditions, achieving larger stirred zones and TMAZ extensions at low heat input conditions (images "a" and "c" vs "b" and "d" at Figure 3). This effect could be attributed to the larger sticking effect between the tool and the material at low heat input conditions resulting in larger material flow regions and larger stirred zones and TMAZ extensions.

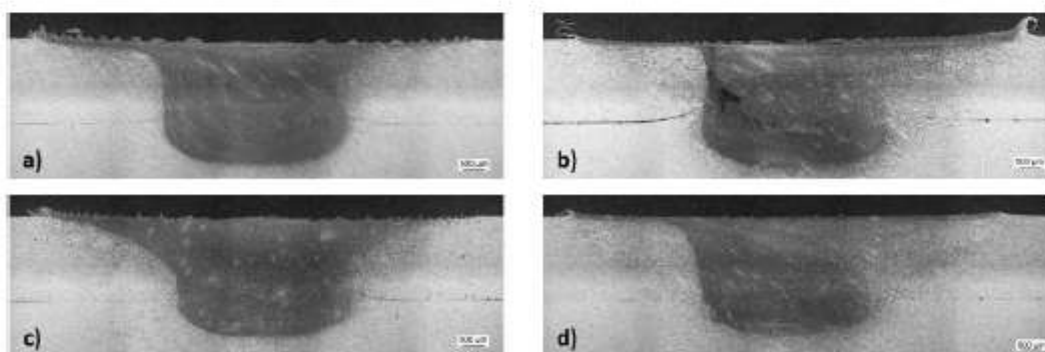


Figure 3: Cross-sections of FSW lap joints performed with a) Cylindrical threaded tool at 800rpm, 254mm/min and 6,4kN; b) Cylindrical threaded tool at 1200rpm, 152mm/min and 5,1kN; c) 3 flat tool at 800rpm, 254mm/min and 6,6kN; d) 3 flat tool at 1200rpm, 152mm/min and 5,1kN.

Apart from volumetric defects at the joint made with the cylindrical threaded tool operated at high heat input conditions, other microstructural features such as hooking and joint line uplifting were observed in the joints as shown in Figure 4, which are characteristic of FSW lap joints. These features can act as top sheet thinning or crack initiation originators so they can be considered as weld defects that are responsible to reduce the joint strength. Taking into account the importance of these features in joint properties, the hook size at the advancing side (H1) and the joint line uplifting (H2) at the retreating side were estimated by optical microscopy and an image processing software, as shown in the detail images at Figure 4.

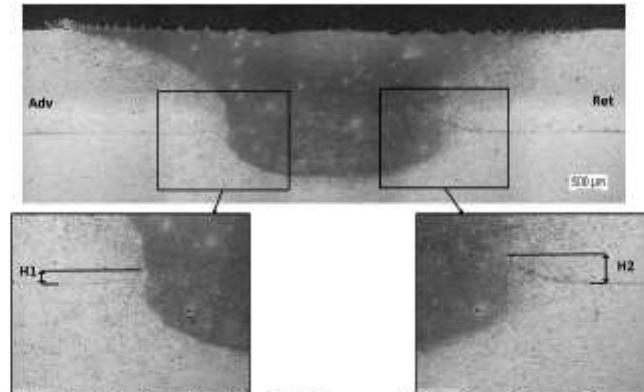


Figure 4: Micrographs showing details of hook features at the advancing (H1) and the retreating (H2) sides of a FSW weld performed at 800rpm and 254mm/min with a 3 flat tool.

The results of hook size measurements at the advancing side (H1) and the retreating side (H2), which were performed in the metallographic specimens obtained from the FSW lap joints produced with the two different tools and two different welding conditions, are plotted in Figure 5. Smaller hook sizes were generally observed in the joints performed with the 3 flat tool in comparison with ones produced with the more conventional cylindrical threaded design. This effect was magnified at high heat input welding conditions (1200 rpm – 152 mm/min) due to the extensive vertical flow of plasticized material at the TMAZ proximities, which is induced in a larger extent by the cylindrical threaded tool in comparison with the 3 flat tool. Therefore larger hook sizes in the range of ~0,4-0,5 mm were identified in joints produced by the cylindrical threaded tool at high heat input conditions in both advancing (H1) and retreating sides (H2). However, a different trend in hook feature formation was identified at the joints performed by the 3 flat tool. In these cases, smaller hook sizes were identified at the advancing side (H1) as well as at the retreating side (H2) of the joints produced using high heat input conditions. From these results it can be concluded that the vertical flow of plasticized material at the TMAZ proximities is minimal in the joints produced by the 3 flat tool, meaning that this tool design is more appropriate for FSW lap joints than the cylindrical threaded tool design.

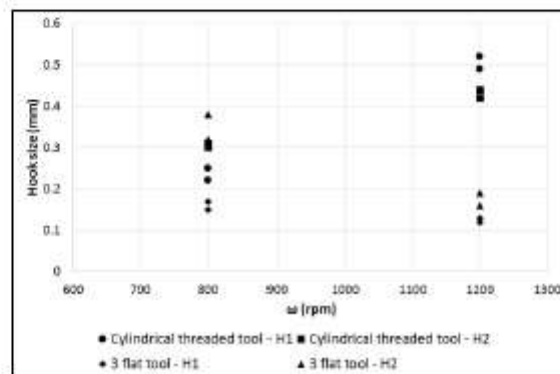


Figure 5: Hook size at the advancing (H1) and retreating (H2) sides for welds performed with different tools and welding parameters.

Therefore, the smallest hook sizes were observed at the joints produced by the 3 flat tool operated at high heat input conditions, being these sizes in the range of ~0,1-0,2 mm. These joints would be expected to offer highest joint strengths although other effects that could reduce the joint properties such as the overaging of the AA7075-T6 alloy at the HAZ should be taken into account.

Conclusions

Microstructural features of AA7075-T6 alloy FSW lap joints produced by two different tool designs and two different welding parameter sets were investigated. The following conclusions can be presented:

- A continuous wormhole defect was produced by the cylindrical threaded tool operated at high heat input welding conditions.
- Larger stirred zones and TMAZ extensions were observed generally using low heat input conditions and the 3 flat tool design to perform the FSW lap joints.
- Using a cylindrical threaded tool design and high heat input conditions, largest hook sizes in the range of ~0,4-0,5 mm were observed.
- Using a 3 flat tool design and high heat input conditions, smallest hook sizes in the range of ~0,1-0,2 mm were observed.
- Different flow patterns were produced by the cylindrical threaded and the 3 flat tool. The 3 flat tool showed the capabilities to produce reduced hook size features and to be operated in a wider parameter window, being a more promising tool design for FSW lap joints.

References

- [1] M.J. Booker, *et al*: "Applying Friction Stir Welding to the Arienne 5 Main Motor Thrust Frame" *Proc 2nd International Symposium on Friction Stir Welding*, Gothenburg, Sweden, 2000.
- [2] R. Talwar, *et al*: "Friction Stir Welding of Airframe Structures" *Proc 2nd International Symposium on Friction Stir Welding*, Gothenburg, Sweden, 2000.
- [3] L. Cederquist, A.P. Reynolds: "Factors affecting the properties of friction stir welded aluminium lap joints", *Weld. J. Res. Suppl.*, 80 (2001), pp. 281.
- [4] E. Aldanondo, *et al*: "Mechanical and microstructural properties of lap joints" *Proc 142nd TMS Annual Meeting & Exhibition – Friction Stir Welding and Processing VII*, San Antonio, USA, March 2013, pp. 195-205.
- [5] M.K. Kulekci, *et al*: "Effects of tool rotation and pin diameter on fatigue properties of friction stir welded lap joints", *Int. J. Adv. Manuf. Technol.*, 36 (2008), pp. 877-882.
- [6] S.B. Jung, *et al*: "Lap joint properties of FSWed dissimilar formed AA5052 and AA6061 Al alloys with different thicknesses", *J. Mat. Sci.*, 43 (2008), pp. 3296.

8.- ARTICLE 5: FRICTION STIR WELD LAP JOINT PROPERTIES IN AERONAUTIC ALUMINIUM ALLOYS

[73] E. Aldanondo, E. Arruti and A. Echeverria, "Friction Stir Weld lap joint properties in aeronautic aluminium alloys," in *Friction Stir Welding and Processing X, in proceedings of the 148th Annual Meeting & Exhibition TMS2017*, San Diego (USA), 2017.

A continuation of the work published in the previous article was carried out in this additional investigation. The properties of FSLW joints produced using the AA7075-T6 alloy were studied in this article as added scientific contribution. We concluded that the new FSW tool design proposed for lap joints could produce welds with improved properties in a wider welding parameter window than the tools with a conventional design.

This work was presented in the Friction Stir Welding and Processing X session of the 148th Annual Meeting & Exhibition TMS2017 in San Diego (USA) and the article was published in the conference book.

FRICION STIR WELD LAP JOINT PROPERTIES IN AERONAUTIC ALUMINIUM ALLOYS

Egoitz Aldanondo¹, Ekaitz Arruti¹, Alberto Echeverria¹

¹IK4 LORTEK;
Arranomendia kalea 4A, Ordizia, 20240, Spain
Tel: +34 943 88 23 03
Egoitz@lortek.es

Keywords: Friction Stir Welding, Lap joints, Aluminium, AA7075-T6

Abstract

A study of properties of Friction Stir Weld lap joints performed with the AA7075-T6 aluminum alloy used in aerospace manufacturing are presented in this work. The effects of different tool designs and welding parameters in the weld cross sectional and mechanical properties of the joints were investigated. The weld cross sectional features were analyzed by metallographic examination while the mechanical properties were studied by microhardness measurements. Typical features of Friction Stir Weld lap joints have been identified such as hook features, cold lap defects or joint line uplifting. The extension of Heat Affected Zone regions and mechanical property reduction was evaluated depending on the welding parameters used to perform the Friction Stir Weld joints. The tool design as well as welding conditions that minimize defects such as effective sheet thinning, hardness drops or wide Heat Affected Zone regions were established.

Introduction

Aircraft structures are commonly manufactured using high strength aluminium alloys such as 2XXX and 7XXX series which are typically combined in lap joint configurations to form skin-stringer stiffened parts. The limitations and difficulties that present such alloys in traditional fusion welding processes resulted in the use of riveting as the main joining technology in the manufacturing of structural elements for aircrafts. However the irruption of a solid state welding technique such as Friction Stir Welding (FSW) opened up new possibilities and many novel structures have been developed in the aerospace industry over the last years [1-5]. The industrial implementation of FSW technology in the manufacturing of primary aircraft structures in some of those developments [3-5] evidences the suitability of the technology for this type of application.

One of the most promising application of FSW in aerospace is the manufacturing of fuselage panels which are generally composed by lap joints between stringer and skin parts. Therefore issues relevant to FSW lap joints have to be dealt with and solved in order to produce joints and parts that comply with the stringent quality requirements of the aeronautic industry. There has been a number of studies focused on that end [6-13] which have shown the main characteristics of joints and the main influential elements that are responsible for such characteristics. Thus typical defects such as hooking, sheet thinning or cold lap defects are well known and some strategies to avoid them or reduce their severity have been described. Among these strategies are the use of double passes [6, 9] as well as the optimization of tool designs and welding parameters in order to maximize the quality of the obtained joints [6-13]. Although some general trends can be extracted from all those works, a general solution for the elimination of the hook features has not been achieved yet and further work is needed for that purpose.

The main results achieved in a work investigating the characteristics of FSW lap joints are presented in this paper. A comparison is made in lap joints produced using a AA7075-T6 aluminium alloy, two different tool designs and several welding parameters. The characteristics of joints are analyzed by metallographic examination and microhardness measurements, which have demonstrated to be useful means to perform a preliminary evaluation of the joint characteristics and investigate the role of the used tool designs and welding parameters in those characteristics.

Experimental details

A series of FSW trials was made in AA7075-T6 aluminium alloy overlapping a 2 mm thick sheet on top of another 3 mm thick sheet. All trials were made in an I-STIR PDS4 machine for FSW process development with the possibility to be operated in position or force control using two different tool designs. Thus a tool containing a conventional threaded probe and a tool containing a probe with three flats and a mixed thread were used as shown in Figure 1. The dimensions for both tools were similar having a shoulder diameter of 10 mm, a probe diameter of 4 mm and a probe length of 2,5 mm. Therefore the penetration of the probe in the bottom sheet is 0,5 mm in all cases. After an initial welding parameter investigation, two welding conditions were selected representing two heat input conditions. A rotational speed of 1200 rpm and welding speed of 152 mm/min were used as high heat input condition resulting in a weld pitch of 0,13 mm/rev; while 800 rpm and 254 mm/min were used as rotational speed and welding speed as cold heat input conditions giving a weld pitch of 0,32 mm/min. Welds were produced using the two welding conditions and two tool designs under force control, adjusting the applied force depending on the welding speed and the rotational speed for each case.

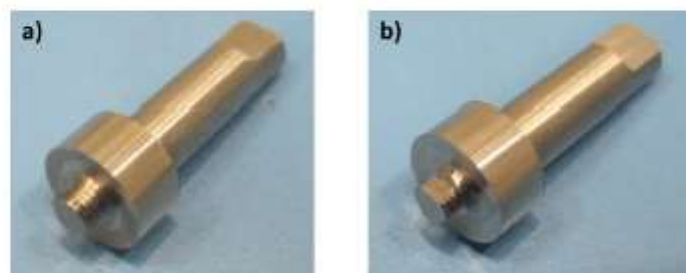


Figure 1: FSW tools used to produce the welds. a) conventional threaded tool and b) tool with 3 flats

Metallographic examination of the welds was conducted with cross-section specimens that were prepared following standard metallographic procedures. These included polishing to a mirror like finish and etching by submerging the specimens into a Keller's reagent for approximately 5 seconds, rinse in water and drying in a warm airflow. Weld cross sectional features of the FSW lap joints were investigated by an Olympus GX51 light optical microscope.

Microhardness measurements were performed using a Vickers indenter, a load of 500 g and a load application time of 15 seconds. The indentations were made with a spacing of 0,5 mm between them, at the midplane of the top sheet and along the transverse cross-section of the welds taking the weld centerline as reference. A length of at least 20 mm (10 mm from the centerline in both directions) was analyzed in order to characterize all relevant microstructural zones. All microhardness measurements were performed in the as welded condition and allowing a time of approximately 30 days between the production of the welds and the measurements.

Results and discussion

Weld cross sectional features and local mechanical properties of the produced FSW lap joints were analyzed by means of metallographic examination and microhardness measurements. The following sections summarize the main results obtained in this work:

Weld cross sectional characterization

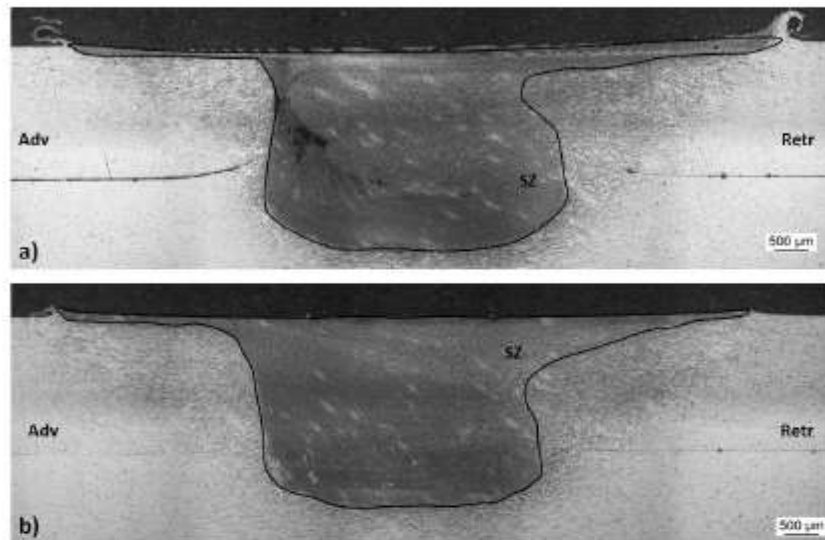


Figure 2: Cross-sections of FSW lap joints produced at 1200 rpm and 152 mm/min (0,13 mm/rev) with a) conventional threaded tool and b) tool with 3 flats

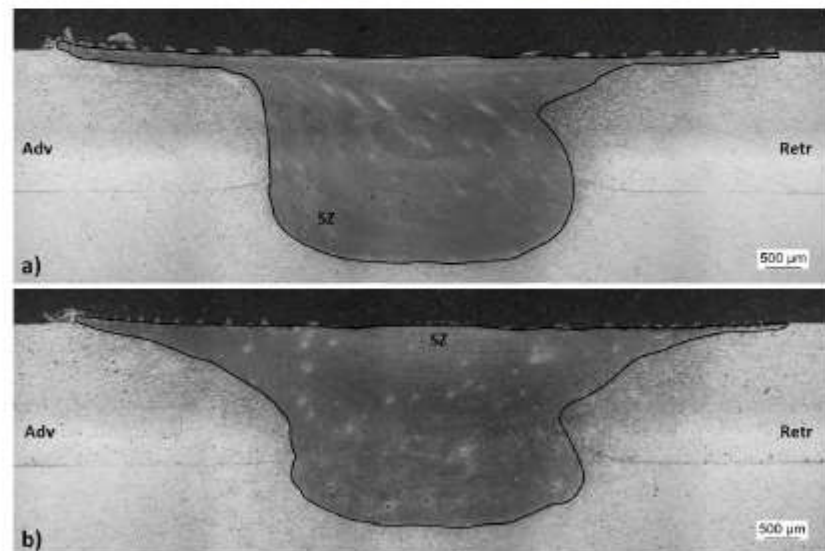


Figure 3: Cross-sections of FSW lap joints produced at 800 rpm and 254 mm/min (0,32 mm/rev) with a) conventional threaded tool and b) tool with 3 flats

Cross-sections of FSW lap joints produced by the employed tools and welding conditions are shown in Figure 2 and Figure 3. The only case where major volumetric defects were found

was in the weld performed by the conventional threaded tool operated at 0,13 mm/rev (image "a" at Figure 2). In this case a continuous wormhole defect can be observed at the advancing side resulting from the inappropriate material flow and consolidation. This major defect can be eliminated by using a weld pitch of 0,32 mm/rev (image "a" at Figure 3) or by using the tool with three flats as shown by the volumetric defect-free joints (image "b" at Figure 2 and image "b" at Figure 3). Therefore the tool with three flats seems to produce a more appropriate plasticized material flow and consolidation being able to eliminate major defects and increasing the process envelope.

The volume of stirred material during FSW is mainly dependent on the tool design and the welding parameters. This volume for the investigated joints is highlighted in Figure 2 and Figure 3, then superposed for comparisons in Figure 4. It can be observed that using the tool with three flats the volume of the stir zone is slightly larger than the volume obtained with the conventional threaded tool for similar welding parameters. This suggests that material flow and consolidation capacity offered by the tool with three flats is more intense and appropriate in comparison to the conventional threaded tool. Thus the process envelope where defect free joints can be obtained is larger for the tool with three flats so that volumetric defect free joints were obtained even at the welds produced under high heat input conditions (0,13 mm/rev in Figure 2 "b").

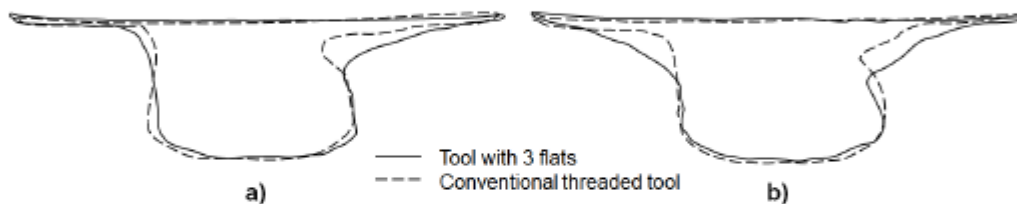


Figure 4: Superposed stir zone regions in FSW lap joints made with different tools and produced at a) 1200 rpm and 152 mm/min (0,13 mm/rev); and b) 800 rpm and 254 mm/min (0,32 mm/rev)

Typical weld cross sectional features of FSW lap joints such as hook features at the advancing side or joint line uplifting as well as cold lap defects at the retreating side were observed in the investigated welds, although their size was found to be generally reduced. The severity and size of those defects was found to be different for different tool designs and welding parameters. As previously reported [13], generally larger hooks and joint line uplifts were found in the welds made by the conventional threaded tool in comparison with those made with the tool with three flats (Figure 2, Figure 3). Therefore the effective sheet thickness of the top sheet was larger in the welds made by the tool with three flats which seems to be beneficial for the joint properties.

Microhardness analysis

Comparisons of microhardness distributions along the welds obtained in the investigated FSW lap joints are shown in Figure 5-Figure 8. W shaped hardness distributions which are typical in FSW of precipitation hardening aluminium alloys can be observed in all cases, although significant differences were found depending on the welding parameters and tool designs used for performing the welds.

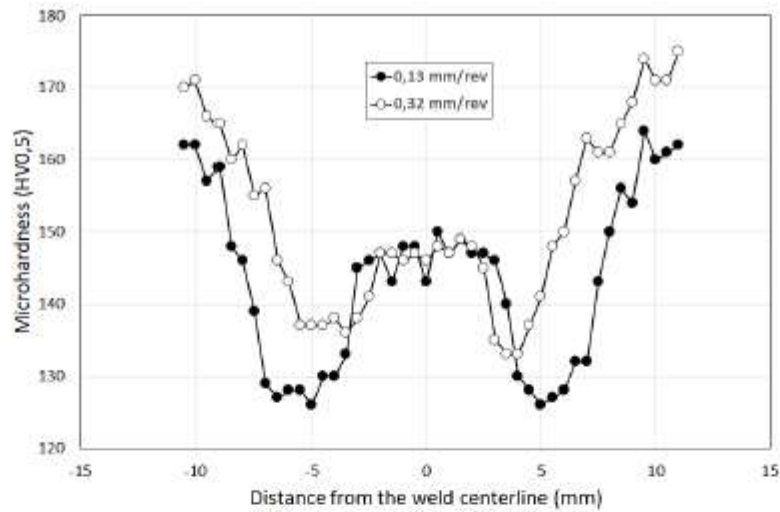


Figure 5: Microhardness values in welds made at 0,13 and 0,32 mm/rev with a conventional threaded tool

The comparison between FSW lap joints made using a different weld pitch of 0,13 and 0,32 mm/rev (Figure 5 and Figure 6) showed the great influence of the welding parameters in the material softening. The use of high heat input parameters, i.e. 1200 rpm and 152 mm/min (0,13 mm/rev), produced lower minimum hardness values and wider heat affected zone (HAZ) regions. This effect results from the higher temperatures and heating of the material achieved at 0,13 mm/rev, which produced a larger overaging effect of the material resulting in hardness drop. The same effect was observed in the welds performed with the conventional threaded tool (Figure 5) as well as with the tool containing three flats (Figure 6). Thus minimum hardness values in the range of 125-130 HV0,5 (~27% drop relative to the base material hardness) were measured in welds performed using a weld pitch of 0,13 mm/rev; while 130-135 HV0,5 was found to be the range for minimum hardness values in welds made at 0,32 mm/rev (~24% drop relative to the base material hardness).

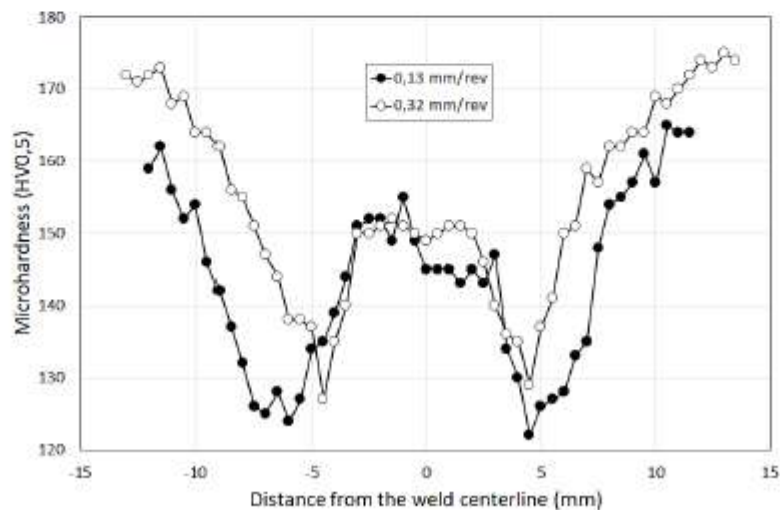


Figure 6: Microhardness values in welds made at 0,13 and 0,32 mm/rev with a threaded tool with 3 flats

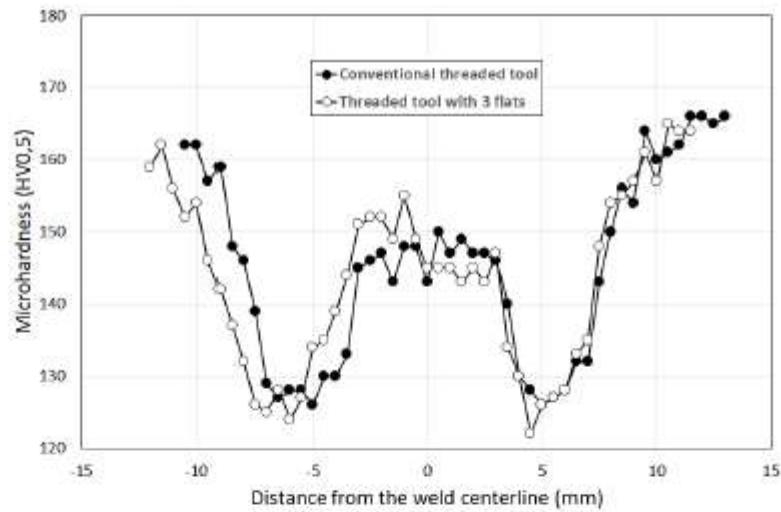


Figure 7: Microhardness values in welds made at 0,13 mm/rev with different tool designs

The comparison of hardness distributions along the welds obtained using the same welding parameters for the investigated two tool designs are shown in Figure 7 and Figure 8. Very similar profiles were obtained for both tools in welds performed using the two investigated weld pitch conditions (0,13 mm/rev in Figure 7 and 0,32 mm/rev in Figure 8), although some trends could be observed. In both cases the welds made by the tool with three flats showed lower minimum hardness values as well as wider HAZ extensions in comparison with the welds made by the conventional threaded tool. This could be explained by a slightly higher overaging effect occurred if the tool with three flats is used. The higher degree of stirring and plastic deformation promoted by this tool, as previously discussed in the weld cross sectional characterization (Figure 4), could be responsible for the achievement of higher temperatures resulting in a higher overaging degree and lower hardness values.

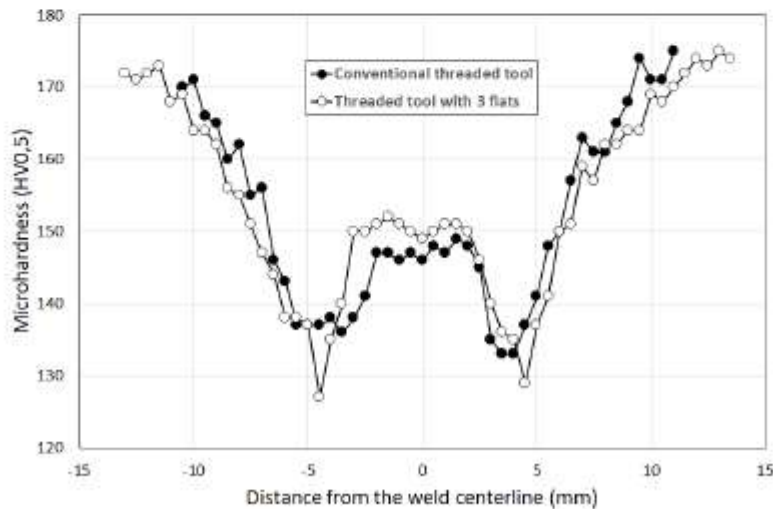


Figure 8: Microhardness values in welds made at 0,32 mm/rev with different tool designs

Conclusions

In the present work weld cross sectional features and mechanical properties of FSW lap joints were investigated in a series of welds made in aluminium alloy AA7075-T6, using different tool designs and welding parameters. The following observations regarding relationships of tool designs, welding parameters and joint properties have been attained:

- The use of low heat input welding parameters, i.e. 800 rpm and 254 mm/min – 0,32 mm/rev, produced volumetric defect free welds.
- When high heat input parameters were used, i.e. 1200 rpm and 152 mm/min – 0,13 mm/rev, the tool with three flats produced defect free welds while a wormhole defect was found in welds made with the conventional threaded tool.
- The tool with three flats showed a higher capacity to promote the appropriate stirring, material flow and consolidation of the plasticized material resulting in a larger process envelope or welding parameter range where defect free joints are obtained.
- Smaller hook features and joint line uplifts were produced by the tool with three flats in comparison with the conventional threaded tool, resulting in a larger effective sheet thickness of the top sheet.
- Lower hardness values and wider HAZ regions were observed in welds made using the high heat input parameters, i.e. 1200 rpm and 152 mm/min – 0,13 mm/rev, for the two tool designs investigated.
- Very similar hardness distribution profiles along the weld were observed in welds performed under same welding parameters for the two tool designs investigated.

Based on the previous observations, it seems clear that better results would be obtained regarding FSW lap joint properties using a tool with three flats rather than using a conventional threaded tool. Although the use of low heat input parameters was found to produce better local mechanical properties, i.e. higher hardness values and smaller HAZ extension, further research is needed in order to evaluate the general mechanical properties of FSW lap joints, as other weld cross sectional features such as hook size or joint line uplifting were found to be in the same range in welds made with low and high heat input welding parameters and the tool with three flats.

References

1. M.J. Booker et al., "Applying Friction Stir Welding to the Ariane 5 Main Motor Thrust Frame", 2nd International Symposium on Friction Stir Welding, Gothenburg, Sweden, 27-29 June 2000.
2. R. Talwar, et al., "Friction Stir Welding of Airframe Structures", 2nd International Symposium on Friction Stir Welding, Gothenburg, Sweden, 27-29 June 2000.
3. B. Christner, "Development and testing of Friction Stir Welding (FSW) as a joining method for primary aircraft structure", 23rd ICAS congress, Toronto, Canada, 8-13 September 2002.
4. B. Christner, "A Friction Stir Welded Jet Aircraft: From Concept to Reality", 11th International Symposium on Friction Stir Welding, Cambridge, UK, 17th May 2016.
5. F. Fernandez, "FSW applied on mid-size aircraft", 8th International Symposium on Friction Stir Welding, Timmendorfer Strand, Germany, 18-20th May 2010.
6. L. Cederquist and A.P. Reynolds: "Factors affecting the properties of friction stir welded aluminium lap joints", *Weld. J. Res. Suppl.*, 80 (2001), pp. 281.

7. E. Aldanondo, et al., "Mechanical and microstructural properties of lap joints", 142nd TMS Annual Meeting & Exhibition – Friction Stir Welding and Processing VII, San Antonio, USA, March 2013, pp. 195-205.
8. G. Buffa et al., "Friction stir welding of lap joints: Influence of process parameters on the metallurgical and mechanical properties", *Materials Science and Engineering A*, 519 (2009), 19-26.
9. L. Dubourg et al., "Process optimisation and mechanical properties of friction stir lap welds of 7075-T6 stringers on 2024-T3 skin", *Materials and Design*, 31 (2010), 3324-3330.
10. S. Ji et al., "Effect of Reverse-threaded Pin on Mechanical Properties of Friction Stir Lap Welded Alclad 2024 Aluminum Alloy", *Journal of Materials Science & Technology*, 32 (2016), 671-675.
11. X. Yang et al., "Defect features and mechanical properties of friction stir lap welded dissimilar AA2024-AA7075 aluminum alloy sheets", *Materials and Design*, 55 (2014), 9-18.
12. H. Liu et al., "The effect of interface defect on mechanical properties and its formation mechanism in friction stir lap welded joints of aluminum alloys", *Journal of Materials Processing Technology*, 238 (2016), 244-254.
13. Aldanondo et al., "Microstructural features in friction stir welded lap joints", 10th International Conference on Trends in Welding Research, Tokyo, Japan, 10-14th October 2016.

9.- ARTICLE 6: DEVELOPMENTS IN STRINGER-SKIN LAP JOINTS BY FSW

[74] E. Aldanondo, E. Arruti, I. Quintana and J. Valer, "Developments in stringer-skin lap joints by FSW," in *12th International Symposium on FSW*, Chicoutimi-Quebec (Canada), 2018.

The work published in this article was another step to the concept of manufacturing of reinforced panels for the aeronautic sector using FSW technology. High strength aluminium alloys typically used in the aeronautic sector were used to produce the FSLW joints. The specific materials were a AA7050-T7651 extrusion on top of a AA2024-T3 and a AlcladAA7475-T761 rolled sheets. The feasibility of a robotic FSW system to produce these welds was also investigated. We concluded that it was possible to obtain high-quality FSLW joints with the mentioned alloys, even with the clad layer, in the robotic FSW system and using the new tool design with three flats and mixed thread.

This work was presented in the *12th International Symposium on FSW* in Chicoutimi-Quebec (Canada) and the article was published in the proceedings of the symposium.

DEVELOPMENTS IN STRINGER-SKIN LAP JOINTS BY FSW

Egoitz Aldanondo¹, Ekaitz Arruti¹, Ion Quintana², Juana Valer³

¹ IK4 LORTEK, Ordizia, Spain

² EDERTEK Technology Centre, Arrasate, Spain

³ AERNNOVA ENGINEERING DIVISION, Vitoria, Spain

SYNOPSIS

Manufacturing aeronautic structures joining extruded profiles or stringers to sheets or skins of aluminium is a very common practice in aeronautic structures. Although riveting is the conventional manufacturing technology to produce such lap joints, the Friction Stir Welding technology has also demonstrated its potential and feasibility in several applications of this kind. The solid state processing nature of FSW has enabled the adoption of FSW for the manufacturing of aircraft structures replacing riveting when aluminium alloys of series 2XXX and 7XXX are used, which was not feasible for other traditional fusion welding processes. Therefore, FSW technology has the potential to continue its implementation as a manufacturing process for aeronautic structures showing benefits such as time saving, light-weighting and overall cost reduction. However, it is very important to develop the appropriate technology and processing conditions to optimize the FSW joint properties and allow the production of high quality structures.

The study presented in this work shows the joint properties obtained in FSW tests performed in stringer-skin type of lap joints. An extruded profile of AA7050-T7651 aluminium alloy was used as stringer, which was welded in the overlap configuration to the skins. Skin materials were AA2024-T3 and AlCladAA7475-T761 alloy sheets of 2 mm in thickness. The AlCladAA7475-T761 sheet also had a cladding layer of pure aluminium in order to improve the corrosion resistance of the material. Different FSW tool designs and welding conditions were used to investigate their effects in the lap joint formation and the associated properties. A robotic FSW system was used for FSW tests showing a good capability to produce FSW lap joints. The weld quality and properties were examined by metallographic analysis and mechanical testing, including microhardness measurements and pull-out tests.

INTRODUCTION

FSW technology has been proposed in several applications as a potential process to substitute riveting as the main joining technology for aeronautic structure manufacturing [1-5]. The implementation of the technology for some aerospace developments involving stringer-skin joints in primary aircraft structures [3-5] evidence

the feasibility of FSW for such applications. However, in order to successfully implement FSW for stringer-skin joining in aeronautic applications, it is essential to optimize the technology to produce high quality joints, having a good understanding of their properties.

There have been a number of investigations focused on producing FSW lap joints and understanding the resulting joint properties [6-14]. It is necessary to optimize the FSW tool designs and processing parameters in order to minimize or avoid the typical imperfections in overlap FSW joints such as cold laps and hooking. Using double pass strategies has been proved [6, 7] to be effective but increases manufacturing time and cost. Other strategies have focused on the optimisation of the tool design, developing special tool geometries for overlap FSW [1, 2, 6-14]. The work reported in this paper focuses on the production of FSW lap joints using different probe designs and welding parameters, as well as in the evaluations of the obtained joint properties.

EXPERIMENTAL DETAILS

FSW lap joints were produced using extrusions of AA7050-T7651 alloy as stringer and AA2024-T3 as well as AlCladAA7475-T761 alloys as skin materials. The thicknesses of all materials in the overlapping joint area were 2mm. All FSW tests reported in this paper were performed using a KUKA KR500-3MT robotic system equipped with a specific FSW spindle and with capability to be operated in force control, which is shown in Figure 1.



Figure 1: Robotic FSW system at IK4 LORTEK used for FSW tests.

FSW joints as shown in Figure 2, Figure 3 and Figure 4 were performed using different FSW probe designs and welding conditions. A FSW tool with a shoulder of 12 mm in diameter was used for all FSW tests with the possibility to substitute probes of different design. Thus, the investigated probes and FSW parameters were the following ones:

- Threaded probe Vs threaded+3 flat probe
- Probe length: 2,2 and 2,5 mm

- FSW parameters:
 - 1000rpm, 150mm/min → weld pitch: 0,15mm/rev
 - 800rpm, 250mm/min → weld pitch: 0,31mm/rev

These 2 FSW parameter sets were used representing high and low heat input conditions in the FSW lap joint production. All FSW lap joints were produced using force control adjusting the appropriate axial force for each rotational speed and welding speed condition.



Figure 2: Part produced by stringer-skin FSW.

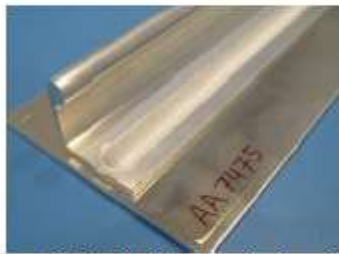


Figure 3: Detail of the beginning of the FSW joint.



Figure 4: Detail of the end of the FSW joint.

FSW lap joints were characterised by metallographic examination, microhardness measurements and pull-out strength static tests.

Metallographic examination of the FSW joints was conducted with cross-section specimens that were prepared following standard metallographic procedures. These included polishing to a mirror like finish and etching by submerging the specimens into a Keller's reagent for approximately 5 seconds, rinse in water and drying in a warm airflow. Weld cross sectional features of the FSW lap joints were investigated by an Olympus GX51 light optical microscope.

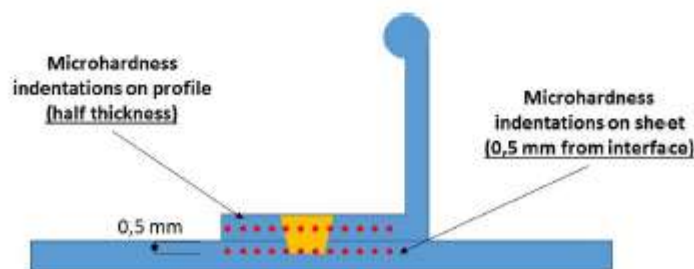


Figure 5: Microhardness scans performed in FSW lap joints with AA7050-T7651 and AlCladAA7475-T761 alloys.

Microhardness measurements were performed using a Vickers indenter and applying a load of 0,5Kg for 15 seconds. Scans of indentations were performed in both the stringer (AA7050-T7651 alloy) and the skin material (AlCladAA7475-T761 alloy) as shown in Figure 5 and with a spacing of 1 mm between indentations.

The mechanical strength of the FSW lap joints was evaluated by static pull-out tests as shown in Figure 6 and Figure 7. A Zwick Roell Z100 tensile testing machine was used for all pull-out testing. A special fixture was designed in order to clamp the specimens and apply the pulling force into the stringer while holding the skin in a fixed place.



Figure 6: Special jig for pull-out testing clamped in the tensile testing machine.

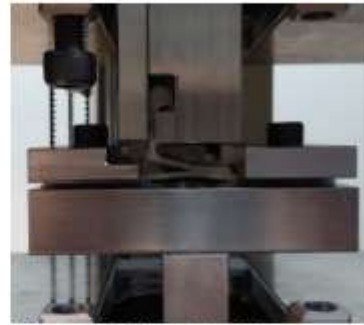


Figure 7: Pull-out test in progress.

RESULTS AND DISCUSSION

FSW lap joints produced using two different probe designs (threaded and threaded+3flats), probe lengths (2,2 and 2,5 mm), weld pitch (0,15 and 0,31 mm/rev) and skin material (AA2024-T3 and AlCladAA7475-T761) were prepared and examined. The desired effects when producing FSW lap joints are an effective mixing of top and bottom alloys in the joint interface by breaking and dispersing the oxides present at the interface, as well as the minimisation of the hook features at the advancing and retreating sides. In the case of using a skin material with a clad layer of pure aluminium, another aim to obtain a good quality weld is to achieve a good mixing of the clad material in the stirred zone. Macrostructural features of all FSW lap joints were analysed paying special attention to the hook size and the material mixing at the joint interface or the presence of cold lap features, as shown in the examples shown in Figure 8 and Figure 9. The following effects were observed:

- The hook sizes produced by the FSW tool with a threaded+3flat probe are slightly smaller in comparison with the ones with the simply threaded probe.
- The hook sizes produced by the FSW tool with a 2,5 mm long probe are larger than the ones produced by a 2,2 mm long probe.
- The FSW lap joints produced with a weld pitch of 0,15 mm/rev show larger hook sizes than the ones produced with a weld pitch of 0,31 mm/rev.
- The FSW lap joints produced by the FSW tool with a 2,5 mm long probe show a more effective cold lap elimination and a more extensive material mixing than the ones produced by a 2,2 mm long probe.

- The FSW lap joints produced with a weld pitch of 0,15 mm/rev show a more effective cold lap elimination and a more extensive material mixing than the ones produced with a weld pitch of 0,31 mm/rev.

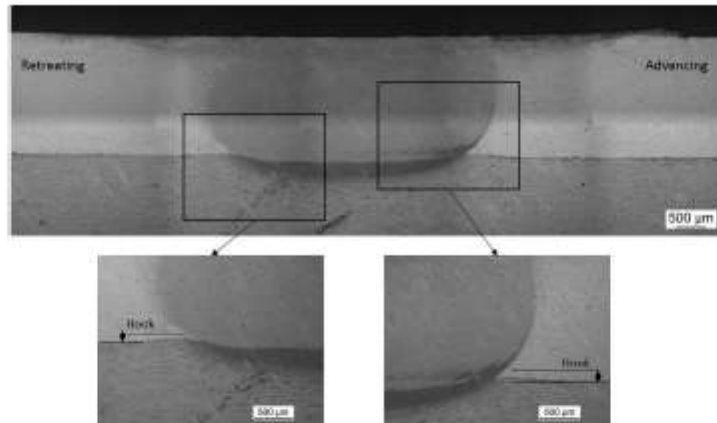


Figure 8: Metallographic cross-section of a FSW lap joint with AA7050-T7651 and AA2024-T3 alloys (probe length 2,2mm-threaded; 0,15mm/rev).

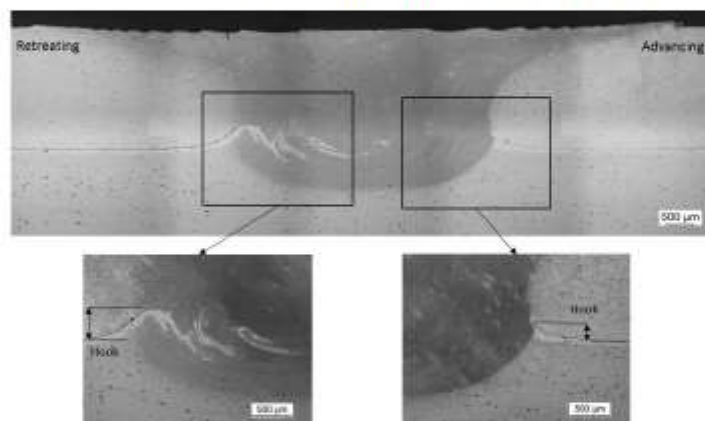


Figure 9: Metallographic cross-section of a FSW lap joint with AA7050-T7651 and AlCladAA7475-T761 alloys (probe length 2,5mm-threaded+3 flats; 0,31mm/rev).

The mentioned effects relative to hook formation and size are represented in the graphs shown in Figure 10 and Figure 11. One can clearly observe that the hook sizes produced by probe lengths of 2,5 mm are larger in comparison with 2,2 mm long probes. However the material mixing at the joint interface and cold lap elimination are more effective in the FSW lap joints produced by 2,5 mm long probes. The fact that the hook sizes produced with a higher weld pitch of 0,31 mm/rev are smaller can be clearly seen as well. Although it is not as obvious as the mentioned effects, the general trend of achieving smaller hook sizes by a threaded+3flat probe can be observed in Figure 10 and Figure 11.

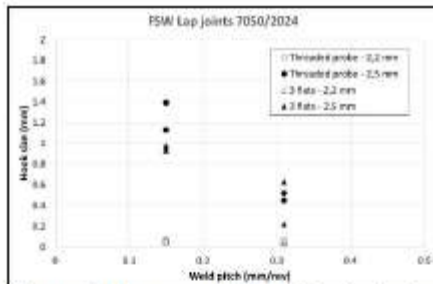


Figure 10: Representation of hook size for FSW lap joints produced under different conditions with AA7050-T7651 and AA2024-T3 alloys.

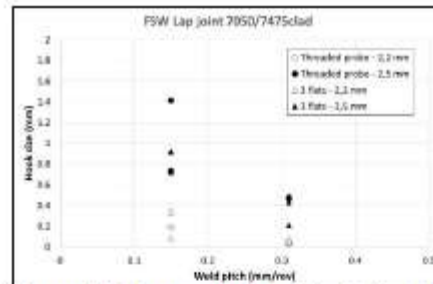


Figure 11: Representation of hook size for FSW lap joints produced under different conditions with AA7050-T7651 and AlCladAA7475-T761 alloys.

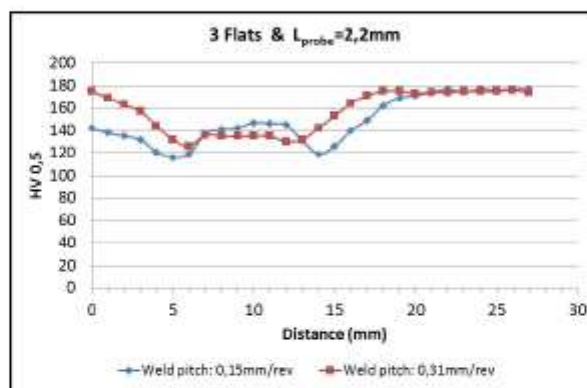


Figure 12: Microhardness measurements in the AA7050-T7651 profile.

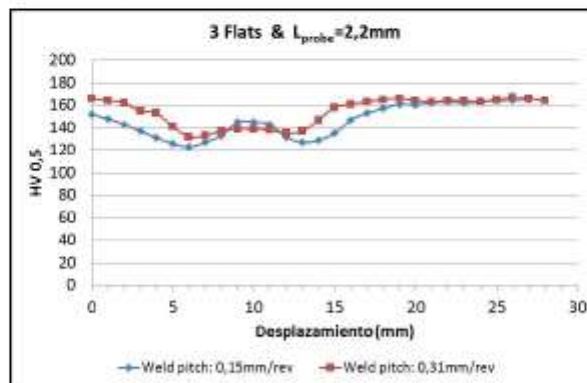


Figure 13: Microhardness measurements in the AlCladAA7475-T761 sheet.

Microhardness scans were performed in the extruded profile AA7050-T7651 (Figure 12) as well as in the sheet AlCladAA7475-T761 (Figure 13) in the FSW lap joints produced using this material combination. The expected effect of having larger HAZ

zones and hardness reductions in the FSW lap joints produced by a lower weld pitch of 0,15 mm/rev can be clearly observed in both extruded profile and the sheet materials. Thus, the following maximum hardness drops were observed:

- Extruded profile AA7050-T7651: From 180HV0,5 at base material to 120HV0,5 at the HAZ (~67% efficiency)
- Sheet AlCladAA7475-T7651: From 160HV0,5 at base material to 120HV0,5 at the HAZ (~75% efficiency)

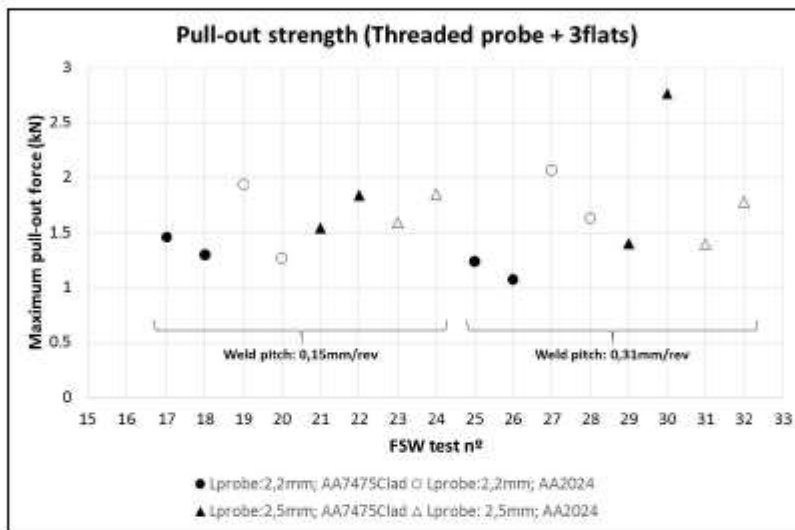


Figure 14: Pull-out strength results for different FSW conditions and alloy combinations.

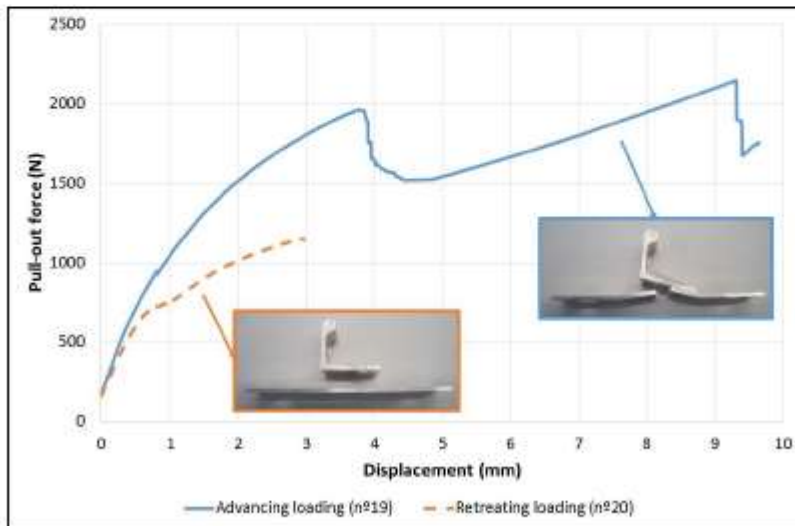


Figure 15: Force-displacement curve and failure mode in pull-out tests of FSW lap joints produced with AA7050-T7651/AA2024-T3 alloys; L_{probe} : 2,2mm; weld pitch 0,15mm/rev.

The average of the maximum pull-out force obtained from three test specimens for each FSW lap joints produced under different conditions is represented in Figure 14. The effect of loading the advancing or the retreating side of the joints was investigated for each FSW condition. In Figure 14 even test numbers represent retreating loaded specimens while odd numbers represent advancing loaded specimens. For FSW lap joints produced by tools with a probe length of 2,2 mm it was observed that the advancing side loading showed higher joint strengths than retreating loading cases (Figure 15). This effect could be explained by a larger bonding effect at the advancing side when low penetration and limited material mixing are achieved in the FSW process. Thus, the advancing loading case showed a sufficient load transferring capability from the stringer to the skin and the failure happened at the HAZ of the skin material. On the other hand, the retreating side showed insufficient joint strength to be able to transfer the load resulting in an interfacial failure of the FSW lap joint.

However, for FSW lap joints produced by tools with a probe length of 2,5 mm the performance of the advancing or retreating loading cases was observed to be different as shown in Figure 16. In these cases, the retreating loading cases showed a higher joint strength than the advancing loading cases. All failures were identified at the weld nugget boundary of the loaded side, being the failure initiation site the hook feature present at this location. The higher severity of the advancing side hook was considered as the main factor for the lower load bearing capability of the FSW lap joints with advancing loading.

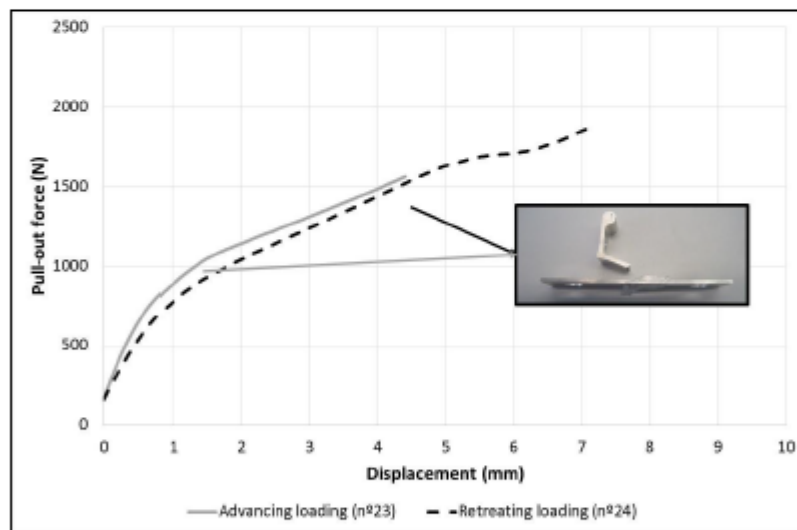


Figure 16: Force-displacement curve and failure mode in pull-out tests of FSW lap joints produced with AA7050-T7651/AA2024-T3 alloys; L_{probe} : 2,5mm; weld pitch 0,15mm/rev.

Some significant difference were also identified in pull-out performance between FSW lap joints produced using the AICladAA7475-T761 or the AA2024-T3 skin materials. In this occasion, the clad layer present at the AICladAA7475-T761 played a significant

role on the joint strength as it can be observed in Figure 17. The following effects were observed:

- In case of using a probe length of 2,2 mm, FSW lap joints produced under similar processing conditions but with AlCladAA7475-T761 and the AA2024-T3 skin materials (n°25 and n°27 in Figure 17) showed different joint performances. The joint with AlCladAA7475-T761 alloy showed a low strength with an interfacial failure which was related to an insufficient stirring and mixing of the clad layer in the weld.
- In case of using a probe length of 2,5 mm, FSW lap joints produced with AlCladAA7475-T761 and the AA2024-T3 skin materials (n°29 and n°31 in Figure 17) showed a similar joint performance. This indicates a good stirring and mixing of the clad layer at the joint interface, resulting in a failure through the hook feature at the advancing side.
- FSW lap joints produced by a probe length of 2,5 mm and AlCladAA7475-T761 as skin material have shown a higher pull-out strength with the retreating loading case in comparison with the advancing loading case (n°30 and n°31 in Figure 17). Thus, the retreating loading specimens generally showed failures on the stringer at higher pull-out forces while the advancing loading specimens showed failures through the hook feature at the boundary of the weld.

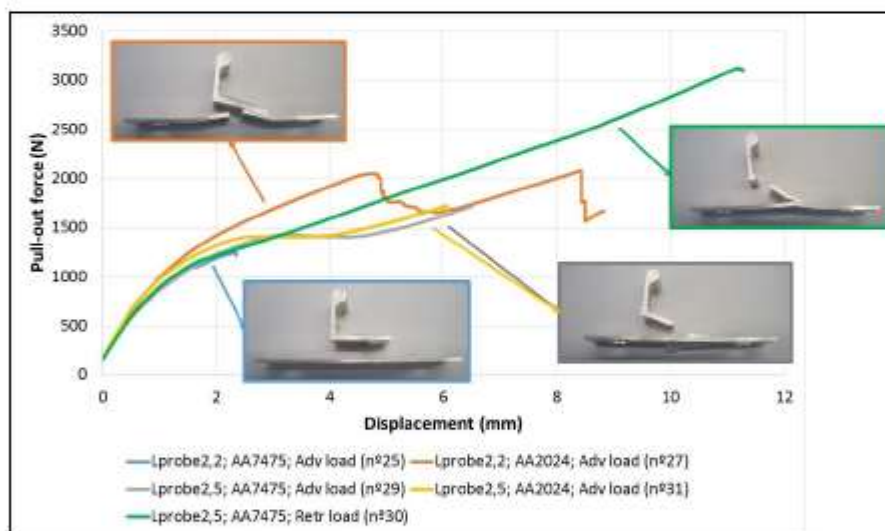


Figure 17: Force-displacement curve and failure mode in pull-out tests of FSW lap joints produced with a weld pitch of 0,31mm/rev.

SUMMARY AND CONCLUSIONS

FSW lap joints were produced using AA7050-T7651 alloy as stringer and AA2024-T3 or AlcladAA7475-T761 alloys as skin materials using different FSW processing conditions. The joint properties were investigated by metallographic examination, microhardness testing and pull-out static strength evaluation. The analysis of the results showed the relationships between processing parameters, micro-macrostructural properties and the mechanical strength of the FSW joints. The effects produced in the two different skin materials with specific detail in the clad layer influence were observed and appropriate FSW processing conditions were identified for each material.

REFERENCES

- [1] M.J. Booker et al., "Applying Friction Stir Welding to the Ariane 5 Main Motor Thrust Frame", 2nd International Symposium on Friction Stir Welding, Gothenburg, Sweden, 27-29 June 2000.
- [2] R. Talwar, et al., "Friction Stir Welding of Airframe Structures", 2nd International Symposium on Friction Stir Welding, Gothenburg, Sweden, 27-29 June 2000.
- [3] B. Christner, "Development and testing of Friction Stir Welding (FSW) as a joining method for primary aircraft structure", 23rd ICAS congress, Toronto, Canada, 8-13 September 2002.
- [4] B. Christner, "A Friction Stir Welded Jet Aircraft: From Concept to Reality", 11th International Symposium on Friction Stir Welding, Cambridge, UK, 17th May 2016.
- [5] F. Fernandez, "FSW applied on mid-size aircraft", 8th International Symposium on Friction Stir Welding, Timmendorfer Strand, Germany, 18-20th May 2010.
- [6] L. Cederquist and A.P. Reynolds: "Factors affecting the properties of friction stir welded aluminium lap joints", *Weld. J. Res. Suppl.*, 80 (2001), pp. 281.
- [7] L. Dubourg et al., "Process optimisation and mechanical properties of friction stir lap welds of 7075-T6 stringers on 2024-T3 skin", *Materials and Design*, 31 (2010), 3324-3330.
- [8] G. Buffa et al., "Friction stir welding of lap joints: Influence of process parameters on the metallurgical and mechanical properties", *Materials Science and Engineering A*, 519 (2009), 19-26.
- [9] S. Ji et al., "Effect of Reverse-threaded Pin on Mechanical Properties of Friction Stir Lap Welded Alclad 2024 Aluminum Alloy", *Journal of Materials Science & Technology*, 32 (2016), 671-675.

- [10] X. Yang et al., "Defect features and mechanical properties of friction stir lap welded dissimilar AA2024-AA7075 aluminum alloy sheets", *Materials and Design*, 55 (2014), 9-18.
- [11] H. Liu et al., "The effect of interface defect on mechanical properties and its formation mechanism in friction stir lap welded joints of aluminum alloys", *Journal of Materials Processing Technology*, 238 (2016), 244-254.
- [12] Aldanondo et al., "Microstructural features in friction stir welded lap joints", 10th International Conference on Trends in Welding Research, Tokyo, Japan, 10-14th October 2016.
- [13] Aldanondo et. al., "Friction Stir Weld lap joint properties in aeronautic aluminium alloys", 146th TMS Annual Meeting & Exhibition – Friction Stir Welding and Processing IX, San Diego, USA, February 2017, pp. 109-118.
- [14] Z. Liu, Z. Zhou, S. Ji, "Improving interface morphology and shear failure load of friction stir lap welding by changing material concentrated zone location", *The International Journal of Advanced Manufacturing Technology*, 95 (2018): 4013-4022.

10.- ARTICLE 7: INFLUENCE OF PIN IMPERFECTIONS ON THE TENSILE AND FATIGUE BEHAVIOUR OF AA7075-T6 FRICTION STIR LAP WELDS

[75] M. Balakrishnan, C. Leitao, E. Arruti, E. Aldanondo and D. M. Rodrigues, "Influence of pin imperfections on the tensile and fatigue behaviour of AA7075-T6 friction stir lap welds," *The International Journal of Advanced Manufacturing Technology*, pp. Published online - 23 May 2018, 2018.

A deeper investigation of the mechanical properties of FSLW joints produced using the AA7075-T6 aluminium alloy was performed in this work. Static tensile strength as well as fatigue strength of the FSLW joints was investigated with welds produced using different tool designs simulating pin imperfections and welding parameters. This was the first approach to the investigation of fatigue performance of these type of welds. We concluded that for base materials above three millimetres in thickness, it was necessary to use tool designs with larger flat features in order to improve the properties of the FSLW joints significantly.

This article was published in the journal "The International Journal of Advanced Manufacturing Technology".



Influence of pin imperfections on the tensile and fatigue behaviour of AA 7075-T6 friction stir lap welds

M. Balakrishnan¹ · C. Leitão² · E. Arruti³ · E. Aldanondo³ · D. M. Rodrigues¹

Received: 27 March 2018 / Accepted: 13 May 2018
© Springer-Verlag London Ltd., part of Springer Nature 2018

Abstract

Friction stir lap welds in AA 7075-T6 aluminium alloy were produced using tools with and without geometrical imperfections and varying welding pitch. Geometrical imperfections, resulting from the damage of the tool during the welding of the hard aluminium alloy, were simulated by machining small flats in the pin threads. Material adhesion to the worn tool was simulated by increasing the welding pitch. The welds produced were characterised, in the as-welded and heat-treated conditions, by performing monotonic and cyclic tensile-shear tests, micro-hardness measurements and metallography. The peak temperatures reached during welding were calculated using the spindle torque. No important differences in heat generation were registered when varying the welding conditions. The morphology and size of the lap weld defects were analysed in order to assess the influence of tool damage on welds properties. Material adhesion to the tool, simulated by increasing the welding pitch, showed to have a stronger influence on defect size than the thread imperfections. The small changes in welds defect size had no important effect on the monotonic strength of the welds, but had important influence on the fatigue behaviour. An increase of around 10% in the effective sheet thickness of the CL joints resulted in an increase of 500% in the fatigue life. Improved fatigue performance was also registered for the welds performed with the tool with pin imperfections indicating that sensitive tool damage will have no negative influence on the performance of the lap welds.

Keywords FSW · Lap welding · Tool · Wear · Fatigue

1 Introduction

The research developed worldwide on friction stir welding (FSW) addressed several aspects of process development and the characterisation of a very wide range of welds [1]. The important influence of the FSW tool characteristics on the thermo-mechanical conditions developed during welding and on defect formation is now well known [2]. Inefficient flow of material around and beneath the tool and/or inadequate heating conditions are considered as the main causes in defect formation [3, 4]. However, it is also well known that

FSW defects' typology also depends on the joint configuration. Hook and cold lap defects are typical in friction stir lap welding (FSLW) but are absent in butt joining. These defects, which result from the interaction between the tool and the top and bottom sheets lap interface, are very sensitive to the tool geometry [5, 6].

Several works addressing the role of the FSLW tool geometry on lap welds defect shape and size can be found in the literature. Most of these works' tested the use of conventional tool geometries, as well as new tool designs, in lap welding of aluminium alloys. Buffa et al. [7] concluded that using tools

✉ D. M. Rodrigues
dulce.rodrigues@dem.uc.pt

M. Balakrishnan
balakrishnan.marimuthu@dem.uc.pt

C. Leitão
cafo.leitao@dem.uc.pt

E. Arruti
earuti@lortek.es

E. Aldanondo
egoitz@lortek.es

¹ ISE, Department of Mechanical Engineering, University of Coimbra, Coimbra, Portugal

² CEMMPRE, Department of Mechanical Engineering, University of Coimbra, Coimbra, Portugal

³ IK4 LORTEK, Ordizia, Gipuzkoa, Spain

with cylindrical-conical pins allows obtaining good lap joining quality for a varied range of rotational speeds. Costa et al. [8, 9] investigated the use of cylindrical and conical pin profiles, with different diameters and taper angles, in similar and dissimilar lap joining of thin aluminium sheets. They concluded that using unthreaded conical pin tools, with a low shoulder/pin diameter ratio, resulted in better joint strength. Babu et al. [10] also concluded that the use of taper cylindrical pins enables controlling the hook geometry in FSLW of Al alloy 2014-T4. Tools with conical threaded pin, cylindrical-conical threaded pin, stepped-conical threaded pin and flared triflute pin were also tested by Salari et al. [11]. They concluded that the stepped-conical threaded pin profile offered better joint integrity in thick plates welding. Park et al. [12] showed that the tool shoulder has also an important role in the quality of the lap joints. The use of an externally assisted stationary shoulder was tested in the welding of AA 6061 Al and AZ31 Mg [13], AA 6061-T6 [14] and AA 2024-T6 [15, 16] alloys. The effect of the tool shoulder diameter and welding pitch was investigated in dissimilar FSLW of AA 6111 and AA 5023 alloys [12]. Improved lap shear strength, as well as improved surface quality, was obtained when larger shoulder diameter tools and fast welding pitch were used.

Analysing the works in the previous paragraph, it becomes clear that the lap welds' quality is very sensitive to the tool geometry. Therefore, additional difficulties in controlling lap welds defects' formation has to be previewed when the FSW tool geometry is changed during welding due to wear. Tool wear occurs during the welding of very hard materials [2, 17], but also during FSW of aluminium alloys, after long utilisation, especially for the hard alloys of the 7xxx series. Prado et al. [18] analysed the evolution of the FSW tool geometry during butt-welding of a metal matrix composite (MMC) with a steel tool. These authors depicted a strong influence of the rotation and traverse speeds on tool degradation. They also found that the degradation of the pin threads had a strong influence on the material flow. Siddiquee and Pandey [19] studied the wear behaviour of a tungsten carbide (WC) tool in FSW of AISI 304 steel. They observed important wear of the pin and analysed the wear mechanisms. Thomson and Babu [20] also analysed the pin wear mechanism in FSW of a high-strength steel with tungsten-based tools and concluded that tool wear mechanisms also depend on the tool material.

None of the works cited on FSW tool wear report the influence of sensitive wear of the pin on the monotonic and fatigue strength of the friction stir welds. This type of analysis is especially important in lap welding by FSW, due to the extreme sensitivity of the lap defect size and morphology on pin geometry. In current work, this subject is analysed by comparing the characteristics of welds produced with cylindrical threaded tools with and without wear. Tool wear was simulated by machining flats to simulate the damage of the pin threads after long utilisation. The two types of tools were

tested in the lap welding of AA7075-T6 aluminium sheets, using two different welding pitches. According to Mehta et al. [21], the welding pitch has a strong influence on the material adhesion to polygonal pins. This way, varying the welding pitch, differences in welding conditions associated with material adhesion to the tool were simulated. The lap joints strength, morphology and defect size were compared in order to assess the influence of pin wear and/or material adhesion on lap joints properties.

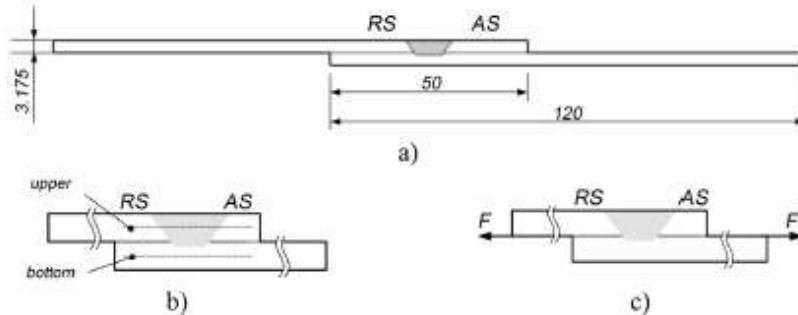
2 Experimental procedure

The base material used in this work was the AA 7075-T6 aluminium alloy supplied in 3.175 mm thick sheets. Figure 1a shows the joint configuration adopted. Two different tools were used: (i) a tool with a threaded cylindrical pin (CL), with the geometry and dimensions specified in Fig. 2a; (ii) a tool with a cylindrical threaded pin in which some flats were machined (FT) in order to simulate geometrical and dimensional imperfections in tool geometry resulting from wear. The geometry and dimensions of the FT tool are specified in Fig. 2b. Table 1 shows the welding parameters used. The same combinations of welding speed and rotational speed were used for both tools. Process parameters were selected in order to obtain welding pitches of 0.15 and 0.30 mm/rev. All welds were produced in an iSTIR PDS4 FSW machine using force control. The axial force was adjusted according to the welding pitch being used 8.9 and 9.6 kN when welding at 0.15 and 0.30 mm/rev, respectively. Using the FSW machine output data, the average torque values, for each welding test, were calculated and used to estimate the peak temperature reached during welding. In the text, the different samples will be labelled according to the tool geometry and welding pitch used to fabricate the lap joints, i.e. the samples of the weld produced with the cylindrical threaded tool and 0.3 welding pitch will be labelled CL030.

Post-welding heat treatment (PWHT), consisting of a solubilisation at 480 °C, for 2 h, was performed in a Temolab oven with a Eurothem controller 32166P. PWHT was conducted with two objectives: (1) to promote abnormal grain growth (AGG) and evidence possible differences in material flow mechanisms during welding, as explained in [22], and (2) to homogenise the strength across the welds, suppressing the influence of the weld softening on the strength of the joints, as explained in [23]. In the text, the welds in the as-welded condition will be labelled AW and the heat-treated welds will be labelled HT.

Hardness measurements were done in both the bottom and top sheets, as illustrated in Fig. 1b. The specimens for metallography were etched with modified Poulton's reagent (6 ml HCl, 8 ml HNO₃, 2.5 ml HF, 2.4 g CrO₃, 12 ml 8.5 ml H₂O). The analysis of microstructures was done using an optical microscope

Fig. 1 Joint configuration (a), hardness measurement lines (b) and loading mode in tensile-shear testing (c)



Leica DM 4000M. The tensile strength of the base metal and the tensile-shear strength of the weld samples were evaluated by performing tests in an INSTRON 4206 uniaxial tensile testing machine. To avoid bending of the samples during loading, two small plates of the same thickness of the welded sheets were fixed at each end of the tensile-shear samples. As represented in Fig. 1c, all the welds were tested using retreating side loading mode. The cyclic loading tensile-shear tests were performed in an INSTRON Electro Plus E1000 machine, supported with INSTRON 8800 acquisition and control system. Sinusoidal loads with a frequency of 15 Hz, a stress ratio set to $R = 0.01$ and stress ranges between 30 and 175 MPa were used. The load amplitude and mean load were calculated taking into account the values of the stress range $\Delta\sigma$, the thickness of the weld, the width of the specimen and the stress ratio.

3 Results and discussion

3.1 Torque and temperature

In Fig. 3 are plotted the average torque (M) values, for each welding test, calculated using the torque evolution during

welding. The peak temperature attained during welding (\bar{T}) was estimated using the equation [24]

$$\bar{T} = T_0 + M\omega \left(\frac{\eta K_0}{2\pi k} \right) \tag{1}$$

where T_0 is the initial temperature of the base material, M the average torque, ω the rotational speed, η the process efficiency, K_0 the modified Bessel function of second kind and 0 order and k the thermal conductivity. A process efficiency of 50% was used. The figure shows that the average torque increased when the welding pitch was increased from 0.15 to 0.30. The increase in the average torque was associated with a slight decrease, of around 8%, in the peak temperature, showing that no important differences in heat generation occurred when changing the tool or the welding pitch. This way, any differences in welds properties/characteristics may be attributed to the differences in the material flow promoted by the tool and considered independent of the thermal cycles induced by the process. More precisely, it is possible to say that the increase of the average torque, when increasing the welding pitch, results from the increase in the volume of material stirred by the tool. In current work, the increase of the volume of

Fig. 2 CL (a) and FT (b) tool geometries and dimensions

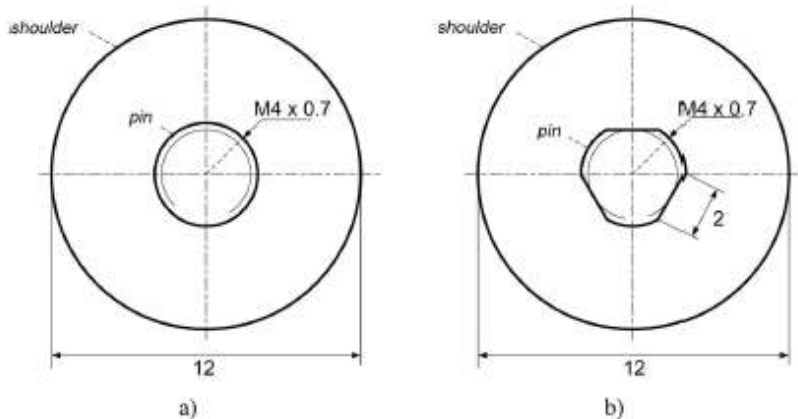


Table 1 Welding parameters

Tool design	ω [rpm]	v [mm/min]	Welding pitch [mm/rev]	Samples
CL	1000	150	0.15	CL015
CL	800	250	0.30	CL030
FT	1000	150	0.15	FT015
FT	800	250	0.30	FT030

material stirred by the tool is used to simulate any possible adhesion of extra material to the tool when welding in an industrial environment.

3.2 Metallographic analysis

In Fig. 4 are shown macrographs of the cross-sections of the welds in the AW (Fig. 4a, b, e and f) and HT (Fig. 4c, d, g and h) conditions. The images relative to the AW welds enable to depict that the morphology of the nugget did not change drastically when the welding conditions were changed. The only spotted difference is a slightly larger nugget size in the shoulder-flow arm region for the welds fabricated with 0.30 welding pitch. This is in agreement with the higher adhesion of material to the tool, already associated to the higher welding torque registered for this welding conditions.

The images relative to the HT samples enable to see that the solution treatment conducted to abnormal grain growth (AGG) in the region of the nugget, that is, in the region of the welds subjected to intense plastic deformation and dynamic recrystallization during the welding. The mechanisms of AGG during PWHT of heat-treatable aluminium alloys are well explained in [22, 23] and will be not addressed in current paper. In current work, only the differences in abnormal grain morphology, between the different welds, will be analysed and related to tool characteristics and welding conditions.

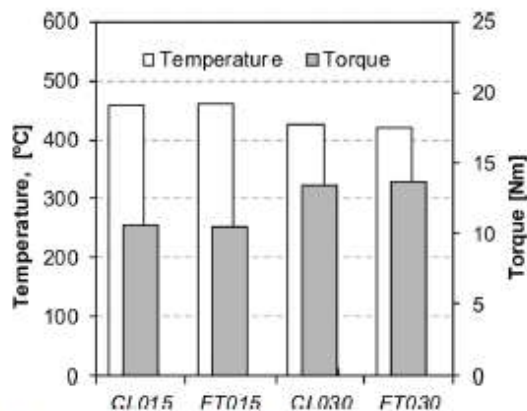


Fig. 3 Average torque (M) and peak temperatures (T)

The images in Fig. 4, relative to the HT welds, enable to see that the abnormal grain size/morphology is not uniform throughout the nugget. The grains are clearly coarser and oriented in the direction of the flow of the material, in the regions of the nugget located in the upper sheet. The grains have smaller dimension and equiaxial shape in the nugget regions in the lower sheet. Observing Fig. 5, where are shown magnified images of the HT welds cross-sections in the region near the original interface of the sheets, it is possible to conclude that for the welds made with 0.15 welding pitch, the abnormal grains, at the advancing side, extend from the upper to the lower sheet. This microstructural continuity indicates that the interface between the sheets was suppressed during the welding. The same is not observed at the advancing side of the welds made with 0.30 welding pitch, for which it is possible to observe a discontinuity in grain size/structure in the region of the original interface of the sheets. These results evidence some influence of material adhesion to the tool on the welding conditions. No differences in abnormal grain size or structure may be observed by comparing the cross-section of the welds made with the CL and FT tools and using the same welding pitch.

The images in Fig. 5 also show the presence of the hook defect, at the advancing side, and of the cold lap defect, at the retreating side, of all the welds. The images enable to conclude that, for the CL015 and FT015 welds, the cold lap defect corresponds to the frontier between the regions with coarse and small abnormal grain. The small abnormal grains occur in the regions of the nugget located in the lower sheet, below the cold lap defect discontinuity, in a region where the upper and lower sheet materials were not mixed under the stirring action of the pin. For the welds CL030 and FT030, the region with the smaller abnormal grain, in the lower sheet, extends from the retreating side, where the cold lap discontinuity can be seen, to the advancing side of the weld, where no previous interface remnant is visible.

No significant influence of the pin imperfections on the interface morphology or defect size can be depicted when comparing the images in Figs. 4 and 5. Welding pitch was the main factor governing welds' characteristics due to its influence on the volume of material stirred by the tool. In order to prove these assumptions, the effective sheet thickness (EST), at the advancing and retreating sides of the welds, as well as the bonded interface width (BIW), was measured. In Fig. 6a-c are shown schemes of the welds, clarifying how the measurements of EST and BIW were done. In Fig. 6d are plotted, for all the welds, the relative sizes %BIW, %EST_{AS} and %EST_{RS}, calculated by dividing the BIW and EST values by the pin diameter and sheet thickness, respectively, as shown by Eqs. (2) to (4) in Fig. 6. The results show that the pin imperfections had no influence on EST, but a small influence on BIW, i.e. a small increase in BIW was registered when changing from

Fig. 4 Cross-sections of the welds in the as-welded (a, b, e, f) and heat-treated (c, d, g, h) conditions

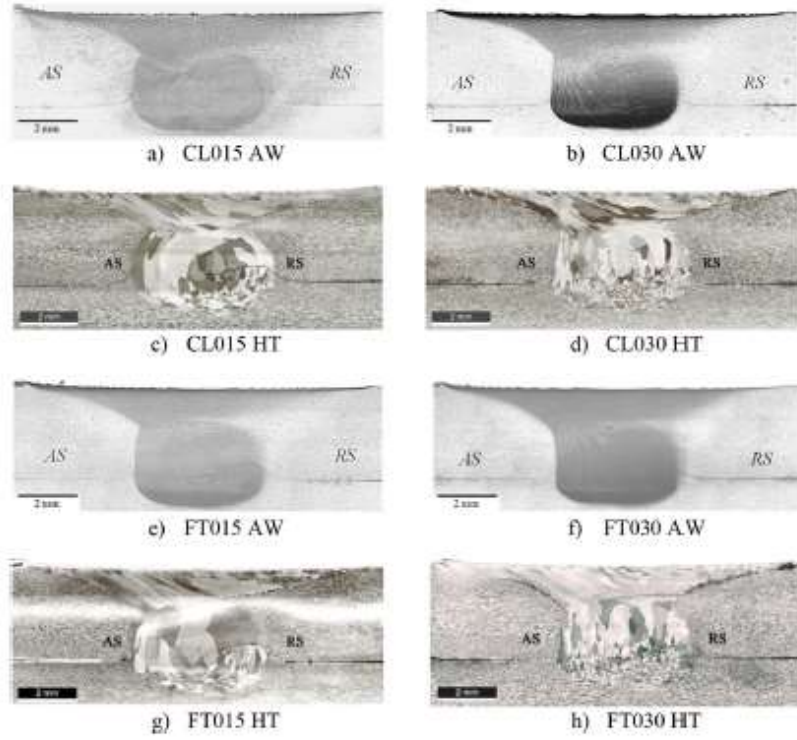


Fig. 5 Details of the bonding region of the welds

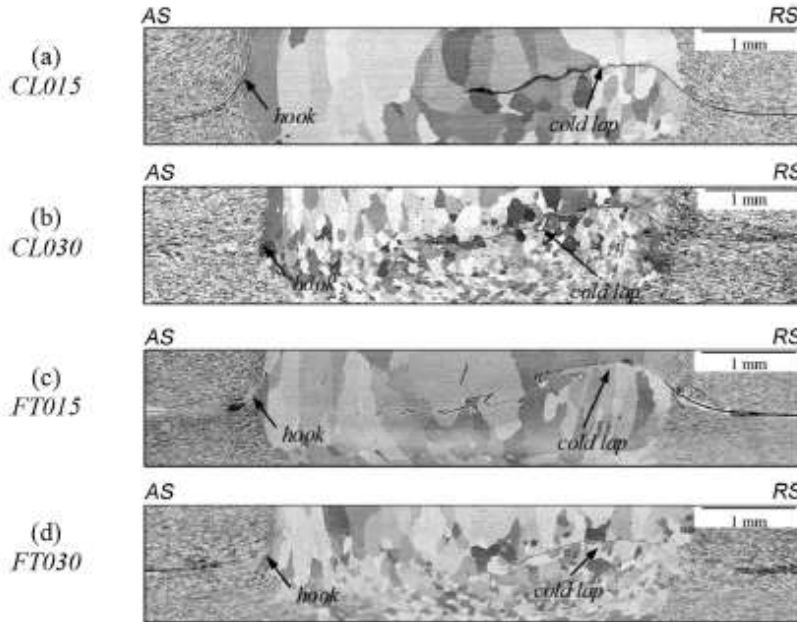
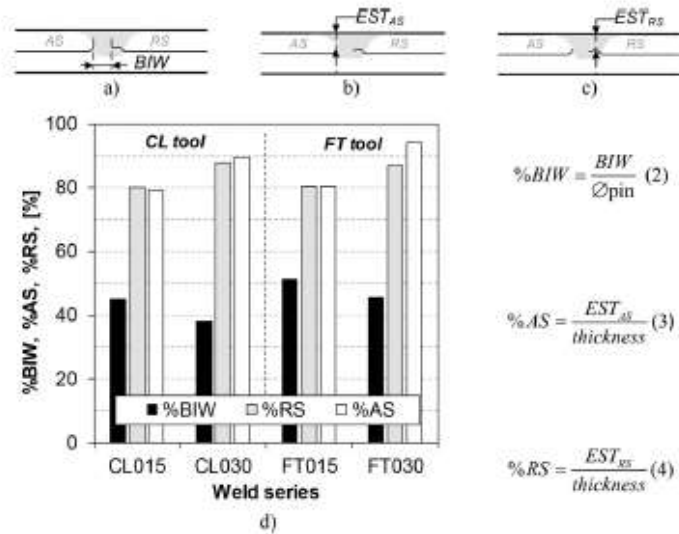


Fig. 6 EST and BIW measurements comparison



the CL to the FT tool. For both pin geometries, both EST_{AS} and EST_{RS} were increased when the welding pitch was increased from 0.15 to 0.30 and BIW was decreased.

4 Mechanical characterisation

4.1 Hardness testing

Figure 7a, b shows the hardness profiles, for the top and bottom sheets, respectively, of the AW and HT welds. In the graphs, it is also represented, by a discontinuous grey line, the average hardness of the base material before welding (7075-T6) and after PWHT (7075-HT). The hardness profiles of the AW joints show a significant decrease in hardness, in the weld, relative to the original base metal. The figures also show that the change of process parameters and tool geometry did not lead to significant differences in the hardness values/distribution, between the different welds. The similarity in hardness distributions corroborates the previous assumption that no important differences in temperature occurred during the different welding operations.

Figure 7 also shows that the hardness profile of the upper sheet, with a W shape, typical of welds in heat-treatable alloys [23, 25–27], is similar for all welds and differs from the lower sheet hardness profile. The differences in hardness profiles shape are easy to be understood considering that the upper sheet profiles intersect the base metal, heat-affected zone (HAZ) and thermo-mechanical affected zone (TMAZ), at both the advancing and retreating sides of the welds, while the hardness profile of the lower sheets only intersects the HAZ under the nugget. This is best illustrated in Fig. 8 where the

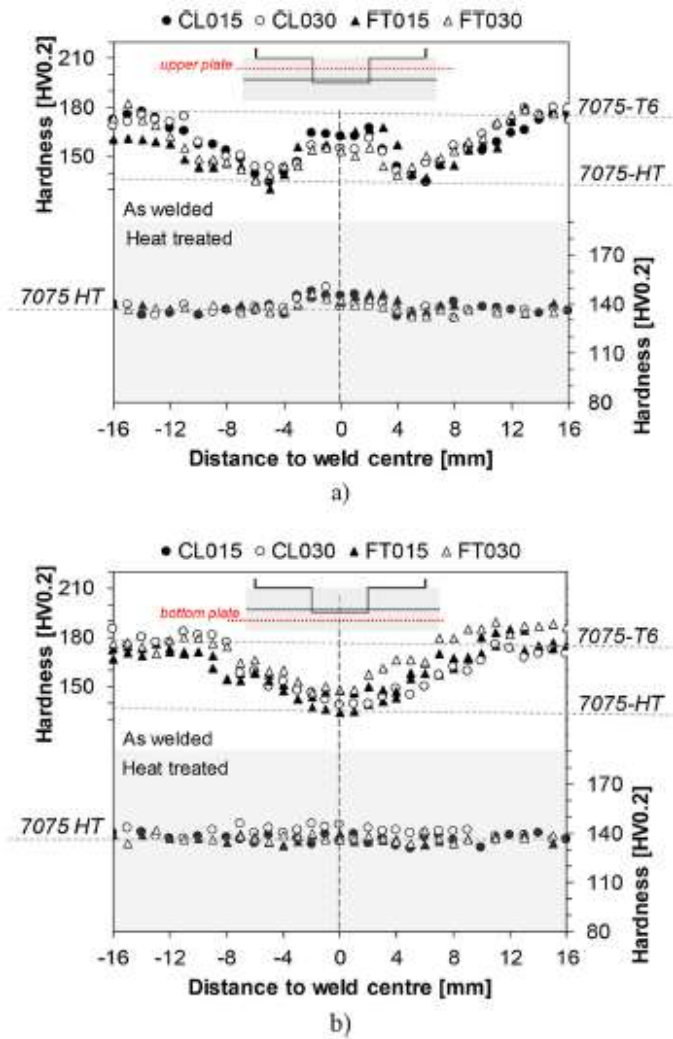
hardness profiles for the CL015 sample were overlapped to an image of the cross-section of the weld. This figure shows that the minimum hardness values were registered not only in the upper sheet HAZ, at the advancing and retreating sides of the welds, but also in the lower sheet HAZ, proving that the heat dissipation was symmetrical around the tool pin. The heat dissipation to the lower sheet, for a joint in which the tool was mainly in contact with the upper sheet, was the reason why a process efficiency of 50% was used in Eq. (1).

Analysing now the hardness profiles for the HT welds, also plotted in Fig. 7, it is possible to conclude that the solution heat treatment resulted in the homogenisation of the hardness along the cross-section of all the welds, both in the lower and upper sheets. The average hardness in the different regions of the weld, and the base metal, after heat treatment, became 137 HV0.2, which is much lower than the original hardness of the base metal (177 HV0.2). As explained in [26], this decrease in hardness, relative to the base material, is associated with the dissolution of the hardening precipitates during the PWHT. The similarities in hardness values between the HAZ of the different welds and the hardness of the HT samples show that the peak temperatures reached during welding were close to that used in the PWHT (480 °C), showing that the values calculated by Eq. (1) are acceptable.

4.2 Tensile testing

The normalised maximum tensile-shear loads (NML) for the AW and HT samples, of all the welds, are plotted in Fig. 9 together with macrographs of some of the samples after rupture. As shown by Eqs. (5) and (6) in the figure, the normalised maximum loads were calculated by dividing the average

Fig. 7 Hardness profiles for the AS and HT welds. Top (a) and bottom (b) sheet.

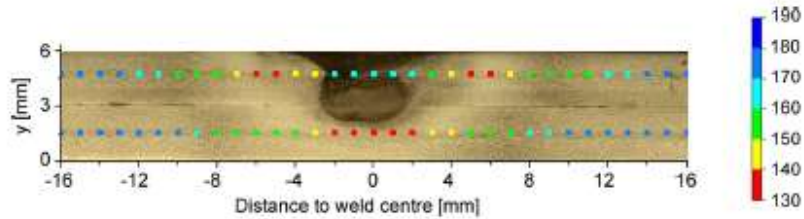


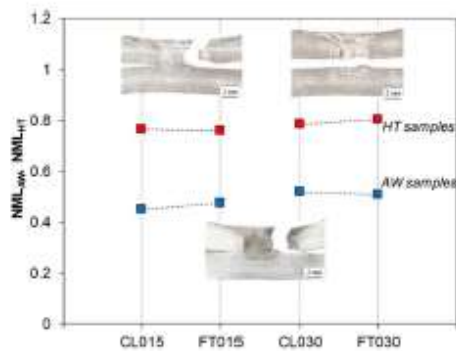
of the maximum loads registered in the tensile-shear tests of the AW and HT samples by the yield load of the base material in the T6 and solubilised conditions, respectively. The yield strength of the base material in the AW and HT conditions was

determined by testing tensile samples of the same width of the tensile-shear weld samples.

Figure 9 shows that the maximum strength of the AW samples was only 40% of that of the base material, in the T6

Fig. 8 Hardness distribution for the CL015 weld in the AW condition





$$NML_{AW} = \frac{F_{max}^{AW}}{F_{max}^{HT}} \quad (5)$$

$$NML_{HT} = \frac{F_{max}^{HT}}{F_{max}^{HT}} \quad (6)$$

Fig. 9 Normalised maximum load for the AW (NML_{AW}) and HT (NML_{HT}) in monotonic loading and macrographs of the tensile-shear samples after failure

condition, but was of the order of 80 to 90% of that of the solution-treated base material, for the HT welds. For the AW welds, the important loss of strength of the joint in comparison to the as-supplied base material strength was determined by the TMAZ and HAZ softening and by the presence of the cold lap defect at the retreating side. For the HT welds, the loss of strength relative to the solution-treated base material was only determined by the cold lap defect, conducting to an improved performance of these joints in tensile-shear loading relative to the AW joints. The figure also enables to observe small differences in maximum load values, between the welds produced with 0.15 and 0.30 welding pitch and the different tools, indicating that tool imperfections/wear will have a very small influence on the monotonic strength of the joints. In spite of the very small differences in monotonic strength, the CL30 and FT30 welds had higher strength than the CL15 and FT15 welds. This small increase in strength, which is related to the increase in EST_{RS} observed in Fig. 6, shows the high sensitivity of these joints to welding defect size.

As exemplified by the AW sample macrograph in the figure, regardless of the process parameters and of the type of tool used in their execution, the rupture of the AW samples occurred in the upper sheet TMAZ, in the region of the sample where the thickness was smallest, that is in the region of the cold lap defect. The macrograph also shows that the rupture was initiated in the cold lap defect, propagating horizontally, into the nugget, and only then vertically, towards the surface of the upper sheet. This way, the final strength of the AW joints was mainly determined by the effective sheet thickness at the retreating side. For the HT samples, significant differences in the mode of rupture were observed between the joints produced with 0.15 and 0.30 welding pitch. More precisely, the welds performed with the higher welding pitch (FT30 and

CL30) had failure by separation of the two sheets, parallel to its original interface. The welds made with the lower welding pitch (FT15 and CL15) had failure by rupture of the upper sheet, in the cold lap defect region, as registered for the AW samples. The differences in the mode of failure are related to the increase in EST_{RS} and decrease in BIW, when increasing the welding pitch, as registered in Fig. 6. The welds FT30 and CL30 that had failure by separation of the two sheets, parallel to the original interface, had slightly higher strength than the FT15 and CL15 joints. This way, it can be concluded that the final strength of the HT joints was determined by the effective bonding width between the two sheets.

4.3 Fatigue testing

The fatigue tests were only conducted for the welds in the AW condition. Figure 10 shows the S-N curves, in a logarithmic scale, for all the welds analysed in this work. The curves relate the stress amplitude applied during the fatigue tests to the number of cycles until the specimens rupture. The results indicate that, regardless of the tool geometry, the fatigue strength was higher for the welds performed with the higher welding pitch (CL30 and FT30) and was lower for the welds performed with the lower welding pitch (CL15 and FT15). Independently of the fatigue strength, all the welds had failure by rupture of the upper sheet, in the cold lap defect region, as shown in Fig. 11a. So the differences in fatigue life, which can reach 500% for the welds produced with the CL tool, may be explained by the differences in EST_{RS} registered in Fig. 6, for the CL15 and CL30 welds. These results also show that lap welds defect size has a much stronger influence on fatigue life than on monotonic strength.

Figure 10 also enables to observe that the fatigue curves for the welds performed with the FT tool fall between that of the

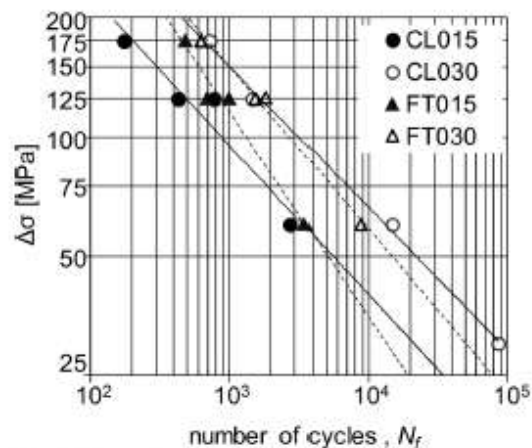
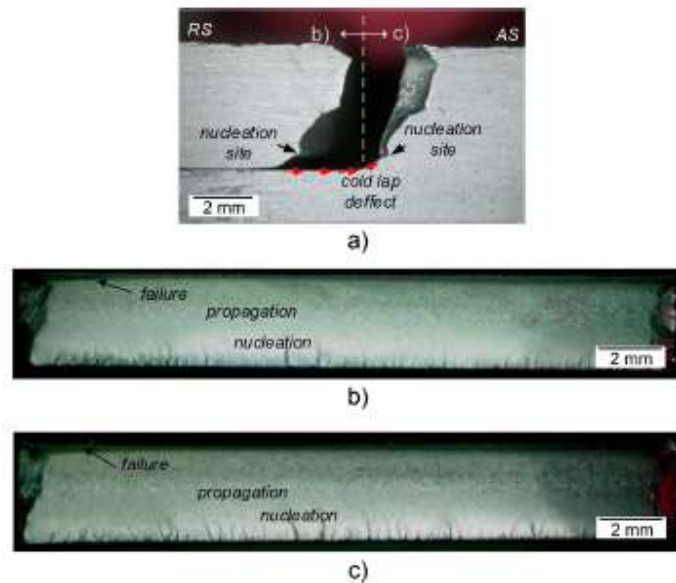


Fig. 10 Fatigue testing results

Fig. 11 Fatigue fracture surfaces



CL30 and CL15 welds. These results show that the probe imperfections had a positive effect on the fatigue strength of the welds performed with 0.15 welding pitch, but small influence on the fatigue strength of the welds performed with 0.30 welding pitch. These results are another evidence that material adhesion to the tool may have a stronger influence on welds properties than the pin imperfections.

Figure 11b, c shows optical microscopy images of the fatigue surfaces of a CL030 specimen tested with a load range of 30 MPa. Despite the reduced magnification, the nucleation zones, where the initiation of the fatigue cracks occurred, are easily seen in the images. Leitao et al. [28] observed similar fracture surfaces in dissimilar aluminium-steel welds produced by FSLW. The analysis of the nucleation zones using scanning electron microscopy (SEM) enabled them to detect the presence of multiple micro-cavities in the interface zone between the base materials, which functioned as nuclei for initiation and propagation of the fatigue crack. From current work, it can be concluded that the size and shape of the micro-cavities, which are influenced by the pin characteristics, are the reason for the differences in fatigue strength between the welds produced with the CL and FT tools. Differences in the interface bonding, between the CL and FT welds, had been already registered when comparing the IBWs in Fig. 6.

5 Conclusions

The monotonic and fatigue behaviour of friction stir lap welded joints, produced with tools with (FT) and without

(CL) geometrical imperfections, was investigated and compared. The following important conclusions were derived:

- (i) Wear of the pin threads and material adhesion to the tool were simulated by machining flats in the pin of a FSW tool and varying the welding pitch, respectively. According to the temperature calculations and hardness measurements, the changes in tool geometry and welding pitch had no influence on heat generation during the process.
- (ii) Torque measurements showed an increase in the volume of material stirred by the tool when increasing the welding pitch, which proved the effectiveness of using this technique in simulating material adhesion to the tool during welding.
- (iii) Metallographic analysis showed that the pin imperfections had no influence on weld morphology or lap welds defect size. According to current results, damage of pin threads during welding of hard aluminium alloys may have no influence on weld quality.
- (iv) The adhesion of material to the tool, simulated by varying the welding pitch, showed to have higher influence on lap welds defect size than the pin imperfections. According to current results, material adhesion to the tool may have a positive effect in decreasing lap welds defect size.
- (v) Mechanical testing results showed that a small decrease in the cold lap weld defect size, associated with an increase in effective plate thickness, has

stronger influence on the fatigue performance of the joints than on the monotonic strength. An increase of around 10% in the effective plate thickness of the CL joints resulted in an increase of 500% in the fatigue strength but had no effect on the monotonic strength of the joints.

- (vi) Both the pin imperfections and material adhesion to the tool may have a positive effect on the fatigue performance of the joints. This is due to the extreme sensitivity of the fatigue strength on the lap interface morphology, which in turn is determined by the material stirring exerted by the tool.

Acknowledgements This research was co-financed through Fundação para a Ciência e a Tecnologia (UID/EMS/00285/2013), COMPETE 2020 (POCI-01-0145-FEDER-007633) and FEDER (CENTRO-01-0145-FEDER-000006). The author, C. Leitão is supported by the Portuguese Foundation for Science and Technology through SFRH/BPD/93685/2013 fellowship. All supports are gratefully acknowledged.

Publisher's Note Springer Nature remains neutral with regard to jurisdictional claims in published maps and institutional affiliations.

References

- Magalhães VM, Leitão C, Rodrigues DM (2017) Friction stir welding industrialisation and research status. *Sci Technol Weld Join* 23:1–10. <https://doi.org/10.1080/13621718.2017.1403110>
- Rai R, De A, Bhadeshia HKDH, DebRoy T (2011) Review: friction stir welding tools. *Sci Technol Weld Join* 16(4):325–342. <https://doi.org/10.1179/1362171811Y.0000000023>
- Leitão C, Louro R, Rodrigues DM (2012) Analysis of high temperature plastic behaviour and its relation with weldability in friction stir welding for aluminium alloys AA5083-H111 and AA6082-T6. *Mater Des* 37:402–409. <https://doi.org/10.1016/j.matdes.2012.01.031>
- Leitão C, Louro R, Rodrigues DM (2012) Using torque sensitivity analysis in accessing friction stir welding processing conditions. *J Mater Process Technol* 212(10):2051–2057. <https://doi.org/10.1016/j.jmatprotec.2012.05.009>
- Cederqvist L, Reynolds AP (2001) Factors affecting the properties of friction stir welded aluminum lap joints. *Welding Journal*: 281–287. doi:citeulike-article-id:12260670
- Yadava MK, Mishra RS, Chen YL, Carlson B, Grant GJ (2010) Study of friction stir joining of thin aluminium sheets in lap joint configuration. *Sci Technol Weld Join* 15(1):70–75. <https://doi.org/10.1179/136217109X12537145658733>
- Buffa G, Campanile G, Fratini L, Prisco A (2009) Friction stir welding of lap joints: influence of process parameters on the metallurgical and mechanical properties. *Mater Sci Eng A* 519(1):19–26. <https://doi.org/10.1016/j.msea.2009.04.046>
- Costa MI, Verdera D, Costa JD, Leitao C, Rodrigues DM (2015) Influence of pin geometry and process parameters on friction stir lap welding of AA5754-H22 thin sheets. *J Mater Process Technol* 225:385–392. <https://doi.org/10.1016/j.jmatprotec.2015.06.020>
- Costa MI, Verdera D, Leitão C, Rodrigues DM (2015) Dissimilar friction stir lap welding of AA 5754-H22/AA 6082-T6 aluminium alloys: influence of material properties and tool geometry on weld strength. *Mater Des* 87:721–731. <https://doi.org/10.1016/j.matdes.2015.08.066>
- Babu S, Ram GDJ, Venkitakrishnan PV, Reddy GM, Rao KP (2012) Microstructure and mechanical properties of friction stir lap welded aluminum alloy AA2014. *J Mater Sci Technol* 28(5): 414–426. [https://doi.org/10.1016/S1005-0302\(12\)60077-2](https://doi.org/10.1016/S1005-0302(12)60077-2)
- Salari E, Jahazi M, Khodabandeh A, Ghasemi-Nanasa H (2014) Influence of tool geometry and rotational speed on mechanical properties and defect formation in friction stir lap welded 5456 aluminum alloy sheets. *Mater Des* 58: 381–389. <https://doi.org/10.1016/j.matdes.2014.02.005>
- Park S-W, Yoon T-J, Kang C-Y (2017) Effects of the shoulder diameter and weld pitch on the tensile shear load in friction stir welding of AA6111/AA5023 aluminum alloys. *J Mater Process Technol* 241:112–119. <https://doi.org/10.1016/j.jmatprotec.2016.11.007>
- Ji S, Li Z, Zhang L, Zhou Z, Chai P (2016) Effect of lap configuration on magnesium to aluminum friction stir lap welding assisted by external stationary shoulder. *Mater Des* 103:160–170. <https://doi.org/10.1016/j.matdes.2016.04.066>
- Zhou Z, Yue Y, Ji S, Li Z, Zhang L (2017) Effect of rotating speed on joint morphology and lap shear properties of stationary shoulder friction stir lap welded 6061-T6 aluminum alloy. *Int J Adv Manuf Technol* 88(5):2135–2141. <https://doi.org/10.1007/s00170-016-8924-6>
- Yue Y, Li Z, Ji S, Huang Y, Zhou Z (2016) Effect of reverse-threaded pin on mechanical properties of friction stir lap welded alclad 2024 aluminum alloy. *J Mater Sci Technol* 32(7):671–675. <https://doi.org/10.1016/j.jmst.2016.03.005>
- Li Z, Yue Y, Ji S, Chai P, Zhou Z (2016) Joint features and mechanical properties of friction stir lap welded alclad 2024 aluminum alloy assisted by external stationary shoulder. *Mater Des* 90:238–247. <https://doi.org/10.1016/j.matdes.2015.10.056>
- Çam G (2011) Friction stir welded structural materials: beyond Al-alloys. *Int Mater Rev* 56(1):1–48. <https://doi.org/10.1179/095066010X12777205875750>
- Prado RA, Murr LE, Soto KF, McClure JC (2003) Self-optimization in tool wear for friction-stir welding of Al 6061+20% Al₂O₃ MMC. *Mater Sci Eng A* 349(1):156–165. [https://doi.org/10.1016/S0921-5093\(02\)00750-5](https://doi.org/10.1016/S0921-5093(02)00750-5)
- Siddiquee AN, Pandey S (2014) Experimental investigation on deformation and wear of WC tool during friction stir welding (FSW) of stainless steel. *Int J Adv Manuf Technol* 73(1):479–486. <https://doi.org/10.1007/s00170-014-5846-z>
- Thompson B, Babu SS (2010) Tool degradation characterization in the friction stir welding of hard metals. *Weld J* 89(12):256S–261S
- Melits M, De A, DebRoy T (2014) Material adhesion and stresses on friction stir welding tool pins. *Sci Technol Weld Join* 19(6):534–540. <https://doi.org/10.1179/1362171814Y.00000000221>
- Attallah MM, Salem HG (2005) Friction stir welding parameters: a tool for controlling abnormal grain growth during subsequent heat treatment. *Mater Sci Eng A* 391(1):51–59. <https://doi.org/10.1016/j.msea.2004.08.059>
- İpekçioğlu G, Erim S, Çam G (2014) Effects of temper condition and post weld heat treatment on the microstructure and mechanical properties of friction stir butt-welded AA7075 Al alloy plates. *Int J Adv Manuf Technol* 70(1):201–213. <https://doi.org/10.1007/s00170-013-5255-8>
- Tello K, Duran U, Mendez P (2009) Scaling laws for the welding arc, weld penetration and friction stir welding. *Proceedings of Eighth Trends in Welding Research*:172–181. doi:<https://doi.org/10.1361/tp2008twr172>
- Yuqing M, Liming K, Fencheng L, Yuhua C, Li X (2017) Effect of tool pin-tip profiles on material flow and mechanical properties of friction stir welding thick AA7075-T6 alloy joints. *Int J Adv Manuf Technol* 88(1):949–960. <https://doi.org/10.1007/s00170-016-8882-z>

26. Golezani AS, Barenji RV, Heidarzadeh A, Pouraliakbar H (2015) Elucidating of tool rotational speed in friction stir welding of 7020-T6 aluminum alloy. *Int J Adv Manuf Technol* 81(5):1155–1164. <https://doi.org/10.1007/s00170-015-7252-6>
27. Aldanondo E, Arruti E, Echeverria A (2017) Friction stir weld lap joint properties in aeronautic aluminium alloys. In: *Friction stir welding and processing IX*. Springer, pp 109–117
28. Leitao C, Arruti E, Aldanondo E, Rodrigues DM (2016) Aluminium-steel lap joining by multipass friction stir welding. *Mater Des* 106:153–160. <https://doi.org/10.1016/j.matdes.2016.05.101>

11.- ARTICLE 8: FRICTION STIR WELDING OF LAP JOINTS USING NEW AL-LI ALLOYS FOR STRINGER-SKIN JOINTS

[76] E. Aldanondo, E. Arruti, A. Echeverria and I. Hurtado, "Friction stir welding of lap joints using new Al-Li alloys for stringer-skin joints," in *Friction stir welding and processing X*, Cham (Switzerland), The Minerals, Metals & Materials Series; Springer, 2019, pp. 77-88.

The work published in this article was the first we performed using Al-Li alloys of the third generation, which is the main focus of the thesis. AA2099-T83 extrusions and AA2060-T8E30 sheets were used to produce FSLW joints due to their excellent balance of high strength and low density. This work supposed a further important step towards the manufacturing concept of lightweight aeronautic fuselage structures using FSW technology and Al-Li alloys. A comparison of the properties of FSLW joints produced using different welding parameters and tool design was carried out. We concluded that the new FSW tool design with three flats and mixed thread that we proposed for lap joints could produce welds with improved properties, also in FSLW joints produced using Al-Li alloys.

This work was presented in the Friction Stir Welding and Processing X session of the 148th Annual Meeting & Exhibition TMS2019 in San Antonio (USA) and the article was published in the conference book.

Friction Stir Welding of Lap Joints Using New Al–Li Alloys for Stringer-Skin Joints



Egoitz Aldanondo, Ekaitz Arruti, Alberto Echeverria and Iñaki Hurtado

Abstract The aeronautic industry is continuously looking for new structural concepts with the aim of reducing dangerous gas emissions as well as reducing manufacturing costs and times. The development of advanced lightweight structures is an effective alternative to achieve the mentioned goals. Reinforced panels produced by the third generation aluminum–lithium alloys and Friction Stir Welding (FSW) can bring new solutions for more efficient aircrafts. This work presents the results obtained in the development and characterization of FSW joints directed to reinforced panel manufacturing. FSW lap joints were produced using aluminum–lithium alloys AA2099-T83 extrusions and AA2060-T8E30 sheets. Several welding parameter combinations and FSW tool designs were used to produce the joints. Joint properties were investigated by metallographic examination, microhardness tests as well as mechanical strength testing. The appropriate FSW conditions to optimize joint properties were established.

Keywords Friction stir welding · Lap joints · Al–Li

Introduction

Riveting has been the dominant joining technology for reinforced panel manufacturing for aircraft structures. However, there are some disadvantages in the riveting processes such as low productivity and lack of potential for weight reduction [1]. Welded integral structures represent benefits such as reductions in the number of necessary parts, weight saving potential as well as significant reductions in manufacturing times and costs. The main welding technologies developed have been

E. Aldanondo (✉) · E. Arruti · A. Echeverria
IK4 LORTEK, Arranomendia Kalea 4A, 20240 Ordizia, Spain
e-mail: Egoitz@lortek.es

I. Hurtado
Faculty of Engineering (MU-ENG), Mondragon Unibertsitatea,
Loramendi Kalea 4, 20500 Arrasate-Mondragon, Spain

© The Minerals, Metals & Materials Society 2019
Y. Hovanski et al. (eds.), *Friction Stir Welding and Processing X*, The Minerals,
Metals & Materials Series, https://doi.org/10.1007/978-3-030-05752-7_8

77

Laser Beam Welding (LBW) and Friction Stir Welding (FSW) [2, 3], resulting in the implementation of some applications in real aircrafts [4–6]. Thus, FSW technology was proposed and investigated as alternative joining technology to riveting for lap joints in stringer to skin applications [7, 8].

Joining stringers to skin by FSW generally requires welding in the lap joint configuration, which has been investigated and reported by several authors using aeronautic aluminum alloys [9–16]. Probably the most important conclusion of these investigations is the importance of the FSW tool design to minimize the main welding imperfections [17] that are typical in FSW lap joints: Hook features and cold lap defects.

Another important aspect to be considered in aircraft structure innovation is the maturation and launch of third-generation aluminum–lithium alloys, which offer high strength, low density and excellent corrosion resistance [18]. These Al–Li alloys such as AA2099 extrusions and AA2060 sheets have been promising candidates for stringer-skin applications and, although some recent investigations have been reported on FSW of these alloys [19], further work is needed to understand the FSW process applied to them.

The work presented in this article reports on investigations of the FSW process applied to lap joints using AA2099-T83 extrusions and AA2060-T8E30 sheets, the understanding of the joint formation mechanism and the evaluation of the resulting lap joint properties.

Experimental Details

Z-shaped extrusions of aluminum alloy AA2099-T83 and sheets of alloy AA2060-T8E30 were used in this work as stringer and skin materials to perform FSW joints in the overlap configuration. The chemical composition of these alloys is shown in Table 1. The thickness of the extrusion in the joining zone was 2 mm and the thickness of the sheet was 2.5 mm. Two different tools were employed to produce the lap joints as shown in Fig. 1. The general dimensions of both tools were similar having a plain shoulder of 10 mm in diameter, a probe diameter of 4 mm and a probe length of 2.5 mm. The difference between the tools was the probe design, one having a conventional threaded cylindrical probe (Fig. 1a) and the other a probe with three flats and a mixed neutral thread (Fig. 1b). Lap joints were produced combining several welding parameters, using rotational speeds between 800 and 1200 rpm and welding speeds between 150 and 250 mm/min. All investigated joints were produced in force control using an I-STIR PDS 4 FSW system adjusting the axial force for each welding parameter condition. Thus, FSW lap joints were produced using weld pitches between 0.125 and 0.31 mm/rev. The type of FSW lap joints produced is shown in Fig. 1c.

Samples for metallographic examination were cut perpendicular to the welding direction, polished to a mirror like finish, etched using Keller's reagent, rinsed in water and dried in a warm airflow. Weld cross-sectional features of the FSW lap

Table 1 Chemical compositions of base materials, wt%

Alloy	Al	Si	Fe	Cu	Mn	Mg	Zn	Ti	Ag	Li	Zr
2060-T8E30	Bal.	0.07	0.07	3.4-4.5	0.1-0.5	0.6-1.1	0.3-0.5	0.1	0.05-0.5	0.6-0.9	0.05-0.15
2099-T83	Bal.	0.05	0.07	2.4-3.0	0.1-0.5	0.1-0.5	0.4-1	0.1	-	1.6-2.0	0.05-0.12

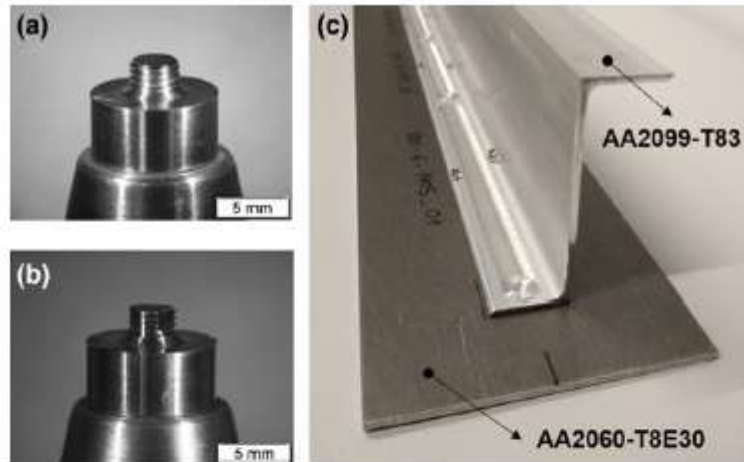


Fig. 1 FSW tools used to produce the FSW joints; a conventional threaded cylindrical tool; b three flats + neutral thread tool; and c FSW lap joint formed by AA2099-T83 extrusion and AA2060-T8E30 sheet

joints were examined by optical microscopy using an Olympus GX51 light optical microscope.

Microhardness tests were performed using a Vickers indenter, a load of 500 g and load application time of 15 s. Scans of indentations of approximately 20 mm in length were carried out, investigating the extension of about 10 mm from the weld centerline in both directions. The spacing between indentations was 0.5 mm. The scans were located in the mid-thickness of the AA2099-T83 extrusion as well as at a distance of 0.5 mm from the joint interface of the AA2060-T8E30 sheet. The microhardness tests were performed in the as welded condition and allowing a time of approximately 60 days between the production of the welds and the measurements.

The static mechanical strength of the FSW lap joints was investigated by pull-out tests, using a special fixture to hold the AA2060-T8E30 sheet firmly and pulling from the AA2099-T83 extrusion in the vertical-perpendicular direction to the sheet surface. All tests were performed at room temperature using a Zwick Roell Z100 tensile testing machine at a constant speed of 1.6 mm/min.

Results and Discussion

The quality of the FSW lap joints produced using different tools and welding parameters was evaluated based on their as welded surface quality, severity of welding imperfections as well as mechanical properties. The following sections summarize the main results obtained in this work:

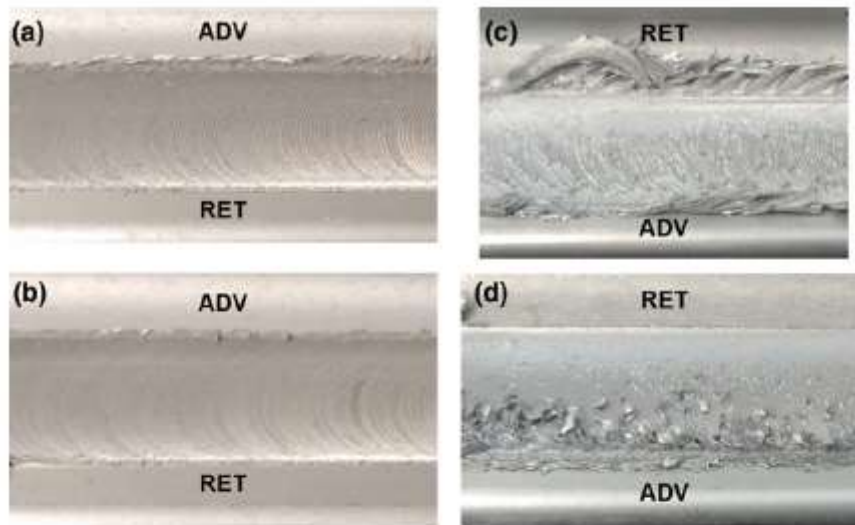


Fig. 2 Close-up images showing the surface quality of welds performed by a tool with three flats at 800 rpm and 250 mm/min; b tool with three flats at 1200 rpm and 250 mm/min; c conventional threaded tool at 800 rpm and 250 mm/min; d conventional threaded tool at 1200 rpm and 250 mm/min

Surface Quality

The surface appearance of FSW lap joints produced by the two tools and different welding parameters is shown in Fig. 2. As a general result, the joints produced by the tool with three flats presented a superior surface quality than those produced with a conventional threaded tool. This can be concluded seen in the images shown in Fig. 2a, b which contain a minimal amount of toe flash in comparison with Fig. 2c, d, which were produced with the conventional threaded tool and presented a larger amount of flash. Thus, it could be concluded that the implementation of flats on the probe produced favorable material flow and consolidation capacity of the FSW tool. This conclusion is in agreement with previous results obtained in FSW lap joining [12, 13], showing that the weldability window and the quality of the lap joints can be higher for tools featuring flats.

Metallographic Examination

Cross-sections of FSW lap joints produced under different welding parameters with both tools are presented in Figs. 3, 4, and 5. No volumetric defects were observed in the welds performed within the range of investigated welding parameters. However, significant differences were observed in typical FSW imperfections [17] of lap joints



Fig. 3 Cross-section of FSW lap joint produced at 1200 rpm and 250 mm/min by a conventional threaded tool

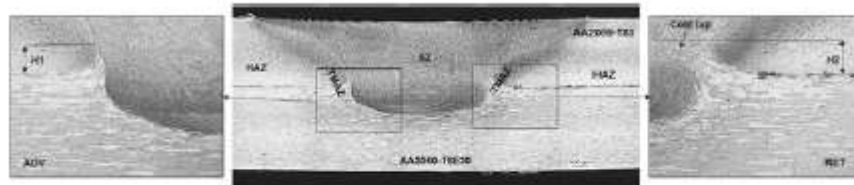


Fig. 4 Cross-section of FSW lap joint produced at 1200 rpm and 250 mm/min by a tool with three flats

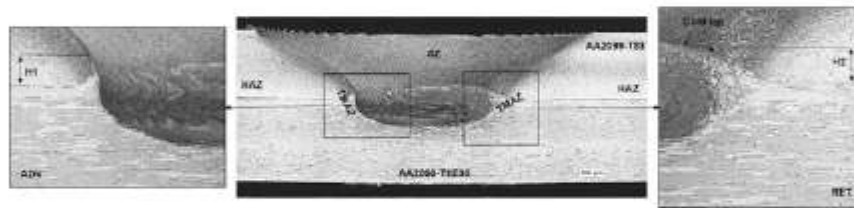


Fig. 5 Cross-section of FSW lap joint produced at 800 rpm and 250 mm/min by a tool with three flats

such as hooks and cold lap defects. Relatively large hook features were observed in both the advancing and the retreating side in joints produced by the conventional threaded tool as it is shown in Fig. 3. The magnified images of the sides show the hook features in the thermomechanically affected zone (TMAZ) regions in the advancing side (or H1) in the left as well as the hook in the retreating side (or H2) in the right. The highly deformed grain orientations of AA2060-T8E30 sheet material of the TMAZ regions are indicative of the vertical material flow induced by the conventional threaded tool, which is the main formation mechanism of the hook features. In addition to this, a cold lap defect feature was observed in the retreating side progressing from the tip of the hook towards the stir zone (SZ).

A reduction on the severity and size of the hook features was observed in FSW lap welds performed by the tool with three flats as shown in Figs. 4 and 5. In addition to that the hook size remained practically the same regardless the rotational speed used to perform the joints. This effect can be observed comparing the hook features in Figs. 4 and 5, which show equivalent FSW lap joints performed at 1200 rpm and

800 rpm, respectively. Thus, it is feasible to increase the rotational speed, without increasing the hook size, in order to produce a higher deformation at the interface, promoting a more extensive mixing of material and limiting the cold lap defect formation. Similar conclusions were obtained in previous works carried out with other aeronautic aluminum alloys [12].

The hooks (H1, H2) of FSW lap joints performed using the two tools previously described herein, and several welding parameters are represented as a function of the weld pitch in Fig. 6. It is clearly shown that the hook features produced by the conventional threaded tool are significantly larger, especially when low weld pitch values are employed. The hook size decreases as the weld pitch increases for the conventional threaded tool due to the less intensive vertical material flow induced at lower rotational speeds and higher welding speeds. This is not the case for the tool with three flats + neutral thread as the hook remains equivalent for all the investigated weld pitch range. The globally neutral nature of the three sections of threads present on the probe eliminates a preferential vertical flow of plasticized material resulting in limited hook formation.

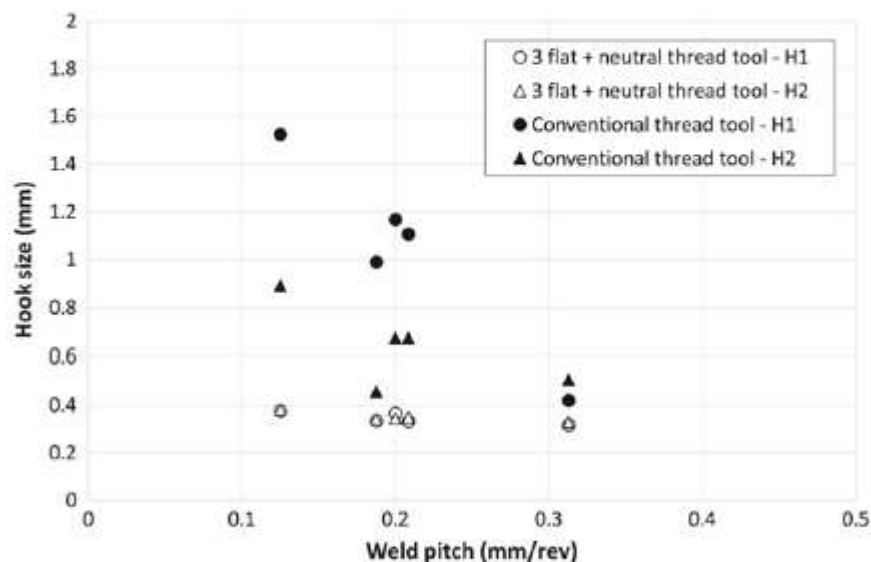


Fig. 6 Representation of the hook size measured in FSW lap joints produced using different welding parameters and weld pitches

Microhardness Testing

The microhardness distribution of different microstructural regions of FSW lap joints in the extrusion AA2099-T83 and the sheet AA2060-T8E30 are presented in Figs. 7 and 8 respectively. The obtained results are in agreement with the conclusions reported by Huang et al. [19], where FSW lap joints with AA2099-T83 and AA2060-T8E30 were investigated. A significant hardness reduction in the HAZ, TMAZ and SZ regions was observed which is typical in FSW of precipitation hardening aluminum alloys [13]. Microstructural phenomena such as dissolution, coarsening and precipitation of the precipitates, which are induced by the complex thermomechanical cycle by the FSW process, directly influence the hardness. Therefore, the hardness distribution usually depends on the FSW parameters used to produce the joints.

A nonsymmetric hardness distribution was observed in the scans performed in the AA2099-T83 extrusion as shown in Fig. 7. A HAZ extension of approximately 9 mm was observed at the advancing side, while the retreating side showed a larger HAZ. The heat accumulation at the edge of the stringer in the retreating side could be the reason for a larger HAZ, producing a more severe overaging effect at this region. In addition to that, the FSW lap joint produced using a weld pitch of 0.21 mm/rev also presented a larger HAZ in comparison with the one performed at 0.31 mm/rev. The higher temperatures and heat accumulation produced by the weld pitch of 0.21 mm/rev could be again the reason for that. This effect was not observed at the advancing side of these FSW lap joints. A maximum hardness reduction of 74 HV0.5 was measured, from 168 HV0.5 of the base material to 94 HV0.5 of the minimum hardness at the HAZ at the advancing side, which represents a ~44% drop.

Figure 8 shows the hardness distribution of the AA2060-T8E30 sheet, where a symmetric HAZ of approximately 16 mm was observed. A maximum hardness drop

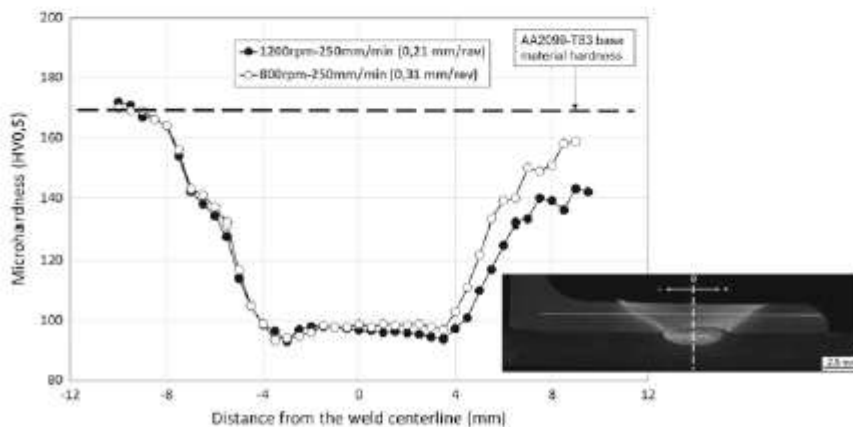


Fig. 7 Microhardness value distributions in the AA2099-T83 extrusion of FSW joints performed using 0.21 mm/rev and 0.31 mm/rev weld pitches and a tool with three flats

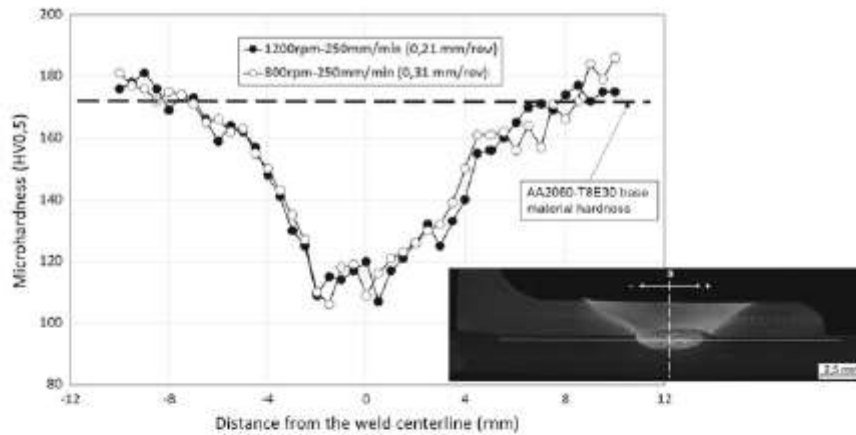


Fig. 8 Microhardness value distributions in the AA2060-T8E30 sheet of FSW joints performed using 0.21 and 0.31 mm/rev weld pitches and a tool with three flats

of ~38% was estimated from 172 HV0.5 of base material to 106 HV0.5 measured at the SZ region boundaries. No significant differences were observed between FSW lap joints performed at 0.21 and 0.31 weld pitches.

Mechanical Strength Testing

Pull-out tests were performed with the aim of evaluating the static mechanical strength of the FSW lap joints produced using several welding parameters and both tools. Figure 9 shows two limit cases that represent the critical influence of the FSW lap joint quality on the joint strength. A maximum pull-out load of 2.8 kN was observed for the FSW lap joint produced by the tool with three flats + neutral thread and welding parameters of 1200 rpm and 250 mm/min. The small hooks and the effective reduction of the cold lap defect shown in Fig. 4 are representative of an appropriate stirring and mixing of materials, producing a good quality weld that presented a failure in the stringer outside the weld. On the other hand, a FSW lap joint produced by the conventional threaded tool at 800 rpm and 150 mm/min presented an interfacial failure, as shown in the top-right image in Fig. 9, with an ultimate pull-out load of 1.95 kN. In this case, the larger size of the hooks and the presence of the cold lap defect in the weld were found to be the main factors that reduced the joint quality and load carrying capacity.

In general, FSW lap joints produced by the tool with three flats + neutral thread presented superior mechanical strength in comparison with the conventional threaded tool, with average ultimate pull-out load values of 2.62 kN and 2.18 kN, respectively.

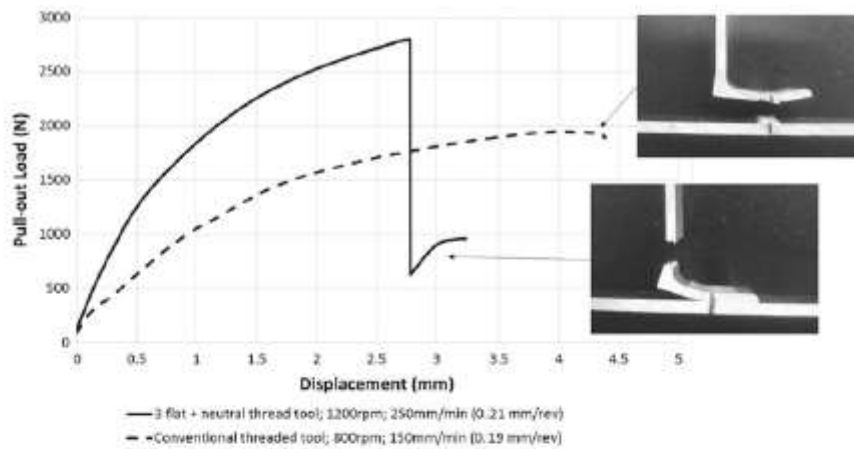


Fig. 9 Pull-out strength and failure mode of FSW lap joints produced by different tools and welding parameters

Thus, it could be concluded that superior weld quality and load carrying capacity can be obtained by the tool with three flats + neutral thread.

Conclusions

In this work, FSW lap joints were performed with AA2099-T83 extrusions and AA2060-T8E30 sheet materials, using different tools and welding parameters, and the joint properties were investigated. The following conclusions could be obtained:

- The tool with three flats + neutral thread can produce FSW lap joints with superior surface quality than the conventional threaded tool.
- The FSW lap joints produced by the tool with three flats + neutral thread present superior weld quality (reduced hooks and cold lap defects) than the ones produced by the conventional threaded tool.
- The tool with three flats + neutral thread allows to increase the rotational speed without promoting vertical flow of plasticized material nor increasing the hook size.
- Hardness drops of approximately 44% and 38% were observed for AA2099-T83 extrusion and AA2060-T8E30, respectively.
- An average ultimate pull-out load of 2.62 kN with a failure outside the joint was achieved in FSW lap joints produced by the tool with three flats + neutral thread. This is a ~20% higher than the values obtained with the joints performed by the conventional threaded tool.

Thus, the main conclusion is that the tool with three flats + neutral thread has the capability to produce FSW lap joints of superior quality and higher load carrying capacity, showing a larger weldability window. Within this window, 1200 rpm and 250 mm/min were identified as the best welding parameters that resulted in the highest weld quality.

Acknowledgements This work has been performed in the frame of the project ecoTECH within the AIRFRAME ITD of the Clean Sky 2 programme of the H2020. The authors acknowledge the funding received for this project under the project ID 807083 of the call H2020-IBA-CS2-GAMS-2017.

References

1. Rendings KH (2001) Aluminium structures used in aerospace—status and prospects. *Mater Sci Forum* 242:11–24
2. Mendez P, Eagar T (2002) New trends in welding in the aeronautic industry. In: *Proceedings of 2nd conference of new manufacturing trends*, Bilbao, Spain
3. Talwar R et al (2000) Friction stir welding of airframe structures. In: *Proceedings of 2nd international symposium on friction stir welding*, Gothenburg, Sweden, pp 27–29
4. Assler H, Telgkamp J (2006) Design of aircraft structures under special consideration of NDT. In: *Proceedings of 9th European conference on NDT*, Berlin (Germany)
5. Christner B (2016) A friction stir welded jet aircraft: from concept to reality. In: *Proceedings of 11th international symposium on friction stir welding*, Cambridge, UK, 17 May 2016
6. Fernandez F (2010) FSW applied on mid-size aircraft. In: *Proceedings of 8th international symposium on friction stir welding*, Timmendorfer Strand, Germany, 18–20 May 2010
7. Tavares SM (2011) Design and advanced manufacturing of aircraft structures using friction stir welding. PhD thesis, Universidade do Porto (Portugal)
8. Freeman J, Moore G, Thomas B, Kok L (2006) Advances in FSW for commercial aircraft applications. In: *6th international symposium on friction stir welding*, Toronto (Canada)
9. Cederquist L, Reynolds AP (2001) Factors affecting the properties of friction stir welded aluminium lap joints. *Weld J Res Suppl* 80:281
10. Dubourg L et al (2010) Process optimisation and mechanical properties of friction stir lap welds of 7075-T6 stringers on 2024-T3 skin. *Mater Des* 31:3324–3330
11. Buffa G et al (2009) Friction stir welding of lap joints: Influence of process parameters on the metallurgical and mechanical properties. *Mater Sci Eng A* 519:19–26
12. Aldanondo E et al (2016) Microstructural features in friction stir welded lap joints. In: *Proceedings of 10th international conference on trends in welding research*, Tokyo, Japan, 10–14 Oct 2016
13. Aldanondo E, Arruti E, Echeverria A (2017) Friction stir weld lap joint properties in aeronautic aluminium alloys. In: *Proceedings of 148th friction stir welding and processing X*, in annual meeting and exhibition TMS2017, San Diego (USA)
14. Ji S et al (2016) Effect of reverse-threaded pin on mechanical properties of friction stir lap welded alclad 2024 aluminum alloy. *J Mater Sci Technol* 32:671–675
15. Yang X et al (2014) Defect features and mechanical properties of friction stir lap welded dissimilar AA2024-AA7075 aluminum alloy sheets. *Mater Des* 55:9–18
16. Liu H et al (2016) The effect of interface defect on mechanical properties and its formation mechanism in friction stir lap welded joints of aluminum alloys. *J Mater Process Technol* 238:244–254

17. ISO, ISO25239 (2011) Friction stir welding—aluminium, Geneva (Switzerland)
18. Eswara Prasad N, Gokhale AA, Wanhil R (2014) Aluminium-lithium alloys: processing, properties and applications. Elsevier-BH, Oxford, UK
19. Huang Y et al (2018) Interface characteristic and tensile property of friction stir lap welding of dissimilar aircraft 2060-T8 and 2099-T83 Al-Li alloys. *Int J Adv Manuf Technol* 94:1253–1261

12.- ARTICLE 9: EFFECT OF TOOL GEOMETRY AND WELDING PARAMETERS ON FRICTION STIR WELDED LAP JOINT FORMATION WITH AA2099-T83 AND AA2060-T8E30 ALUMINIUM ALLOYS

[77] E. Aldanondo, J. Vivas, P. Álvarez y I. Hurtado, «Effect of tool geometry and welding parameters on friction stir welded lap joint formation with AA2099-T83 and AA2060-T8E30 aluminium alloys,» *Metals*, vol. 10, nº 872, 2020.

In this work, further investigation was performed in order to understand better the plasticised material flow and weld formation mechanisms in the manufacturing of FSLW joints using AA2099-T83 (extrusion) and AA2060-T8E30 (sheet) Al-Li alloys. A welding parameter optimisation was carried out and the conditions resulting in high-quality FSLW joints were defined. The benefits of the proposed FSW tool design for lap joints having three flats and mixed thread were confirmed.

This article was the first of the three articles that are to be considered for the completion of the thesis as a compendium of publications. It was published in the journal "Metals".

Article

Effect of Tool Geometry and Welding Parameters on Friction Stir Welded Lap Joint Formation with AA2099-T83 and AA2060-T8E30 Aluminium Alloys

Egoitz Aldanondo ^{1,*}, Javier Vivas ¹, Pedro Álvarez ¹ and Iñaki Hurtado ²

¹ LORTEK Technological Centre, Basque Research and Technology Alliance (BRTA), Arranomendia kalea 4A, 20240 Ordizia, Spain; jvivas@lortek.es (J.V.); palvarez@lortek.es (P.A.)

² Mondragon Unibertsitatea, Faculty of Engineering (MU-ENG), Loramendi Kalea 4, 20500 Arrasate-Mondragon, Spain; ihurtado@mondragon.edu

* Correspondence: Egoitz@lortek.es; Tel: +34-943-882-303

Received: 27 May 2020; Accepted: 23 June 2020; Published: 1 July 2020



Abstract: In this paper the effect of tool geometry and welding parameters on friction stir welded lap joints with AA2099-T83 and AA2060-T8E30 aluminium alloys has been investigated through the study of the material flow and weld formation along with the reaction forces during friction stir welding (FSW) for various sets of welding parameters and two FSW tools with different geometrical features. The results showed that welding parameters and tool probe geometry strongly affect the characteristics of the typical defect features (hook and cold lap defects) of the friction stir welded lap joints. From the relationship established between the welding parameters, tool probe geometry and the hook and cold lap defect formation, some guidelines are concluded with the objective of guaranteeing appropriate FSW lap joint properties.

Keywords: friction stir welding; lap joint; aluminium alloy; defect feature; tool geometry; process forces; aeronautic

1. Introduction

Currently, riveting is the most used joining technology for manufacturing reinforced panels of aircraft structures [1]. However, there are important disadvantages in the use of this technology that have to be solved. Among them, the low productivity and the significant contribution to weight increase are the most significant ones. By contrast with riveting, welded structures show remarkable benefits such as reductions in the number of parts to produce the structures, weight saving as well as significant reductions in manufacturing time and cost. Nowadays the most promising alternative joining technologies to riveting for the manufacturing of aircraft structures are laser beam welding (LBW) [2–4] and friction stir welding (FSW) [5–7]. Indeed, these technologies have already been satisfactorily implemented in different parts of real aircrafts [8]. This paper explores FSW as an alternative to riveting for stringer to skin lap joint manufacturing applied to reinforced panel applications in aeronautics.

As a solid-state welding technology, FSW presents clear benefits over other welding technologies as it makes possible to reduce typical disadvantages that arise in welding of high strength aluminium alloys, such as welding defects (porosity, hot-cracking) and residual stresses. In order to obtain joints of sufficiently high quality, it is important to avoid welding defects as well as to reduce and control the residual stresses as they can reduce the fatigue life of aircraft structures significantly [9]. Although the effect of residual stresses in the fatigue life of aircraft structures is not in the scope of the present work, several authors have shown the possibility to evaluate the residual stresses using different methods [10,11].

There are several works that have already studied FSW applied to lap joints, and more concretely, stringer to skin lap joints for aeronautic applications [12–25]. Dubourg et al. [16] investigated the effects of FSW parameters on the lap joint formation mechanisms using 2024-T3 and 7075-T6 alloys and they concluded that the material flow induced by the tool had critical effects on the FSW joint properties. Ji et al. [21,22] investigated the effects of different tool-probe thread designs on the FSW lap joint properties. They concluded that the thread design of the probe was critical on the plasticized material flow and the resulting lap joint properties. Lap joints were produced using large penetration tools showing that different thread designs can lead to different material flow and joint properties. Thus specific thread designs for large penetration welds were proved to be beneficial compared to conventional threads, producing lap joints with smaller defect features and higher mechanical properties. The most important conclusion that can be extracted from these works is that both FSW tool design and welding parameters play a key role on the minimization of the welding defects that are characteristic of these type of joint configuration: hook and cold lap defects. According to the ISO25239 standard for FSW aluminium alloys [23], the hook is the most relevant imperfection in FSW lap joints and its relevance in mechanical properties of the joints have been shown previously by Rodrigues et al. [24]. Therefore, it is important to define appropriate tool designs and welding parameters to avoid the formation of hooks of important size in order to optimize the mechanical properties of FSW lap joints.

Regarding current innovation trends in new aircraft structure concepts, the research, maturation and launch of the third generation of aluminium-lithium alloys must be mentioned [26,27]. These alloys present a high strength, low density and excellent corrosion resistance. For stringer-skin applications AA2099 (extrusion) and AA2060 (sheet) Al-Li alloys are considered as some of the most interesting candidates for stringer and skin materials respectively. Huang et al. reported results on FSW lap joints using these alloys [27] showing the influence of process parameters to obtain defect-free joints using a screwed tool-probe design. They showed the feasibility to obtain volumetric defect-free joints using very specific process parameters, i.e., 800 rpm and 200 mm/min, but they reported the formation of cavities using lower or higher welding speeds.

The present work was focused on the manufacturing of FSW lap joints using AA2099-T83 and AA2060-T8E30 aluminium alloys. Thus, the main purpose was to investigate the effect of FSW tool geometry and welding parameters on the main FSW lap joint defect formation, understanding material flow and weld formation mechanisms.

2. Materials and Methods

Z shaped extrusions of aluminium alloy AA2099-T83 with a thickness of 2 mm and sheets of aluminium alloy AA2060-T8E30 with a thickness of 2.5 mm were used as base materials in this work. Both alloys were in a T8 hardened temper condition resulting from a combination of solution heat treatment, cold working and artificial aging steps during their production. The materials were provided by Arconic and Israel Aerospace Industries (IAI) (Lod, Israel) and their indicative chemical compositions are shown in Table 1.

Table 1. Chemical compositions of base materials, wt. %.

Alloy	Al	Si	Fe	Cu	Mn	Mg	Zn	Ti	Ag	Li	Zr
AA2060-T8E30	Bal.	0.07	0.07	3.4–4.5	0.1–0.5	0.6–1.1	0.3–0.5	0.1	0.05–0.5	0.6–0.9	0.05–0.15
AA2099-T83	Bal.	0.05	0.07	2.4–3.0	0.1–0.5	0.1–0.5	0.4–1	0.1	-	1.6–2.0	0.05–0.12

FSW joints were performed in overlap configuration where the alloy AA2099-T83 was used as stringer and placed on top of the alloy AA2060-T8E30 which was used as skin. An example of this lap joint is shown in Figure 1a. 120 mm long joints were performed for each investigated welding condition.

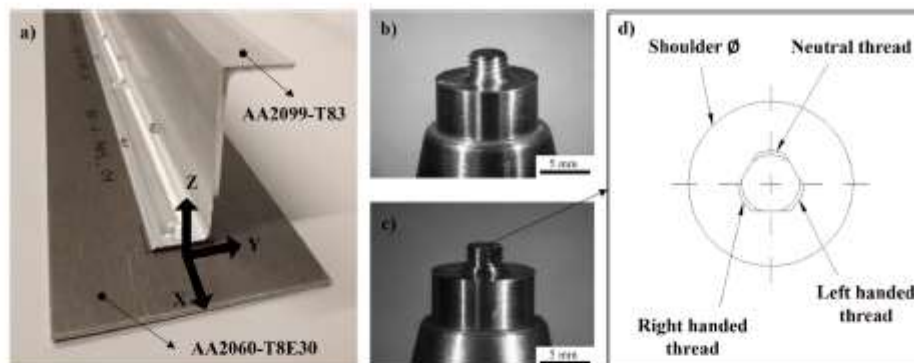


Figure 1. (a) Friction stir welding (FSW) lap joint between AA2099-T83 extrusion and AA2060-T8E30 sheet and FSW tools used to produce them; (b) conventional threaded tool; (c) 3 flats + mixed thread tool; and (d) sketch showing details of the top view of the 3 flats + mixed thread tool.

Two types of FSW tools were employed to produce lap joints. Both FSW tools had a plane shoulder of 10 mm in diameter and a probe with 4 mm in diameter and 2.5 mm in length. The difference between the tools was the probe design. One probe design consisted in a conventional right handed thread cylindrical probe (Figure 1b) while the other tool had a probe with 3 flats and 3 types of threads in the 3 cylindrical sections (Figure 1c,d). The flats were used to divide the probe in three different threaded sections. All threads were produced with the same pitch and depth dimensions being the only difference among them the thread orientation. One section had a right handed thread, another one a left handed thread and the other one was a neutral thread with no inclination. The main purpose of this probe design was to avoid any preferential vertical plasticized material flow in order to reduce the hook formation, while promoting sufficient flow at the faying surface to break the oxide layers and produce the mixture between the parts to be welded.

The joints were made in an I-STIR PDS 4 machine for FSW (MTS Systems Corp., Eden Prairie, MN, USA) at LORTEK operated in load control. The welding parameters utilised for this study are summarised in Table 2. The axial loads for each tool and welding parameter set were adjusted in initial FSW tests performed under position control so that sufficient contact by the shoulder was guaranteed. All the welds were performed with a tilt angle of 1.5°.

Table 2. Welding parameters used for different FSW lap joints.

Rotational Speed (rpm)	Welding Speed (mm/min)
800 and 150	800 and 250
1200 and 150	1200 and 250

The in-plane reaction forces during the FSW process were recorded by the controller using the pressure transducers and load cells implemented in the FSW machine. Thus, reaction forces in the welding direction (X) and perpendicular to the welding direction (Y) were recorded as well as the spindle torque. A frequency of 40 Hz was employed to log the process forces and torque. An average value of the forces and torque was calculated from all the recorded values in the steady-state region of each weld. These values are used in the later Section 4 where the process forces and torque are discussed.

After welding, specimens for metallographic analysis were cut from the welds, perpendicular to the welding direction. All specimens were obtained from the middle of the 120 mm long joints. Standard grinding and polishing procedures were followed, and diluted Keller's reagent was used for

revealing the microstructure. Weld cross-sections were then examined by optical microscopy using an Olympus GX51 light optical microscope (Olympus Corp., Tokyo, Japan).

3. Results and Discussion

3.1. Material Flow and Weld Formation

No volumetric defects such as wormholes, cavities or cracks were found in any of the analyzed cross sections. However, as expected, the macrostructural features of the FSW lap joints were found to be different depending on the employed tool and welding parameters. Figure 2 shows a low magnification cross section of a selected FSW lap joint. The retreating and advancing sides are denoted by RET and ADV respectively. The typical microstructural zones that form FSW lap joints are the base material (BM), the heat affected zone (HAZ), the thermomechanically affected zone (TMAZ) and the weld nugget (WN). The BM is the zone that remains unaffected by the FSW process and shows the characteristic microstructures of extrusions and sheets of stringer and skin aluminium alloys, respectively. The HAZ is the microstructural zone affected by the heat generated in the FSW process and undergoes changes in the precipitate size and distribution as well as grain growth compared to the base material. The TMAZ is the zone where the material is affected by the heat and the plastic deformation. This zone is characterized by the presence of deformed and relatively coarse grains. These grains are formed mainly due to dynamic recovery as the levels of temperature and deformation suffered are not sufficient to induce any dynamic recrystallization. Finally, the WN exhibits a microstructure formed by fine equiaxed grains. This grain structure is produced by continuous dynamic recrystallization as, in contrast to the TMAZ, the temperature and plastic deformation are high enough to cause this phenomenon.

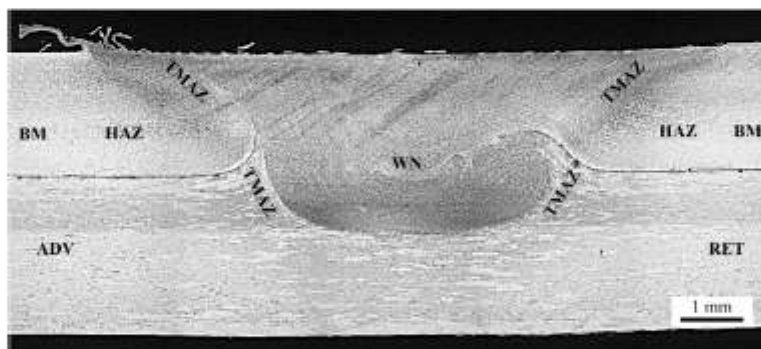


Figure 2. Cross-section and microstructural zones of a friction stir welding (FSW) lap joint produced using a conventional threaded tool at 1200 rpm and 250 mm/min. Tool translation movement was forward from the shown cross-section.

In addition to the microstructural zones, two types of joint features were observed in all the FSW lap joints: hooks and cold lap defects. An example of these joint features can be observed in Figure 3, which shows a metallographic cross-section of a FSW lap joint produced by the conventional threaded tool. The formation of these joint features results from the material flow at the faying surface between the AA2099-T83 extrusion (stringer) and the AA2060-T8E30 sheet (skin). During the welding process the plasticized material around the tool at the advancing side suffers an upward flow (labelled as flow I in Figure 4) due to the shearing effect caused by the thread of the probe. A similar effect at the retreating side also produces an upward flow (labelled as flow II in Figure 4). Both vertical flows are responsible for creating the hooks at the advancing and the retreating sides. Finally, the material flows downward (labelled as flow III in Figure 4) dragged by the action of the shoulder to fill the cavity left

by the probe at the rear of the tool. The insufficient flow and mixture of the plasticized metal at the faying surface at the retreating side induces the formation of the cold lap defect.

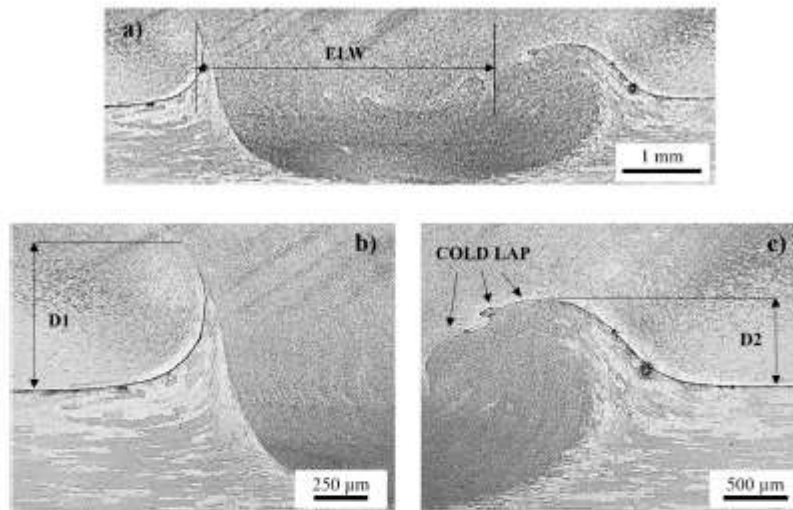


Figure 3. Example of hook and cold lap defects and their characteristic measurements in a friction stir welding (FSW) lap joint: (a) effective lap width (ELW); (b) hook height at the advancing side (D1); and (c) cold lap defect and hook height at the retreating side (D2). Tool translation movement was forward from the shown cross-section.

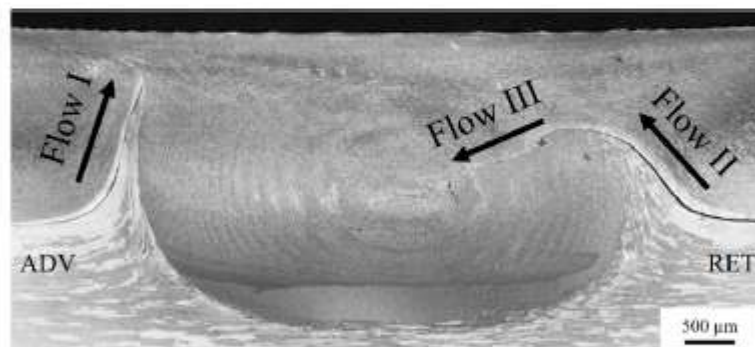


Figure 4. Material flow produced by the conventional threaded tool operated at 1200 rpm and 150 mm/min. Tool translation movement was forward from the shown cross-section.

Figures 5 and 6 show the transverse cross-sections of the welds performed with the conventional threaded tool and the 3 flats + mixed thread tool respectively. In each macro-section the advancing side is on the left. It is interesting to note that volumetric defect free welds were obtained for both tools under all investigated welding parameters. However, it is clearly observed that the hook and cold lap defect features strongly vary with the welding parameters and tool geometry.

It is well known that formation of hook and cold lap defects result in a sheet thinning and in a reduction of the effective lap width (ELW) respectively, which deteriorate mechanical properties of FSW lap joints [28–30]. In order to quantify the size of these joint features as a function of the tool geometry and welding parameters, the ELW and the height of the hooks were measured as shown

in Figure 3. Note that the ELW is defined as the horizontal distance from the tip of the hook at the advancing side to the edge of the cold lap defect at the retreating side [14].

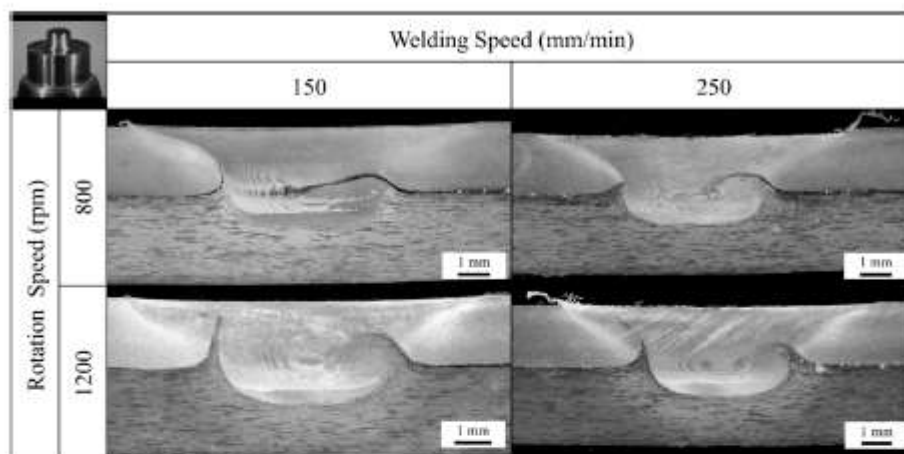


Figure 5. Transverse macro-sections of the friction stir welding (FSW) lap joints performed with the conventional threaded tool. The advancing side is located at the left of the image for all macro-sections. Tool translation movement was forward from the shown cross-section.

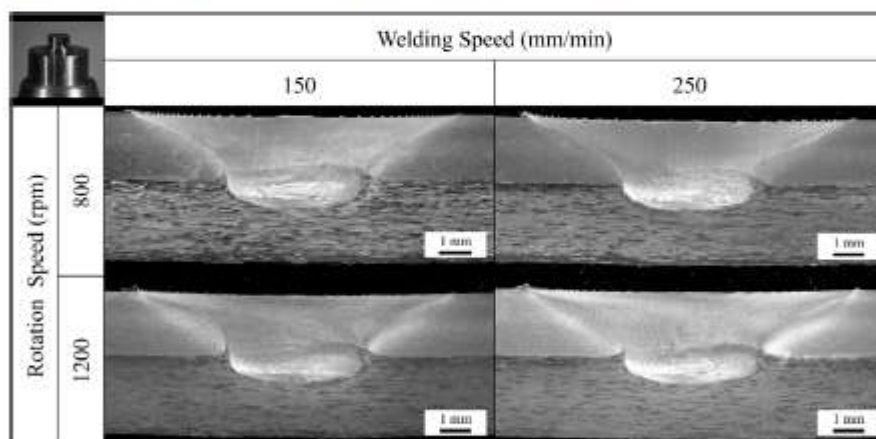


Figure 6. Transverse macro-sections of the friction stir welding (FSW) lap joints performed with the 3 flats + mixed thread tool. The advancing side is located at the left of the image for all macro-sections. Tool translation movement was forward from the shown cross-section.

Figure 7 depicts the ELW as a function of the welding speed for the studied tool geometries and welding parameters. The results show that at the lowest welding speed the 3 flats + mixed thread tool shows a slightly larger ELW than the conventional threaded tool. However, this result is the opposite at the highest welding speed where the conventional threaded tool presents a substantially larger ELW, for both rotational speeds. This effect can be explained due to the more extensive material flow and plasticized material mixture produced by the conventional threaded tool when using a higher welding speed.

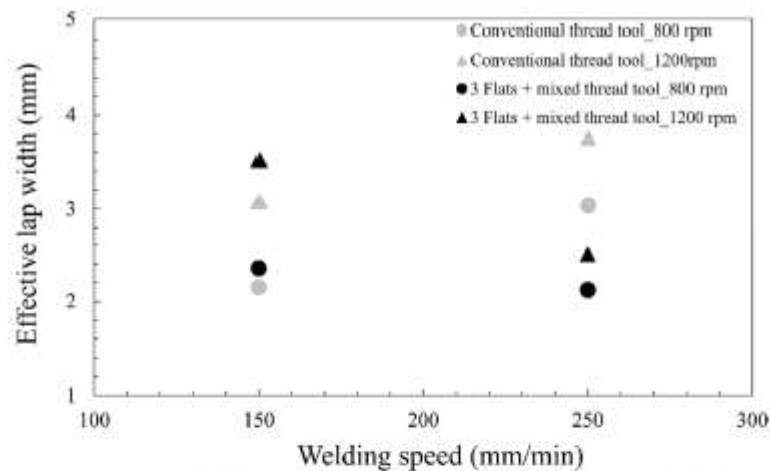


Figure 7. Effective lap width (ELW on Figure 3a) as a function of welding speed for the studied tool geometries and rotational speeds.

As it can be observed in Figure 7, an increase of the welding speed results in an increment of the ELW for the conventional threaded tool. These results contrast with those obtained for the 3 flats + mixed thread tool which decreases its ELW when increasing the welding speed. These different trends are attributed to the material flow induced by the tool probe design. While the conventional threaded tool prevents the material flow labelled as III in Figure 4, the 3 flats + mixed thread tool seems to enhance it.

These results indicate the importance of using the 3 flats + mixed thread tool at low welding speed and the conventional threaded tool at high welding speed with the aim of obtaining the largest ELW possible. A large ELW is desired to guarantee optimum mechanical performance of FSW lap joints [31].

On the other hand, the increase of rotational speed allows increasing the ELW for both tools. As it can be clearly observed in Figures 5 and 6, this is mainly because the cold lap defect extends over a larger horizontal distance into the weld nugget at the lower rotational speed. Then, a high rotational speed favours the material flow, plastic deformation, plasticised metal mixture and a more effective oxide dispersion at the faying surface. However, the use of higher rotational speeds also favours flow I and II resulting in an increment of the hook height in the advancing and the retreating sides when using the conventional threaded tool as can be observed in Figure 5. This effect is not observed in the welds produced by the 3 flats + mixed thread tools (Figure 6).

From the values represented in Figure 7, an increment of 30% of the ELW was estimated in average in the joints produced by the conventional threaded tool.

Figure 8 depicts hook heights at advancing and retreating sides as a function of the welding speed for the studied tool geometries and rotational speeds. Note again that hook at the retreating side is closely related to cold lap feature. As expected, larger hook heights were measured on the joints performed by the conventional threaded tool for all investigated welding parameters. The highly deformed grain orientations of AA2060-T8E30 sheet material of the TMAZ regions are indicative of the vertical material flow induced by the conventional threaded tool (flow I and II on Figure 4), which is the main formation mechanism of the hook at the advancing and the retreating sides.

For the conventional threaded tool, when increasing welding speed hook height decreases, particularly for 1200 rpm rotational speed. This can be explained by the fact that at higher welding speed the material upward flow (flow I and flow II on Figure 4) is limited due to the lower capability of shearing effect provided by the probe. For the same reason, the increase of the rotational speed

increases the hook height by favouring the upward material flow in the TMAZ. Thus, it can be concluded that the hook size tends to be larger with higher rotational speeds or lower welding speeds.

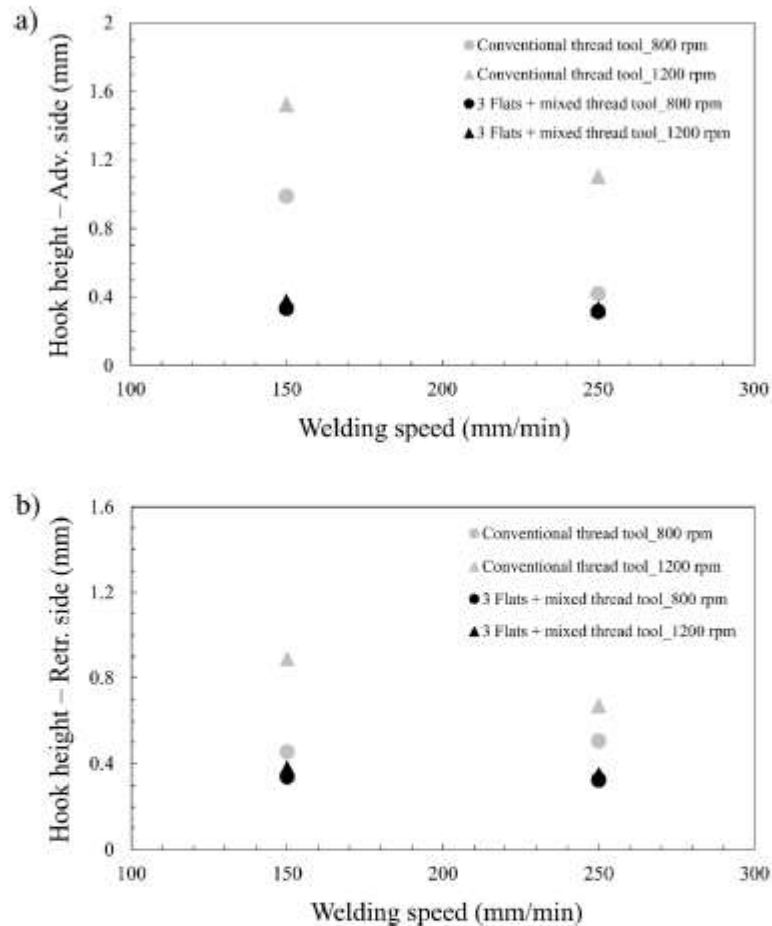


Figure 8. (a) Hook height at the advancing side (D1 on Figure 3b) and (b) hook height at the retreating side (D2 on Figure 3c) as a function of welding speed for the studied tool geometries and rotational speeds.

In the case of the 3 flats + mixed thread tool no important differences were observed in the hook heights under the investigated welding parameters. These results may be attributed to the 3 different threads along with the 3 flats that form the probe of this tool. These geometrical features allow avoiding an excess of upward material flow that would increase the hook height at higher rotational speeds or lower welding speeds. It is important to note that this tool allows keeping the hook height short, i.e., less than 0.4 mm, under a wide range of welding parameters. This short height of the hook has been shown to increase the mechanical strength of FSW lap joints by several authors, specially the fatigue strength [24]. In addition to this, hook heights below 0.4 mm would allow to comply with the acceptance criteria B established by the new revision of the ISO25239 standard for quality requirements of FSW lap joints.

From the values represented in Figure 8, an increment of 138% of the hook heights was estimated in average in the joints produced by the conventional threaded tool.

3.2. Reaction Forces during FSW Process

In-plane reaction forces (X-Force and Y-Force) are shown in Figure 9 as a function of welding speed for the studied tool geometries. The circles indicate the average reaction forces recorded for welds produced at 800 rpm of rotational speed and the triangles are for the welds produced at 1200 rpm. The general trend shows an increase in the reaction forces if higher welding speeds are used.

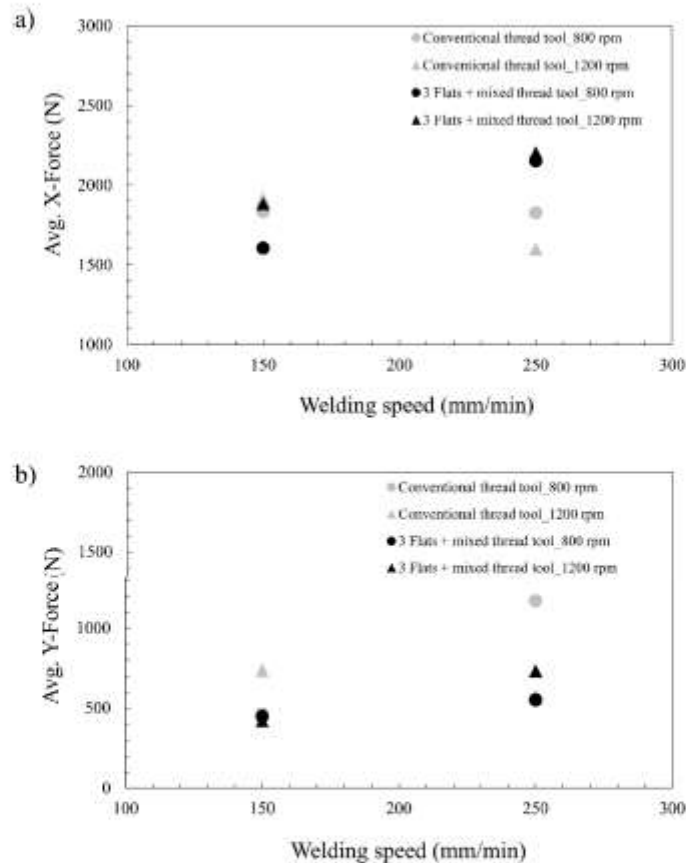


Figure 9. (a) Average X-Force and (b) average Y-force as a function of welding speed for the studied tool geometries and rotational speeds.

For the conventional threaded tool the increase of welding speed diminishes X-Force at 1200 rpm but do not produce an important change at 800 rpm. For the Y force, when increasing welding speed, the force increases at 800 rpm and slightly decreases at 1200 rpm.

In the case of the 3 flats + mixed thread tool, it can be observed that X-force and Y-force increase with increasing welding speed and increased rotational speed leads to an increase in X-force at 150 mm/min and Y-force at 250 mm/min. However, the increase of rotational speed does not affect the X-Force at 250 mm/min and Y-Force at 150 mm/min.

From these particular trends, it can be deduced that the X-force and Y-force do not have a clear trend with the welding parameters and other aspects are influencing their values [32,33]. Many authors have investigated the influence of defect formation on the in-plane reaction forces (X- force and Y-Force). Reza-E-Rabby et al. [34] reported that volumetric defects strongly affect the in-plane forces in bead on plate welds. In this regard, since there were no volumetric defects in the investigated FSW

welds, the lack of a clear trend between the welding parameters and X-force and Y-force could be explained based on the influence of the hook and cold lap defect formation. The formation of these joint features alters the material flow around the tool and, in consequence, the values of X-Force and Y-force. The different hook and cold lap defect size along with different tool geometry may justify the differences in force values. Unfortunately, the relationship between the material flow and defect formation for each tool geometry cannot be well understood only with these results and further work should be done in the future to shed light on this topic.

Figure 10 depicts the torque as a function of the welding speed for the studied tool geometries and rotational speeds. A clear relationship between welding speed, rotational speed and torque for both tool geometries can be observed, i.e., the higher the welding speed, the higher the torque; and the higher the rotational speed, the lower the torque. Note, that the torque is similar for both tool geometries which implies that the shoulder size is the main factor affecting the torque and the effect by the probe features is not significant.

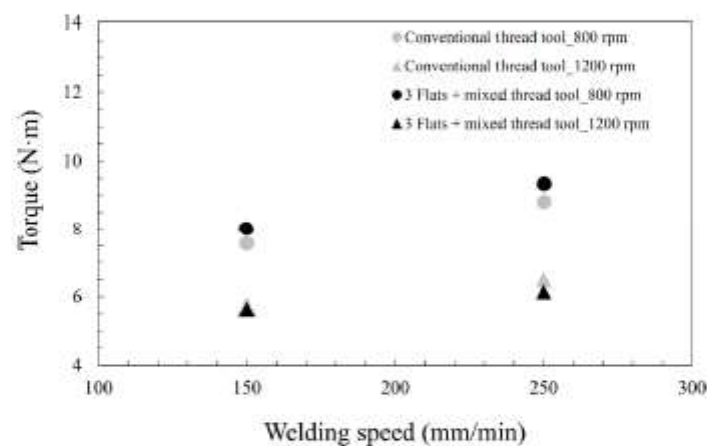


Figure 10. Torque as a function of welding speed for the studied tool geometries and rotational speeds.

4. Conclusions

The effect of tool geometry and welding parameters on the properties of PSW lap joints of AA2099-T83 and AA2060-T8E30 Al-Li alloys has been studied in regard to hook and cold lap defect formation and process reaction forces. The following conclusions can be drawn from the present work:

- Generally larger ELW values were obtained using the conventional threaded tool, although also larger hook heights were formed by this tool geometry. The increment of the ELW and the hook heights was estimated in a 30% and a 138% respectively.
- The 3 flats + mixed thread tool showed the capability to keep the hook height values low irrespective of the employed welding parameters. Therefore, the capability to limit the vertical material flow at the faying surface of the materials has been demonstrated.
- For both tools, a general trend was observed showing an increase of the reaction forces (X and Y) and torque values when increasing the welding speed. A clear trend showing an increase of the torque values when using lower rotational speeds and higher welding speeds was observed.
- The reaction forces during PSW depend on the welding parameters and tool geometry, which influence the formation of hooks and cold lap defects. No clear relationship between these joint features and reaction forces was found in this investigation.

Based on these conclusions, it can be stated that the tool geometry with 3 flats + mixed thread presents clear advantages for PSW lap joint manufacturing in comparison with the conventional

threaded tool design, as it is well known that smaller hook features result in an increment of the mechanical strength of FSW lap joints [21–24]. The 3 flats + mixed thread tool showed an estimated improvement of 138% in hook height while the detrimental effect in ELW was estimated in 30% in comparison with the conventional threaded tool.

Author Contributions: Conceptualization, E.A.; formal analysis, E.A. and J.V.; investigation, E.A. and J.V.; methodology, E.A.; supervision, P.Á. and L.H.; writing—original draft, E.A.; writing—review and editing, E.A., J.V., P.Á. and L.H. All authors have read and agree to the published version of the manuscript.

Funding: This work has been performed in the frame of the project ecoTECH within the AIRFRAME ITD of the Clean Sky 2 programme of the H2020. The authors acknowledge the funding received for this project under the project ID 807083 of the call H2020-IBA-CS2-GAMS-2017).

Acknowledgments: The authors want to thank Arconic and IAI for supplying the base materials used in this work.

Conflicts of Interest: The authors declare no conflict of interest.

References

1. Starke, E.A.; Staley, J.T. Application of modern aluminum alloys to aircraft. *Progress Aerosp. Sci.* **1996**, *32*, 131–172. [\[CrossRef\]](#)
2. Alexopoulos, N.D.; Gialos, A.A.; Zeimpekis, V.; Velonaki, Z.; Kashaev, N.; Riekehr, S.; Karanika, A. Laser beam welded structures for a regional aircraft: Weight, cost and carbon footprint savings. *J. Manuf. Syst.* **2016**, *39*, 38–52. [\[CrossRef\]](#)
3. Sánchez Amaya, J.M.; Amaya-Vázquez, M.R.; Botana, F.J. 8—Laser welding of light metal alloys: Aluminium and titanium alloys. In *Handbook of Laser Welding Technologies*; Katayama, S., Ed.; Woodhead Publishing Series in Electronic and Optical Materials; Woodhead Publishing: Cambridge, UK, 2013; pp. 215–254, ISBN 978-0-85709-264-9.
4. Gialos, A.A.; Zeimpekis, V.; Alexopoulos, N.D.; Kashaev, N.; Riekehr, S.; Karanika, A. Investigating the impact of sustainability in the production of aeronautical subscale components. *J. Clean. Prod.* **2018**, *176*, 785–799. [\[CrossRef\]](#)
5. Aldanondo, E.; Arruti, E.; Alvarez, P.; Echeverria, A. Mechanical and Microstructural Properties of FSW Lap Joints. In *Friction Stir Welding and Processing VII*; Mishra, R., Mahoney, M.W., Sato, Y., Hovanski, Y., Verma, R., Eds.; Springer International Publishing: Cham, Switzerland, 2016; pp. 195–203. ISBN 978-3-319-48108-1.
6. Arbogast, W.J. A flow-partitioned deformation zone model for defect formation during friction stir welding. *Scr. Mater.* **2008**, *58*, 372–376. [\[CrossRef\]](#)
7. Guerra, M.; Schmidt, C.; McClure, J.C.; Murr, L.E.; Nunes, A.C. Flow patterns during friction stir welding. *Mater. Charact.* **2002**, *49*, 95–101. [\[CrossRef\]](#)
8. Kashaev, N.; Ventzke, V.; Çam, G. Prospects of laser beam welding and friction stir welding processes for aluminum airframe structural applications. *J. Manuf. Process.* **2018**, *36*, 571–600. [\[CrossRef\]](#)
9. Edwards, L.; Fitzpatrick, M.E.; Irving, P.E.; Sinclair, I.; Zhang, X.; Yapp, D. An Integrated Approach to the Determination and Consequences of Residual Stress on the Fatigue Performance of Welded Aircraft Structures. *J. ASTM Int.* **2006**, *3*. [\[CrossRef\]](#)
10. Richter-Trummel, V.; Moreira, P.M.G.P.; Ribeiro, J.; de Castro, P.M.S.T. The contour method for residual stress determination applied to an AA6082-T6 friction stir butt weld. *Mater. Sci. Forum* **2011**, *681*, 177–181. [\[CrossRef\]](#)
11. Guo, J.; Fu, H.; Pan, B.; Kang, R. Recent progress of residual stress measurement methods: A review. *Chin. J. Aeronaut.* **2020**. [\[CrossRef\]](#)
12. Zhang, H.; Wang, M.; Zhang, X.; Zhu, Z.; Yu, T.; Yang, G. Effect of Welding Speed on Defect Features and Mechanical Performance of Friction Stir Lap Welded 7B04 Aluminum Alloy. *Metals* **2016**, *6*, 87. [\[CrossRef\]](#)
13. Chen, H.; Fu, L.; Liang, P.; Liu, F. Defect features, texture and mechanical properties of friction stir welded lap joints of 2A97 Al-Li alloy thin sheets. *Mater. Charact.* **2017**, *125*, 160–173. [\[CrossRef\]](#)
14. Song, Y.; Yang, X.; Cui, L.; Hou, X.; Shen, Z.; Xu, Y. Defect features and mechanical properties of friction stir lap welded dissimilar AA2024-AA7075 aluminum alloy sheets. *Mater. Des.* **2014**, *55*, 9–18. [\[CrossRef\]](#)
15. Buffa, G.; Campanile, G.; Fratini, L.; Prisco, A. Friction stir welding of lap joints: Influence of process parameters on the metallurgical and mechanical properties. *Mater. Sci. Eng. A* **2009**, *519*, 19–26. [\[CrossRef\]](#)

16. Dubourg, L.; Merati, A.; Jahazi, M. Process optimisation and mechanical properties of friction stir lap welds of 7075-T6 stringers on 2024-T3 skin. *Mater. Des.* **2010**, *31*, 3324–3330. [[CrossRef](#)]
17. Liu, H.; Hu, Y.; Peng, Y.; Dou, C.; Wang, Z. The effect of interface defect on mechanical properties and its formation mechanism in friction stir lap welded joints of aluminum alloys. *J. Mater. Process. Technol.* **2016**, *238*, 244–254. [[CrossRef](#)]
18. Chen, G.; Li, H.; Wang, G.; Guo, Z.; Zhang, S.; Dai, Q.; Wang, X.; Zhang, G.; Shi, Q. Effects of pin thread on the in-process material flow behavior during friction stir welding: A computational fluid dynamics study. *Int. J. Mach. Tools Manuf.* **2018**, *124*, 12–21. [[CrossRef](#)]
19. Xu, Z.; Li, Z.; Lv, Z.; Zhang, L. Effect of Welding Speed on Joint Features and Lap Shear Properties of Stationary Shoulder FSIWeld Alclad 2024 Al Alloy. *J. Mater. Eng. Perform.* **2017**, *26*, 1358–1364. [[CrossRef](#)]
20. Zhou, Z.; Yue, Y.; Ji, S.; Li, Z.; Zhang, L. Effect of rotating speed on joint morphology and lap shear properties of stationary shoulder friction stir lap welded 6061-T6 aluminum alloy. *Int. J. Adv. Manuf. Technol.* **2017**, *88*, 2135–2141. [[CrossRef](#)]
21. Ji, S.; Li, Z.; Zhou, Z.; Wu, B. Effect of Thread and Rotating Speed on Material Flow Behavior and Mechanical Properties of Friction Stir Lap Welding Joints. *J. Mater. Eng. Perform.* **2017**, *26*, 5085–5096. [[CrossRef](#)]
22. Liu, Z.; Zhou, Z.; Ji, S. Improving interface morphology and shear failure load of friction stir lap welding by changing material concentrated zone location. *Int. J. Adv. Manuf. Technol.* **2018**, *95*, 4013–4022. [[CrossRef](#)]
23. ISO25239 (2011) *Friction Stir Welding—Aluminium, Part 5: Quality and Inspection Requirements*; The International Organization for Standardization (ISO): Geneva, Switzerland, 2011.
24. Balakrishnan, M.; Leitão, C.; Arruti, E.; Aldanondo, E.; Rodrigues, D.M. Influence of pin imperfections on the tensile and fatigue behaviour of AA 7075-T6 friction stir lap welds. *Int. J. Adv. Manuf. Technol.* **2018**, *97*, 3129–3139. [[CrossRef](#)]
25. Eswara Prasad, N.; Gokhale, A.A.; Wanhill, R.J.H. Aluminium–Lithium Alloys. In *Aerospace Materials and Material Technologies: Volume 1: Aerospace Materials*; Prasad, N.E., Wanhill, R.J.H., Eds.; Indian Institute of Metals Series; Springer: Singapore, 2017; pp. 53–72, ISBN 978-981-10-2134-3.
26. Starke, E.A. Chapter 1—Historical Development and Present Status of Aluminum–Lithium Alloys. In *Aluminum–Lithium Alloys*; Eswara Prasad, N., Gokhale, A.A., Wanhill, R.J.H., Eds.; Butterworth-Heinemann: Boston, MA, USA, 2014; pp. 3–26. ISBN 978-0-12-401698-9.
27. Meng, X.; Xu, Z.; Huang, Y.; Xie, Y.; Wang, Y.; Wan, L.; Lv, Z.; Cao, J. Interface characteristic and tensile property of friction stir lap welding of dissimilar aircraft 2060-T8 and 2099-T83 Al–Li alloys. *Int. J. Adv. Manuf. Technol.* **2018**, *94*, 1253–1261. [[CrossRef](#)]
28. Costa, M.I.; Verdura, D.; Costa, J.D.; Leitao, C.; Rodrigues, D.M. Influence of pin geometry and process parameters on friction stir lap welding of AA5754-H22 thin sheets. *J. Mater. Process. Technol.* **2015**, *225*, 385–392. [[CrossRef](#)]
29. Li, Z.; Yue, Y.; Ji, S.; Chai, P.; Zhou, Z. Joint features and mechanical properties of friction stir lap welded alclad 2024 aluminum alloy assisted by external stationary shoulder. *Mater. Des.* **2016**, *90*, 238–247. [[CrossRef](#)]
30. Shirazi, H.; Kheirandish, S.; Pouraliakbar, H. Employing hooking and effective sheet thickness to achieve optimum failure load in lap joints of friction stir welded AA5456 aluminum. *Theor. Appl. Fract. Mech.* **2020**, *105*, 102423. [[CrossRef](#)]
31. Yue, Y.; Li, Z.; Ji, S.; Huang, Y.; Zhou, Z. Effect of Reverse-threaded Pin on Mechanical Properties of Friction Stir Lap Welded Alclad 2024 Aluminum Alloy. *J. Mater. Sci. Technol.* **2016**, *32*, 671–675. [[CrossRef](#)]
32. Reza-E-Rabby, M.; Reynolds, A.P. Some effects of tool geometric features on friction stir weld response parameters. *Sci. Technol. Weld. Join.* **2018**, *23*, 575–584. [[CrossRef](#)]
33. Reza-E-Rabby, M.; Reynolds, A.P. Effect of Tool Pin Thread Forms on Friction Stir Weldability of Different Aluminum Alloys. *Procedia Eng.* **2014**, *90*, 637–642. [[CrossRef](#)]
34. Reza-E-Rabby, M.; Tang, W.; Reynolds, A.P. Effects of thread interruptions on tool pins in friction stir welding of AA6061. *Sci. Technol. Weld. Join.* **2018**, *23*, 114–124. [[CrossRef](#)]



13.- ARTICLE 10: FRICTION STIR WELDING OF AA2099-T83 AND AA2060T8E30 ALUMINIUM ALLOYS WITH NEW CR-FREE SURFACE TREATMENTS AND SEALANT APPLICATION

[78] E. Aldanondo, J. Vivas, P. Álvarez, I. Hurtado y A. Karanika, «Friction stir welding of AA2099-T83 and AA2060-T8E30 aluminium alloys with new Cr-free surface treatments and sealant application,» *Metals*, vol. 11, nº 644, 2021.

Having optimised the welding process parameters and tool design resulting in high-quality FSLW joints between selected Al-Li alloys in the as-delivered condition, in this work we investigated the feasibility to produce FSLW joints using those base materials with innovative surface treatments, as well as sealant in the joint interface. Cr-free TFSA and Sol-Gel treatments were applied to the AA2099-T83 extrusions and AA2060-T8E30 sheets by HAI and FSLW joints were produced using the previously optimised welding conditions. A sealant typically used to improve the corrosion resistance of the joints in aeronautic structures was also applied in the overlapping interface of the joints before the FSW process. The properties of the FSLW joint were investigated and compared to the properties of the joints produced without any surface treatment nor sealant application. We concluded that it is feasible to produce good quality FSLW joints using surface treated Al-Li alloys and applying a sealant in the overlapping interface, we did not observe significant variations in the mechanical properties. These conclusions opened the possibility for manufacturing lightweight and corrosion resistant structures for the aeronautic sector using FSW technology.

This article was the second of the three articles that are to be considered for the completion of the thesis as a compendium of publications. It was published in the journal "Metals".

Article

Friction Stir Welding of AA2099-T83 and AA2060-T8E30 Aluminium Alloys with New Cr-Free Surface Treatments and Sealant Application

Egoitz Aldanondo ^{1,*}, Javier Vivas ¹, Pedro Álvarez ¹, Iñaki Hurtado ² and Alexandra Karanika ³

¹ LORTEK Technological Centre, Basque Research and Technology Alliance (BRTA), 20240 Ordizia, Spain; jvivas@lortek.es (J.V.); palvarez@lortek.es (P.A.)

² Faculty of Engineering (MU-ENG), Mondragon Unibertsitatea, 20500 Arrasate-Mondragon, Spain; ihurtado@mondragon.edu

³ Hellenic Aerospace Industry S.A., 32009 Schimatari, Greece; akaranika@haicorp.com

* Correspondence: egoitz@lortek.es; Tel: +34-943-882-303

Abstract: The feasibility for friction stir welding (FSW) surface-treated AA2099-T83 aluminium extrusions with AA2060-T8E30 aluminium sheets in the overlap configuration and using a sealant at the interface was investigated in this work. New Cr-free surface treatments such as thin film sulphuric acid anodising (TFSA) and sol-gel were applied to the parent materials, and a sealant was applied before applying the FSW process. FSW welds were produced using several combinations of surface treatments and sealant application with no significant influence on FSW process stability and performance. The metallographic examination of the welds showed that a good protection of the crevice was achieved with some sealant accumulation at the edges of the overlapping region. The microstructural analysis showed no sealant remnants but the presence of some oxide remnants in the stir zone (SZ) of the welds, especially in the TFSA treated parent material cases. However, these remnants did not show any significant effect in the static pull-out strength of the joints and failures at the most stressed zone of the AA2099-T83 extrusions outside the FSW weld region were consistently obtained.

Keywords: friction stir welding; lap joint; surface treatment; thin film sulphuric acid anodizing; sol-gel; sealant; aluminium; aeronautic



Citation: Aldanondo, E.; Vivas, J.; Álvarez, P.; Hurtado, I.; Karanika, A. Friction Stir Welding of AA2099-T83 and AA2060-T8E30 Aluminium Alloys with New Cr-Free Surface Treatments and Sealant Application. *Metals* **2021**, *11*, 644. <https://doi.org/10.3390/met11040644>

Academic Editor: Evgeniy A. Kolubayev

Received: 25 February 2021

Accepted: 8 April 2021

Published: 15 April 2021

Publisher's Note: MDPI stays neutral with regard to jurisdictional claims in published maps and institutional affiliations.



Copyright: © 2021 by the authors. Licensee MDPI, Basel, Switzerland. This article is an open access article distributed under the terms and conditions of the Creative Commons Attribution (CC BY) license (<https://creativecommons.org/licenses/by/4.0/>).

1. Introduction

The transportation industry in general and the aerospace industry in particular are continuously demanding lightweight load-bearing structures in order to achieve improvements in fuel consumption efficiency and reduction of CO₂ emissions [1,2]. Although riveting is the dominant joining technology for manufacturing aircraft structures, other modern technologies such as friction stir welding (FSW) have been proposed as alternatives due to important benefits over riveting [3–8]. Weight saving and reduced manufacturing costs and times have been listed as some of the main advantages shown by FSW applied to the manufacturing of efficient aircraft structures [9,10]. This innovative manufacturing technology required the execution of lap joints by FSW, among other joint configurations and design possibilities [4]. Thus, the need to produce lap joints by FSW promoted the interest and investigations of this type of joint configuration by several authors [11–18]. These studies showed the importance of using an appropriate FSW tool design and welding parameters in order to achieve high-quality welds using different types of aluminium alloys.

High-strength aluminium alloys are key engineering materials widely considered for the manufacturing of efficient aircraft structures due to their low density and potential to produce light, strong structures [19]. The continuous search for low density and high strength in modern aluminium alloys promoted the maturation of the third generation

of Al-Li alloy family. After many years of intense research and development efforts, numerous Al-Li alloys have been produced in several product forms, showing improved properties in comparison to the traditional 2XXX and 7XXX aluminium alloys such as higher modulus and higher specific strength [20]. Thus, the commercial availability of aluminium products with alloys such as AA2060 and AA2099 opens new opportunities to design efficient aeronautical and space structures. The possibility for producing joints by FSW using these alloys was investigated by some authors showing their potential for manufacturing stiffened panels by joining AA2099-T83 stringers to AA2060-T8E30 skin [18,21]. Other authors also showed the possibility of using other Al-Li alloys to produce FSW joints [22,23].

Another important issue to be considered for the design and manufacturing of aircraft structures is the corrosion resistance. In order to achieve a long-term operational capability, a variety of corrosion protection methods such as surface treatments and sealants are used in the aerospace industry. Operational considerations, societal concerns, as well as registration, evaluation, authorization and restriction of chemicals (REACH) regulations are creating a growing demand for the development of new effective and environmentally friendly technologies [24,25]. In addition to that, there is a continuous need to reduce the environmental footprint of the manufacturing technologies, as established in the advisory council for aviation research and innovation (ACARE) targets [26]. Thus, materials used in manufacturing airframe components need to become more resistant in corrosion and more eco-compliant in order to achieve an eco-friendly life cycle. This includes a significant decrease of hazardous materials during the manufacturing phase. In this context, chrome-free surface treatments such as thin film sulphuric acid anodising (TFSAA) and out-of-bath Sol-Gel sprayable application are being developed aiming at the replacement of current chromate anticorrosive protection processes [27].

From a general manufacturing of aircraft structures point of view, it is necessary to investigate the feasibility to combine surface treatments, sealants, and joining technologies. Several authors investigated the feasibility of FSW and its derivatives such as refill friction stir welding (RFSSW) for joining surface-treated aluminium alloys in the overlap configuration using sealants [28–32]. These studies demonstrated a good potential of FSW technologies to weld surface-treated aluminium alloys using sealants with appropriate welding conditions and materials. However, these studies focused mostly on conventional high-strength aluminium alloys of 2XXX and 7XXX series, as well as in standard chrome-based surface treatments such as Alodine-1200S Aero Chromate Chemical Film. The effects produced when combining FSW, Al-Li alloys, and innovative chrome-free surface treatments have not been investigated before in spite of being highly interesting. Thus, the present work focused on investigating the properties of FSW joints produced using surface-treated Al-Li alloys with sealant application and comparing their properties with FSW joints produced using non-treated alloys.

2. Materials and Methods

2.1. Base Materials and Surface Treatments

Lap joints were produced using Z-shaped extrusions of AA2099-T83 aluminium alloy on top of rolled sheets of AA2060-T8E30 aluminium alloy. The thickness of the AA2099-T83 extrusions was 2 mm, while the thickness of the AA2060-T8E30 sheets was 2.5 mm. The nominal chemical compositions of these aluminium alloys are shown in Table 1. First, 500 mm long extrusions were placed on top of sheets measuring 100 mm × 600 mm for the manufacturing of the welded coupons. Welded coupons composed by several combinations of surface treatments as well as sealant application at the matching interface between overlapping base materials were produced by FSW and examined. Thus, six different coupons were produced using two different types of surface treatments and the application of a sealant, as shown in Table 2.

Table 1. Chemical composition of base materials, wt %.

Alloy	Al	Si	Fe	Cu	Mn	Mg	Zn	Ti	Ag	Li	Zr
AA2060-T8E30	Bal.	0.07	0.07	3.4–4.5	0.1–0.5	0.6–1.1	0.3–0.5	0.1	0.05–0.5	0.6–0.9	0.05–0.15
AA2099-T83	Bal.	0.05	0.07	2.4–3.0	0.1–0.5	0.1–0.5	0.4–1	0.1	-	1.6–2.0	0.05–0.12

Table 2. Friction stir welded coupon identification with the applied surface treatments and sealant.

Coupon Code ID	Surface Treatment	Sealant
C1	-	-
C2	TFSAA	-
C3	Sol Gel	-
C4	-	Naftoseal [®] MC-780-Class C
C5	TFSAA	Naftoseal [®] MC-780-Class C
C6	Sol Gel	Naftoseal [®] MC-780-Class C

Coatings of the AA2099-T83 aluminium extrusions and the AA2060-T8E30 sheets were produced by the Hellenic Aerospace Industry (HAI) using two different surface treatment techniques: (i) thin film sulphuric acid anodising (TFSAA) and (ii) sprayable application of sol-gel treatment (AC131 from 3M[™]). Both treatments are fully chromium free and REACH compliant. Prior to both (i) and (ii) treatments, the aluminium surfaces were given the following surface preparation: alkaline degreasing, rinsing, alkaline etching, rinsing, desmutting, and final rinsing.

TFSAA was initially performed in an experimental, lab-scale setup and then scaled-up in semi-industrial and final industrial conditions. During the anodising cycle the current density, and the electrolyte temperature were recorded. The experimental setup for TFSAA and the process parameters are given in Figure 1.



Parameter Description	Value
Sulphuric acid	43 g/L
D.I. water	Rem
Temperature	24–27 °C
Total immersion time	24–26 min
Final voltage	15–15.5 V (ramp-up max 5 V/min)
Cathodes	Pb
Agitation	Magnetic stirring

Figure 1. Experimental setup for the thin film sulphuric acid anodising (TFSAA) alongside TFSAA process parameters.

The sol-gel treatment by AC131 was applied with a spray-gun in order to reduce the needs of waste management. The treatment was performed respecting the pot life of the AC131 sol-gel solution, which is limited to few days.

The sealant selected for this investigation was Naftoseal[®] MC-780-class C (Chemetall GmbH, Frankfurt am Main, Germany), which is a two-component, manganese-dioxide cured polysulfide polymer system with reduced density typically used for fuel tank and fuselage seals in aerospace manufacturing. The application of the sealant in the extrusion-sheet interface was performed in the uncured state right after mixing the two components and prior to the execution of the PSW process. A constant thickness of 0.2 mm

of sealant was applied using an adhesive tape of the same thickness, removing the sealant remnants and the tape itself prior to the FSW process.

2.2. Friction Stir Welding Procedure

The AA2099-T83 extrusions and AA2060-T8E30 sheets were friction stir welded at LORTEK in the overlap configuration in an I-STIR PDS 4 machine operated in force control. The welding tool, which in previous investigations was shown to have an optimised design for the manufacturing of lap joints [17,21], consisted of a probe with 3 flats and a mixed thread with a diameter of 4 mm and a length of 2.5 mm. The shoulder had a flat shoulder of 10 mm in diameter. A specifically designed fixture and clamping system was used for the positioning of the AA2099-T83 extrusions on top of the AA2060-T8E30 sheets. All welds were performed at a clockwise rotational speed of 1200 rpm, a welding speed of 250 mm/min, and a forge force of 6.25 kN. The advancing side of the welds was oriented toward the vertical section of the extrusions and the retreating side toward the free side of the extrusions. The tilt angle of the tool was 1.5° in all cases. The main process parameters such as the torque, forge force, and penetration by the welding tool were recorded for their analysis during the FSW process using the controller of the FSW machine. The setup for the FSW process showing the specific fixture, welding tool, and the materials mounted on the FSW machine table as well as some completed FSW coupons can be observed in Figure 2.

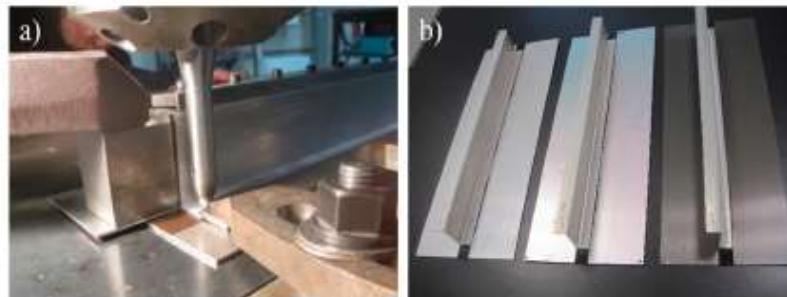


Figure 2. (a) Setup for the FSW process and (b) example of completed FSW coupons C4, C5, and C6.

2.3. FSW Weld Property Characterisation

The properties of the FSW welds were assessed by metallographic characterisation and static mechanical strength tests (pull-out tests). Cross-sectional specimens were cut perpendicular to the welding direction from each of the welded coupons. The specimens were prepared using standard procedures for mounting, grinding, and polishing to a mirror-like surface finish using a colloidal silica suspension. After this preparation, the specimens were etched using a diluted Keller's reagent to reveal the microstructure. The initial metallographic examination of the cross-sectional specimens was performed by optical microscopy using an Olympus GX51 light optical microscope, before and after the chemical etching of the specimens in order to allow a more clear observation of the influences of the coatings in the welded region. The specimens were also characterised making use of both a Fei Nova NanoSEM 450 scanning electron microscope (SEM) and an Oxford Instruments X-Max 50 energy-dispersive X-ray spectroscopy (EDS) system.

The influence of the coatings and sealant in the static strength of the FSW joints was investigated by pull-out tests using a Zwick Roell Z100 tensile testing machine with a load capacity of 100 kN and a constant testing speed of 1.6 mm/min. Thirty mm wide test samples were cut from the welded coupons using electrical discharge machining (EDM). In these tests, the AA2060-T8E30 was clamped in a special fixture designed for the tests, and a pull-out force perpendicular to the weld surface was applied to the AA2099-T83 extrusion

until fracture. Three samples from each FSW coupon, C1–C6, were tested, and average values of the maximum pull-out force were calculated.

3. Results

3.1. Reaction Forces and Tool Penetration during FSW

The torque, forge force, and penetration feedback signals were analysed in order to study the effects of the coatings and sealant on the FSW process stability. The representation of these signals as a function of time during the FSW process for coupon C1 can be observed in Figure 3, which is representative also for the rest of the coupons, C2–C6. The penetration of the tool during the plunging phase was carried out in position control at a constant speed of 5 mm/min until a penetration value of 2.5 mm. An initial peak of forge force, as indicated in detail A, was observed at the beginning of the plunging phase followed by a reduction, as shown in detail B, when the material below the probe of the tool was heated and softened. At the end of the plunging phase, a large increase of the forge force was observed when the tool shoulder contacted the material, as shown in detail C. As expected, a similar evolution of the torque was observed at this point where the contact of the shoulder with the material produced an increase in its value. Detail D indicates how the forge force decreased again during the dwell time of 1 s applied for the homogenisation of the heat in the shoulder contact region before starting the tool travelling phase.

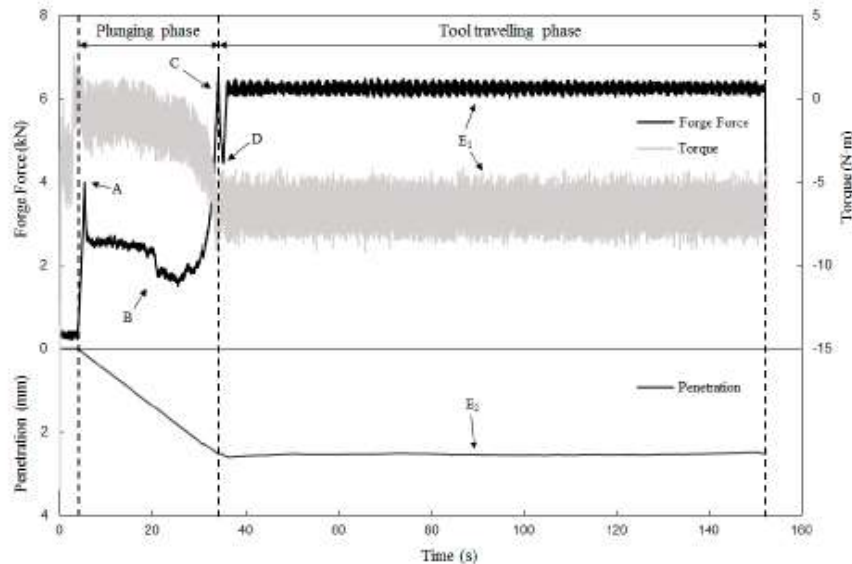


Figure 3. Representation of the forge force, torque, and tool penetration values as a function of time during the FSW process for the coupon C1.

The evolution of the forge force and torque during the tool travelling phase are indicated by detail E1 in Figure 3, whereas the evolution of the penetration is indicated by detail E2. This travelling phase was performed in force control so that the commanded value of the forge force was maintained at 6.25 kN. Slight variations of the tool penetration can be observed, which are produced by the FSW machine in order to maintain the commanded forge force value. The relatively constant values observed for penetration and torque during the tool travelling phase were indicative of a stable FSW process. Note that these two values are not commanded in the force control mode employed in these FSW welds.

Average values of torque and tool penetration during the travelling phase in the period comprehended between 40 and 140 s were calculated for all welded coupons. The representation of these values is shown in Figure 4. Similar values with no significant variations were observed for the torque and the tool penetration in all coupons. A maximum variation of 8% between the maximum and minimum torque average values calculated for the C1–C6 coupons was determined. Regarding the penetration, the maximum variation was 4%. These variations are indicative that the FSW process was stable and not significantly influenced by the surface conditions nor the sealant application before FSW.

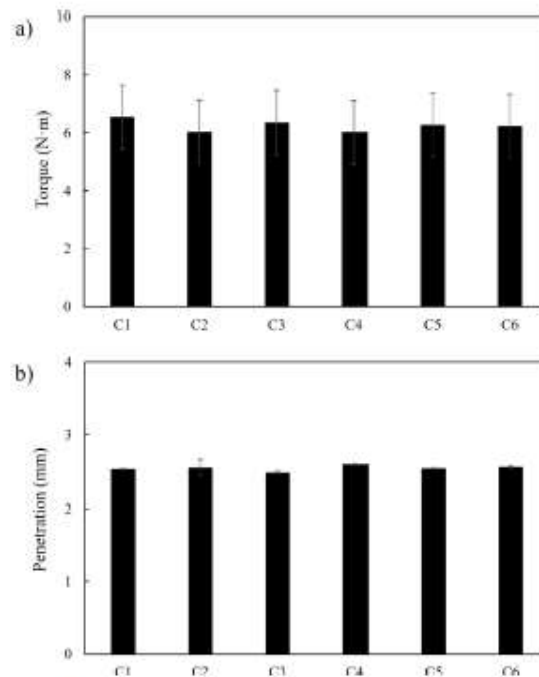


Figure 4. (a) Torque and (b) penetration average values obtained during the friction stir welding (FSW) process for C1–C6 coupons.

3.2. Metallographic Characterisation

A metallographic characterisation was performed in order to investigate the effects of the coatings and sealant on the microstructure of the welds. Cross-sectional macrographs of the weld specimens obtained from C1–C6 coupons are shown in Figure 5. No significant differences nor measurable volumetric defects were observed in the macrographs, showing similar macrostructural characteristics and shapes for all examined welds. All welds showed good soundness with all the typical FSW microstructural weld zones such as the stirred zone (SZ), thermo-mechanically affected zone (TMAZ), heat-affected zone (HAZ), and parent metal (PM). A small hook imperfection, which is a typical feature found in FSW lap joints [33], was consistently observed and similar in size in all welds at the AA2099-T83 extrusion and AA2060-T8E30 sheet interface in both advancing and retreating sides. These macrostructural characteristics are similar to the characteristics reported previously for similar welds by the authors [21].

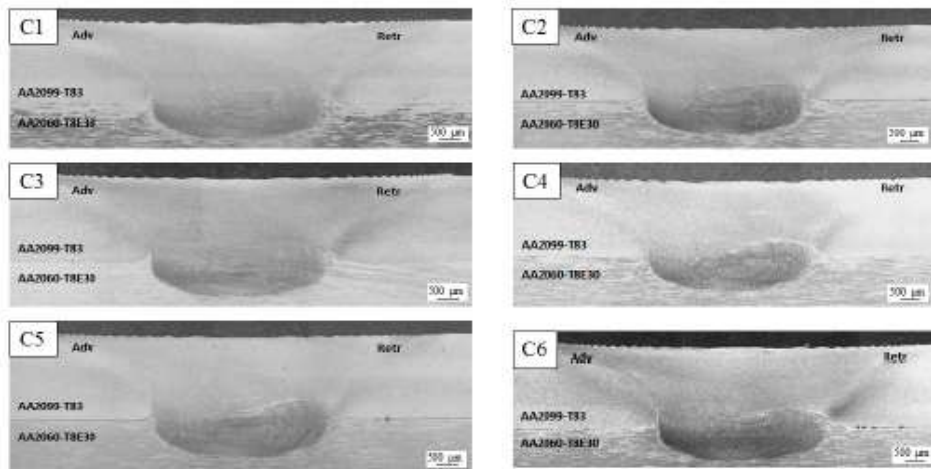


Figure 5. Cross-sectional macrographs of the FSW welds for C1–C6 coupons.

Figure 6 shows a cross-sectional macrograph of the weld specimen obtained from coupon C4 and higher magnification ($5\times$) micrographs of the crevice region in the AA2099-T83 extrusion and AA2060-T8E30 sheet interface. An accumulation of the Naftoseal[®] MC-780-Class C sealant in the crevice region can be clearly observed in details A and B, i.e., at the edges of the matching interfaces between the overlapping parent materials, indicating that a good protection of this crevice region was obtained by the sealant. These sealant accumulations were consistently observed also in the other coupons C5 and C6 that were produced using the sealant in the extrusion–sheet interface. It is worth noting that no macrostructural defects are observed in these welds using sealant at the matching interface. Thus, the achievement of a good protection of the crevice at the extrusion–sheet interface without impairing the weld quality seems to be feasible by combining un-cured sealant application and FSW.

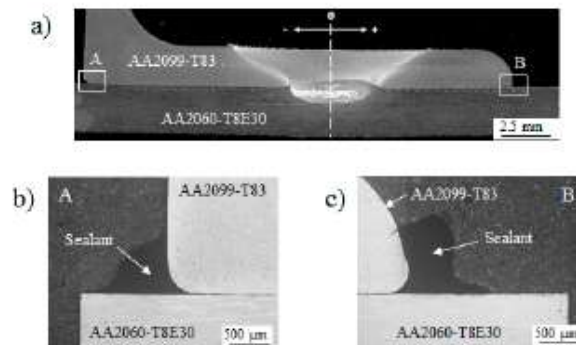


Figure 6. (a) Cross-sectional macrograph of the FSW weld in coupon C4; (b) magnified image of detail A in Figure 6a; and (c) magnified image of detail B in Figure 6a.

Further microstructural details of the FSW welds were investigated using SEM observation complemented with EDS chemical analysis. Figure 7 shows the results obtained for such analysis performed with the FSW weld from coupon C1, which was produced with

as-received base materials and without sealant application. The macrograph and the detail shown in Figure 7a were performed after chemical etching and before chemical etching respectively in order to get a more clear observation of the weld features. It can be observed that a very clear SZ region was obtained with no major contaminant agents, except in a reduced cold lap region located in the hook region of the retreating side (highlighted in detail A in Figure 7a). SEM observation and EDS analysis shown in Figure 7b revealed the presence of oxide remnants at the interface between the AA2099-T83 extrusion and the AA2060-T8E30 sheet, which are indicative of a non-complete break, dispersion, and mixing of the inherent oxide layer present at the surface of the parent materials before the FSW process.

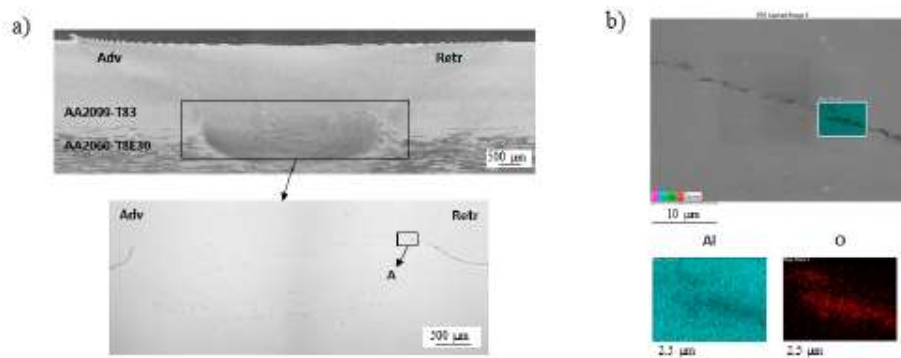


Figure 7. (a) Cross-sectional macrograph of the FSW weld from coupon C1 and (b) SEM image and EDS analysis of the region indicated as detail A in Figure 7a.

Figure 8 shows the cross-sectional macrograph of coupon C2, as well as the SEM observation and the EDS analysis carried out at the interface between the AA2099-T83 extrusion and the AA2060-T8E30 sheet, as indicated by detail A in Figure 8a. The SEM analysis (Figure 8b) revealed the presence of continuous thin layers of aluminium oxide at the surface of both AA2099-T83 and AA2060-T8E30 alloys as a result of the TPSAA process applied to the parent materials before the FSW process. The thickness of the oxide layer in the AA2099-T83 extrusion was approximately 3 µm, whereas in the AA2060-T8E30 sheet, it was approximately 1 µm. The chemical composition analysis carried out by EDS in both oxide layers, which are represented as points P1 and P2 in Figure 8b, revealed an identical composition for both coatings, which was mainly composed of aluminium, oxygen, and sulphur. The sulphur content of the coating was indicative of the characteristics of the anodising process based on the use of sulphuric acid.

The microstructural analysis of the weld in coupon C2, which is shown in Figure 9, revealed an important presence of fragment remnants in the SZ. These fragment remnants can be observed as black particles in Figure 9b, and their dimension was estimated between 3 and 7 microns. It was found that the SZ region located in the advancing side was free from these fragment remnants, while the retreating side was more populated. At the centre of the SZ, the fragment remnants were relatively small and dispersed into the aluminium matrix, while closer to the edge of the retreating side, a continuous, thin layer formed by the remnants was observed. The EDS analysis of the fragment remnants showed a similar composition to the thin aluminium oxide layers identified at the surfaces of the parent materials (Figure 8) with the presence of some sulphur content. Therefore, it can be concluded that the presence of these fragment remnants is related to the incomplete break, dispersion, and mixing of the thin aluminium oxide coatings, which are originally at the surface of the TPSAA anodised parent materials before the FSW process. The morphology,

size, and distribution of the fragment remnants is a consequence of the plasticised metal flow promoted by the tool during the FSW process.

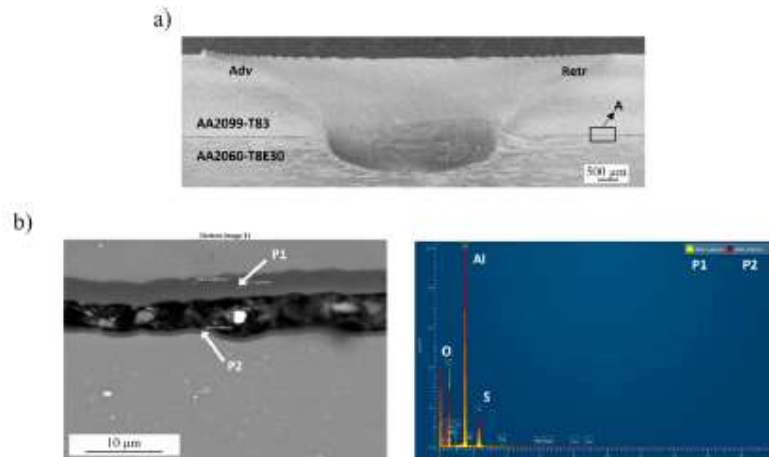


Figure 8. (a) Cross-sectional macrograph of the FSW weld from coupon C2 and (b) SEM image of the region indicated as detail A in Figure 8a (left) and EDS analysis (right) of points P1 and P2 shown in Figure 8b.

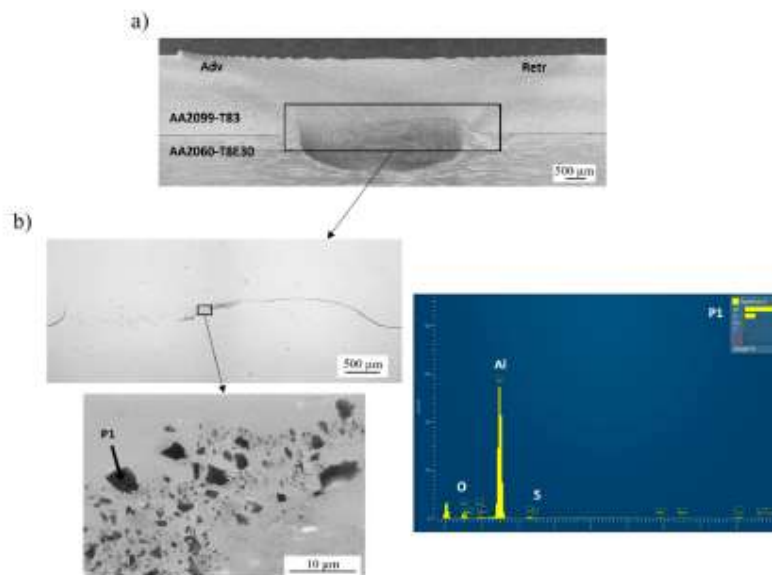


Figure 9. (a) Cross-sectional macrograph of the FSW weld from coupon C2 and (b) details of the SZ interface by optical microscopy, SEM, and EDS analysis of the fragment remnants.

Figure 10 shows a macrograph of the weld from coupon C6 and the detailed analysis of the crevice region between both parent materials. Similarly to the results shown in Figure 6, an accumulation of sealant at the crevice region was observed in the detail A

from Figure 10a, which is magnified in the image of Figure 10b. The EDS analysis of the sealant corresponding to point P1 in Figure 10b revealed a high sulphur content with lower contents of other elements such as oxygen and manganese. This result is consistent with the composition of the sealant, which is a manganese-dioxide cured polysulphide polymer system. Thus, in the same way as the sulphur content was used for the tracing and identification of aluminium oxide fragment remnants coming from the coatings produced in the TFSAA treatments, the sulphur of the sealant was used for tracing the sealant remnants that could be present at C4, C5, and C6 welds. It is important to mention that the sulphur content in the sealant is significantly higher than in the aluminium oxide fragment remnants. This fact, along with the shape of the analysed remnants, made it possible to identify clearly their origin and nature.

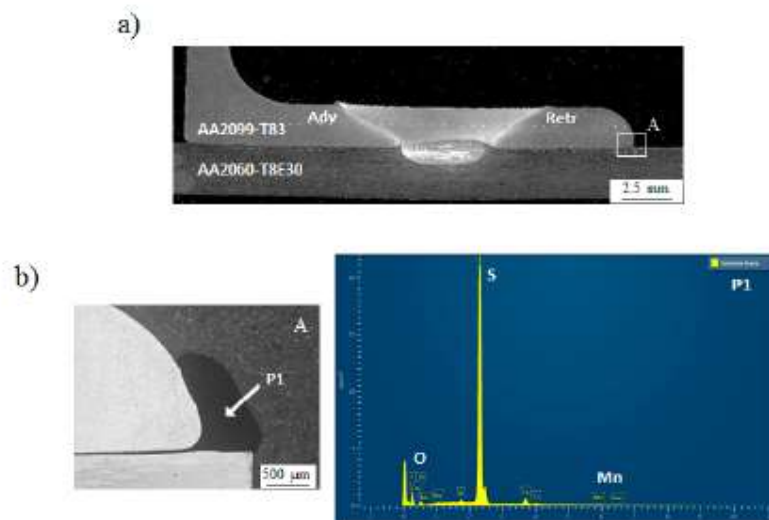


Figure 10. (a) Cross-sectional macrograph of the FSW weld from coupon C6 and (b) detail of the region indicated as detail A in Figure 10a and EDS analysis of the sealant.

Figure 11 shows the microstructural analysis carried out in the cross-section of the FSW weld obtained from coupon C6. The detail image obtained from the specimen before etching that can be observed in Figure 11a revealed a clear SZ region at the advancing side of the weld, while traces of remnants were present towards the retreating side. One could expect that these remnants had been formed as a result of a non-complete break, dispersion, and mixing of the Sol-Gel coating, sealant, and the inherent oxides that were present at the surface of the parent materials before the FSW process. Figure 11b presents the EDS analysis of the region indicated as detail A in Figure 11a. The compositional analysis of the remnants revealed contents of aluminium and copper, which are the main alloying elements of the parent metals, as well as oxygen very likely from the inherent oxide layer of the surface of the parent metals. Traces of sulphur that could indicate the presence of sealant remnants were not observed in any of the welds produced combining sealant application and FSW, i.e., coupons C4, C5, and C6. Thus, it seems that the sealant was displaced from the weld region towards the edges during the FSW process due to the pressure applied by the tool.

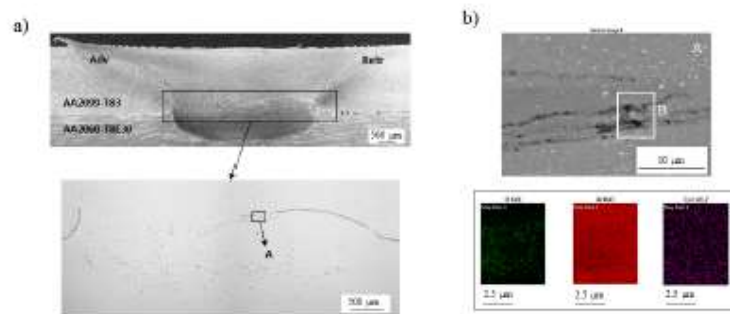


Figure 11. (a) Cross-sectional macrograph and detail magnification of the FSW weld from coupon C6 and (b) SEM image and EDS analysis of the region indicated as detail A in Figure 11a.

3.3. Pull-Out Strength

Quasi-static pull-out tests were performed in order to evaluate the influence of the coatings and sealant application in the strength of FSW welds. In these tests, the AA2060-T8E30 sheet was clamped, and a pulling force perpendicular to the weld surface was applied to the AA2099-T83 extrusion until the failure of the specimens, as shown in Figure 12. The maximum pull-out force for all specimens obtained from each FSW coupon C1–C6 as well as some examples of the failure mode observed for all specimens are presented in Figure 13. Very consistent maximum pull-out values of approximately 4.4 kN were obtained, except for the FSW specimens corresponding to coupon C3 that showed values of approximately 3.6 kN. This represents a reduction of 18% in the strength of the joints performed with Sol-Gel treated parent materials. This reduction was related to the larger distance of the weld with respect to the vertical part of the AA2099-T83 extrusion (indicated as “d” in Figure 12a), which generated a higher bending moment (M in Figure 12b) and stress concentration resulting in the failure of the stringer. This bending effect was reported by Mota de Siqueira et al. during pull-out tests carried out with similar overlap joint configurations [34]. For all the specimens tested in this study, the failure occurred consistently in the most stressed zone (region “e” in Figure 12b) at the AA2099-T83 extrusion outside the FSW weld region, as represented in Figure 12c. Figure 13b shows some examples of such failures.

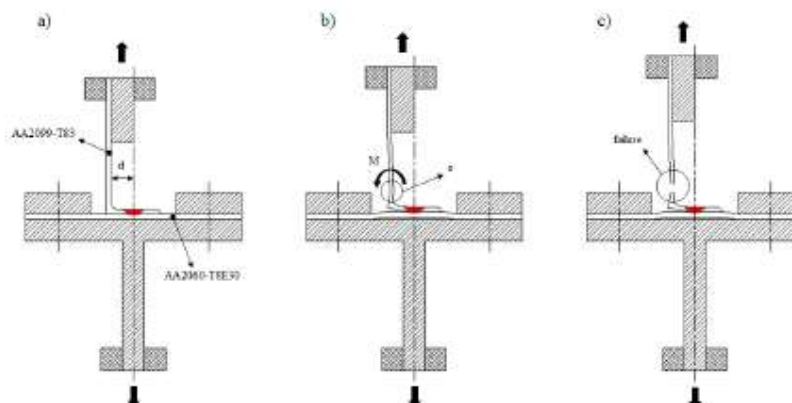


Figure 12. Representation of the progress in pull-out tests. (a) Test initiation; (b) before failure; and (c) after failure.

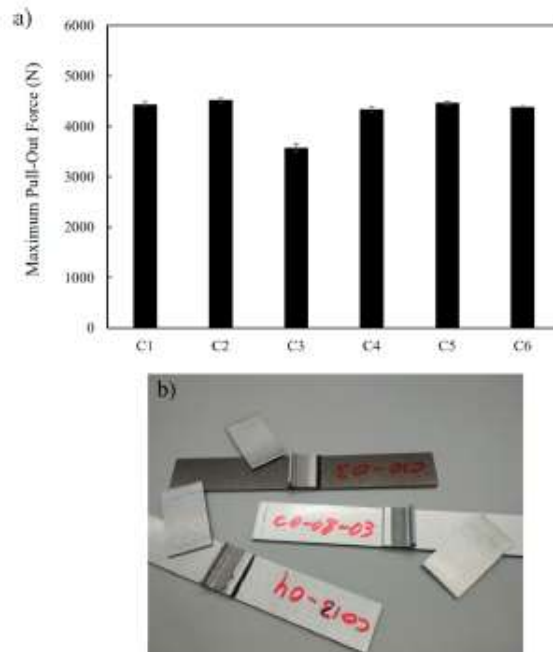


Figure 13. (a) Representation of maximum pull-out force values for FSW coupons C1–C6 and (b) examples of stringer failure in specimens obtained from FSW coupons C2, C4, and C6.

Although a lower strength could be expected especially for FSW specimens obtained from coupons C2 and C5 due to the fragment remnants present in the retreating side of the SZ, they showed similar strength to the other specimens except for the mentioned C3 case.

Therefore, the failure was never located at any region of the FSW welds (SZ, TMAZ or HAZ). All FSW welds showed higher strength than the most stressed zone located in the AA2099-T83 extrusions due to the bending effects and stress concentrations produced during the pull-out loading tests.

4. Conclusions

The influence of TFSAA and Sol-Gel surface treatments as well as the application of sealant before FSW was investigated in lap joints produced using AA2099-T83 aluminium Z-shaped extrusions on top of AA2060-T8E30 aluminium sheets. Based on the obtained results, the following conclusions were obtained:

- No significant differences were observed in the force controlled FSW process after comparing the resulting torque and tool penetration during welding of non-treated, TFSAA treated, and Sol-Gel treated aluminium components (coupons C1, C2, and C3). The FSW process is similar and stable for all these conditions.
- No significant differences were observed in the FSW process after comparing welding with and without sealant application at the interface of aluminium extrusions and sheets (C1, C2, C3 vs. C4, C5, and C6). The FSW process is similar and stable for all investigated surface treatments and sealant application conditions. The consistent accumulation of sealant observed at the stringer–skin crevice region at the edge of the matching interface between overlapping parent materials could provide good protection against corrosion for this type of joints and structures.

- All investigated welds (C1–C6) presented similar macrostructural characteristics, such as a small hook imperfection, and no measurable volumetric defects were observed in any of them. However, the use of surface-treated parent materials, especially those with the TFSAA treatment, showed aluminium oxide fragment remnants at the retreating region of the SZ in the welds.
- No sealant remnants were observed in any of the welds of the investigated FSW coupons. The sealant seems to be displaced from the weld region towards the edges by the pressure applied by the tool during the FSW process.
- Consistent failures at the stringer (AA2099-T83 extrusion) outside the weld region and comparable failure loads were observed in pull-out static tests for all FSW specimens due to the bending effect and stress concentration at this point. Therefore, all tested FSW welds showed higher strength than the most stressed point of the joints despite the presence of the aluminium oxide remnants observed in some cases (C2 and C5).

According to the obtained results, FSW of TFSAA or Sol-Gel-treated third generation Al-Cu-Li aluminium alloys combined with sealant application at the crevice of the lap joints seems a feasible and promising technique for the manufacturing of lightweight aeronautic structures with good corrosion resistance. FSW could be applied directly on the surface-treated sheets and extrusions without the need for any pre-processing step to eliminate the coatings.

Author Contributions: Conceptualisation, E.A. and A.K.; formal analysis, E.A.; investigation, E.A., J.V., A.K. and I.H.; methodology, E.A. and A.K.; supervision, P.A. and I.H.; writing—original draft, E.A. and A.K.; writing—review and editing, E.A., P.A., I.H. and J.V. All authors have read and agreed to the published version of the manuscript.

Funding: This work has been performed in the frame of the project ecoTECH within the AIRFRAME ITD of the Clean Sky 2 programme of the H2020. The authors acknowledge the funding received for this project under the project ID 807083 of the call H2020-IBA-CS2-GAMS-2017.

Data Availability Statement: The data presented in this study are available on request from the corresponding author.

Acknowledgments: The authors would like to acknowledge Manuel De La Torre from BASF and Chemetall for providing the necessary Naftoseal[®] MC-780-class C sealant to perform the tests reported in the present work.

Conflicts of Interest: The authors declare no conflict of interest.

References

1. Rendings, K.H. Aluminium structures used in aerospace—Status and prospects. *Mater. Sci. Forum* **2001**, *242*, 11–24. [[CrossRef](#)]
2. Starke, E.A.; Staley, J.T. Application of modern aluminum alloys to aircraft. *Prog. Aeronaut. Sci.* **1996**, *32*, 131–172. [[CrossRef](#)]
3. Mendez, P.; Eagar, T. New trends in welding in the aeronautic industry. In Proceedings of the 2nd Conference of New Manufacturing Trends, Bilbao, Spain, 19–20 November 2002.
4. Tavares, S.M. Design and Advanced Manufacturing of Aircraft Structures Using Friction Stir Welding. Ph.D. Thesis, Universidade do Porto, Porto, Portugal, July 2011.
5. Murphy, A.; McCune, W.; Quirn, D.; Price, M. The characterization of friction stir welding process effects on stiffened panel structures. *Thin Walled Struct.* **2007**, *45*, 339–351. [[CrossRef](#)]
6. Talwar, R.; Bolser, D.; Lederich, R.J.; Baumann, J. Friction stir welding of airframe structures. In Proceedings of the 2nd International Symposium on Friction Stir Welding, Gothenburg, Sweden, 27–29 June 2000.
7. Assler, H.; Telgkamp, J. Design of aircraft structures under special consideration of NDT. In Proceedings of the 9th European Conference on NDT, Berlin, Germany, 25–29 September 2006.
8. Freeman, J.; Moore, G.; Thomas, B.; Kok, L. Advances in FSW for commercial aircraft applications. In Proceedings of the 6th International Symposium on Friction Stir Welding, Toronto, ON, Canada, 10–13 October 2006.
9. Christner, B. A friction stir welded jet aircraft: From concept to reality. In Proceedings of the 11th International Symposium on Friction Stir Welding, Cambridge, UK, 17 May 2016.
10. Fernandez, F. FSW applied on mid-size aircraft. In Proceedings of the 8th International Symposium on Friction Stir Welding, Timmendorfer Strand, Germany, 18–20 May 2010.
11. Cederquist, L.; Reynolds, A.P. Factors affecting the properties of friction stir welded aluminium lap joints. *Weld. J. Res. Suppl.* **2001**, *80*, 281.

12. Dubourg, L.; Merati, A.; Jahazi, M. Process optimisation and mechanical properties of friction stir lap welds of 7075-T6 stringers on 2024-T3 skin. *Mater. Des.* **2010**, *31*, 3324–3330. [[CrossRef](#)]
13. Buffa, G.; Campanile, G.; Fratini, L.; Prisco, A. Friction stir welding of lap joints: Influence of process parameters on the metallurgical and mechanical properties. *Mater. Sci. Eng. A* **2009**, *519*, 19–26. [[CrossRef](#)]
14. Song, Y.; Yang, X.; Cui, L.; Hou, X.; Shen, Z.; Xu, Y. Defect features and mechanical properties of friction stir lap welded dissimilar AA2024-AA7075 aluminum alloy sheets. *Mater. Des.* **2014**, *55*, 9–18. [[CrossRef](#)]
15. Liu, H.; Hu, Y.; Peng, Y.; Dou, C.; Wang, Z. The effect of interface defect on mechanical properties and its formation mechanism in friction stir lap welded joints of aluminum alloys. *J. Mater. Process. Technol.* **2016**, *238*, 244–254. [[CrossRef](#)]
16. Balakrishnan, M.; Leitão, C.; Arruti, E.; Aldanondo, E.; Rodrigues, D.M. Influence of pin imperfections on the tensile and fatigue behaviour of AA 7075-T6 friction stir lap welds. *Int. J. Adv. Manuf. Technol.* **2018**, *97*, 3129–3139. [[CrossRef](#)]
17. Aldanondo, E.; Arruti, E.; Echeverria, A. Friction stir weld lap joint properties in aeronautic aluminium alloys. In *Friction Stir Welding and Processing IX*; Hovanski, Y., Mishra, R., Sato, Y., Upadhyay, P., Yan, D., Eds.; The Minerals, Metals & Materials Series; Springer: Cham, Switzerland, 2017. [[CrossRef](#)]
18. Meng, X.; Xu, Z.; Huang, Y.; Xie, Y.; Wang, Y.; Wan, L.; Lv, Z.; Cao, J. Interface characteristic and tensile property of friction stir lap welding of dissimilar aircraft 2060-T8 and 2099-T83 Al-Li alloys. *Int. J. Adv. Manuf. Technol.* **2018**, *94*, 1253–1261. [[CrossRef](#)]
19. Pacchione, M.; Telgkamp, J. Challenges of the metallic fuselage. In Proceedings of the 25th International Congress of the Aeronautical Sciences, Hamburg, Germany, 3–8 September 2006.
20. Prasad, N.E.; Gokhale, A.A.; Wanhill, R.J.H.; Merken, S.; Freeland, J. (Eds.) *Aluminium-Lithium Alloys: Processing, Properties and Applications*; Elsevier Inc.: Oxford, UK, 2014.
21. Aldanondo, E.; Vivas, J.; Álvarez, P.; Hurtado, I. Effect of tool geometry and welding parameters on friction stir welded lap joint formation with AA2099-T83 and AA2060-T8E30 aluminium alloys. *Metals* **2020**, *10*, 872. [[CrossRef](#)]
22. Jandaghi, M.R.; Pouraliakbar, H.; Hong, S.I.; Pavese, M. Grain boundary transition associated intergranular failure analysis at TMAZ/SZ interface of dissimilar AA7475-AA2198 joints by friction stir welding. *Mater. Lett.* **2020**, *280*, 128557. [[CrossRef](#)]
23. Jandaghi, M.R.; Badini, C.; Pavese, M. Dissimilar friction stir welding of AA2198 and AA7475: Effect of solution treatment and aging on the microstructure and mechanical strength. *J. Manuf. Process.* **2020**, *57*, 712–724. [[CrossRef](#)]
24. Shahzad, M.; Chaussumier, M.; Chieragath, R.; Mabru, C.; Rezaei-Aria, F. Influence of anodising process on fatigue life of machined aluminium alloy. *Procedia Eng.* **2010**, *2*, 1015–1024. [[CrossRef](#)]
25. Dursun, T.; Soutis, C. Recent developments in advanced aircraft aluminum alloys. *Mater. Des.* **2014**, *56*, 862–871. [[CrossRef](#)]
26. European Aeronautics. *A Vision for 2020 Aircraft and an Air Transport System that Are Responding to Society's Needs*; Report of the group of personalities; European Aeronautics: Brussels, Belgium, 2001.
27. Karanika, A.; Vourdas, N.; Makrikostas, A.; Marini, R.; Plagianakos, T.; Kalogeropoulos, S. Development of new environmentally friendly anticorrosive surface treatments for new Al-Li alloys protection within the frame of Clean Sky2. *Procedia Struct. Integr.* **2018**, *10*, 66–72. [[CrossRef](#)]
28. Boldsaiikhan, E.; Fukada, S.; Fujimoto, M.; Kamimuki, K.; Okada, H. Refill friction stir spot welding of surface-treated aerospace aluminium alloys with faying-surface sealant. *J. Manuf. Process.* **2019**, *42*, 113–120. [[CrossRef](#)]
29. Kubit, A.; Wydrzynski, D.; Trzepieciniski, T. Refill friction stir spot welding of 7075-T6 aluminium alloy single-lap joints with polymer sealant interlayer. *Compos. Struct.* **2018**, *201*, 389–397. [[CrossRef](#)]
30. Maciel, R.; Bento, T.; Braga, D.F.O.; da Silva, L.F.M.; Moreira, P.M.G.P.; Infante, V. Fatigue properties of combined friction stir and adhesively bonded AA6082-T6 overlap joints. *Fatigue Fract. Eng. Mater. Struct.* **2020**, *43*, 1–12. [[CrossRef](#)]
31. Gibson, B.T.; Wilkes, D.M.; Cook, G.E.; Strauss, A.M. In-process detection of faying surface sealant application flaws in friction stir welding. *J. Aircr.* **2013**, *50*, 567–575. [[CrossRef](#)]
32. Gibson, B.T.; Cox, C.D.; Ballun, M.C.; Cook, G.E.; Strauss, A.M. Automatic tracking of blind sealant paths in friction stir lap joining. *J. Aircr.* **2014**, *51*, 824–832. [[CrossRef](#)]
33. ISO25239. *Friction Stir Welding-Aluminium, Part 5: Quality and Inspection Requirements*; The International Organization for Standardization (ISO): Geneva, Switzerland, 2011.
34. Mota de Siqueira, R.H.; Capella de Oliveira, A.; Riva, R.; Abdalla, A.J.; Fernandes de Lima, M.S. Comparing mechanical behaviour of aluminium welds produced by laser beam welding (LBW), friction stir welding (FSW), and riveting for aeronautical structures. *Weld. Int.* **2016**, *30*, 497–503. [[CrossRef](#)]

14.- ARTICLE 11: FRETTING FATIGUE AS A LIMITING FACTOR ON THE DURABILITY OF FRICTION STIR WELDED LAP JOINTS USING AA2099-T83 AND AA2060-T8E30 ALUMINIUM ALLOYS

[79] E. Aldanondo, O. Zubiri, J. Vivas, P. Álvarez y I. Hurtado, «Fretting fatigue as a limiting factor on the durability of friction stir welded lap joints using AA2099-T83 and AA2060-T8E30 aluminium alloys,» *Journal of Manufacturing and Materials Processing*, vol. 6, nº 94, 2022.

The fatigue performance and the influences of surface treatments and sealants in the FSLW joints produced using AA2099-T83 and AA2060-T8E30 alloys were investigated in this work. FSLW joints were produced using optimised welding conditions and tested under hoop-stress loading conditions in order to investigate their fatigue performance. Two different fracture modes were identified, and the fretting fatigue was observed to be the limiting factor for the fatigue life of FSLW joints tested under low stress levels and high number of cycles. We concluded that the surface treatments and the sealant applied in the FSLW joints reduced the severity of fretting fatigue effects and extended the fatigue life of the joints. These conclusions supposed another important step to open the possibility for manufacturing lightweight and corrosion resistant structures for the aeronautic sector using FSW technology and Third-Generation Al-Li alloys.

This article was the third of the three articles that are to be considered for the completion of the thesis as a compendium of publications. It was published in the journal “Journal of Manufacturing and Materials Processing”.



Article

Fretting Fatigue as a Limiting Factor on the Durability of Friction Stir Welded Lap Joints Using AA2099-T83 and AA2060-T8E30 Aluminium Alloys

Egoitz Aldanondo ^{1,*}, Oier Zubiri ¹, Javier Vivas ¹, Pedro Álvarez ¹ and Iñaki Hurtado ²

¹ LORTEK Technological Centre, Basque Research and Technology Alliance (BRTA), Arranomendia kalea 4A, 20240 Ordizia, Spain

² Mechanical and Manufacturing Department, Mondragon University, Loramendi 4, 20500 Arrasate, Spain

* Correspondence: egoitz@ortek.es



Citation: Aldanondo, E.; Zubiri, O.; Vivas, J.; Álvarez, P.; Hurtado, I. Fretting Fatigue as a Limiting Factor on the Durability of Friction Stir Welded Lap Joints Using AA2099-T83 and AA2060-T8E30 Aluminium Alloys. *J. Manuf. Mater. Process.* **2022**, *6*, 94. <https://doi.org/10.3390/jmmp6050094>

Academic Editor: Enkhsaikhan Boldsaikhan

Received: 28 July 2022

Accepted: 23 August 2022

Published: 26 August 2022

Publisher's Note: MDPI stays neutral with regard to jurisdictional claims in published maps and institutional affiliations.



Copyright: © 2022 by the authors. Licensee MDPI, Basel, Switzerland. This article is an open access article distributed under the terms and conditions of the Creative Commons Attribution (CC BY) license (<https://creativecommons.org/licenses/by/4.0/>).

Abstract: Friction stir welding (FSW) has been proposed as an alternative modern joining technology and demonstrated important benefits for the manufacturing of efficient and lightweight aircraft structures using high-strength aluminium alloys. These structures are required to be corrosion-resistant and thus, it is necessary to use technologies such as surface treatments and sealants in their manufacturing and assembly. In this work, the feasibility of combining innovative Cr-free surface treatments, sealants and FSW technology was investigated with the focus on the durability of the joints in fatigue. FSW lap joints were produced using AA2099-T83 extrusions and AA2060-T8E30 sheets in the as-received or surface-treated condition. A sealant was also applied in some cases at the overlapping interface before the FSW process. Static tensile tests and fatigue tests were carried out applying hoop-stress loading conditions. Different fracture modes were identified depending on the stress levels applied in the fatigue tests: High stress levels resulted in fractures in the HAZ of the FSW joints, while the specimens tested at low stress levels showed fractures out of the FSW joint. In general, FSW joints produced using surface-treated aluminium components and sealant presented improved fatigue life and extended durability in comparison with non-treated aluminium joints. The surface treatments and sealant at the interface of AA2099-T83 extrusions and AA2060-T8E30 sheets reduced the friction and local damage produced due to the sliding movement during the fatigue tests, minimizing the fretting fatigue effect, which was found to be the main limiting factor on the durability and fatigue life of the FSW joints.

Keywords: friction stir welding; lap joint; surface treatment; sealant; hoop stress; fretting fatigue; Al-Li alloys

1. Introduction

Aircraft structures are usually manufactured using high-strength aluminium alloys, such as 2xxx and 7xxx series, due to their good mechanical performance: low density, high stiffness, corrosion resistance, fracture toughness and fatigue growth resistance [1]. However, the difficulties in welding these alloys by conventional fusion welding processes has limited the possibilities for an efficient manufacturing, opening a new research field for the use of alternative joining technologies based on solid-state processes. One of the most recognized solid-state joining processes for high-strength aluminium alloys is friction stir welding (FSW) [2–5]. FSW has been successfully used as an alternative to riveting in aircraft structural components for joining precipitation-hardening aluminium alloys such as 2024-T3 [6], 7075-T6 [7] and even dissimilar joining 2024-T3 to 7075-T6 alloys [8].

Another important issue to be considered for the design and manufacturing of aircraft structures such as fuselage panels is the corrosion resistance, since this is essential for a long-term operational capability. In order to achieve this using aluminium alloys, a great variety of corrosion protection methods exist, such as surface treatments and sealants. For

the adequate selection of these protection methods, it is important to consider the operational considerations, societal concerns and REACH regulations [9], which are creating a growing demand for the development of new effective and environmentally friendly surface treatment technologies. In addition to this, there is a continuous need to reduce the environmental footprint of the manufacturing technologies, as established in the ACARE targets [10]. Thus, the materials employed in the manufacturing of current and future aircraft structures need to become more resistant to corrosion and, at the same time, more eco-compliant to achieve an environmentally friendly life cycle [11]. This implies a significant decrease in hazardous materials for their manufacturing. In this context, chrome-free surface treatments such as thin film sulphuric acid anodizing (TFSA) and out-of-bath sprayable Sol-Gel application play an important role as a replacement for conventional anticorrosive protection processes using chromates [12].

The need to combine surface treatments, sealants and joining technologies is a continuous challenge in the manufacturing of structures such as reinforced fuselage panels. In fact, several authors investigated the feasibility of FSW and its derivatives such as refill friction stir spot welding (RFSSW) for joining surface-treated aluminium alloys in the overlap configuration using sealants [13–17]. These studies showed a promising potential of FSW technologies to join surface-treated aluminium alloys using sealants in appropriate welding conditions. In one of our previous works, the feasibility for FSW surface-treated AA2099-T83 aluminium extrusions with AA2060-T8E30 aluminium sheets in the overlap configuration using a sealant at the interface was investigated [18]. The new Cr-free surface treatments TFSA and Sol-Gel were applied to the parent materials and the static behavior by pull-out tests was investigated, showing that these corrosion protection methods had no significant effects on pull-out static mechanical properties.

The fatigue behavior of representative FSW joints used for the manufacturing of fuselage panels has been investigated [19–21]. L. Dubourg et al. [20] optimized the FSW process and the mechanical properties of friction stir lap welds of 7075-T6 stringer on 2024-T3 skin, focusing on the defects associated with this joint configuration, such as top-sheet thinning, voids, hooking and kissing-bonds. H. J. Schmidt et al. [21] investigated the crack scenarios and crack growth rates in integral structures and built-up structures of fuselage panels with FSW joints. However, although it is extremely significant, the fatigue performance of FSW joints combined with surface treatments and sealants has not been investigated previously.

Thus, the present work is focused on investigating the fatigue behavior of FSW joints produced using surface-treated high-strength aluminium alloys with sealant application and comparing their properties with FSW joints produced using non-treated alloys. At this point, the analysis of fatigue behavior of welded joints, it is important to highlight the significant contribution that infrared (IR) thermography methods can make, allowing us to study the location of the failure area in real time. Thermography methods have been satisfactorily employed to assess the fatigue behavior and the damage evolution of materials and their welded components [22–24].

2. Experimental Procedure

2.1. Materials and Surface Treatments

Z-shaped extrusions of AA2099-T83 aluminium alloy as stringers and rolled sheets of AA2060-T8E30 aluminium alloy as skins were used to manufacture the stringer-skin lap joints. Both alloys belong to the third generation of aluminium–lithium (Al–Li) alloys that present excellent properties such as high strength, low density and excellent corrosion resistance. The thickness of the AA2099-T83 stringers was 2 mm, while the thickness of the AA2060-T8E30 skins was 2.5 mm. The nominal chemical compositions of the stringer and skin aluminium alloys are shown in Table 1.

Table 1. Chemical composition of base materials, wt %.

Alloy	Al	Si	Fe	Cu	Mn	Mg	Zn	Ti	Ag	Li	Zr
Skin AA2060-T8E30	Bal.	0.07	0.07	3.4–4.5	0.1–0.5	0.6–1.1	0.3–0.5	0.1	0.05–0.5	0.6–0.9	0.05–0.15
Stringer AA2099-T83	Bal.	0.05	0.07	2.4–3.0	0.1–0.5	0.1–0.5	0.4–1	0.1	-	1.6–2.0	0.05–0.12

Before FSW, skins and stringers were subjected to different combinations of surface treatments as well as sealant application at the matching interface. Table 2 summarizes the welded coupons and their surface conditions before the FSW process.

Table 2. FSW coupon identification with the applied surface treatments and sealant.

Coupon ID	Surface Treatment	Sealant
C01	-	-
C02	TFSAA	-
C03	Sol Gel	-
C04	-	Naftoseal [®] MC-780-Class C
C05	TFSAA	Naftoseal [®] MC-780-Class C
C06	Sol Gel	Naftoseal [®] MC-780-Class C

TFSAA and Sol-Gel (AC131 from 3M) surface treatments, which are fully chromium-free and REACH compliant, were applied by the Hellenic Aerospace Industry S.A. (HAI). For more information on the composition of the surface treatments and sealant and how they were applied on the stringers and skins, the readers are referred to a previous work of the authors [18].

2.2. Friction Stir Welding Procedure

The Z-shaped AA2099-T83 stringers and the AA2060-T8E30 skins were friction stir welded at LORTEK in the overlap configuration in an I-STIR PDS 4 machine operated in force control. 500-mm-long stringers were friction stir welded in the central position of 600-mm-long and 200-mm-wide skins. The FSW tool (Figure 1a) consisted of a probe with three flats and a mixed thread with a diameter of 4 mm and a length of 2.5 mm. The shoulder had a flat shoulder of 10 mm in diameter. The fixtures and clamping system used for the positioning and clamping of the Z-shaped stringer on top of the skin are shown in Figure 1b.

All coupons were produced using the same FSW parameters at a clockwise rotational speed of 1200 rpm, a welding speed of 250 mm/min, and a forge force of 6.25 kN. The tilt angle of the tool was 1.5° in all cases. The selection of these FSW parameters was based on the optimization study performed by the authors in one of our previous works [2]. The advancing side of the welds was oriented towards the vertical section of the extrusions and the retreating side towards the free edge.

2.3. FSW Joint Characterisation

The FSW coupons C01–C06 were characterised by metallographic characterisation, microhardness measurements, static tensile tests and fatigue tests under hoop-stress loading conditions. In this loading condition, tensile stresses are applied to the AA2060-T8E30 skin as is shown by the red arrows in Figure 2.

For the metallographic characterisation, cross-sectional specimens were cut perpendicular to the welding direction from each of the welded coupons. The specimens were prepared using standard procedures for mounting, grinding, and polishing to a mirror-like surface finish using a colloidal silica suspension. After this preparation, the specimens were etched using a diluted Keller's reagent to reveal the microstructure. The initial metallographic examination of the cross-sectional specimens was performed by optical microscopy

using an Olympus GX51 light optical microscope. Hardness measurements were made using the Vickers hardness scale with a sampling step of 0.5 mm and a load of 5 N applied for 15 s.

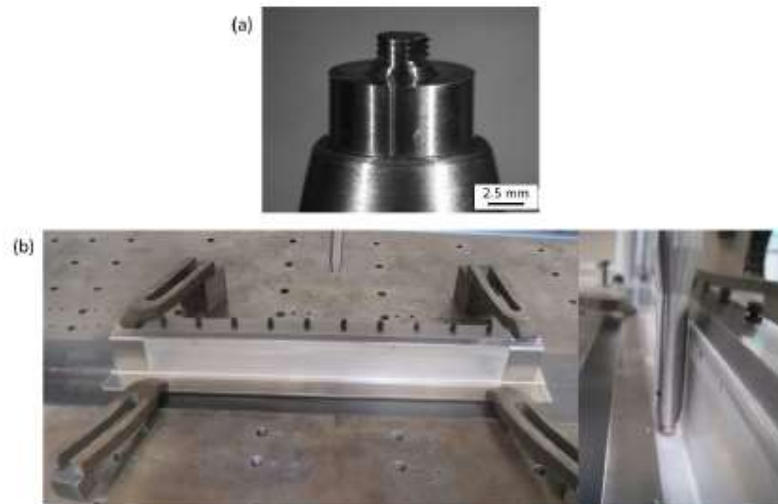


Figure 1. (a) FSW tool and (b) Setup for the FSW process.

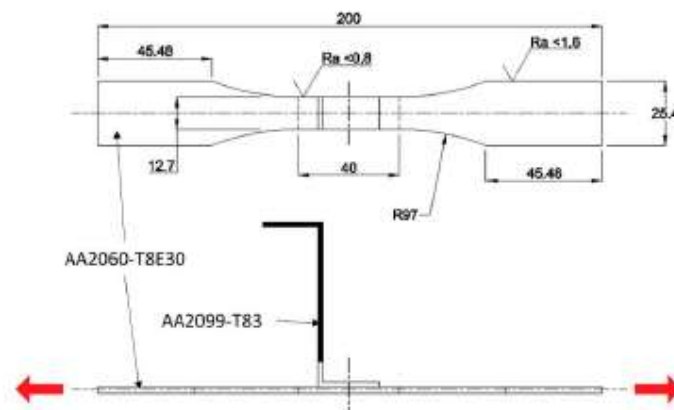


Figure 2. FSW specimens machined from the coupons used for the static tensile and fatigue tests under hoop-stress loading conditions (indicated by the red arrows).

Specimens for static tensile tests and fatigue tests were prepared following the recommendation by the BS EN 6072 standard. 30-mm-wide specimens were cut from the welded coupons using electrical discharge machining (EDM) and final mechanical milling was applied to achieve the final geometry. The geometry of the final specimens is shown in Figure 2. For the static tensile tests, a Zwick Roell Z100 tensile testing machine with a load capacity of 100 kN was used at a constant testing speed of 1.6 mm/min. The fatigue behaviour of the FSW joints was studied by fatigue strength data as represented in basic S-N diagrams. The fatigue performance was evaluated using an MTS hydraulic testing machine. Fatigue tests were conducted in load control, using a sinusoidal waveform at 10 Hz and $R = 0.1$. Fatigue stress levels among 15–70% of the AA2060-T8E30 base material's

yield strength were applied as hoop-stress loading on the AA2060-T8E30 skin. During the fatigue tests, an IR camera (model FLIR A655sc series) was employed to record the temperature field evolution on the surface of the specimens. Optical field-of-view conditions were achieved by installing the camera at a distance of approximately 0.5 m between specimens and the lens of the camera. After finishing the fatigue tests, the fractured specimens were examined using scanning electron microscopy (SEM) as well as energy dispersive spectroscopy (EDS) to determine the fatigue crack behaviour and the influence of the weld microstructure and surface conditions on the nucleation site.

3. Results

3.1. Static Tensile Tests

Static tensile tests were performed under hoop-stress loading conditions with specimens machined from coupons C01–C06. Two specimens from each coupon were tested showing very similar results. A summary of the obtained results can be observed in Figure 3a. Very similar yield stress and UTS values were obtained for all specimens showing no significant influence of the surface treatments and sealant application in the performance of the FSW joints. Yield strength values between 410–424 MPa were obtained showing a minor variability of approximately 3% among all tested specimens. In terms of UTS, a variability of approximately 2% was observed with values between 486–498 MPa. All specimens showed an equivalent fracture mode with an initiation in the HAZ and propagation at 45° through the AA2060-T8E30 skin as shown in Figure 3b.

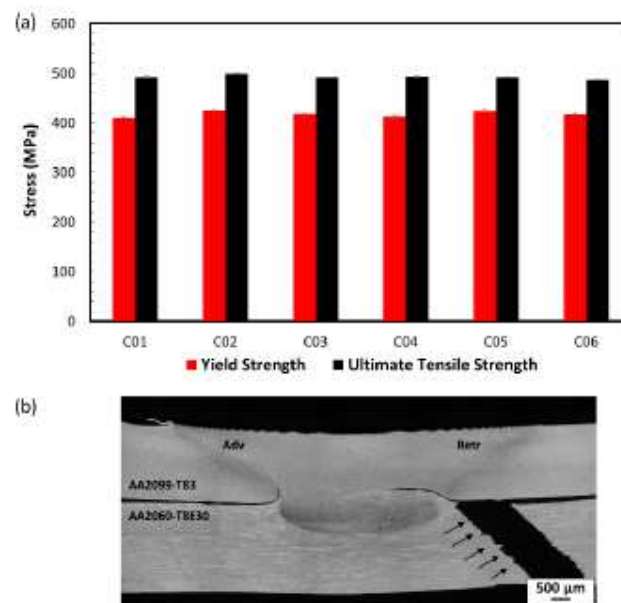


Figure 3. (a) Yield strength and ultimate tensile strength values obtained for specimens machined from C01–C06 and (b) metallographic cross-section of a fractured C01 (non-treated without sealant) specimen showing the fracture initiation at the HAZ.

The initiation of the fracture in the HAZ can be explained by the hardness reduction of the AA2060-T8E30 base material in this zone, in addition to the coincidence with the lowest effective thickness of the AA2060-T8E30 sheet in the close vicinity of the FSW joint. Figure 4 shows the microhardness values obtained for the AA2060-T8E30 alloy in a scan of indentations performed parallel to the interface between the AA2060-T8E30 sheet and the

AA2099-T83 stringer (A–B line in Figure 4a). Although the lowest values of approximately 110 HV0.5 were obtained in the stir zone (SZ), the larger effective thickness provided by the FSW joint in this zone compensates for the lower strength avoiding the fracture through the SZ. The hardness increases to values in the range of 120–130 HV0.5 in the HAZ of the advancing and retreating sides, where the effective thickness of the AA2060-T8E30 sheet decreases to its minimum value of 2.5 mm. Thus, the fracture is initiated in the region where the thickness is the lowest and the hardness values are still significantly low in the HAZ of the FSW joints.

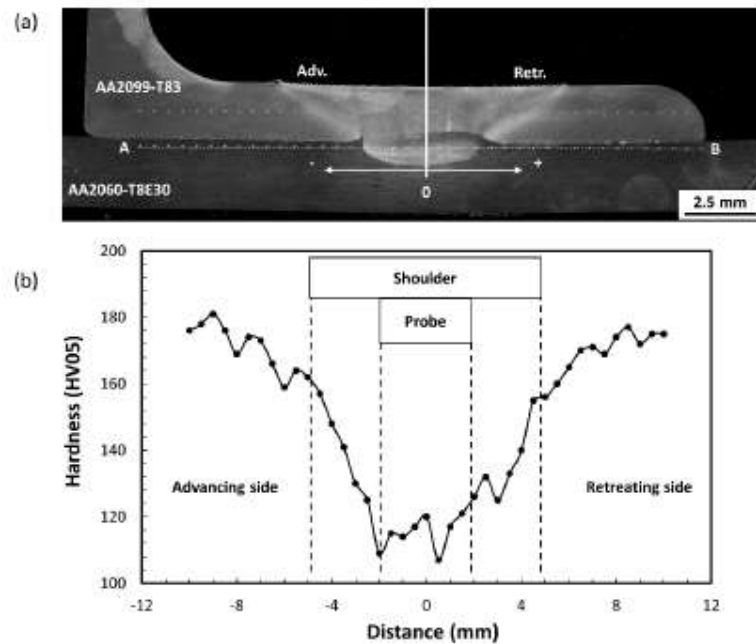


Figure 4. (a) Metallographic cross-section of a specimen obtained from coupon C01 and (b) micro-hardness scan measurements in the A–B line shown in Figure 4a.

3.2. Fatigue Tests

Basic S–N curves were obtained for the FSW joints machined from the C01–C06 coupons after the fatigue tests carried out under dynamic hoop-stress loading conditions. Several comparative analyses of the S–N curves are presented in Figures 5–7, where the stress level in the y axis is represented as a percentage of the yield strength of the base material.

Figure 5 shows the comparison between the FSW joints produced using bare aluminium alloys (C01) and those produced using surface-treated aluminium alloys, TFSAA in C02 and Sol-Gel treatment in C03. According to these results, surface-treated FSW joints obtained from C02 and C03 showed a slightly better fatigue behavior and extended life compared to the FSW joints obtained from the coupon C01. A similar conclusion can be obtained from the results shown in Figure 6, where the fatigue life of FSW joints obtained from coupon C01 is compared to the ones produced using the same bare aluminium substrates, but sealant in the stringer-skin interface prior to FSW (coupon C04). The fatigue specimens containing sealant showed a better fatigue performance and durability in comparison with the reference FSW joints from coupon C01. Figure 7 shows the comparison between the reference FSW joints machined from coupon C01 and those obtained from the

coupons produced using a combination of surface-treated aluminium alloys and sealant in the stringer-skin interface, coupons C05 and C06. Once again, the FSW joints containing surface treatments and sealant showed a longer fatigue life than the reference FSW joints. According to these results it could be stated that both the use of surface-treated aluminium alloys and the application of sealant improved the fatigue life of the FSW joints, when they are applied either in an individual or a combined way.

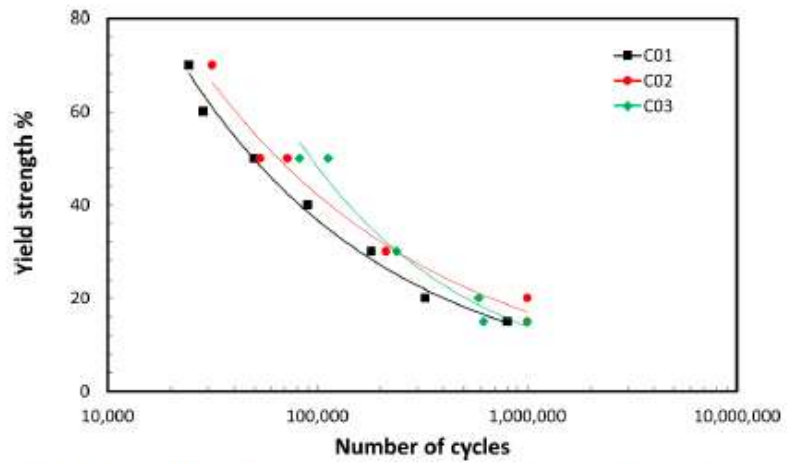


Figure 5. S-N curves of FSW joints showing a comparison between FSW specimens produced with bare aluminium alloys (C01) and surface-treated aluminium alloys without sealant (C02 and C03).

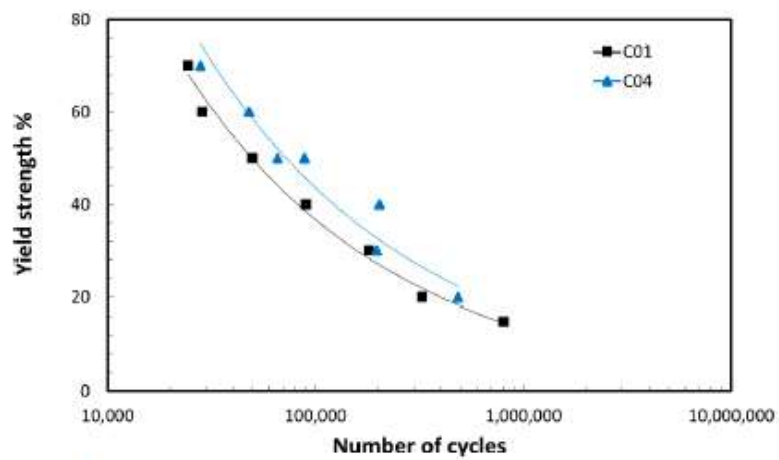


Figure 6. S-N curves of FSW joints showing a comparison between FSW specimens produced with bare aluminium alloys without sealant (C01) and with sealant (C04).

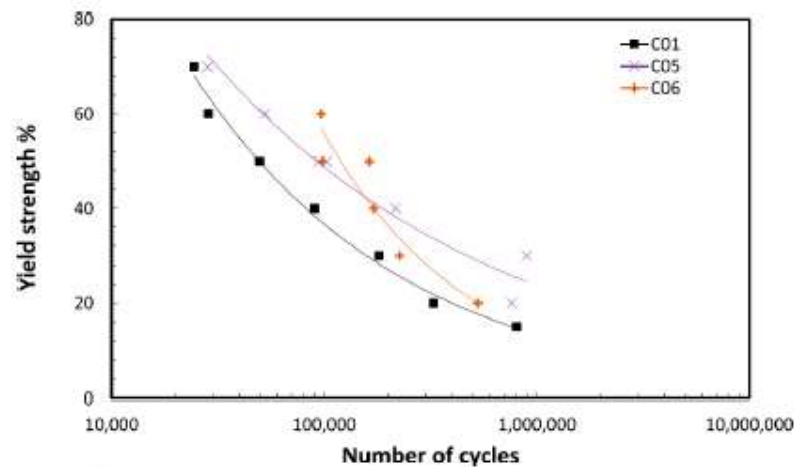


Figure 7. S-N curves of FSW joints showing a comparison between FSW specimens produced with bare aluminium alloys without sealant (C01) and surface-treated aluminium alloys with sealant (C05 and C06).

The fracture analysis of the FSW joints in the fatigue tests allowed us to distinguish two main fracture modes as shown in the S-N data represented in Figure 8. The specimens tested in high-stress loading conditions showed failures at a relatively low number of cycles with a fracture initiation and propagation in the HAZ of the FSW joint (indicated in red in Figure 8). On the other hand, the specimens tested in low-stress loading conditions presented a higher number of cycles until fracture and they showed a fracture located out of the FSW joint (indicated in blue in Figure 8). This type of failure could be related to fretting fatigue phenomena [25,26] occurring at random locations in the contacting stringer-skin interface out of the FSW joints, generating an initial damage and fracture initiation point for a later fracture out of the FSW joint.

The monitoring of the FSW specimens during the fatigue tests by IR thermography allowed us to capture the instants when the fracture occurred for the two different failure modes identified (Figure 9). The positions of the AA2099-T83 stringer, the AA2060-T8E30 skin and the FSW joint were highlighted with black lines for a better clarity of the images. The image in Figure 9a shows the instant when the fracture of the specimen C05_A, which was tested at relatively low stress conditions as indicated in Figure 8, occurred. It can be clearly observed that the fracture initiation and final fracture occurred out of the FSW joint after 216,817 cycles. On the other hand, the image in Figure 9b shows the instant of the fracture of the specimen C05_B, tested in high-stress loading conditions (Figure 8). It can be observed that the fracture occurs in the HAZ of the FSW joint after 52,306 cycles. Although it was not possible to achieve an accurate quantification of temperature variations during the fatigue tests, IR thermography allowed us to clearly distinguish the fracture initiation points. Thus, IR thermography was found to be an effective technique to carry out qualitative studies in the fatigue tests of FSW joints.

Similar results were obtained after the metallographic characterisation of specimens fractured in fatigue tests (Figure 10). The cross-section shown in Figure 10a corresponds to a specimen machined from coupon C05 that failed in low-stress loading conditions after 897,334 cycles. It can be clearly observed that the fracture initiation and final failure occur out of the FSW joint. On the other hand, the cross-section of a specimen tested in high-stress loading conditions can be observed in Figure 10b. A fracture initiation and crack growth through the HAZ can be clearly observed prior to the final fracture after 28,187 cycles.

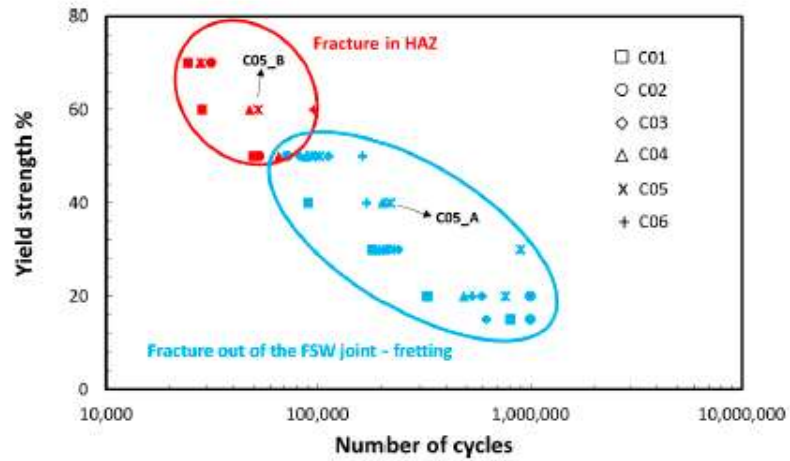


Figure 8. S-N data of FSW joints showing different fracture modes in high- and low-stress loading conditions.

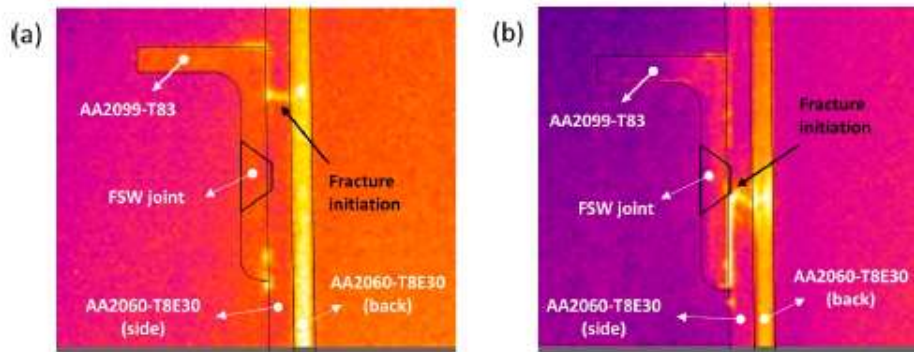


Figure 9. Thermographic images of FSW joints showing the instant of the fracture in the fatigue tests; (a) specimen C05_A showing the fracture out of the FSW joint at 216,817 cycles and (b) specimen C05_B showing the fracture in the HAZ at 52,306 cycles.

Therefore, from these results, it could be stated that specimens tested in high-stress loading conditions presented a fracture initiation in the HAZ in a similar zone as in the fractures observed in the static tensile tests (Figure 3b). However, the crack growth occurs along the HAZ due to the reduced hardness of the material in this zone. The specimens tested under low-stress conditions showed a fracture out of the FSW joint due to fretting effects produced as a consequence of the frictional contact and sliding movement between the stringer and the skin at their interface. The precise location of the fracture initiation point was randomly distributed along the stringer-skin interface out of the FSW joint, depending on the damage accumulation caused by the frictional contact and the sliding movement between the stringer and the skin.

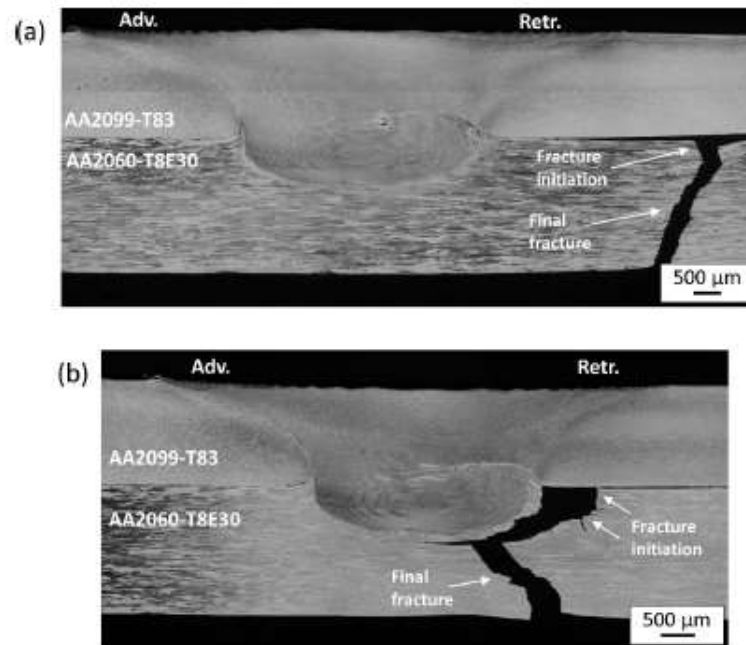


Figure 10. Metallographic cross-sections of FSW showing different fracture modes; (a) specimen from coupon C05 tested at 30% of the YS showing the fracture out of the FSW joint and (b) specimen from coupon C05 tested at 70% of the YS showing the fracture in the HAZ.

The presence of surface lubricants has been proposed as a palliative method to reduce fretting fatigue problems and extend the fatigue life of structures [27]. In the FSW joints analysed in this work, the lubricant effect produced by the surface treatments and the applied sealant explains the observed improvement in the fatigue life of these FSW joints. Their presence could reduce the frictional effects at the interface, minimizing the fretting effects and delaying the fracture initiation as well as the final fracture of the FSW specimens.

3.3. Fracture Surface Analysis

The fracture surfaces were investigated in more detail using SEM and EDS techniques. The results obtained in the analysis of the specimen C05_A, which was tested in low-stress loading conditions, are shown in Figures 11–13. A general view of the fractured specimen can be observed in Figure 11a and a more detailed view of the fracture surface in Figure 11b. Small regions of black phases were observed at the stringer-skin matching interface, which are indicated as point A1 in Figure 11a, suggesting these phases could act as fatigue crack nucleation points. A detailed analysis of these black phases indicated as regions A1-1 and A1-2 in Figure 12 revealed that they consisted of accumulated aluminium oxides as a result of local sliding and frictional contact between the stringer and skin surfaces at the point A1. Once the fatigue crack was initiated at this point, three main regions were observed for its propagation, indicated as zones A, B and C in Figure 11b. A detailed observation of the fracture surface by SEM allowed us to identify these zones and representative SEM images are shown in Figure 13.

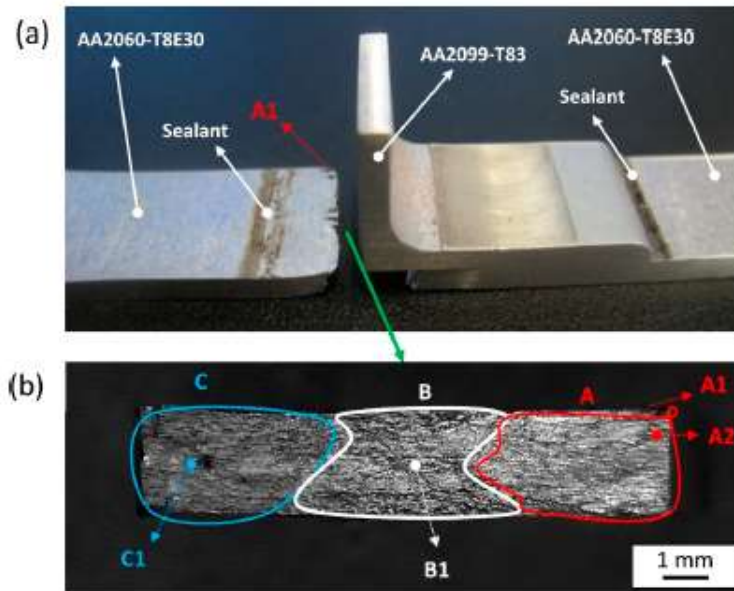


Figure 11. Fracture surface analysis of specimen C05_A showing the fracture out of the FSW joint at 216,817 cycles (a) general view of the fractured specimen and (b) perpendicular view of the fracture surface indicated by the green arrow.

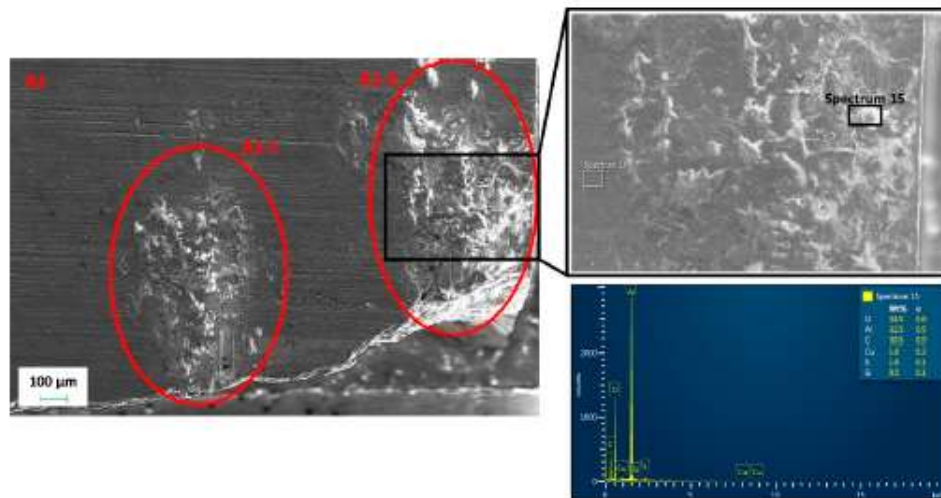


Figure 12. SEM image and EDS analysis of the zone A1 indicated in Figure 11.

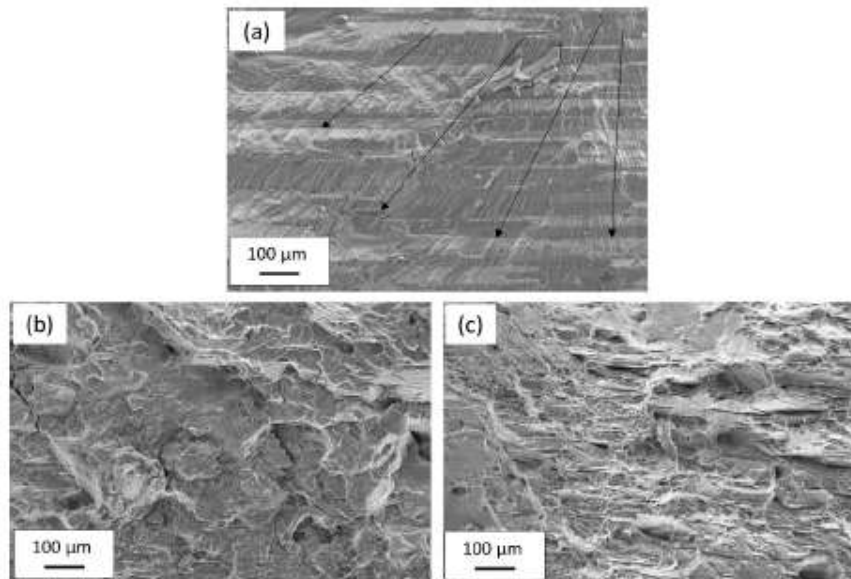


Figure 13. SEM observations of the fracture surface of specimen C05_A shown in Figure 11b; (a) image obtained at point A2 indicated in Figure 11b; (b) point B1 in Figure 11b and (c) point C1 in Figure 11b.

Figure 13a shows a SEM image obtained at point A2 indicated in Figure 11b, which is considered to be close to the initial fatigue crack nucleation point. A very flat surface without significant plastic deformation and the progress of the crack during the cyclic loading of the fatigue test can be observed. This propagation goes from the top surface towards the bottom in thickness as well as from the edge of the specimen towards its centre as indicated by the arrows in Figure 13a. A representative SEM image of the transition zone B obtained at point B1 indicated in Figure 11b can be observed in Figure 13b. A combination of zones showing limited plastic deformation and crack growth bands with other zones showing dimples indicative of ductile fracture with significant plastic deformation could be observed in this zone B. Finally, an SEM image obtained at point C1 in Figure 11b can be observed in Figure 13c. A surface formed of multiple dimples indicative of substantial plastic deformation and ductile fracture could be observed, which was representative of zone C, where the final fracture occurred.

This type of fracture, originated by oxides accumulated at the stringer-skin interface, was representative of the fractures caused by fretting effects in low-stress loading conditions and after a relatively high number of cycles. Thus, fretting effects are the main limiting factor of the fatigue life of stringer-skin FSW joints in the overlap configuration in the high-cycle fatigue regime.

The fractures that occurred in high-stress loading conditions were also investigated by SEM observation of the fracture surfaces. The results obtained in the analysis of the specimen C05_B, that presented a representative fracture in the HAZ of the FSW joint, are shown in Figures 14 and 15. The general view of the fractured specimen can be observed in Figure 14a. No presence of black phases was observed at the stringer-skin interface. A more detailed view of the fracture surface can be observed in Figure 14b showing the main zones which form the final fracture surface: the fatigue crack nucleation and propagation zone (indicated as D) as well as the final fracture zone (indicated as E). Representative images obtained by SEM showing the characteristics of these zones can be observed in Figure 15. Thus, Figure 15a shows details of the initial fatigue crack nucleation point indicated as

point D1 in Figure 14b. A flat surface showing no plastic deformation can be observed where propagation bands starting at the top surface indicate the fracture initiation point. The propagation of the fatigue crack, which is indicated by the black arrows in Figure 15a, goes from the top surface towards the bottom in the thickness direction and from the central zone towards the edges in the width of the specimen. Once the crack propagates to cover the zone D, the final fracture occurs in the zone E. SEM images obtained at points E1 and E2 indicated in Figure 14b are shown in Figures 15b and 15c, respectively. Multiple dimples can be observed in these zones indicating a ductile fracture with plastic deformation.

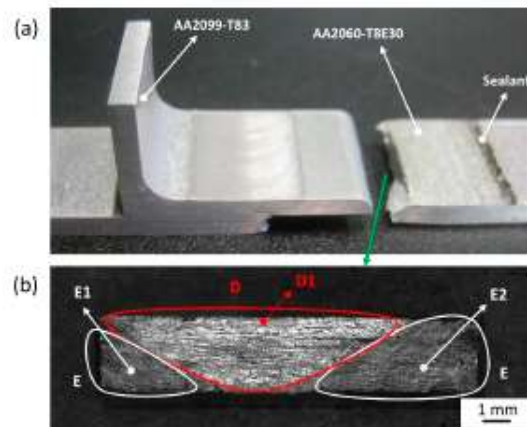


Figure 14. Fracture surface analysis of specimen C05_B showing the fracture in the HAZ at 52,306 cycles; (a) general view of the fractured specimen and (b) perpendicular view of the fracture surface indicated by the green arrow.

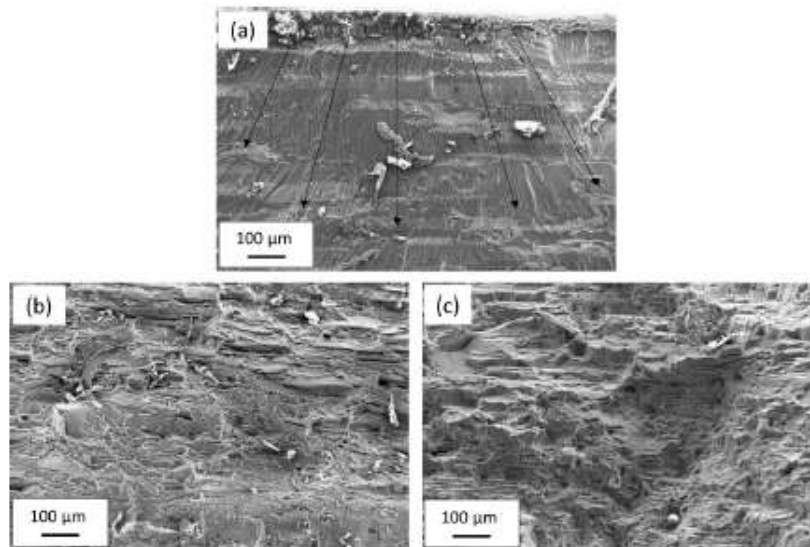


Figure 15. SEM observations of the fracture surface of specimen C05_B shown in Figure 14b; (a) image obtained at point D1 indicated in Figure 14b; (b) point E1 in Figure 14b and (c) point E2 in Figure 14b.

4. Conclusions

The fatigue behaviour of stringer-skin overlapped FSW joints under hoop-stress loading conditions was investigated. AA2099-T83 extrusions and AA2060-T8E30 rolled sheets were used to produce the FSW joints in the as-received and surface-treated conditions. A sealant was also applied at the stringer-skin interface before FSW for some conditions. Based on the results obtained in this work, the following conclusions could be drawn:

- All investigated FSW joints showed an equivalent performance in the static tensile tests carried out under hoop-stress loading conditions. The surface treatments (TFSA and Sol-Gel) and sealant applied before the manufacturing by FSW did not induce significant effects on the joint properties.
- Two different fracture modes were identified as the main failure mechanisms in the fatigue tests performed under hoop-stress loading conditions. Fractures in the HAZ were observed in tests performed with relatively high stress levels, while the fracture mode in low-stress level tests was found to occur out of the FSW joint.
- IR thermography was found to be a suitable technique for a qualitative analysis of the fatigue performance of FSW joints, allowing us to identify the fracture initiation and propagation locations.
- Fretting fatigue was identified as the main limiting factor of the fatigue life for FSW joints tested at low stress levels. The local damage caused by the frictional contact and sliding movement at the stringer-skin interface was found to create aluminium oxide accumulations that acted as the fatigue crack initiation points.
- FSW joints produced using surface-treated aluminium components and sealant at the stringer-skin interface showed an improved fatigue life in comparison with the FSW joints produced using bare aluminium components. The lubricant effect and reduced friction produced by the surface treatments and sealant at the stringer-skin interface resulted in reduced fretting effects and extended durability of the FSW joints.

Generally, it was concluded that it is feasible to combine FSW manufacturing using surface-treated aluminium alloys and sealants at the stringer-skin interface in order to produce efficient, high-strength and corrosion-resistant aeronautic structures. The possibility of FSW surface-treated aluminium components using sealants was demonstrated and the resulting joints showed improved durability in fatigue tests under hoop-stress loading conditions.

Author Contributions: Conceptualisation, E.A.; formal analysis, E.A.; investigation, E.A., O.Z., J.V. and L.H.; methodology, E.A., O.Z. and J.V.; supervision, P.A. and L.H.; writing—original draft, E.A. and J.V.; writing—review and editing, E.A., P.A., L.H. and J.V. All authors have read and agreed to the published version of the manuscript.

Funding: This work was performed in the frame of the project ecoTECH within the AIRFRAME ITD of the Clean Sky 2 programme of the H2020. The authors acknowledge the funding received for this project under the AIRFRAME ITD grant agreement 945521.

Institutional Review Board Statement: Not applicable.

Informed Consent Statement: Not applicable.

Data Availability Statement: Data will be available upon request through the corresponding author.

Acknowledgments: The authors would like to acknowledge Manuel De La Torre from BASF and Chemetall for providing the necessary Naftoseal® MC-780-class C sealant to perform the tests reported in the present work. The authors also thank Maria del Carmen Taboada for her assistance in the fracture surface analysis by SEM and Uxue Irastorza for her support with the metallographic examination tests. Finally, the authors are also thankful to Alexandra Karanika and her team in the Hellenic Aerospace Industry S.A. (HAI) for the application of the surface treatments to the aluminium components.

Conflicts of Interest: The authors declare no conflict of interest.

References

- Starke, E.A.; Staley, J.T. Application of modern aluminum alloys to aircraft. *Prog. Aerosp. Sci.* **1996**, *32*, 131–172. [CrossRef]
- Aldanondo, E.; Vivas, J.; Álvarez, P.; Hurtado, I. Effect of Tool Geometry and Welding Parameters on Friction Stir Welded Lap Joint Formation with AA2099-T83 and AA2060-T8E30 Aluminium Alloys. *Metals* **2020**, *10*, 872. [CrossRef]
- Torkamani, H.; Vivas Méndez, J.; Lecart, C.; Aldanondo Begiristain, E.; Álvarez Moro, P.; Antti, M.-L. Effect of Rotation Speed and Steel Microstructure on Joint Formation in Friction Stir Spot Welding of Al Alloy to DP Steel. *J. Manuf. Mater. Process.* **2022**, *6*, 24. [CrossRef]
- Ambrosio, D.; Aldanondo, E.; Wagner, V.; Dessein, G.; Garnier, C.; Vivas, J.; Cahuc, O. A Semi-Empirical Model for Peak Temperature Estimation in Friction Stir Welding of Aluminium Alloys. *Sci. Technol. Weld. Join.* **2022**, *27*, 491–500. [CrossRef]
- Jacquín, D.; Guillemot, G. A Review of Microstructural Changes Occurring during FSW in Aluminium Alloys and Their Modelling. *J. Mater. Process. Technol.* **2021**, *288*, 116706. [CrossRef]
- Murphy, A.; Price, M.; Wang, P. The integration of strength and process modeling of friction-stir-welded fuselage panels. In Proceedings of the 46th AIAA/ASME/ASCE/AHS/ASC Structures, Structural Dynamics and Materials Conference, Austin, TX, USA, 18–21 April 2005; American Institute of Aeronautics and Astronautics: Reston, VA, USA, 2005.
- Su, J.-Q.; Nelson, T.W.; Sterling, C.J. Microstructure Evolution during FSW/FSP of High Strength Aluminum Alloys. *Mater. Sci. Eng. A* **2005**, *405*, 277–286. [CrossRef]
- Cavaliere, P.; Nobile, R.; Panella, F.W.; Squillace, A. Mechanical and Microstructural Behaviour of 2024–7075 Aluminium Alloy Sheets Joined by Friction Stir Welding. *Int. J. Mach. Tools Manuf.* **2006**, *46*, 588–594. [CrossRef]
- Understanding REACH—ECHA. Available online: <https://echa.europa.eu/regulations/reach/understanding-reach> (accessed on 25 July 2022).
- ACARE Advisory Council for Aviation Research and Innovation. Available online: <https://www.acare4europe.org/> (accessed on 25 July 2022).
- Darsun, T.; Soutis, C. Recent Developments in Advanced Aircraft Aluminium Alloys. *Mater. Des. (1980–2015)* **2014**, *56*, 862–871. [CrossRef]
- Karanika, A.; Vourdas, N.; Makrikostas, A.; Marini, R.; Plagianakos, T.; Kalogeropoulos, S. Development of New Environmentally Friendly Anticorrosive Surface Treatments for New Al-Li Alloys Protection within the Frame of Clean Sky2. *Procedia Struct. Integr.* **2018**, *10*, 66–72. [CrossRef]
- Boldsakhan, E.; Fukada, S.; Fujimoto, M.; Kamimuki, K.; Okada, H. Refill Friction Stir Spot Welding of Surface-Treated Aerospace Aluminum Alloys with Faying-Surface Sealant. *J. Manuf. Process.* **2019**, *42*, 113–120. [CrossRef]
- Kubit, A.; Wydrzynski, D.; Trzepieciniski, T. Refill Friction Stir Spot Welding of 7075-T6 Aluminium Alloy Single-Lap Joints with Polymer Sealant Interlayer. *Compos. Struct.* **2018**, *201*, 389–397. [CrossRef]
- Maciel, R.; Bento, T.; Braga, D.F.O.; da Silva, L.F.M.; Moreira, P.M.G.P.; Infante, V. Fatigue Properties of Combined Friction Stir and Adhesively Bonded AA6082-T6 Overlap Joints. *Fatigue Fract. Eng. Mater. Struct.* **2020**, *43*, 2169–2180. [CrossRef]
- Gibson, B.T.; Wilkes, D.M.; Cook, G.E.; Strauss, A.M. In-Process Detection of Faying Surface Sealant Application Flaws in Friction Stir Welding. *J. Aircr.* **2013**, *50*, 567–575. [CrossRef]
- Gibson, B.T.; Cox, C.D.; Ballun, M.C.; Cook, G.E.; Strauss, A.M. Automatic Tracking of Blind Sealant Paths in Friction Stir Lap Joining. *J. Aircr.* **2014**, *51*, 824–832. [CrossRef]
- Aldanondo, E.; Vivas, J.; Álvarez, P.; Hurtado, I.; Karanika, A. Friction Stir Welding of AA2099-T83 and AA2060-T8E30 Aluminium Alloys with New Cr-Free Surface Treatments and Sealant Application. *Metals* **2021**, *11*, 644. [CrossRef]
- Kashaev, N.; Ventzke, V.; Çam, G. Prospects of Laser Beam Welding and Friction Stir Welding Processes for Aluminum Airframe Structural Applications. *J. Manuf. Process.* **2018**, *36*, 571–600. [CrossRef]
- Dubourg, L.; Merati, A.; Jahazi, M. Process Optimisation and Mechanical Properties of Friction Stir Lap Welds of 7075-T6 Stringers on 2024-T3 Skin. *Mater. Des.* **2010**, *31*, 3324–3330. [CrossRef]
- Schmidt, H.J.; Schmidt-Brandecker, B. Fatigue and damage tolerance behaviour of advanced structures in aeronautics. In *Fracture of Materials and Structures from Micro to Macro Scale. 18th European Conference on Fracture*; Deutscher Verband für Materialforschung und -prüfung: Berlin, Germany, 2010.
- Chhith, S.; De Waele, W.; De Baets, P.; Van Hecke, T. On-Line Detection of Fretting Fatigue Crack Initiation by Lock-in Thermography. *Tribol. Int.* **2017**, *108*, 150–155. [CrossRef]
- Ummenhofer, T.; Medgenberg, J. On the Use of Infrared Thermography for the Analysis of Fatigue Damage Processes in Welded Joints. *Int. J. Fatigue* **2009**, *31*, 130–137. [CrossRef]
- Yang, H.; Cui, Z.; Wang, W.; Xu, B.; Xu, H. Fatigue Behavior of AZ31B Magnesium Alloy Electron Beam Welded Joint Based on Infrared Thermography. *Trans. Nonferrous Met. Soc. China* **2016**, *26*, 2595–2602. [CrossRef]
- Crocco, D.; De Agostinis, M.; Fini, S.; Olmi, G.; Robusto, F.; Scapecchi, C. Fretting Fatigue in Mechanical Joints: A Literature Review. *Lubricants* **2022**, *10*, 53. [CrossRef]
- Szolwinski, M.P.; Farris, T.N. Mechanics of Fretting Fatigue Crack Formation. *Wear* **1996**, *198*, 93–107. [CrossRef]
- Lindley, T.C. Fretting fatigue. In *Encyclopedia of Materials: Science and Technology*; Buschow, K.H.J., Cahn, R.W., Flemings, M.C., Ilschner, B., Kramer, E.J., Mahajan, S., Veyssi re, P., Eds.; Elsevier: Oxford, UK, 2001; pp. 3347–3351, ISBN 978-0-08-043152-9.

15.- SUMMARY OF RESULTS, CONCLUSIONS AND FUTURE LINES

15.1.- SUMMARY OF RESULTS

The main results of this thesis are summarized in this chapter. The results are divided in two sections:

- Initial results: This section summarizes the results obtained in the previous investigations which were carried out before the presentation of the research project proposed to complete the thesis and employing conventional aluminium alloys. These results are a summary of the articles 1-7 presented in chapters 4-10 of this thesis and are discussed in section 15.1.1.
- Main results: The main results leading to the completion of the thesis are a summary of articles 8-11 reported in chapters 11-14. These results represent the core of the work carried out during the execution of the research project proposed to complete the thesis and are reported in section 15.1.2.

All these results are focused on the FSW process development and characterisation studies of joints produced in the overlap configuration using different aluminium alloys. The basic details of work performed in each of the articles included in this thesis are summarised in Table 4. The three articles considered for the completion of the thesis as a compendium of publications are highlighted in yellow and the fourth complementary article is highlighted in green:

Table 4: Summary of the work performed and published in each article.

	Al alloys	Tool design	Studied phenomena Characterisation tests
Article 1	AA6082-T6	<ul style="list-style-type: none"> • Cylindrical threaded • Cylindrical non-threaded 	<ul style="list-style-type: none"> • Tool probe design/length • Welding parameters • Metallographic examination • Static tensile shear strength
Article 2	AA6082-T6/AA5457-H22	<ul style="list-style-type: none"> • Cylindrical threaded • Cylindrical non-threaded 	<ul style="list-style-type: none"> • Tool probe design/length • Welding parameters • Material flow • Metallographic examination • Static tensile shear strength
Article 3	AA6063-T5/AA2024-T3	<ul style="list-style-type: none"> • Cylindrical threaded • Three flats + mixed thread • Triflute thread 	<ul style="list-style-type: none"> • Tool probe design • Welding parameters • Material flow • Metallographic examination • Static tensile shear strength • Static tensile tests (hoop stress)
Article 4	AA7075-T6	<ul style="list-style-type: none"> • Cylindrical threaded • Three flats + mixed thread 	<ul style="list-style-type: none"> • Tool probe design • Welding parameters • FSW process data • Metallographic examination • Lap joint metallurgical features
Article 5	AA7075-T6	<ul style="list-style-type: none"> • Cylindrical threaded • Three flats + mixed thread 	<ul style="list-style-type: none"> • Tool probe design • Welding parameters • Metallographic examination • Lap joint metallurgical features and defects • Microhardness analysis

Article 6	<ul style="list-style-type: none"> AA7050-T7651 AA2024-T3 Alclad AA7475-T761 	<ul style="list-style-type: none"> Cylindrical threaded Three flats + mixed thread 	<ul style="list-style-type: none"> Tool probe design Welding parameters Metallographic examination Lap joint metallurgical features and defects Microhardness analysis Static pull-out strength
Article 7	AA7075-T6	<ul style="list-style-type: none"> Cylindrical threaded Three flats + conventional thread 	<ul style="list-style-type: none"> Tool probe design Welding parameters Metallographic examination Lap joint metallurgical features and defects Estimation of T^o Effects of post-weld heat treatment Microhardness analysis Static tensile-shear strength Fatigue strength (tensile shear load)
Article 8	AA2099-T83/AA2060-T8E30	<ul style="list-style-type: none"> Cylindrical threaded Three flats + mixed thread 	<ul style="list-style-type: none"> Tool probe design Welding parameters Metallographic examination Lap joint metallurgical features and defects Microhardness analysis Static pull-out strength
Article 9	AA2099-T83/AA2060-T8E30	<ul style="list-style-type: none"> Cylindrical threaded Three flats + mixed thread 	<ul style="list-style-type: none"> Tool probe design Welding parameters Metallographic examination Material flow Lap joint metallurgical features and defects FSW process data
Article 10	AA2099-T83/AA2060-T8E30	<ul style="list-style-type: none"> Three flats + mixed thread 	<ul style="list-style-type: none"> FSW process data Metallographic examination Lap joint metallurgical features and defects SEM+EDS analysis Effects of surface treatments Effects of sealant Static pull-out strength
Article 11	AA2099-T83/AA2060-T8E30	<ul style="list-style-type: none"> Three flats + mixed thread 	<ul style="list-style-type: none"> Tool probe design Static tensile strength Fatigue strength (tensile shear load) Microhardness analysis Metallographic examination SEM+EDS analysis Fracture mode analysis Effects of surface treatments Effects of sealant

15.1.1.- Initial results

Initial work was performed and reported by the author related to FSW technology investigations in lap joint configuration [69] [70] [71] [72] [73] [74] [75]. The results obtained from this work were published in several articles before starting the work proposed for the research project of this thesis. These articles are included in this thesis as articles 1-7 in chapters 4-10, because the obtained conclusions were relevant for the selection of the FSW tool design and welding parameters for the targeted Al-Li alloys. Moreover, the experimental approach, testing and validation tasks were comparable, and they enabled the understanding of the underlying physical phenomena.

Initial investigations in FSLW were carried out with AA6082-T6 and AA5754-H22 aluminium alloys, analysing the material flow, joint formation mechanisms, joint defects and the static strength of the joints [69] [70]. The dissimilar material combination

employed was very useful to have an insight of the material flow leading to the final joint macrostructure [70]. Conventional cylindrical threaded and non-threaded FSW tool-probes were used in these initial FSW tests, which demonstrated to have an enormous impact on the metallographic properties of the joints as shown in Figure 39. Thus, the different probe designs resulted in different joint formation mechanisms that produced large differences in joint strength, showing the huge impact of the tool-probe design in the properties of FSLW joints. However, none of the tool-probes used in this study was able to avoid important defects such as the hook formation in FSLW joints.

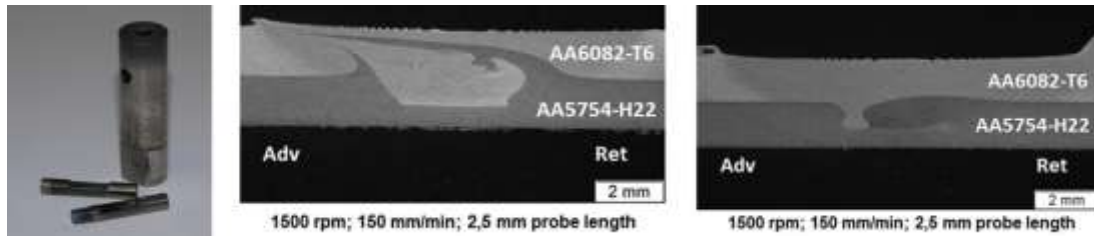


Figure 39: Threaded and non-threaded FSW tool-probe designs (left) and macrosections of FSLW joints produced using the same welding parameters but different tool-probe designs (right) [70].

Subsequent FSLW tests focused on developing tool-probe design improvements, introducing a new tool-probe design featuring three flats and a mixed thread. The aluminium alloys used for this study were AA6063-T5 extrusions on top of a AA2024-T3 sheet. The main conclusion was that the new tool-probe was able to minimize the defect formation in FSLW joint showing reduced hook size, as shown in Figure 40. This effect occurred due to a reduction of the vertical upwards flow of the material of the bottom sheet. Further FSLW tests followed using AA7075-T6 aluminium sheets [72], as well as AA2198-T8 alloy sheets [73]. The results, as shown in Figure 41, Figure 42 and Figure 43, confirmed the improvements in the quality of the joints produced by the probe featuring flats and mixed thread in comparison with the conventional threaded probe, due to its capability to minimize the hook size which is a potential defect in FSLW joints.

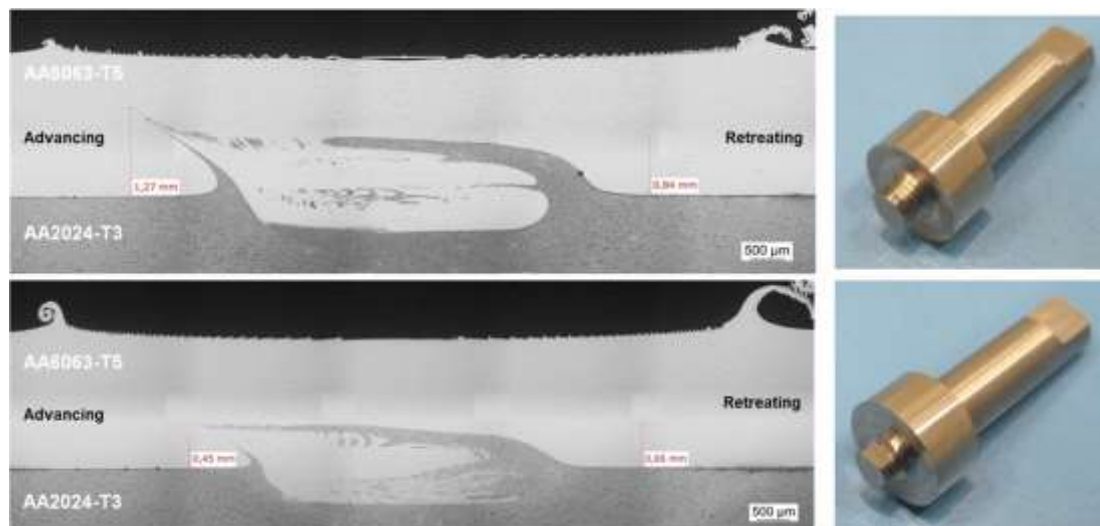


Figure 40: Macrosections and FSW tool-probes used for FSLW tests; cylindrical threaded tool-probe (top) and tool-probe with three flats and mixed thread (bottom) [71].

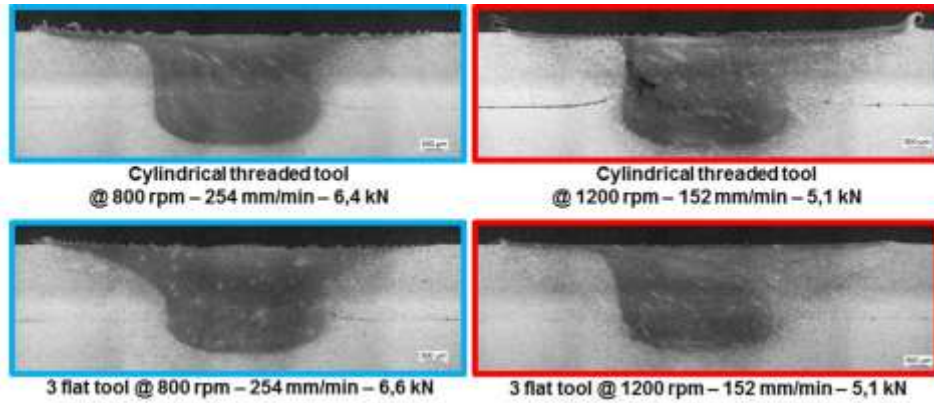


Figure 41: Macrosections of FSLW joints produced by the 2 different tool-probe designs and welding parameters with AA7075-T6 aluminium sheets [72].

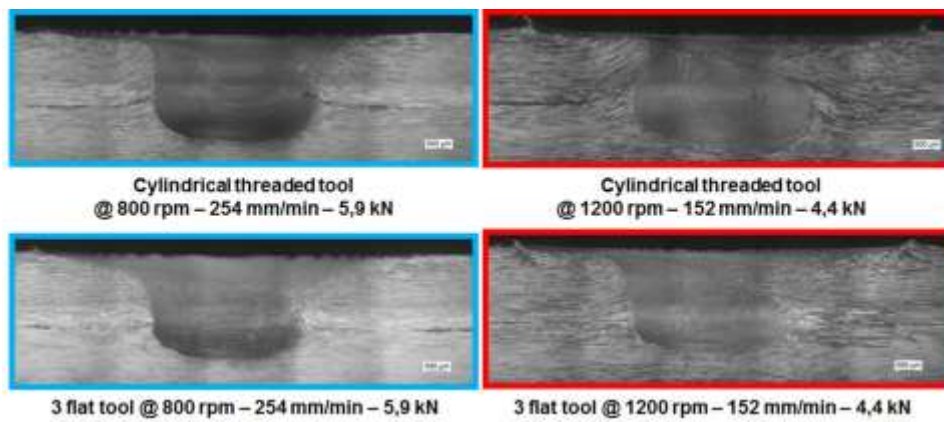


Figure 42: Macrosections of FSLW joints produced by the 2 different tool-probe designs and welding parameters with AA2198-T8 aluminium sheets [73].

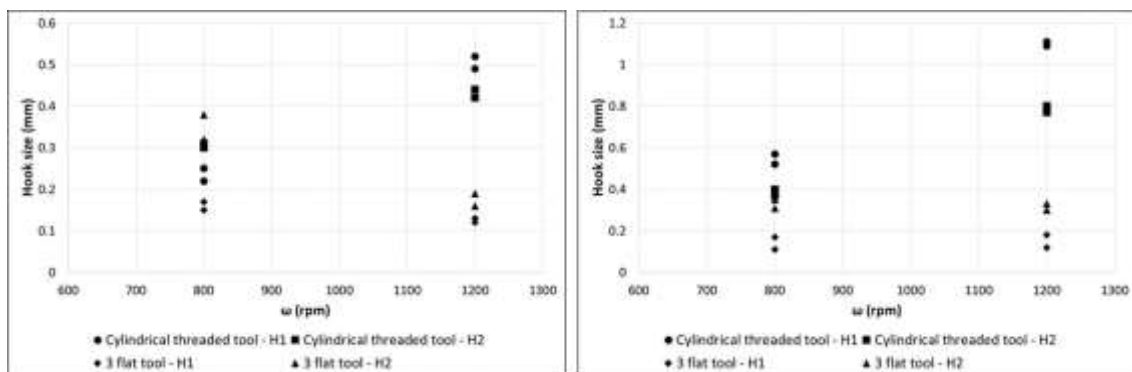


Figure 43: Graphic representation of the hook size measured in FSLW joints produced by 2 different tool-probe designs and welding parameters with AA7075-T6 (left) [72] and AA2198-T8 (right) [73].

Macrosections of FSLW joints produced under several FSW process conditions with AA7075-T6 aluminium sheets can be observed in Figure 41. The joints produced by the conventional threaded probe presented narrower SZ regions and showed tunnelling defects in the advancing side when high heat input welding parameters were used, i.e. 1200rpm and 152mm/min. In addition to that, this conventional threaded probe produced larger hook imperfections, especially using high heat input welding parameters. These

issues were avoided by the use of the probe featuring three flats and mixed thread. The capability to achieve larger SZ regions and absence of any volumetric defect was demonstrated over a wide range of welding parameters. Equivalent results as the ones obtained with AA7075-T6 alloy were also achieved with the 2mm thick AA2198-T8 Al-Li alloy sheets (Figure 42). A particular characteristic provided by the probe with three flats and mixed thread was that, contrary to the case with the conventional threaded probe, the hook size was not dependant of the welding parameters. Thus, the use of different heat input conditions, i.e. different relationships between rotational and welding speed, was found to be feasible with the new probe design, achieving a similar hook size formation. These results are represented in Figure 43. However, the effectiveness of the new probe to avoid the cold lap defects as well as the joint strength were not thoroughly investigated in these works.

The use of probe designs featuring three flats and a conventional thread were also compared with cylindrical conventional threaded tools in FSLW tests performed with AA7075-T6 aluminium sheets [75]. FSLW joints were performed using several welding conditions and their properties studied in terms of microstructural examination, microhardness measurements as well as joint strength in static tensile and fatigue testing. Although the tool-probe with flats showed a slightly better capacity to minimize lap joint imperfections such as hooks and cold lap defects, the mechanical performance of the joints was found to be very similar for the joints produced by both probe designs. This suggested that the size of the flat features in the probe was not sufficiently large to produce significant improvements in FSLW joint quality.

Figure 44 shows the macrographs of FSLW joints as well as a quantification of characteristic microstructural features of such welded joints, such as the effective sheet thickness (EST) and the bonded interface width (BIW), produced using different FSW conditions (tool design and welding parameters). From these results, it was concluded that the benefits of using a FSW tool design with three flats and a conventional thread were limited in comparison with a cylindrical conventional threaded tool. In any case, the tool featuring three flats did show the capability of improving the characteristics of FSLW joints, producing smaller hook sizes and incrementing the EST and the BIW.

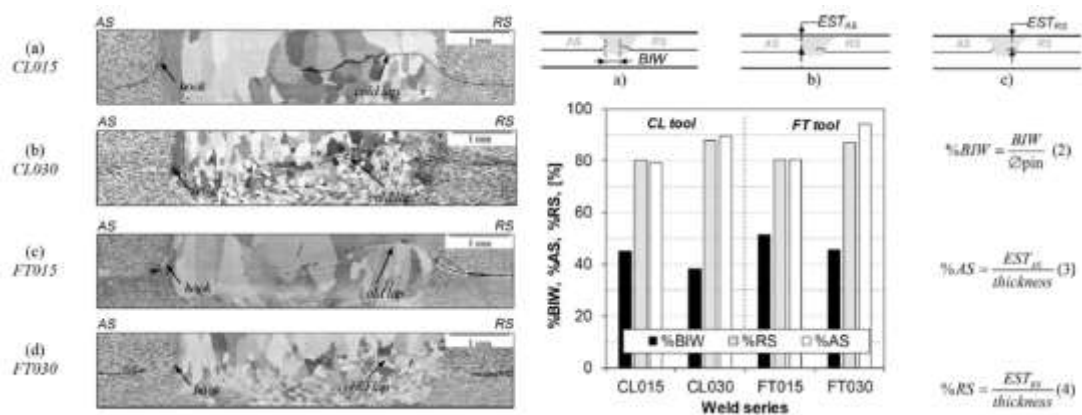


Figure 44: Hook and cold lap defect details (left); and EST and BIW representation (right) in FSLW joints performed by several probe designs and welding parameters [75].

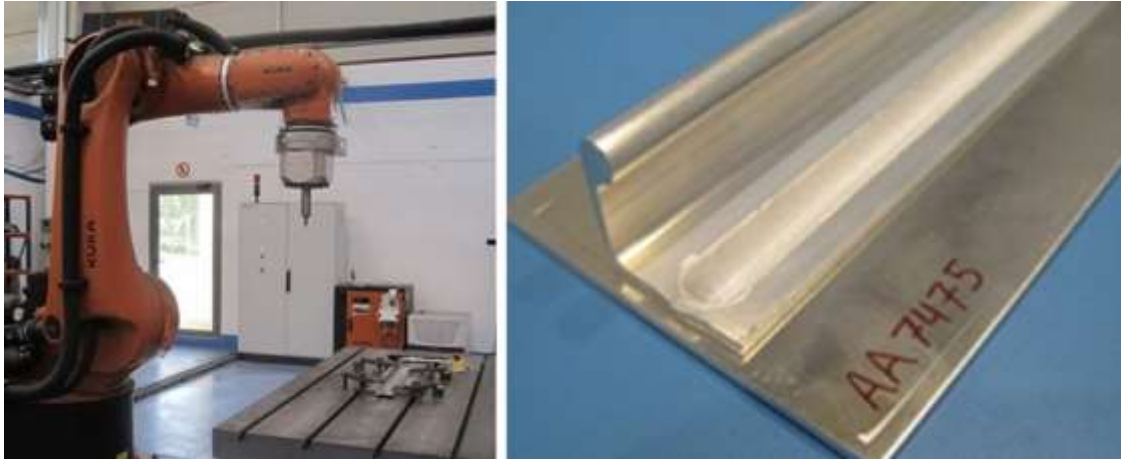


Figure 45: Robotic FSW system at LORTEK used for FSLW tests (left) and a FSLW joint (right) made with AA7050-T7651 extrusion (stringer) and AlcladAA7475-T761 sheet (skin) [74].

All the discussed results were mainly obtained in FSLW joints produced by overlapped sheets of several medium and high strength aluminium alloys. FSLW were also performed in stringer-skin lap joint configurations using conventional aluminium alloys typically employed in the aeronautic industry [74]. AA7050-T7651 aluminium extrusions (stringer) on top of AA2024-T3 and Alclad AA7475-T761 aluminium sheets (skins) were selected to produce FSLW joints. The robotic FSW system used for the tests and an example of a FSLW joint are shown in Figure 45. FSLW joints were produced employing several welding parameter-sets and tool-probe designs, including probe length and flats-thread features. The basic characterisation of the joint properties was performed by metallographic examination, microhardness measurements and static pull-out tests.

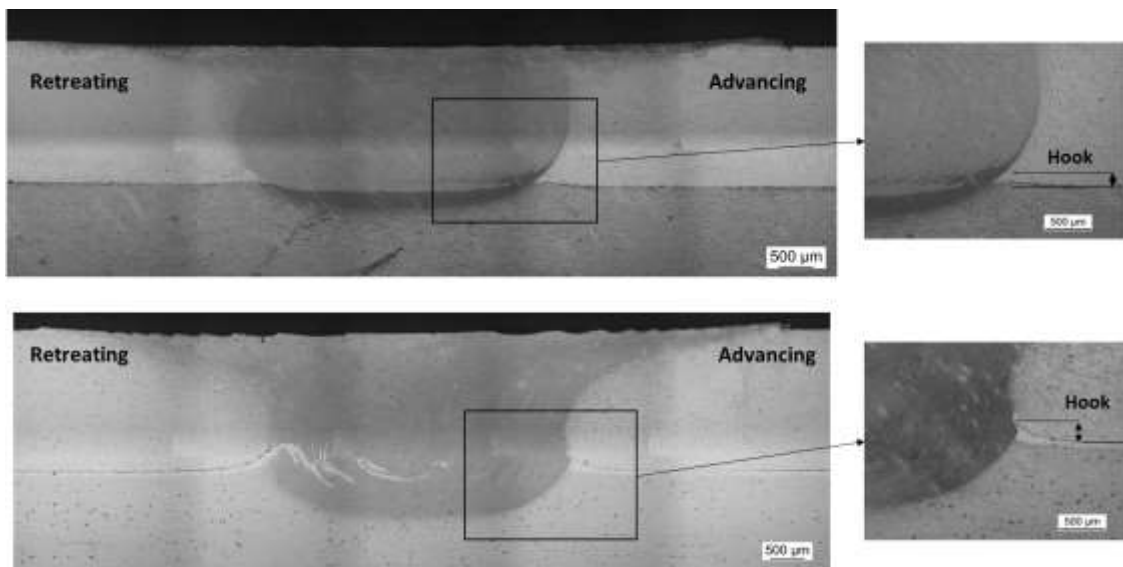


Figure 46: Macrosections of FSLW joints made with AA7050-T7651 extrusion on top of an AA2024-T3 sheet (top) or AlcladAA7475-T761 sheet (bottom) [74].

The clad material (pure aluminium layer) present at the surface of the Alclad AA7475-T761 sheet with the aim of enhancing corrosion performance played a major role in the joint formation mechanism and the resulting joint properties. Thus, it was necessary to adjust the FSW process conditions in order to maximize the pull-out joint strength depending on the aluminium alloys used as skin material (AlcladAA7475-T761 or

AA2024-T3). Figure 46 shows macrosections of FSLW produced under different processing conditions and base aluminium alloy materials. The hook size was minimized by using a small penetration of the probe in the skin during the FSW process (Figure 46-top). However, the material mixing and cold lap defect elimination was not effective with these FSW process conditions, especially for the Alclad AA7475-T761 alloy as the clad layer mixing and dispersion in the SZ was not effective enough. Therefore, the use of larger probe lengths produced better results as the clad layer was more effectively disrupted and dispersed in the SZ of the weld (Figure 46-bottom). In the pull-out strength results shown in Figure 47, one can observe that, depending on the aluminium alloy used as skin, the FSW processing conditions have to be carefully selected in order to maximize the joint strength. This includes the right selection of the advancing and retreating side orientation in the weld, as the strength for each side was shown to be different [74].

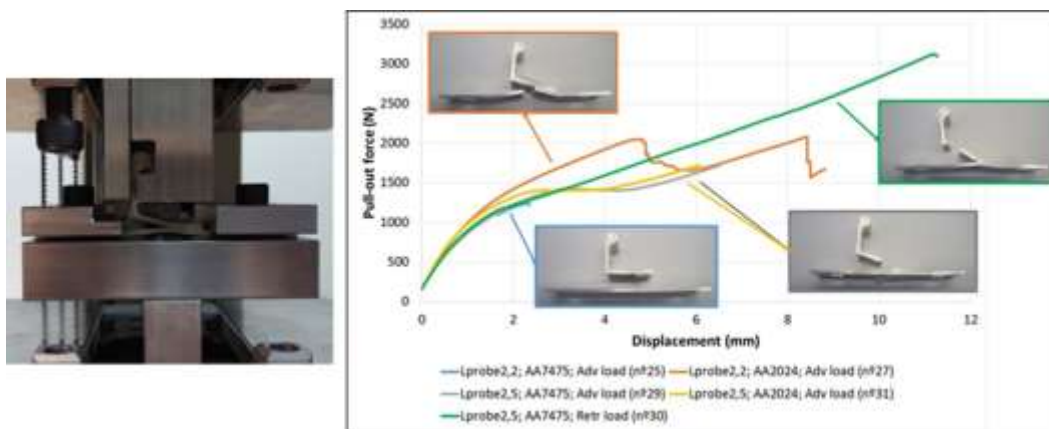


Figure 47: Pull-out strength test (left) and strength results (right) with stringer-skin FSLW joints produced by different tool-probe designs, alloy combinations and loading conditions [74].

All these results showed that there are many factors to be taken into account for the FSW manufacturing of lap joints to achieve high quality FSLW joints such as targeted alloys, thicknesses, FSW tool design, weld orientation, processing parameters... Therefore, the work proposed in the research project presented to complete the thesis was focused on the FSW process developments for the selected Al-Li alloys in stringer-skin type joints, which are of high relevance for the development of lightweight integrally reinforced aircraft structures:

- AA2060-T8E30 skin sheet (thickness 2,5 mm) – AA2099-T83 stringer extrusion (thickness 2 mm in the overlapped area). These materials were supplied by ALCOA-ARCONIC (Figure 48 - left).
- AA2198-T8 skin sheet (thickness 2,5 mm) – AA2196-T8511 stringer extrusion (thickness 2,5 mm in the overlapped area). These materials were supplied by CONSTELLIUM (Figure 48 - right).

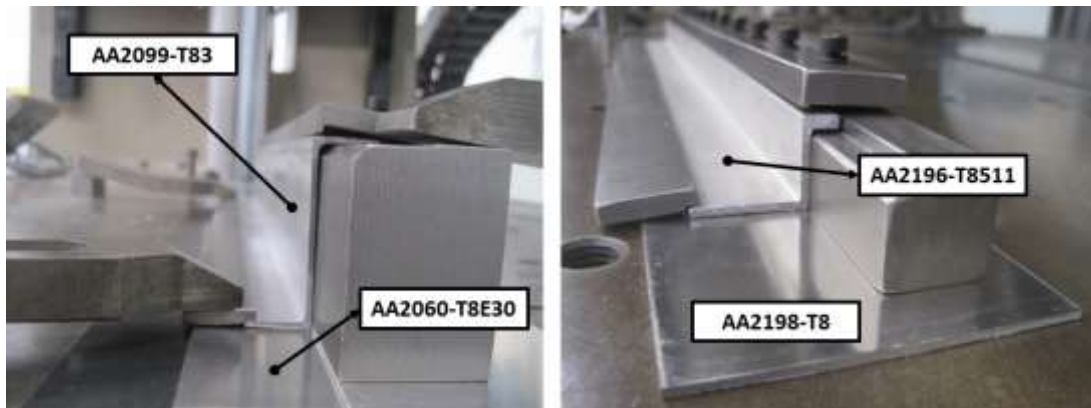


Figure 48: Selected Third-Generation Al-Li alloy materials and clamping arrangements developed for FSLW tests.

All the initial results discussed in this section were considered for the FSLW developments with these new Al-Li alloys. Thus, the necessary clamping arrangements were designed and manufactured (Figure 48). FSW tool-probes were also designed, as shown in Figure 49, and manufactured. Surface treatment application to the Al-Li materials was coordinated with partners of ecoTECH (HAI and AKZONOBEL), as well as sealant selection for subsequent FSLW tests. Thus, the work to be performed to complete the thesis was planned and ready to start at the time when the research project was presented.

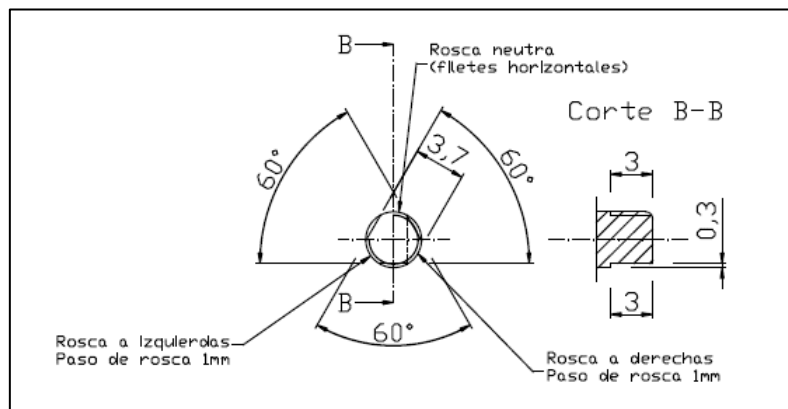


Figure 49: FSW tool-probe design with “mixed threads + three flat” concept.

Following the recommendations made by the evaluation committee after the presentation of the research project, it was decided to focus the main work to complete the thesis in the alloy combination supplied by ALCOA-ARCONIC, i.e., AA2060-T8E30 sheet and AA2099-T83 extrusion. Nevertheless, the performed work was not limited to this combination and further work has also been done using the other alloys, mainly AA2198-T8 sheet. All these results are discussed in the following section 15.1.2.

15.1.2.- Main results

The work and results leading to the completion of this thesis, which are discussed in this section, were published mainly in three scientific articles [77] [78] [79] complemented by a fourth one [76]. These articles are included in this thesis as articles 8-11 in chapters

11-14. The work was focused on investigating the microstructural and mechanical properties of FSLW joints produced using AA2099-T83 and AA2060-T8E30 Al-Li alloys. These properties were investigated for joints produced using different FSW conditions and relevant manufacturing conditions to ensure high corrosion resistance (surface treatments and sealant application).

The initial work was focused on the FSW process optimization to obtain high quality FSLW joints using AA2099-T83 extrusions as stringers and AA2060-T8E30 sheets as skin materials without any surface treatment [76] [77] (chapters 11 and 12 respectively). The chemical compositions of these alloys are shown in Table 5.

Table 5: Chemical compositions of base materials, wt.%.

Alloy	Al	Si	Fe	Cu	Mn	Mg	Zn	Ti	Ag	Li	Zr
AA2060-T8E30	Bal.	0.07	0.07	3.4-4.5	0.1-0.5	0.6-1.1	0.3-0.5	0.1	0.05-0.5	0.6-0.9	0.05-0.15
AA2099-T83	Bal.	0.05	0.07	2.4-3.0	0.1-0.5	0.1-0.5	0.4-1	0.1	-	1.6-2.0	0.05-0.12



Figure 50: i-STIR PDS 4 FSW machine used for FSW manufacturing tests (left); clamping configuration developed to produce the FSW coupons using AA2099-T83 extrusions on top of AA2060-T8E30 sheets (right).

FSW manufacturing tests were performed in the i-STIR PDS 4 FSW machine at LORTEK using the specific clamping system and configuration designed and manufactured for the base materials (Figure 50). FSLW joints were produced using different tool designs and process parameters. An example of a FSLW joint can be observed in Figure 51a. The general dimensions of both tools were similar having a shoulder of 10 mm in diameter, a probe of 4 mm in diameter and a probe length of 2.5 mm. The main difference of the tools was the design of the probe. The first design was a conventional threaded cylindrical probe (Figure 51b) typically used in conventional FSW processes for butt joint configurations. The new design proposed for lap joints was a probe with three flats and a mixed neutral thread (Figure 51c). The flats divided the probe in three different threaded sections where three different thread orientations were machined as indicated in Figure 51d. The main purpose of this tool design specifically proposed for lap joints was to avoid vertical plasticized material flow during the FSW process in order to reduce the hook formation, while promoting sufficient material flow at the faying surface of the materials to break the oxide layers and produce the mixture between the materials to be welded.

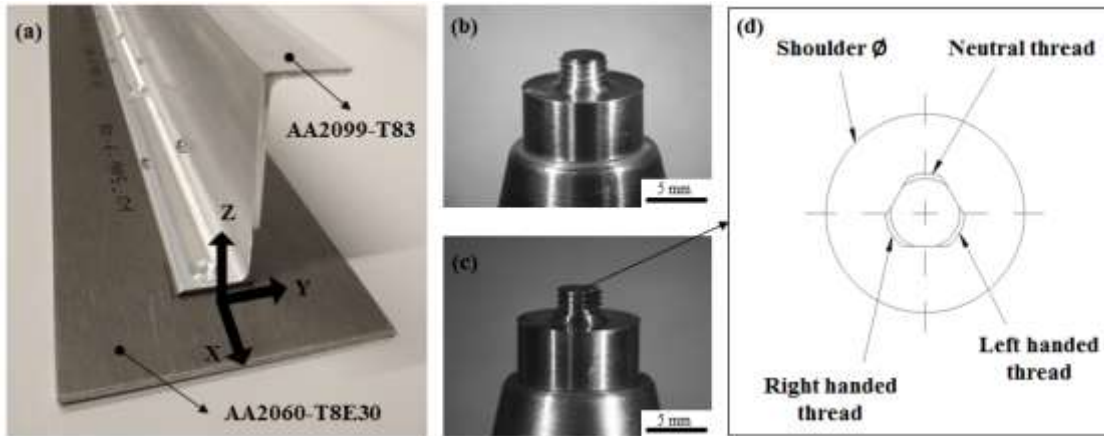


Figure 51: (a) FSLW joint produced using AA2099-T83 and AA2060-T8E30 alloys; (b) conventional tool; (c) new tool proposed for lap joints; (d) sketch with details of the new three flat + mixed thread tool.

In addition to the different tool designs, FSLW joints were also produced employing several combinations of welding parameters. The rotational speed ranged between 800 and 1200 rpm and the welding speed was varied from 150 to 250 mm/min. A macro-microstructural analysis was performed with specimens cut from the FSLW joints and prepared using typical metallographic preparation techniques. The cross-sections were examined by optical microscopy in order to investigate the metallographic properties of the FSLW joints.

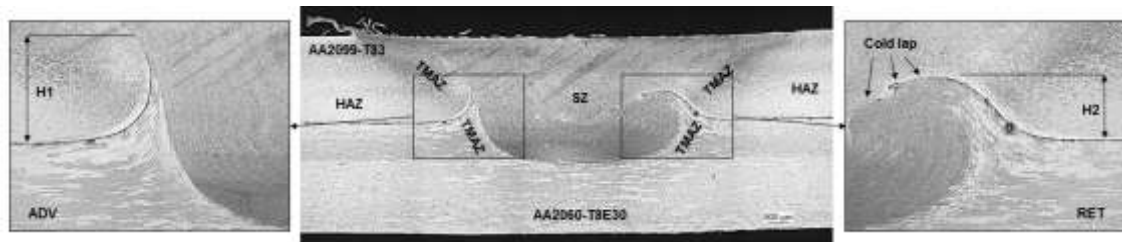


Figure 52: Cross-section of FSLW joint produced at 1200 rpm and 250 mm/min using a conventional threaded tool.

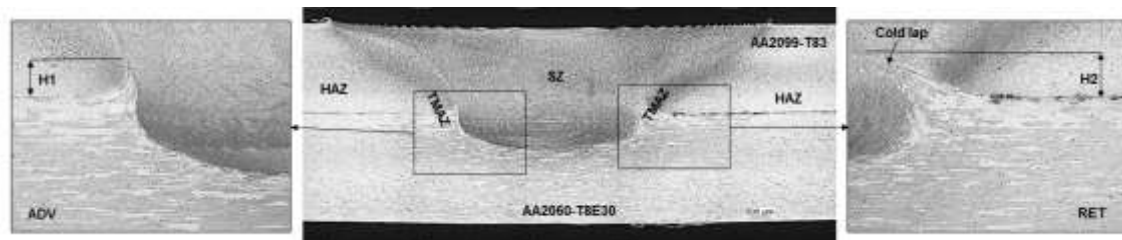


Figure 53: Cross-section of FSLW joint produced at 1200 rpm and 250 mm/min using a three flat + mixed thread tool.

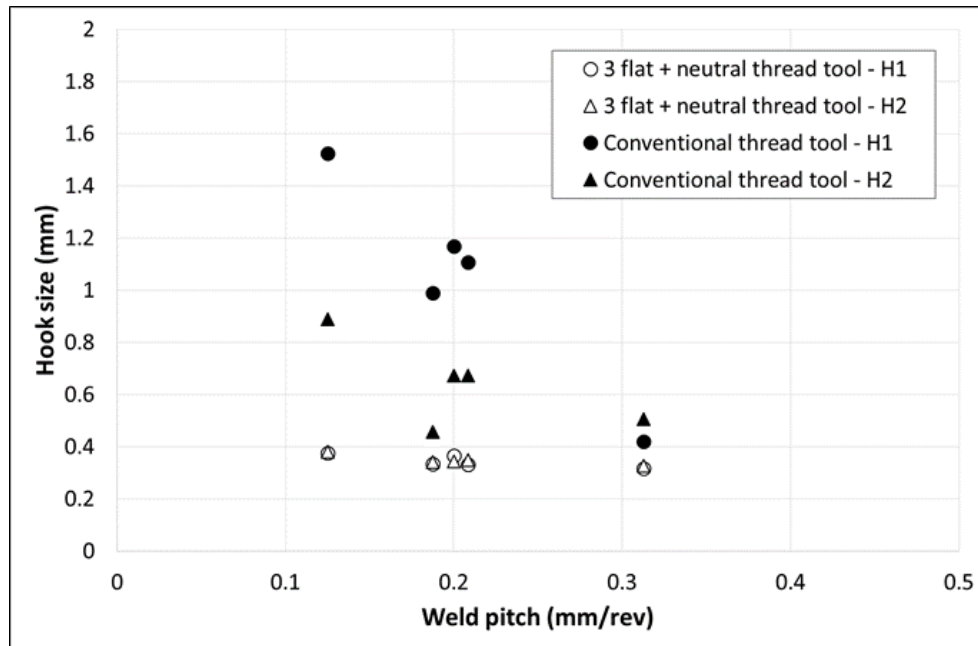


Figure 54: Representation of the hook size measured in FSLW joints produced using different welding parameters (weld pitch) and tool designs.

The macro-microstructural analysis evidenced the benefits of using the new three flat + mixed thread tool for the manufacturing of FSLW joints in comparison with the conventional threaded tool. Figure 52 and Figure 53 show the clear differences in the metallographic properties of the FSLW joints that were obtained using the same welding parameters but different tool design. It was clearly observed that the new three flat + mixed thread tool was able to minimize the hook defects of the FSLW joints. This effect was observed for a wide range of welding parameters as it can be observed in Figure 54. The hook size of the FSLW joints produced under different welding parameters (weld pitch) and heat input conditions was kept in reduced values using the new three flat + mixed thread tool. This was not the case for the conventional cylindrical threaded tool which produced a significant increase of the hook defect in FSLW joints produced using small weld pitch conditions, i.e., high rotational speed and low welding speed conditions. Thus, it was concluded that the proposed new tool design was capable of limiting the vertical material flow of plasticized material resulting in small hooks in both the advancing and retreating sides.

In order to evaluate the effectiveness of the welding conditions to minimize the cold lap defect and hooks, the most relevant metallographic features of FSLW joints were quantified and analyzed. Thus the effective lap width (ELW) and hook height at the advancing (D1) and retreating (D2) sides were measured as indicated in Figure 55 and represented in the graphs shown in Figure 56 and Figure 57.

The conclusions related to the hook formation mechanisms and the capability of the new three flat + mixed thread tool to reduce this defect were similar to the ones obtained previously. This tool showed the capability to limit the vertical flow of plasticized material during the FSW process, minimizing the hooks produced in the FSLW joints (Figure 56). This is the case for the hooks produced in the advancing side (Figure 56a) as well as in the retreating side (Figure 56b). On the contrary, the conventional cylindrical threaded tool showed an important material flow in the vertical direction especially using high heat input conditions, i.e., low weld pitch (high rotational speed and low welding speed). This resulted in a significant increment of the hook size which can reduce the strength of the FSLW joints.

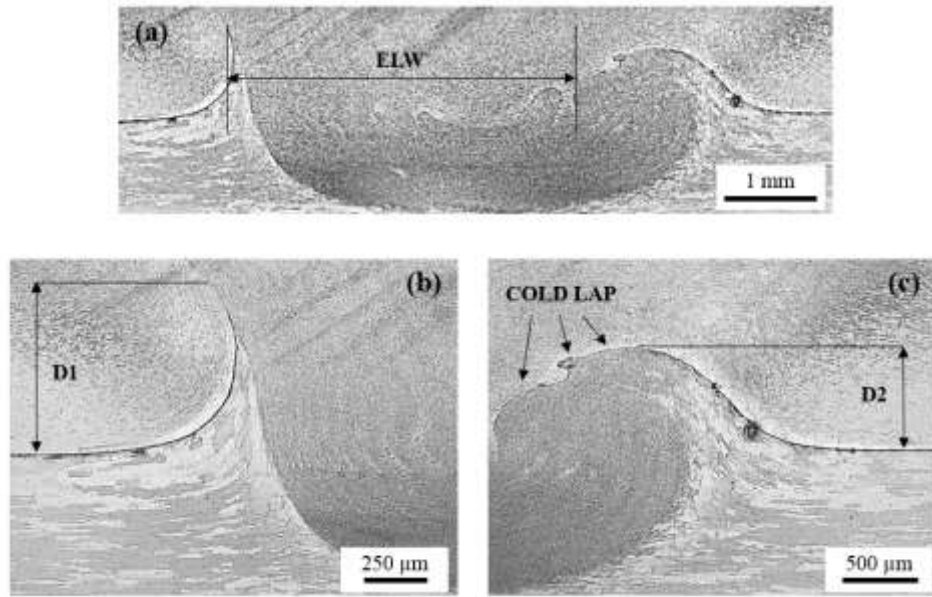


Figure 55: Cross-section showing the characteristic features of FSLW joints; (a) effective lap with (ELW); (b) hook at the advancing side (D1); (c) cold lap defect and hook at the retreating side (D2).

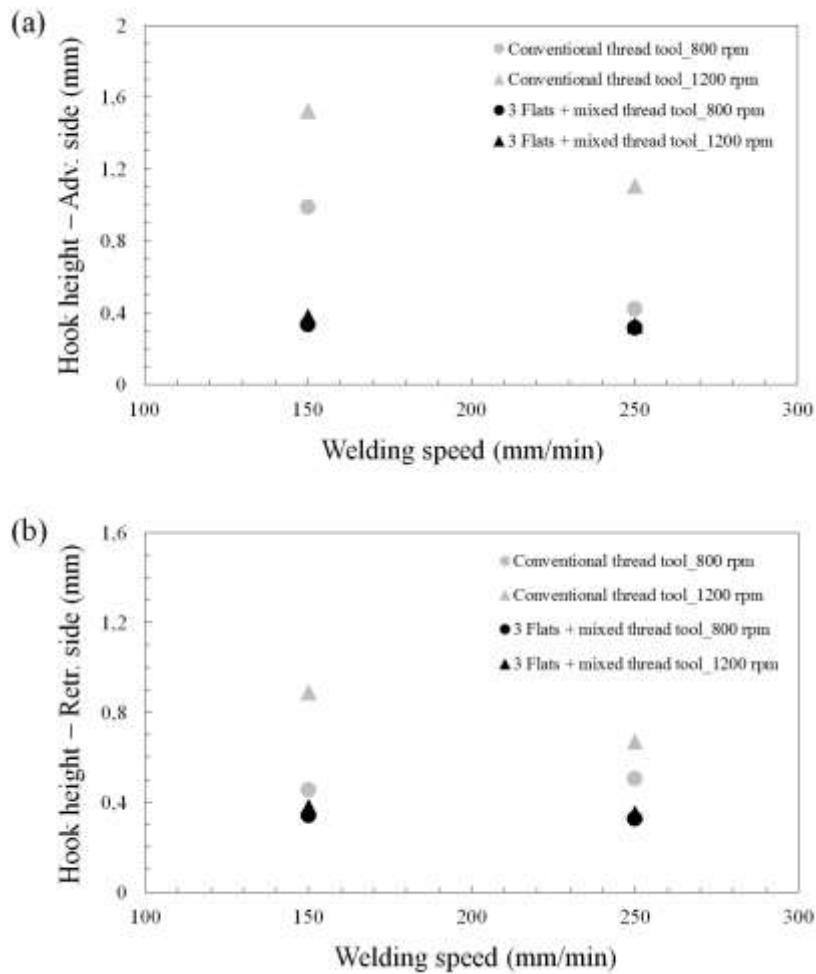


Figure 56: Representation of the (a) hook height in the advancing side; and (b) hook height in the retreating side; in FSLW joints produced using different welding parameters and tool designs.

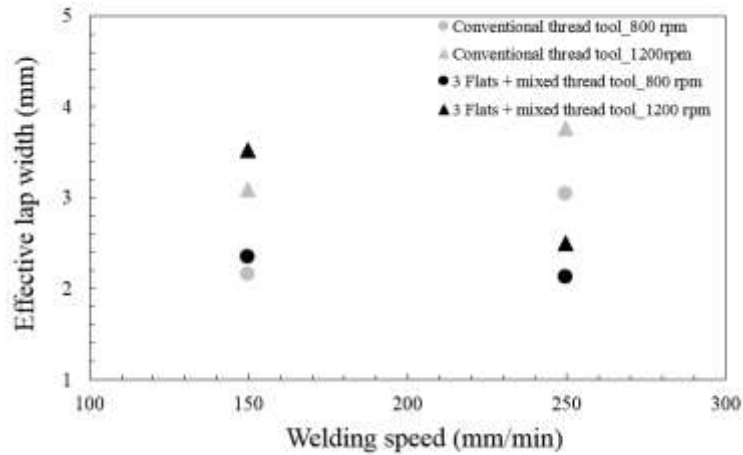


Figure 57: Representation of the ELW in FSLW joints produced using different welding parameters and tool designs.

The results related to the ELW produced in the FSLW joints were not as clear as for the hook formation case (Figure 57). Generally, it was observed that a higher rotational speed resulted in larger ELW. While at lower welding speeds the ELW produced using different tools were comparable, at higher welding speeds the conventional threaded tool produced a larger ELW. This was related to a more energetic material flow and mixing produced by the threads in the vertical direction by the conventional tool, but this effect also entails the formation of large hooks. On the contrary, the new three flat + mixed thread tool showed a good capability to limit the vertical material flow and to promote sufficient material flow at the faying surface of the materials, resulting in FSLW joints with a large ELW and small hooks.

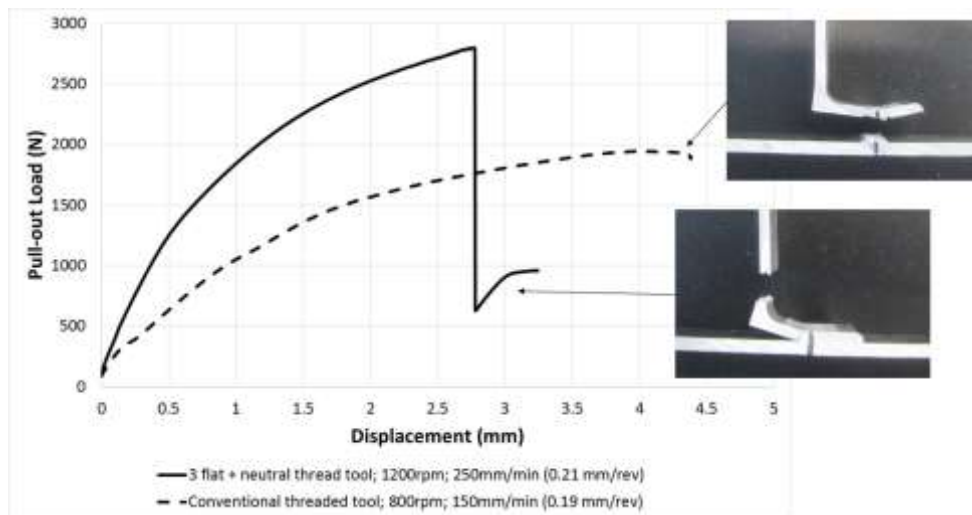


Figure 58: Pull-out strength and failure mode of FSLW joints produced using different tools and welding parameters.

The static mechanical strength of the FSLW joints was investigated by pull-out tests, where the AA2060-T8E30 sheet/skin was firmly hold in a fixture and a pulling force in the vertical direction was applied to the AA2099-T83 extrusion/stringer. Specimens cut from FSLW joint-coupons produced using different tools and welding parameters were tested in order to investigate their mechanical strength and the relationship with their metallographic characteristics. In general, FSLW joints produced using the three flat +

mixed thread presented superior mechanical strength in comparison with the conventional threaded tool. An example of the failure modes and the strength curves obtained for different specimens can be observed in Figure 58. Welding conditions resulting in poor material flow and mixing at the stringer/skin interface resulted in low strength and interfacial failures of the FSLW joints. On the contrary, welding conditions that produced FSLW joints with small hooks and sufficiently large ELW showed a good load carrying capability and failures in the base alloy AA2099-T83 outside the FSLW joint. It was concluded that a superior weld quality and load carrying capacity can be obtained using the new three flat + mixed thread tool. Thus, the welding conditions that produced FSLW joints with an optimized quality were identified:

- Tool design: Three flat + mixed thread
- Rotational speed: 1200 rpm
- Welding speed: 250 mm/min
- Forge force: 6.25 kN
- Joint configuration: Advancing side oriented towards the vertical side of the AA2099-T83 stringer

Once an advanced tool design and appropriate welding conditions were identified, the work continued with the investigation to determine the feasibility to process by FSW surface treated base materials including the use of a sealant at the AA2099-T83 stringer and the AA2060-T8E30 skin interface. These conditions were representative of typical manufacturing practices used in the manufacturing of aeronautic structures in order to improve their corrosion resistance. This work, results and conclusions were published in another scientific article [78], which is included in this thesis in chapter 13.

AA2060-T8E30 sheet/skin and AA2099-T83 extrusions/stringers were surface treated using two innovative Cr-free surface treatments:

1. Thin Film Sulfuric Acid Anodizing (TFSAA)
2. AC131 Sol-Gel

These surface treatments were performed by Hellenic Aerospace Industry (HAI) so the test plan and logistics for materials were coordinated with them in a great collaborative work established in the project ecoTECH. As another corrosion protection technique, the sealant Naftoseal MC-780-class C was selected to be applied at the interface between the stringers and skin before the welding process. Examples of surface treated base materials as well as sealant preparation and application in the AA2060-T8E30 skin surface can be observed in Figure 59.

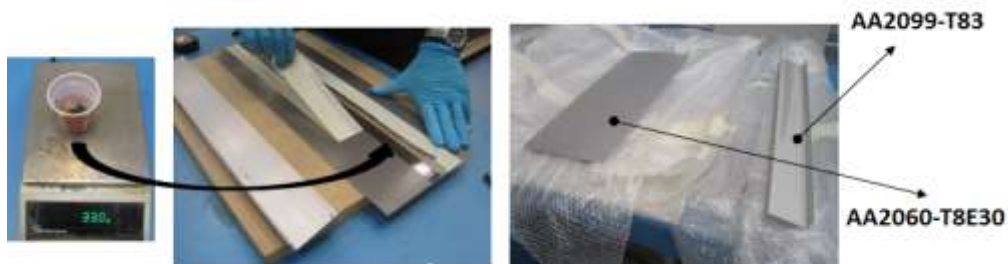


Figure 59: Sealant preparation and application in AA2060-T8E30 sheet without any surface treatment (left); and surface treated base materials (right).

FSW manufacturing tests were performed using several combinations of base materials with different surface treatments and sealant application in the stringer-skin interface. The same I-STIR PDS 4 FSW machine and previously optimized welding parameters were employed to produce the FSLW joint-coupons. The FSW process setup and the FSLW joint-coupons showing different surface conditions can be seen in Figure 60. Thus, FSLW joint-coupons C1-C6 were produced using different combinations of applied surface treatments and sealant. The manufacturing conditions for each coupon are detailed in Table 6.

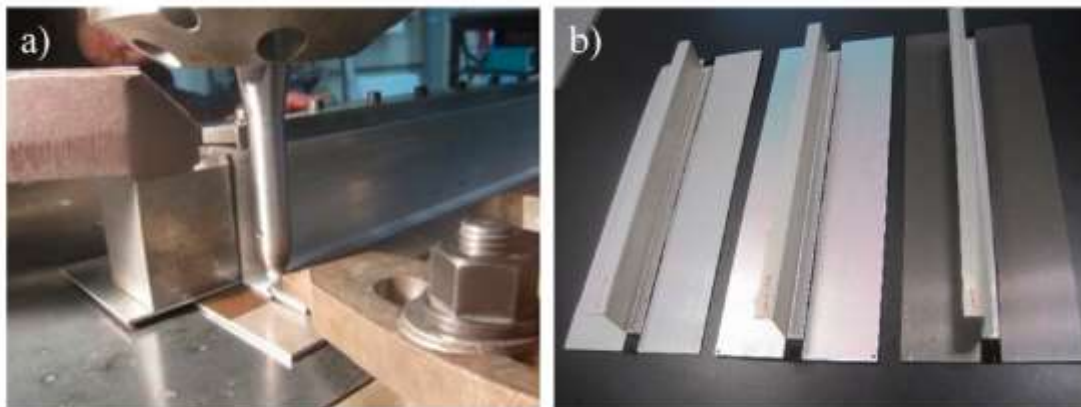


Figure 60: (a) Setup for the FSW process manufacturing; and (b) Examples of FSLW joint-coupons produced using base materials with different surface conditions and sealant.

Table 6: Friction stir welded coupon identification with the applied surface treatments and sealant.

Coupon Code ID	Surface Treatment	Sealant
C1	-	-
C2	TFSAA	-
C3	Sol Gel	-
C4	-	Naftoseal® MC-780-Class C
C5	TFSAA	Naftoseal® MC-780-Class C
C6	Sol Gel	Naftoseal® MC-780-Class C

The FSW process stability was investigated observing the general performance of the FSW process execution, visual inspection of the produced FSLW joints as well as analyzing the critical process data recorded by the FSW machine.

The general FSW process performance as well as the visual appearance of the FSLW joints was similar for all C1-C6 coupons, meaning the process was stable even for the cases where base materials were coated and the sealant applied at the stringer/skin interface.

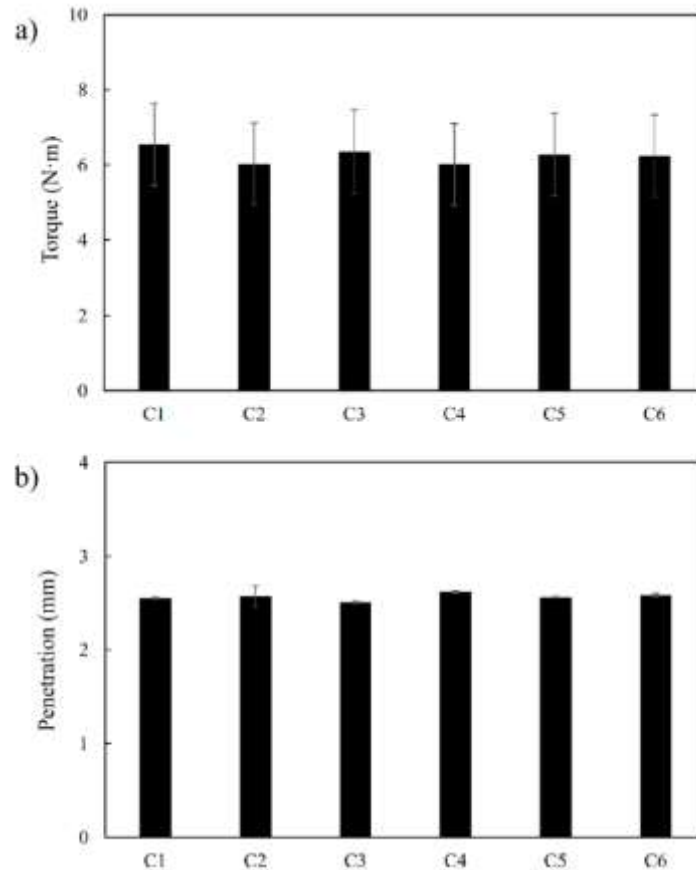


Figure 61: (a) Torque and (b) tool penetration average values obtained during the FSW process for C1-C6 coupons.

The analysis of critical data of the FSW process led to the same conclusion. Taking into account the command parameters were a constant rotational speed (1200 rpm) and a constant axial forge force (6.25 kN), the principal data that were analyzed as critical feedback values were the torque and the tool penetration. Average values obtained during the manufacturing of the C1-C6 FSLW joint-coupons are shown in Figure 61. According to these results, no significant difference was observed between the FSLW joints performed using base materials without any surface treatment (C1) and the ones with TFSA (C2) or Sol-Gel (C3). The application of sealant (C4-C6) did not suppose any significant difference in the average torque and penetration values either. Therefore, it was concluded that the application of the surface treatments TFSA and Sol-Gel to the base materials, as well as the application of sealant at the stringer/skin interface did not introduce any relevant difficulties for the manufacturing process of FSLW joints. Thus, the manufacturing of surface treated AA2060-T8E30 and AA2099-T83 alloys using a sealant was observed to be feasible opening the possibility to apply innovative Cr-free corrosion protection techniques during FSLW joint manufacturing.

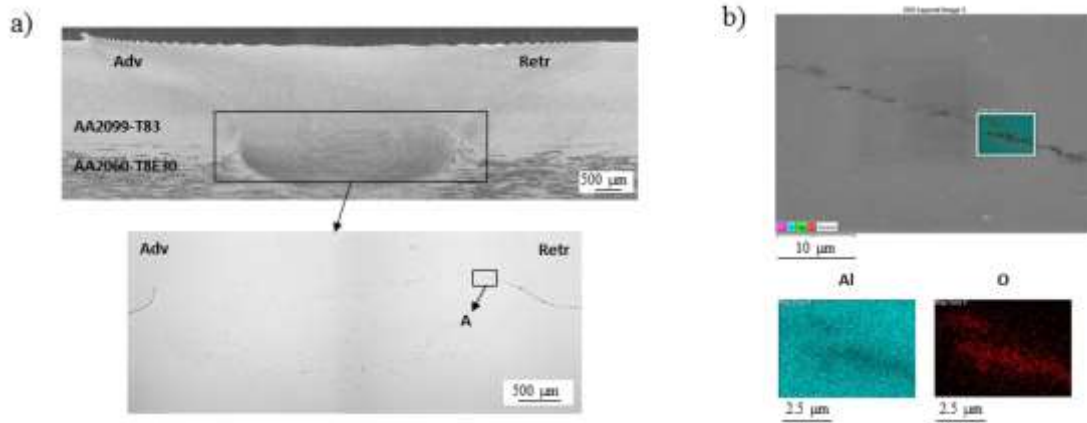


Figure 62: (a) Cross-section of FSLW joint C1 and (b) SEM image and EDS analysis of region A in Figure 62a.

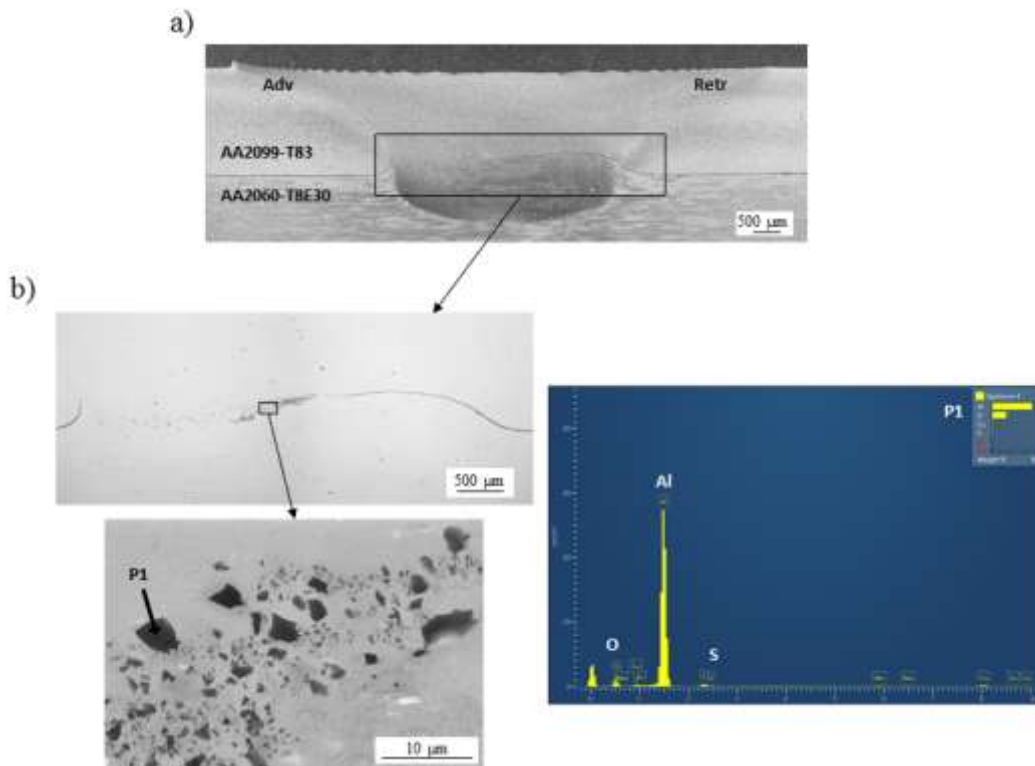


Figure 63: (a) Cross-section of FSLW joint C2 and (b) details of the SZ interface by optical microscopy, SEM and EDS analysis of the fragment remnants.

Although the FSLW manufacturing seemed feasible, the microstructure and properties of the FSLW joints produced using surface treated base materials and sealant were more deeply investigated. Thus, a metallographic characterization of the FSLW joints was performed using optical and scanning electron microscopy (SEM) complemented with energy dispersive spectroscopy (EDS) analysis. A summary of the obtained results is shown in Figure 62, Figure 63 and Figure 64.

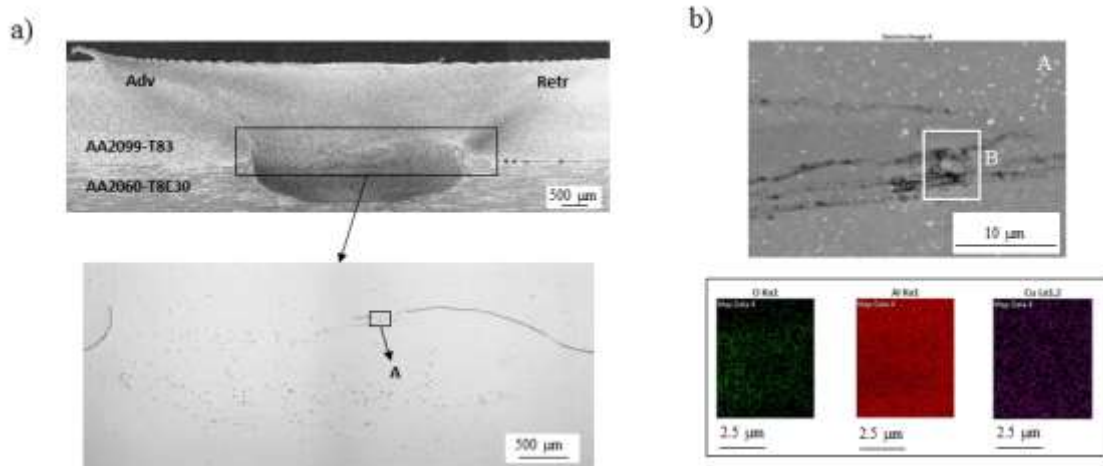


Figure 64: (a) Cross-section and detail magnification of FSLW joint C6 and (b) SEM image and EDS analysis of region A in Figure 64a.

The results of the metallographic analysis showed a very clear stirred zone (SZ) region free of major contaminant agents, although some minor oxides were observed in the close proximity to the retreating side (Figure 62). However, in FSLW joints performed using TFSA treated base materials (C2 and C5) an important presence of fragment remnants was observed in the SZ (Figure 63), which were mainly located towards the retreating side of the weld. The SEM and EDS analysis of these remnants revealed their aluminium oxide nature with the presence of some sulphur content. Thus, it was concluded that the presence of these fragments was the consequence of the incomplete break, dispersion and mixing of the thin aluminium oxide coating generated at the surface of the AA2060-T8E30 and AA2099-T83 alloys during the TFSA process. The FSLW joints produced using Sol-Gel treated alloys and sealant at the stringer/skin interface also showed some traces of remnants located towards the retreating side of the weld (Figure 64). The compositional analysis of these remnants revealed contents of aluminium and copper as well as oxygen very likely coming from the base composition of the alloys and the inherent oxide layer present at the surface of the parent materials. No traces of sealant were found in the SZ of the welds suggesting it was eliminated from the weld zone due to the pressure applied by the tool during the FSLW process.

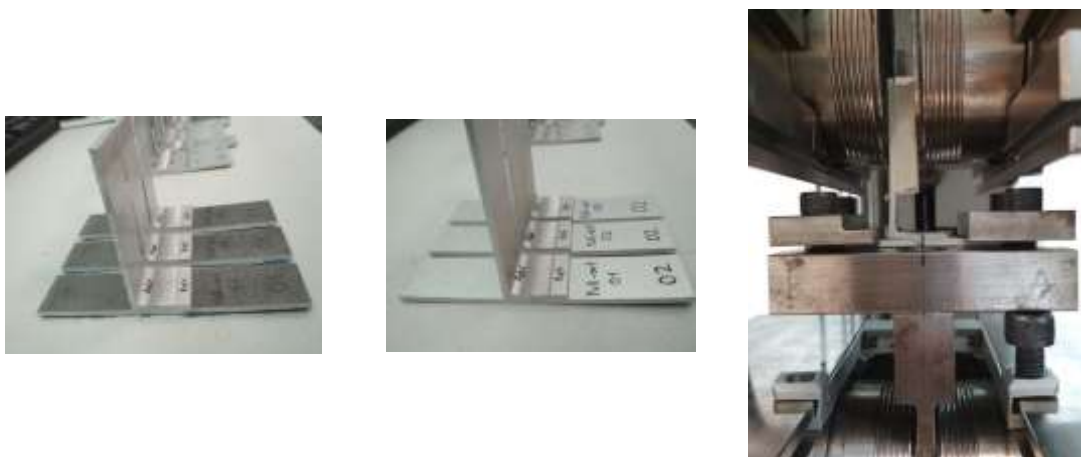


Figure 65: Examples of the specimens (C1-left; C2-middle) used for the static pull-out tests (right).

The presence of the remnants found in the SZ of the welds was expected to impact on the mechanical strength of the FSLW joints, especially in the pull-out strength of the

joints produced using TFSA treated base materials (C2 and C5). In order to evaluate this impact, static pull-out tests were performed with specimens cut from the FSLW joint-coupons C1-C6. Examples of some of these specimens and the pull-out test setup can be observed in Figure 65. A representation of the test progress and final failure that was observed for all tested specimens is illustrated in Figure 66.

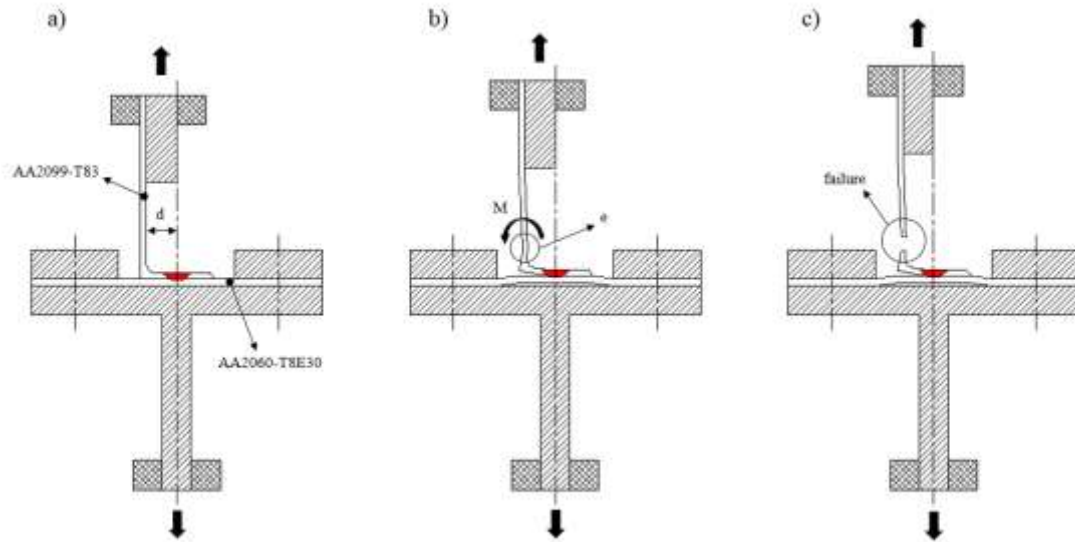


Figure 66: Representation of the progress in pull-out tests. (a) Initiation; (b) before failure; and (c) after failure.

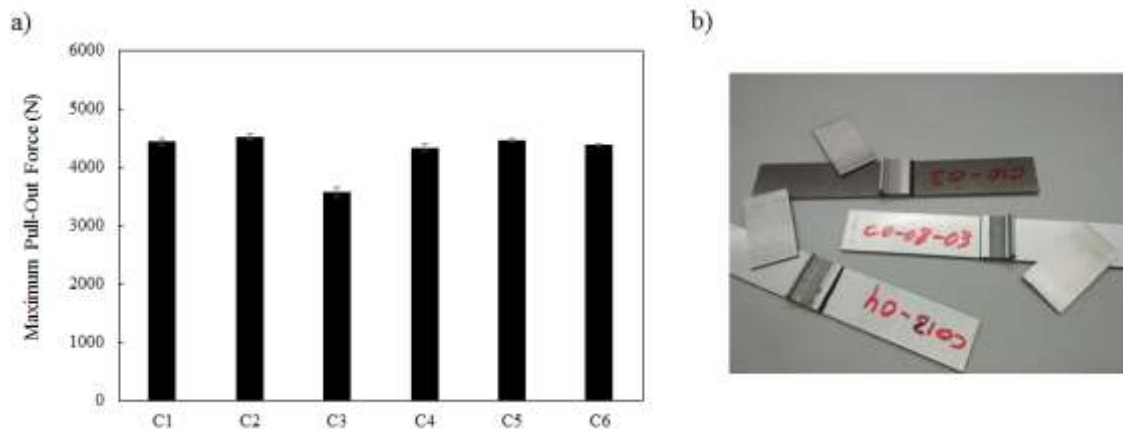


Figure 67: (a) Representation of maximum pull-out force values for FSLW joint-coupons C1-C6; and (b) examples of stringer failure in specimens obtained from FSW coupons C2, C4 and C6.

The maximum pull-out force obtained for all the FSLW joints C1-C6 and some examples showing the failure mode of the specimens can be observed in Figure 67. Very consistent pull-out strength values were observed for all FSLW joints C1-C6. For all specimens, the failure occurred consistently at the AA2099-T83 extrusion outside the weld region, showing a sufficiently high strength and load carrying capacity of all the FSLW joints irrespective of the surface condition of the base materials before the FSW process. Thus, although a lower strength was expected for the FSLW joints produced using surface treated base materials, especially C2 and C5 due to the presence of aluminium oxide remnants, they showed a similar strength as the rest of FSLW joints.

According to the obtained results, FSLW of TFSAA or Sol-Gel treated AA2060-T8E30 and AA2099-T83 alloys combined with sealant application seemed a feasible and promising technique for the manufacturing of lightweight aeronautic structures with good corrosion resistance. The selected surface treatments are of high interest in order to eliminate the use of Cr-based treatments and the application of sealants is also a standard practice in the manufacturing of corrosion resistant structures in the aeronautic industry. FSLW could be applied directly on the surface treated sheets and extrusions without the need for any pre-processing step to eliminate the coatings, showing no significant reductions in the static strength of the FSLW joints.

Although the performance of the FSLW joints under static stress was very good, their performance under fatigue loading was still unknown. Thus, the next work focused on the investigation of the fatigue resistance of the FSLW joints. This work, results and conclusions were published in a scientific article [79], which is included in this thesis in chapter 14.

Equivalent FSLW joint coupons C01-C06 were produced using the same alloys, same surface treatments and same sealant as indicated previously in Table 6. FSW machine and process conditions were also the same as the ones used to produce the high-quality FSLW joint-coupons. Specimens for static tensile and fatigue tests under hoop-stress loading conditions, which is the most representative to simulate the pressurization-depressurization cycles of a fuselage structure, were machined from all C01-C06 coupons. The dimensions and geometry of the specimens are shown in Figure 68, the setup for static tensile test in Figure 69 and the setup for fatigue tests in Figure 70. IR thermography was used to monitor the failure of the specimens in the fatigue tests.

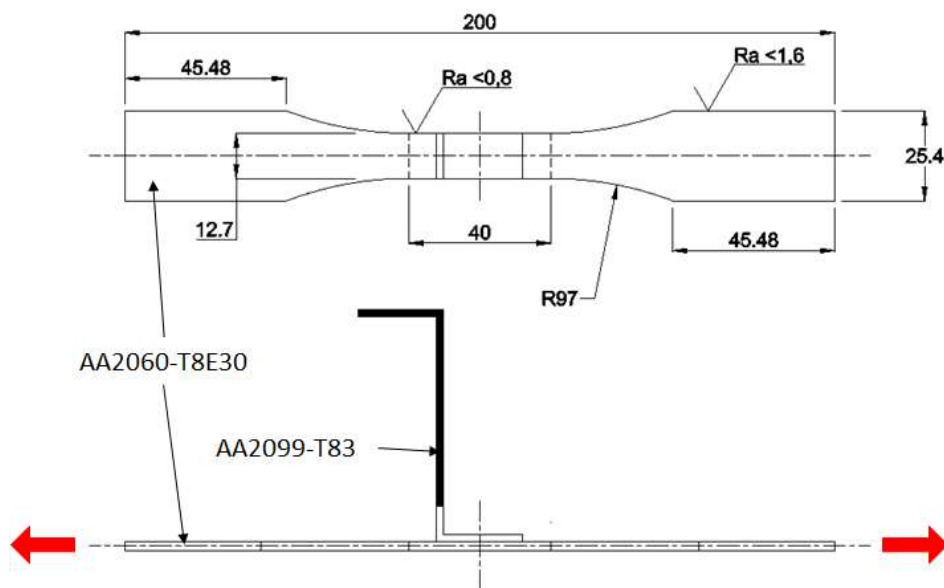


Figure 68: Sketch of the specimens machined from the FSLW joint-coupons C1-C6 for the static tensile and fatigue tests under hoop-stress loading conditions.



Figure 69: Specimens machined from coupons C3 (left); C6 (right); and the setup for the static tensile tests (middle).



Figure 70: Setup for the fatigue tests monitored by IR thermographic cameras.

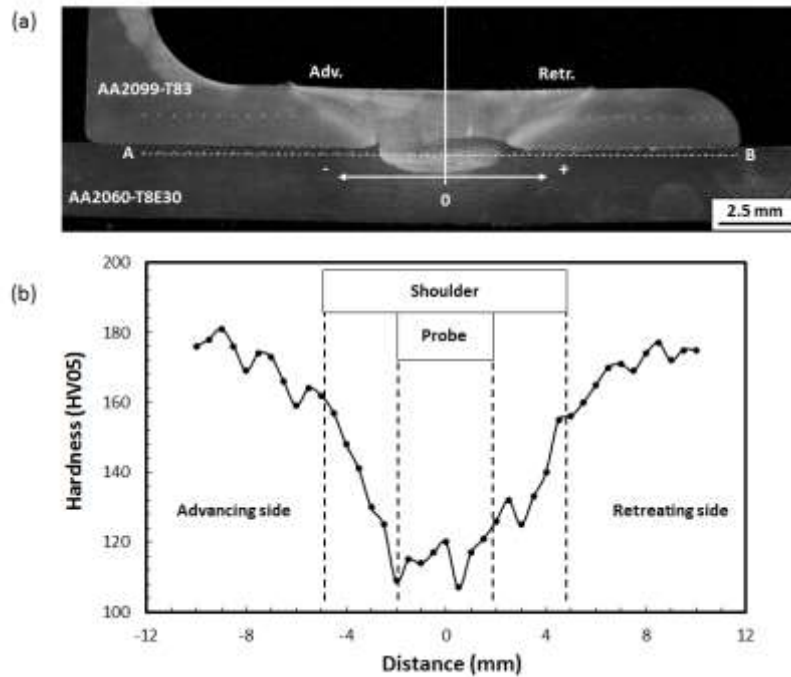


Figure 71: (a) Cross-section of a specimen cut from FSLW joint C01; (b) microhardness scan measurements in the A-B line shown in Figure 71a.

Microhardness measurements were performed in order to investigate the hardness distribution of the different microstructural zone within the welds (Figure 71). As it was expected working with precipitation hardening aluminium alloys such as AA2060-T8E30 and AA2099-T83, the region showing the minimum hardness was the HAZ, which typically suffers from an overaging effect due to the temperatures reached during the FSW process with the consequent reduction in hardness.

The results obtained in the static tensile tests showed a very similar performance between the FSLW joints C01-C06 as shown in Figure 72. Consistent and equivalent yield strength (YS) and ultimate tensile strength (UTS) values were observed for all tested specimens irrespective of the applied surface treatments and the use of sealant for the manufacturing of the FSLW joints. Consistent fractures with the initiation in the HAZ of the AA2060-T8E30 sheet, which was identified as the region with lowest hardness, were observed for all C01-C06 FSLW joints indicating that the surface treatments and the use of sealant at the stringer/skin interface did not produce significant effects in the performance of FSLW joints.

Similar to the static pull-out testing case reported above, a lower fatigue life was expected for the FSLW joints produced using surface treated base materials and the use of sealant. The presence of remnants in these welds was expected to reduce their fatigue life due to the stress concentration and crack initiation effect they could induce. However, the results obtained in the fatigue tests showed a slightly better fatigue behavior and extended life for FSLW joints produced using surface treated base materials and use of sealant. Basic S-N curves were plotted for the C01-C06 coupons after the execution of fatigue tests under hoop-stress loading conditions. These S-N curves and a comparison between them can be observed in Figure 73, Figure 74 and Figure 75.

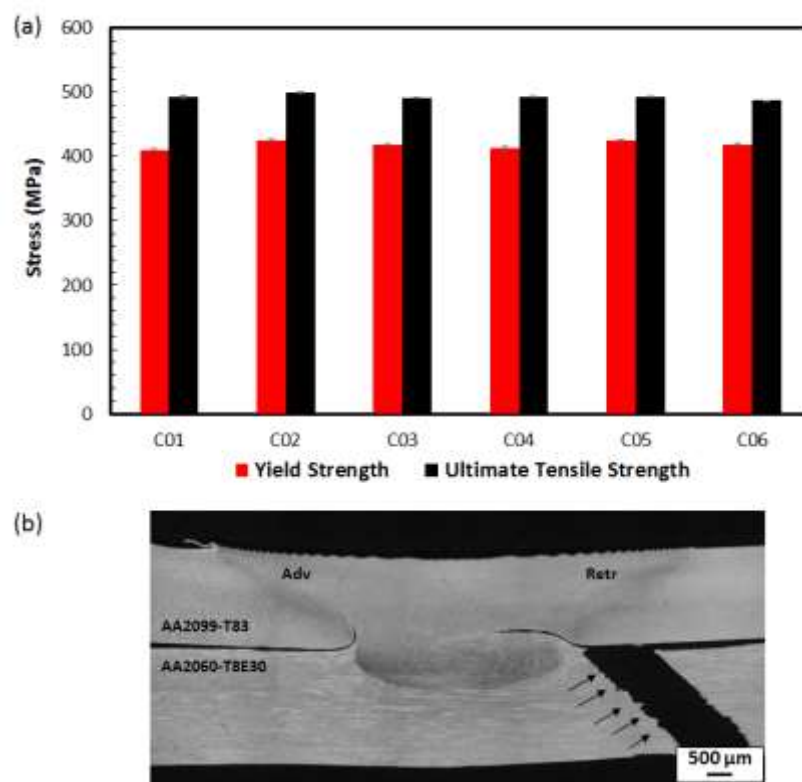


Figure 72: (a) Yield strength and ultimate tensile strength values obtained for the FSLW joints C01-C06 in static tensile tests; and (b) metallographic cross-section of a fractured C01 specimen showing the fracture initiation at the HAZ.

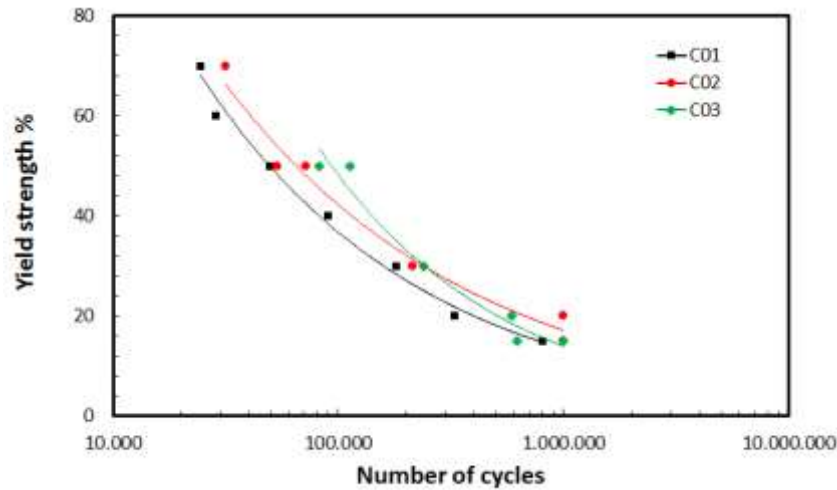


Figure 73: S-N curves of FSLW joints showing a comparison between FSW specimens produced using bare aluminium alloys (C01) and surface treated alloys without sealant (C02 and C03).

Figure 73 shows a comparison between the FSLW joints produced using bare aluminium alloys (C01) with those produced using surface treated aluminium alloys in order to show the effect of surface treatments in the fatigue life of the FSLW joints. In general, it was observed that the specimens with surface treatments presented a longer fatigue life until fracture. A similar trend was observed in the comparison of the fatigue life of FSLW joints produced with (C04) and without (C01) sealant applied at the stringer-skin interface, which is shown in Figure 74. Specimens produced with sealant showed a consistently longer fatigue life than the reference specimens without any sealant. Similarly, the effect of combining surface treated base materials and use of sealant for the manufacturing of FSLW joints showed an extension of the fatigue life compared to reference FSLW joints manufactured without any surface treatment nor sealant (Figure 75).

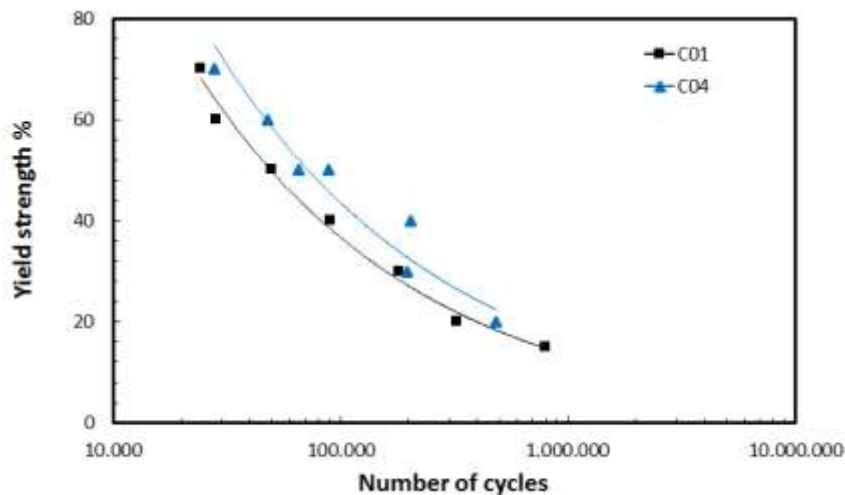


Figure 74: S-N curves of FSLW joints showing a comparison between FSW specimens produced using bare aluminium alloys without sealant (C01) and with sealant (C04).

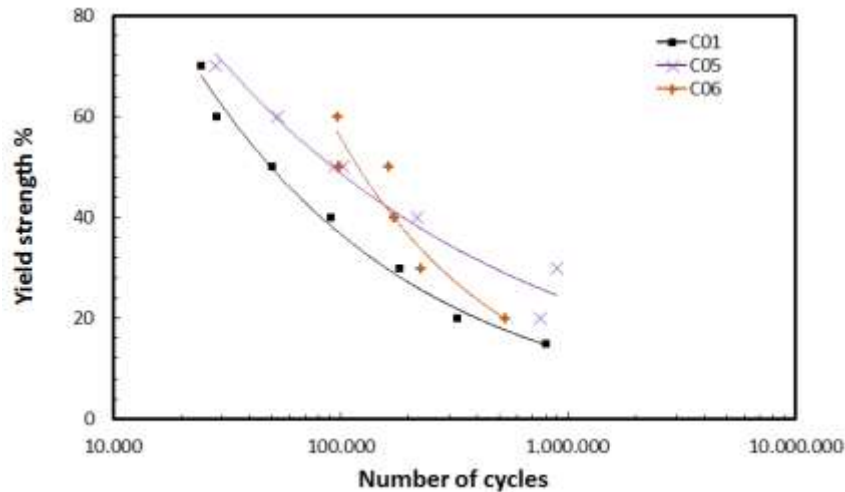


Figure 75: S-N curves of FSLW joints showing a comparison between FSW specimens produced using bare aluminium alloys without sealant (C01) and surface treated aluminium alloys with sealant (C05 and C06).

According to these results it was concluded that the use of surface treated aluminium alloys and the application of sealant improved the fatigue life of FSLW joints when they are applied either in an individual or a combined way. Considering this surprising result, the fracture mode of FSLW joints in fatigue tests was analyzed in order to investigate the mechanisms leading to the failure.

Two different fracture modes were observed depending on the stress level used for each particular test and specimen. The specimens tested in high-stress loading conditions showed failures at a relatively low number of cycles and presented a fracture initiation and propagation in the HAZ of the FSLW joints (indicated in red in Figure 76). On the other hand, the specimens tested in low-stress loading conditions, presented a fracture located out of the FSLW joint (indicated in blue in Figure 76), showing failures at higher number of cycles.

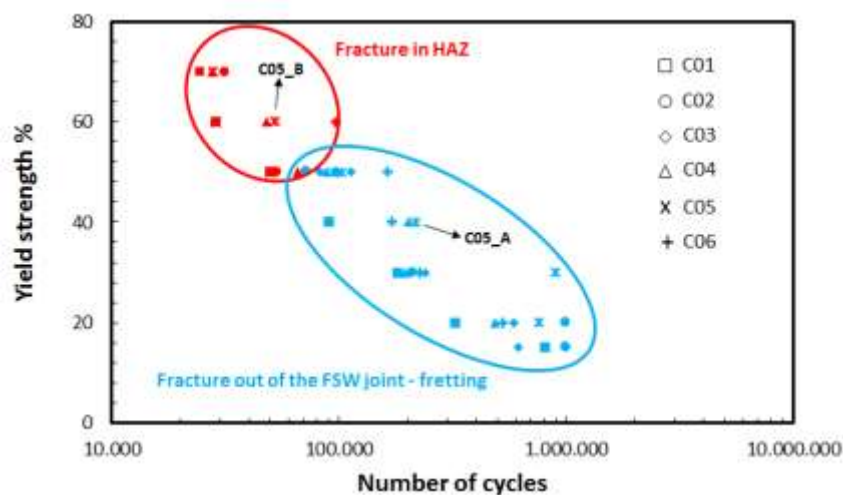


Figure 76: S-N data of FSLW joints showing different fracture modes in high and low stress loading conditions.

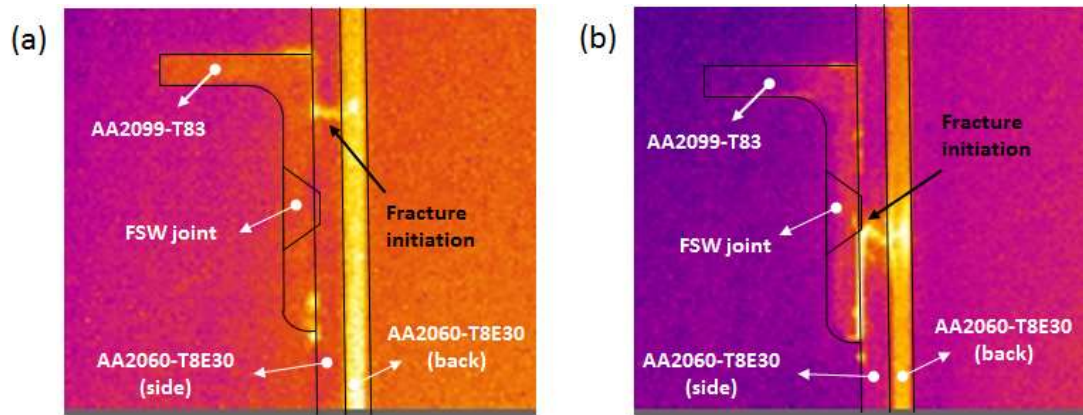


Figure 77: IR thermographic images showing the instant of the fracture in fatigue tests; (a) fracture out of the FSLW joint at high n° of cycles (specimen C05_A in Figure 76); and (b) fracture at the HAZ of the FSLW joint at low n° of cycles (specimen C05_B in Figure 76).

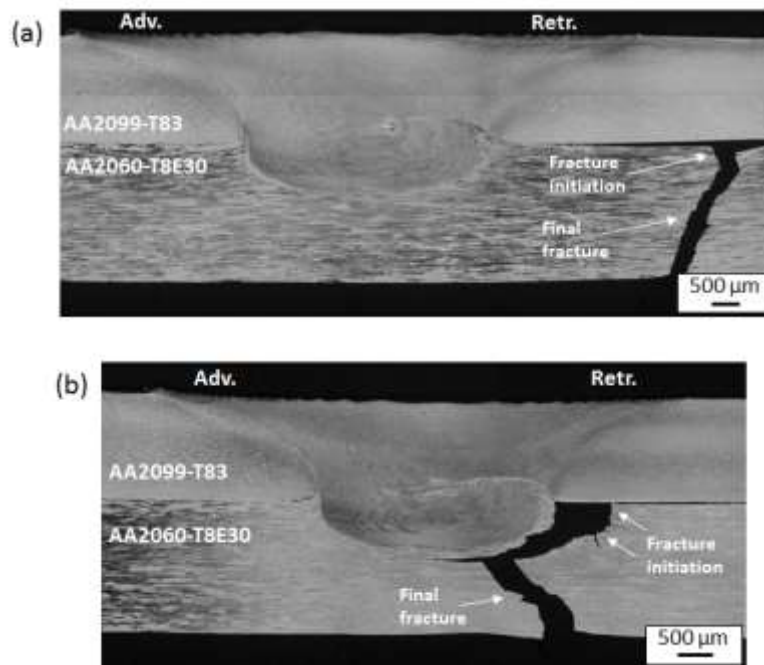


Figure 78: Cross-sections of FSLW joints showing different fracture modes; (a) fracture out of the FSLW joint (specimen from coupon C05 tested at a 30% of the YS); and (b) fracture at the HAZ of the FSLW joint (specimen from coupon C05 tested at a 70% of the YS).

These two different fracture modes were captured using IR thermographic cameras that were employed to monitor the specimens during the fatigue tests. Figure 77a shows the instant when the failure of a specimen tested in low-stress loading conditions occurs, showing the fracture out of the FSLW joint. A cross-section of this type of fracture can be observed in Figure 78a, where it can be clearly seen the initiation and final fracture occurred out of the FSLW joint. Fretting fatigue effects produced as a consequence of the frictional contact and sliding movement between the AA2099-T83 stringer and the AA2060-T8E30 skin during the fatigue tests were observed to be the origin of the fracture initiation. On the other hand, Figure 77b shows the instant when the fracture occurred in a specimen tested in high-stress loading conditions, with the fracture at the HAZ of the FSLW joint. The fracture initiation and crack growth through the HAZ before the final fracture can be clearly observed in the cross-section shown in Figure 78b.

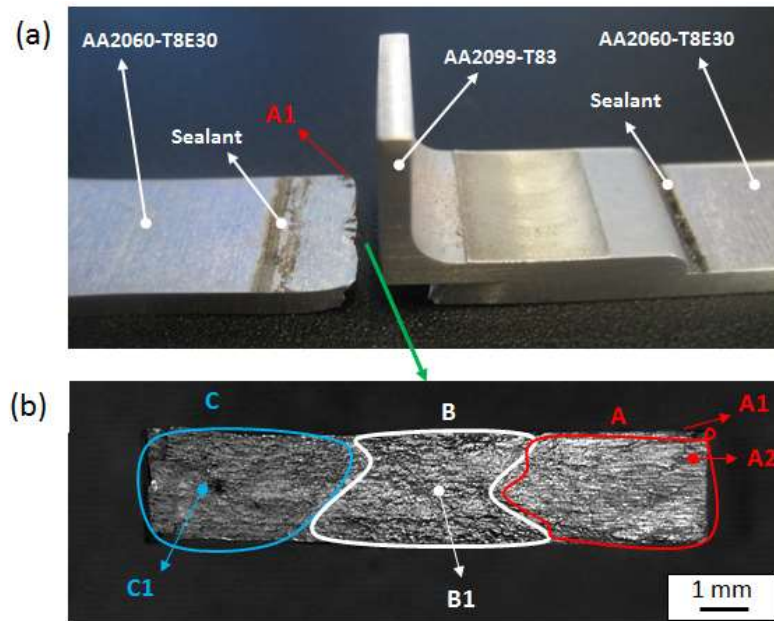


Figure 79: Fracture surface analysis of specimen C05_A (indicated in Figure 76) showing the fracture out of the FSLW joint; (a) general view of fractured specimen; and (b) perpendicular view of the fracture surface.

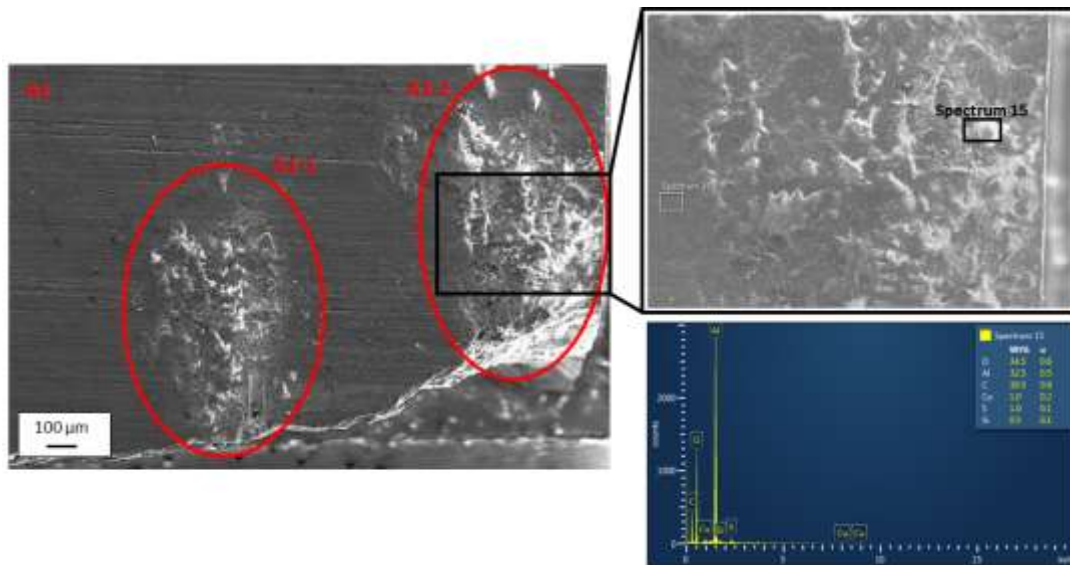


Figure 80: SEM image and EDS analysis of the zone A1 indicated in Figure 79.

The analysis of fracture surfaces was performed using SEM and EDS techniques. A summary of the results obtained in the analysis of the specimen C05_A, which was tested at relatively low-stress loading conditions and showed a fracture out of the FSLW joint, are presented in Figure 79, Figure 80 and Figure 81. Small regions of black phases were observed (indicated as A1 in Figure 79) at the stringer/skin matching interface suggesting they could act as fatigue crack nucleation points. A detailed analysis of these black phases (Figure 80) revealed they consisted of accumulated aluminium oxides as a result of localized fretting effects at random locations of stringer/skin interfaces. Once the fatigue crack was initiated, three main regions (A, B and C in Figure 79b) were observed for its propagation. Details of these three regions are shown in Figure 81.

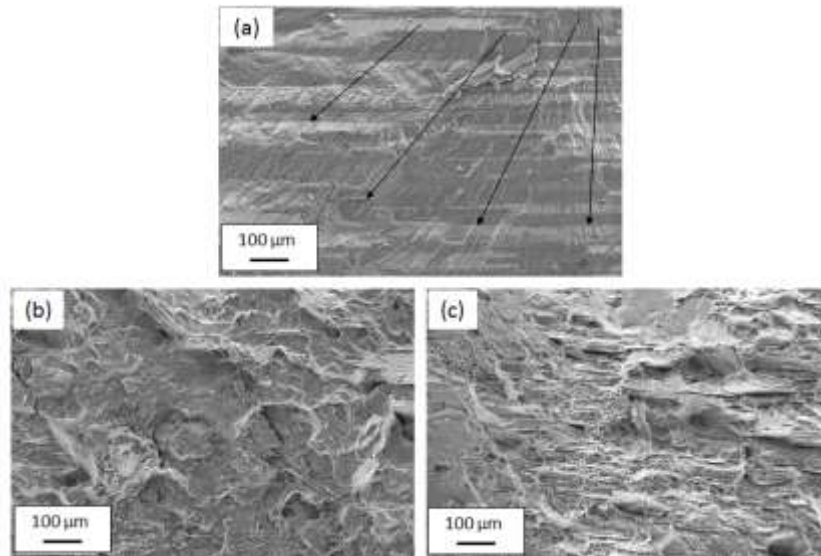


Figure 81: SEM observations of the fracture surface of specimen C05_A shown in Figure 79b; (a) point A2; (b) point B1; and (c) point C1.

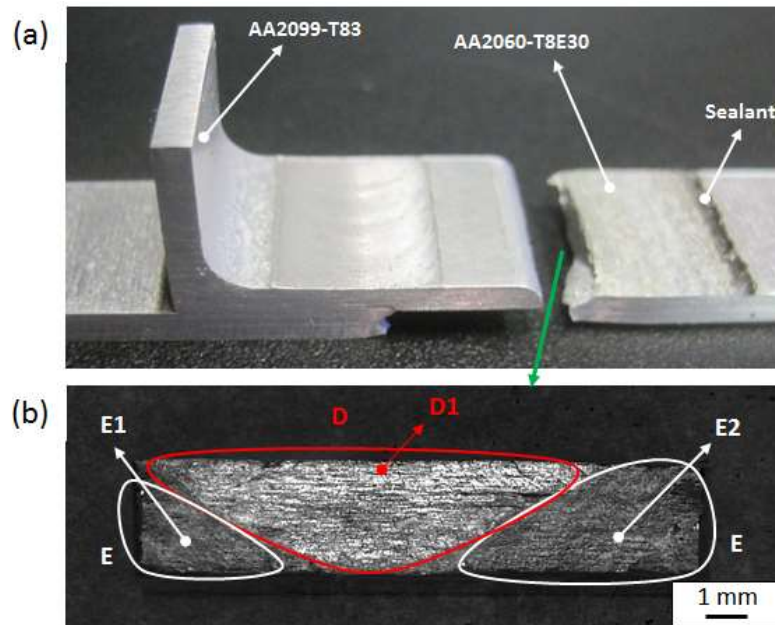


Figure 82: Fracture surface analysis of specimen C05_B (indicated in Figure 76) showing the fracture in the HAZ of the FSLW joint; (a) general view of fractured specimen; and (b) perpendicular view of the fracture surface.

The fracture surface analysis of specimen C05_B, which was tested under high-stress loading conditions and showed a fracture in the HAZ of the FSLW joints, was also carried out. The main results are presented in Figure 82 and Figure 83. No presence of black phases was observed in the specimens that presented this type of fracture mode. A detailed observation of the fracture surface revealed the presence of a fatigue crack nucleation and propagation region (indicated as D in Figure 82b) as well as the final fracture region (indicated as E in Figure 82b). Details of these regions are shown in Figure 83, where the fatigue crack initiation point (indicated as D1 in Figure 82b) presented a flat surface where propagation bands started at the top surface (Figure 83a). The propagation of the crack continued to grow until the final fracture occurred in region

E presenting a ductile fracture with multiple dimples as shown in Figure 83b and Figure 83c.

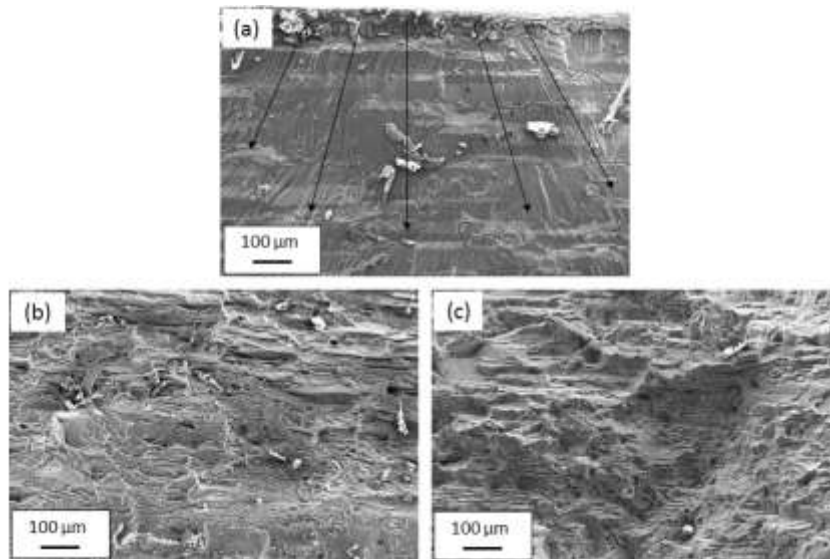


Figure 83: SEM observations of the fracture surface of specimen C05_B shown in Figure 82b; (a) point D1; (b) point E1; and (c) point E1.

According to all these results, it was concluded that fretting effects were the main limiting factor of the fatigue life of stringer/skin FSLW joints in the high-cycle fatigue regime. In addition to that, the possibility of manufacturing FSLW joints using surface treated aluminium components with a sealant in the stringer/skin interface was demonstrated and the resulting joints showed an improved durability in fatigue tests under hoop-stress loading conditions.

Generally, it was concluded that it is feasible to combine FSLW manufacturing using surface treated aluminium alloys and sealants at the stringer/skin interface in order to produce efficient, high-strength and corrosion resistant aeronautic structures.

Although the main contents and work to complete this thesis are covered in articles 8-11 which are included in chapters 11-14, some other complementary work was also performed or is in progress at the time when the thesis is presented. This work includes corrosion tests, FSW tests using AA2198-T8 and AA2196-T8511 alloys and the development of a representative fuselage panel demonstrator. Additional information of this experimental work, main findings and conclusions are presented in the following sections.

CORROSION TESTS

The effectiveness of the corrosion protection techniques considered for the FSLW joints was investigated by a basic test plan. FSLW joint-coupons were manufactured using AA2099-T83 and AA2060-T8E30 alloys with the welding conditions that were previously optimized and different surface treatments and sealant were applied to them. Some of these coupons were subjected to neutral salt spray (NSS) corrosion tests according to the ASTM-B117 standard. These tests as well as the application of the relevant surface treatments (TFSA and Sol-Gel) and a new Cr-free primer and top-coat developed by AKZONOBEL were carried out at HAI, so the FSLW joint preparation, logistic and tests were coordinated with them. The FSLW joint-coupon description and test plan for this study are summarized in Table 7.

Table 7: FSLW joint-coupon description and test plan.

Coupon 1	2060-2099 as welded	No corrosion test
Coupon 2	2060-2099 + TFSA	No corrosion test
Coupon 3	2060-2099 + TFSA + Primer	With corrosion test
Coupon 4	2060-2099 + TFSA + Primer + TopCoat	With corrosion test
Coupon 5	2060-2099 + SolGel	No corrosion test
Coupon 6	2060-2099 + SolGel + Primer	With corrosion test
Coupon 7	2060-2099 + SolGel + Primer + TopCoat	With corrosion test
Coupon 8	2060-2099 with sealant MC780-C as welded	No corrosion test
Coupon 9	2060-2099 with sealant MC780-C + SolGel	No corrosion test
Coupon 10	2060-2099 with sealant MC780-C + SolGel + Primer	With corrosion test
Coupon 11	2060-2099 with sealant MC780-C + SolGelPrimer + TopCoat	With corrosion test

Static pull-out tests were performed with specimens cut from all the FSLW joint-coupons which underwent corrosion test in order to evaluate any eventual loss of properties due to corrosion effects. The FSLW joints that were not exposed to the NSS tests were tested in the as manufactured condition, while the rest of the coupons were tested after the completion of the corrosion tests and NSS exposure. The disposition of the FSLW joint-

coupons that were subjected to the NSS exposure can be observed in Figure 84, as well as an example of a FSLW joint-coupon after completion of the corrosion test and examples of specimens prepared for the subsequent static pull-out tests.



Figure 84: Disposition of the FSLW joint-coupons in the NSS chamber during the ASTM-B117 NSS corrosion test (left); FSLW joint-coupon 4 after NSS exposure (middle); and specimens cut from FSLW joint-coupons ready for static pull-out tests (right).

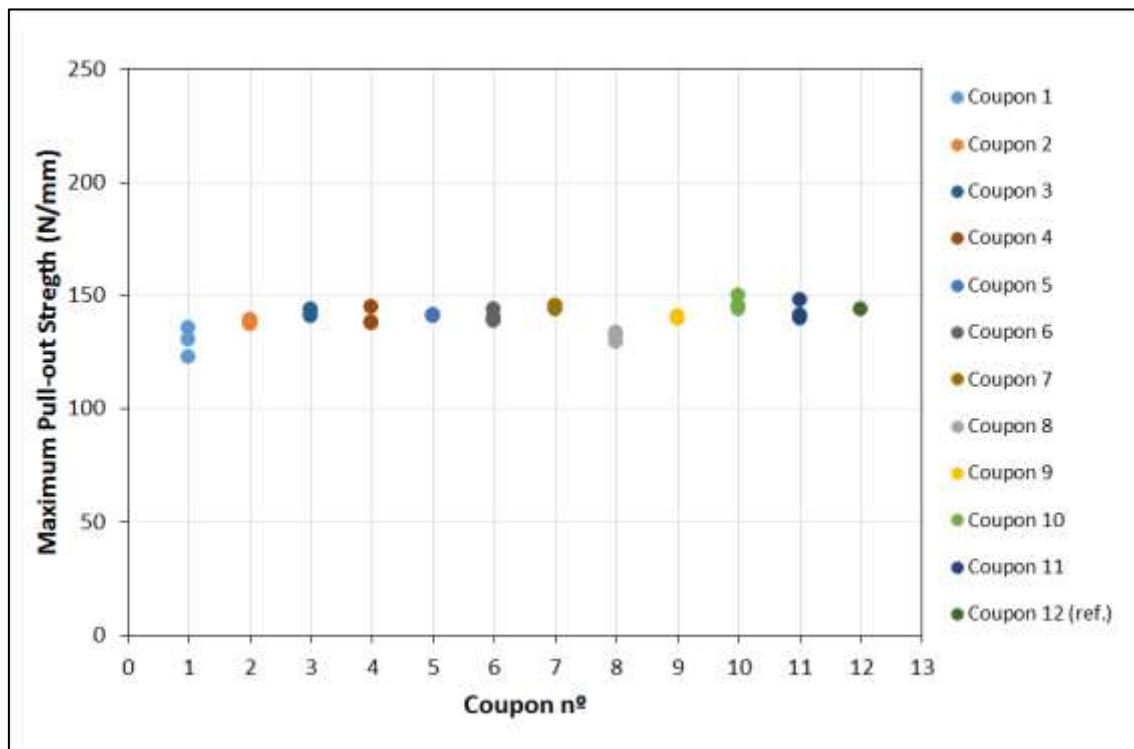


Figure 85: Results of static pull-out tests of FSLW joints produced and corrosion tested according to the conditions shown in Table 7.

The results obtained in the pull-out tests are shown in Figure 85. No significant differences were observed in the joint strength between the FSLW joints that were not exposed to NSS tests and those that were exposed. Therefore, it was concluded that the corrosion protection techniques investigated in this test plan (TFSA, Sol-Gel, primer, top-coat and sealant) were effective in the protection of the FSLW joints against corrosion.

FSLW TEST RESULTS WITH AA2198-T8/AA2196-T8511 ALLOYS

In addition to the investigation work carried out with the Third-Generation Al-Li alloys AA2099-T83 and AA2060-T8511, which was the core that led to the completion of this thesis, similar work was also performed using Al-Li alloys AA2198-T8 sheet as skin and AA2196-T8511 extrusion as stringers. Thus, FSLW process development was performed including tool, clamping system and welding parameter optimization assisted by an extensive joint characterization by means of metallographic examination, mechanical testing as well as corrosion testing. An example of a FSLW joint produced by this alloy combination can be observed in Figure 86, where a 2.5 mm thick AA2196-T8511 extrusion was welded by FSW on top of a 2.5 mm thick AA2198-T8 sheet.



Figure 86: FSLW joint-coupon manufactured using a AA2198-T8 sheet/skin and a AA2196-T8511 extrusion/stringer.

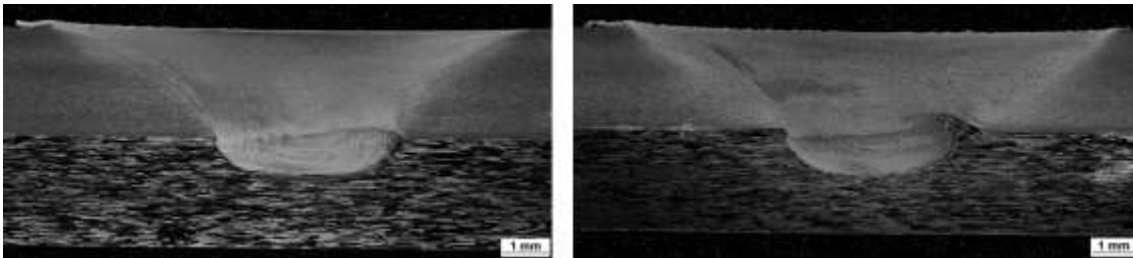


Figure 87: Cross-sections of FSLW joints produced with AA2198-T8 sheet and AA2196-T8511 extrusion at 800 rpm and 250 mm/min (left) and 1200 rpm and 150 mm/min (right).

Macrographic cross-sections of FSLW joints are shown in Figure 87. The tool design with three flat + mixed thread that produced excellent results with the AA2060-T8E30/2099-T83 alloy combination was tested for the AA2198-T8/AA2196-T8511 combination too. The obtained results were equivalent and FSLW joints with excellent properties were produced using this tool design, avoiding the generation of hook defects while achieving a good oxide break, dispersion and plasticized material mixing during the FSW process.

Fatigue tests under hoop-stress loading were performed using these FSLW joints with the particular characteristic that the FSLW joint-coupons were prepared using pocketing techniques. The pocketing is a technique that is typically used in the manufacturing of fuselage skin sections and consists of machining the free areas that are located between reinforcements (stringers, frames...) that are joined to the skin. Thus, a reduction of thickness and important weight savings can be achieved. As a result of the pocketing, the areas of the skin where the reinforcements are joined have typically a larger thickness than the surrounding free areas. With the purpose of investigating this thickness variation effect on the fatigue performance of the FSLW joints, the AA2198-T8 skin sections were machined to simulate the pocketing effect and FSLW joints were

manufactured. Examples of these FSLW joints are shown in Figure 88-left. In Figure 88-right, examples of specimens machined from the FSLW joint-coupons can be observed.

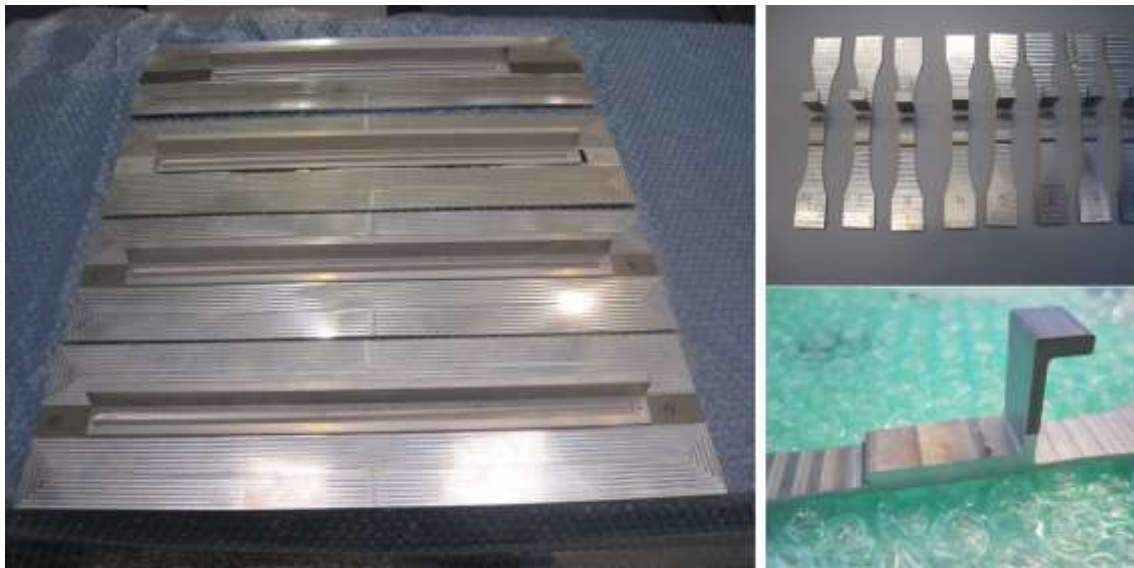


Figure 88: FSLW joint-coupons manufactured using pocketed AA2198-T8 sheet/skins (left), specimens for static tensile and fatigue testing machined from the coupons (top-right) and detail of a machined specimen showing the pocketed region (bottom-right).

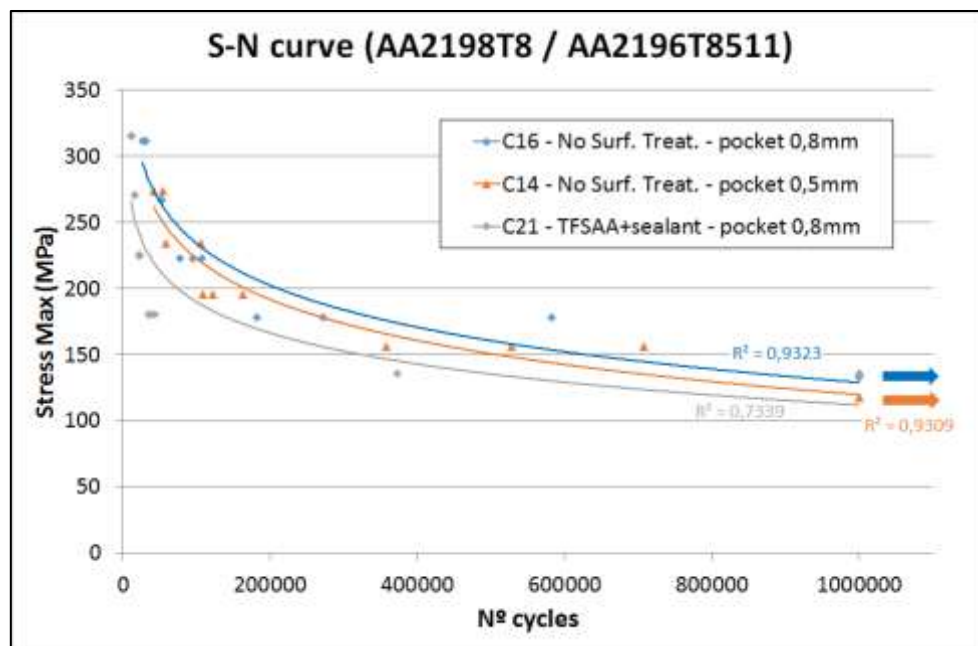


Figure 89: S-N curves of FSLW joints produced using pocketed AA2198-T8 sheet/skins and AA2196-T8511 extrusion/stringers.

The results of the fatigue tests showed that fretting fatigue effects were avoided in pocketed FSLW joints, incrementing the fatigue stress limit and life significantly (Figure 89). Having a smaller thickness outside the FSLW joint area promotes a preferential deformation in these sections with smaller thickness. The consequence of this effect is that the sliding movement and frictional contact between the stringer and skin was reduced, so that fretting effects were significantly minimized. Thus, fractures in the pocketed region were observed in most of these specimens suggesting the FSLW joint

area was stronger than the pocketed area even under hoop-stress fatigue loading conditions. In this case, the effect of the surface treatments and sealant that allows to reduce the fretting effects and extend the fatigue life of the non-pocketed FSLW joints is not significant as it can be observed in Figure 89.

After these interesting conclusions obtained for the pocketed specimens, a similar study was also carried out with pocketed FSLW joints using the AA2060-T8E30/AA2099-T83 alloy combination. As it can be seen in the comparative results shown in Figure 90, it was confirmed the possibility to extend the fatigue life of FSLW joints by reducing the fretting effects when pocketing techniques were employed.

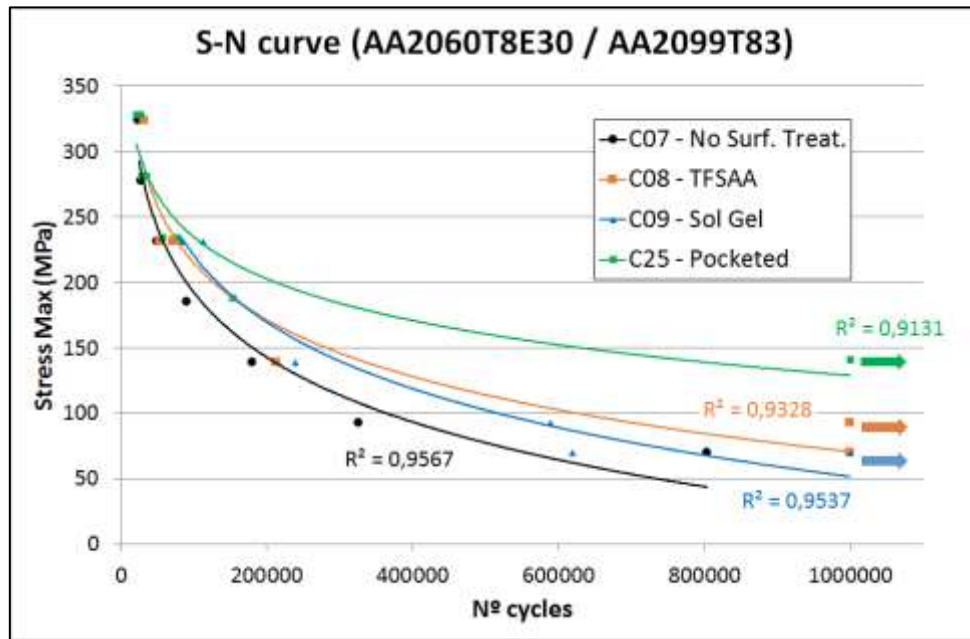


Figure 90: S-N curves of FSLW joints showing a comparison between pocketed and non-pocketed FSW specimens produced using AA2060-T8E30 and AA2099-T83 alloys.

Although the main work to complete this thesis was focused on FSLW joints using Al-Li alloys with thicknesses between 2 and 2.5 mm, new challenges arose when the possibility to use smaller thicknesses for the reinforcements (stringers, frames) was considered, due to weight saving purposes during the design phase of a representative fuselage panel demonstrator. Thus, the possibility to produce FSLW joints using down to 1 mm thick AA2198-T8 sheets was investigated.

FSW tests were performed in the robotic FSW system at LORTEK, which was the facility selected for the manufacturing of the fuselage panel demonstrators to be developed in the project ecoTECH. The robotic FSW system and the clamping arrangement for the tests can be seen in Figure 91. FSLW joints were produced using thicknesses down to 1 mm for the top AA2198-T8 sheet, obtaining good results in terms of process stability and repeatability. The quality of the resulting FSLW joints was investigated by metallographic examination and static tensile tests under hoop-stress loading conditions. FSLW joints of excellent quality could be produced as it can be observed in the cross-sections of Figure 92 and Figure 93. The new tool design with three flat + mixed thread was capable of avoiding defects that can be typically found in FSLW joints such as hooks and cold lap defects.



Figure 91: Robotic FSW system used for FSLW tests using AA2198-T8 sheets of small thicknesses.

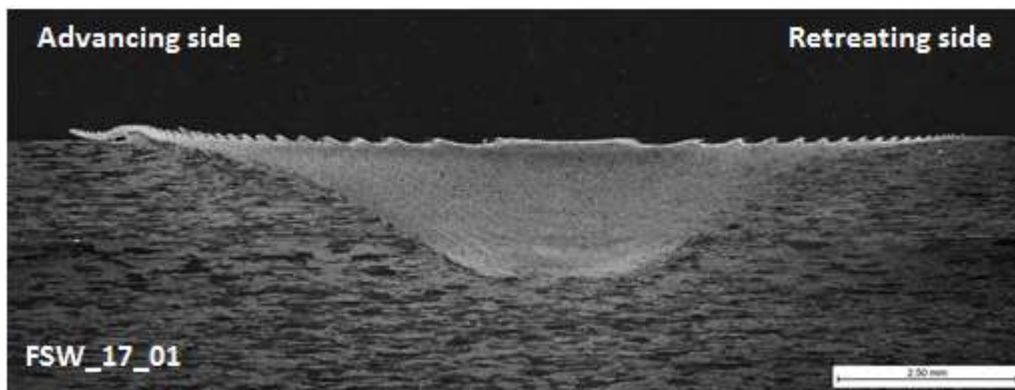


Figure 92: Cross-section of a FSLW joint produced using a 1.3 mm thick AA2198-T8 sheet on top of a 2.3 mm thick AA2198-T8 sheet.

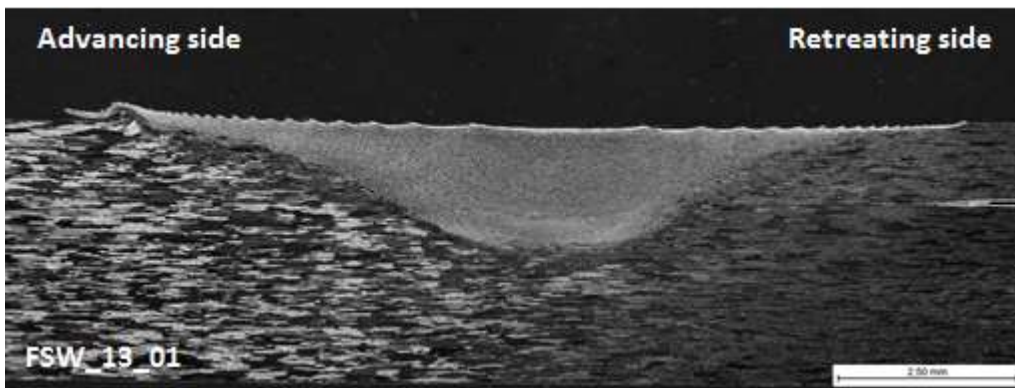


Figure 93: Cross-section of a FSLW joint produced using a 1 mm thick AA2198-T8 sheet on top of a 2.3 mm thick AA2198-T8 sheet.

Static tensile tests under hoop-stress loading conditions were carried out with specimens cut from the FSLW joints manufactured using AA2198-T8 sheets with thicknesses down to 1 mm. Figure 94 shows a summary of the results obtained in these tests, comparing the strength of FSLW joints produced using sheets of thicknesses of 1 mm, 1.3 mm and 2.5 mm. Very consistent and similar strength values were obtained for all conditions.

Therefore, it was concluded that the manufacturing of FSLW joints using AA2198-T8 sheets of thicknesses down to 1 mm was feasible.

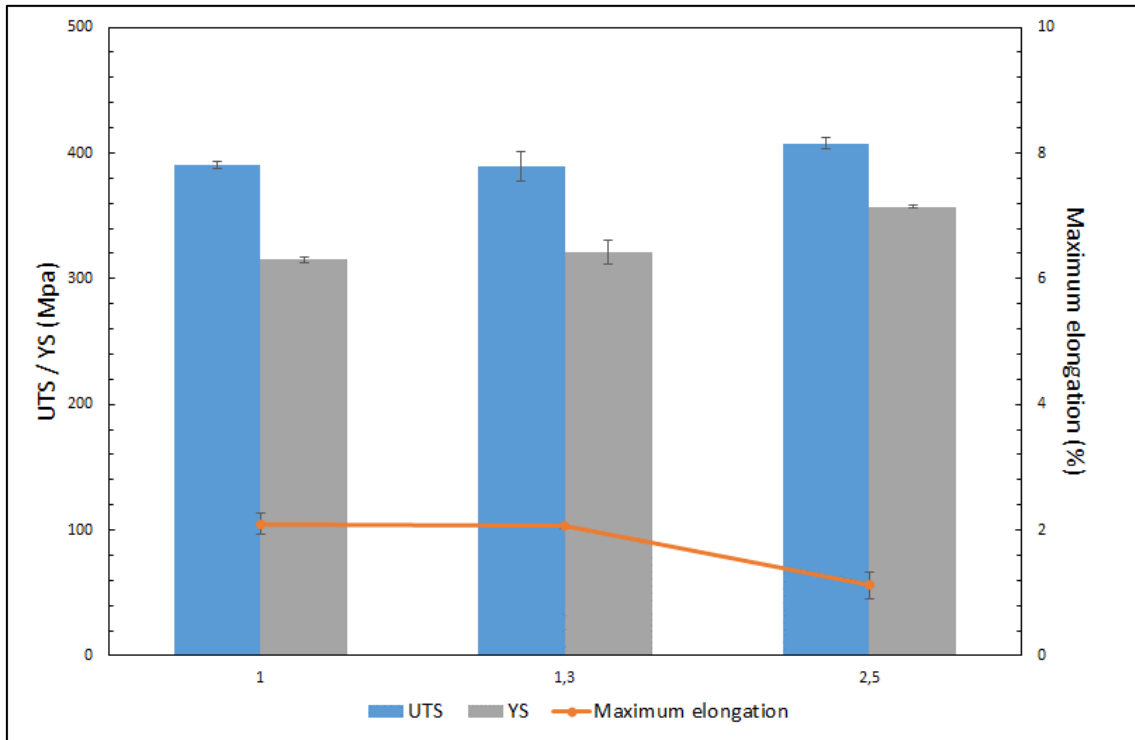


Figure 94: Static tensile test results of FSLW joints produced using AA2198-T8 sheets of different thicknesses.

FUSELAGE PANEL DEMONSTRATOR

With the green light for the use of 1 mm thick sheets, a fuselage panel demonstrator to be developed in the project ecoTECH was designed in a collaborative work between IAI, HAI and LORTEK. The general design of this demonstrator as well as details of the reinforcements (stringers, frames) are shown in Figure 95. The following materials were selected:

- Skin: AA2198-T8 formed sheet; thickness 2.3 mm.
- Stringers: AA2198-T8 formed sheet; thickness 1 mm.
- Frames: AA2198-T8 formed sheet; thickness 1.2 mm.

FSLW process was selected as the joining technology for the manufacturing of this demonstrator. Thus, it was required to develop all the necessary FSW technology adaptations for the FSLW manufacturing of the stringer-skin (linear longitudinal reinforcements) and frame-skin (curved transversal reinforcements) such as tools, clamping systems, welding parameters, etc...

After freezing the final design of the demonstrator, the design and manufacturing of the clamping systems for stringer-skin and frame-skin FSLW joints were carried out. In parallel, new tools and the appropriate tool-holder were designed and manufactured too. The initial welding parameters for both stringer-skin and frame-skin FSLW joints were estimated as a starting point for the manufacturing tests. The tool design and welding

parameters were defined based on the results obtained in the work carried out in this thesis.

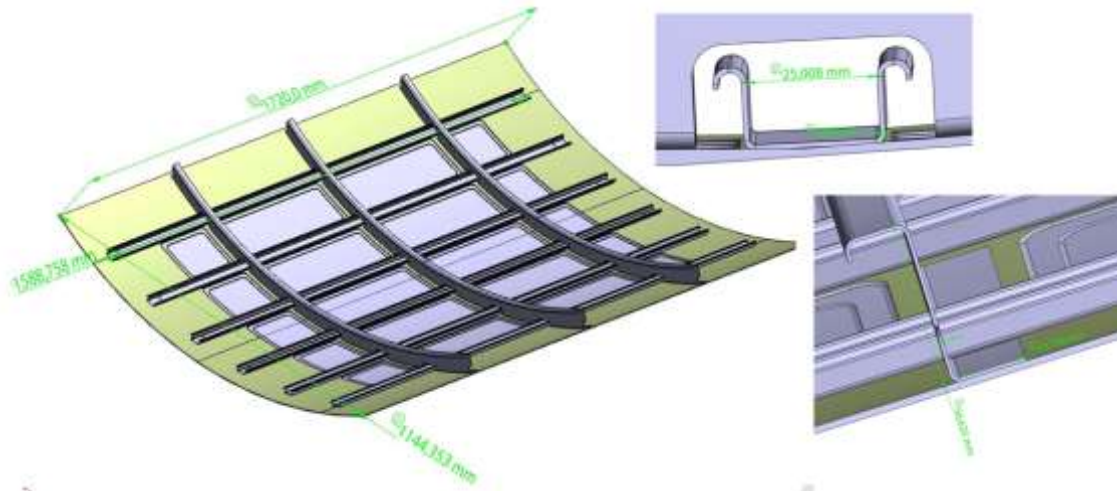


Figure 95: General design of fuselage panel demonstrator to be manufactured by FSLW and details of the design of stringers and frames.

Once all FSW technology adaptations were completed and the materials prepared (skin, stringers and frames) the FSLW manufacturing tests started. After some necessary welding parameter adjustments due to the specific curvature and properties of curved components, the manufacturing tests in the first fuselage panel demonstrator were carried out and the FSLW manufacturing of the initial fuselage panel demonstrator was successfully completed at the time when this thesis was submitted. This initial demonstrator is presented in Figure 96.



Figure 96: Initial fuselage panel demonstrator manufactured in the robotic FSW system at LORTEK.

This type of innovative aeronautic structure can present important benefits such as weight saving, reduction of manufacturing time and cost, reduction of energy

consumption and gas emissions during the operational life of the aircraft as well as environmental benefits in the end of life (EoL) processes for recycling. The next activities in the project ecoTECH will try to evaluate and quantify the mentioned benefits and perform a comparison with conventional technologies.

15.2.- CONCLUSIONS

The aeronautic industry is continuously seeking for new materials and technologies in order to overcome the challenges identified for future green aircraft. Among many other challenges, innovative lightweight structures for airframe represent an attractive solution to reduce the overall weight of the aircraft, which would result in improved energy efficiency and reduction of harmful gas emissions.

The main objective of the work carried out in this thesis was to investigate the potential of the FSW technology to be implemented in the manufacturing of integral reinforced panels for aircraft structures made of Third-Generation Al-Li alloys. In order to accomplish this main objective, some specific objectives were established and at the end of the thesis it can be stated that all of them have been met. These objectives were:

1. Develop FSW tools with improved design to avoid or minimize characteristic imperfections that can be found in lap joints.
A new FSW tool design for lap joint configurations has been developed having three flats and a mixed thread. This new design showed the capability to minimize characteristic imperfections such as hooks and cold lap defects.
2. Perform FSW tests and create stringer-skin joints with the selected AA2060-T8E30, AA2099-T83, AA2198-T8 and AA2196-T851 Al-Li alloys.
FSLW joints have been produced using all the above-mentioned alloys using different welding parameters. We concluded that FSW technology can be used to produce stringer-skin joints and we established appropriate welding parameter-sets and operational windows.
3. Perform FSW tests and create stringer-skin joints with the above-mentioned alloys including sealant at the stringer-skin interface; and with surface treated aluminium alloys.
FSLW joints have been produced using surface treated aluminium alloys. Cr-free innovative surface treatments such as TFSAA and Sol-Gel were applied to the aluminium components before FSW. FSLW joints were also produced applying a sealant in the stringer-skin interface before FSW. We concluded that it is feasible to produce FSW joints consistently using surface treated components and sealant, which are technics typically employed by the aeronautic industry for the protection against corrosion.
4. Perform an extensive FSW joint characterisation including microstructural examination, static and fatigue strength analysis.
The properties of FSLW joints produced under different base material preparation and welding conditions have been investigated. Microstructural examination was carried out by optical microscopy and SEM observation complemented by EDS. The static strength was evaluated by pull-out tests as well as tensile tests under hoop-stress loading conditions. The fatigue strength was also evaluated under hoop-stress loading conditions.

5. Investigate the effects of FSW tool design, welding parameters, sealants and surface treatments on joint formation mechanisms, joint imperfections and the resulting joint properties.

FSLW joint formation mechanisms have been analysed for different tool designs, base material preparation and welding conditions. The FSLW joint imperfections and properties were investigated by microscopy, static and fatigue tests.

6. Conclude on the potential of FSW technology for the manufacturing of advanced aircraft structures and define required manufacturing conditions.

The FSW technology has shown a great potential for the manufacturing of integral reinforced fuselage panels using Third-Generation Al-Li alloys. A fuselage panel demonstrator was manufactured in the robotic FSW system at LORTEK using the welding parameters optimised in previous tests, achieving TRL 5.

This thesis is mainly focused on the FSW technology development towards the optimization of the joint quality in overlap welds using AA2099-T83 extrusions/stringers and AA2060-T8E30 sheet/skin. The main work was presented in three articles achieving the following main conclusions:

- The three flat + mixed thread tool showed the capability to keep the hook height values low while offering sufficient material mixing capability at the faying surface of the materials for an effective dispersion of surface oxides.
- The three flat + mixed thread tool presents clear advantages for FSW lap joint manufacturing in comparison with the conventional threaded tool design. It was possible to produce FSLW joints of superior quality and higher load carrying capacity, showing a larger weldability window.
- FSW of surface treated Al-Li components using sealant was feasible. The FSW process did not show any instability and the pull-out strength values of the FSLW joints were comparable to the FSLW joints produced without surface treatments nor sealant.
- Consistent failures at the stringer (AA2099-T83 extrusion) out of the weld region and comparable failure loads were observed in the pull-out static tests for all the tested FSLW joints, irrespectively of the surface treatment condition or the application of sealant.
- All investigated FSLW joints showed an equivalent performance in the static tensile tests carried out under hoop-stress loading conditions. The surface treatments (TFSA and Sol-Gel) and sealant applied before the manufacturing by FSW did not induce significant effects on the properties of the FSLW joints.
- Fretting fatigue was identified as the main limiting factor of the fatigue life for FSLW joints tested at low stress levels under hoop-stress loading conditions. The local damage caused by the frictional contact and sliding movement at the stringer-skin interface was found to create aluminium oxide accumulations that acted as the fatigue crack initiation points.
- Fatigue life of FSLW joints was incremented by using surface treated materials and sealant. The lubricant effect and reduced friction produced by the surface treatments and sealant at the stringer-skin interface resulted in reduced fretting effects and extended durability of the FSLW joints.

Generally, it has been concluded that it is feasible to combine FSW manufacturing using surface treated Al-Li alloys and sealants in order to produce efficient, high-strength and corrosion resistant aeronautic structures. A fuselage panel demonstrator has been manufactured in the robotic FSW system at LORTEK. This type of structures can present important benefits such as weight saving, reduction of manufacturing time and costs, reduction of energy consumption and environmental benefits in the EoL processes for recycling.

15.3.- FUTURE LINES

In this thesis, we have shown the potential of the FSW technology for the manufacturing of advanced fuselage structures using Third-Generation Al-Li alloys. In order to increase the TRL and MRL levels of this type of innovative structures, it is necessary to continue the research activities and some future lines that should be explored are suggested as follows:

- Perform pull-out tests under fatigue loading conditions in order to understand better the effects of surface treatments and sealant in the properties of FSLW joints.
- Manufacturing of more fuselage panel demonstrators to be used in static and dynamic tests at panel level. 3 more fuselage panel demonstrators will be manufactured in the near future.
- Perform a study of robustness and reliability of the FSW process applied to the manufacturing of fuselage panel demonstrators.
- Carry out a cost analysis and comparison with conventional technologies used in the manufacturing of fuselage panels.
- Perform static and dynamic loading tests to the fuselage panel demonstrators in order to validate. A CfP project called DEMONSTRATE was launched under the project ecoTECH with the objective of testing the innovative fuselage panel demonstrators. The tests will be performed in the first semester of 2023 and it is expected to achieve TRL 6 if the results are satisfactory.
- Develop EoL procedures for the innovative fuselage panels. A CfP project called ReINTEGRA was launched under the project ecoTECH with the objective of investigating appropriate EoL procedures for the fuselage panels manufactured using Third-Generation Al-Li alloys and welding technologies. An environmental impact analysis and comparison with conventional technologies will be done before the end of the project in 2023.
- Development of suitable NDT technologies to evaluate the quality of FSLW joints produced in the fuselage panel demonstrators.
- Develop new programs for continuous FSW manufacturing in the robotic FSW system in order to reduce the manufacturing time of fuselage panels.

Many of the mentioned future lines will be conducted within the activities of the project ecoTECH during 2023. In case the results obtained in the tests at panel level are satisfactory, further steps towards the increment of TRL and MRL levels should be taken, for example, demonstrations in flight tests. The objective will be to advance towards the certification and qualification of the innovative fuselage panels and an implementation of the FSW technology for their manufacturing.

BIBLIOGRAPHY

- [1] "Advisory Council for the Aviation Research and Innovation in Europe (ACARE)," [Online]. Available: <http://www.acare4europe.org/>. [Accessed 20 04 2018].
- [2] "Clean Sky Joint Undertaking," [Online]. Available: www.cleansky.eu. [Accessed 20 04 2018].
- [3] "Single European Sky ATM Research Joint Undertaking," [Online]. Available: <https://www.sesarju.eu/>. [Accessed 10 05 2018].
- [4] J. Munroe, K. Wilkins and M. Gruber, "Integral Airframe Structures (IAS) - Validated Feasibility Study of Integrally Stiffened Metallic Fuselage Panels for Reducing Manufacturing Costs," NASA/CR-2000-209337, Prepared by Boeing for Langley Research Center under contracts NAS1-20014 and NAS1-20267, USA, 2000.
- [5] S. M. Tavares, *Design and advanced manufacturing of aircraft structures using Friction Stir Welding*, Universidade do Porto (Portugal): PhD Thesis, 2011.
- [6] M. Mrazova, "Advanced composite materials of the future in aerospace industry," *INCAS BULLETIN*, vol. 5, no. 3, pp. 139-150, 2013.
- [7] F. Eberl, S. Gardiner, G. Campanile, G. Surdon, M. Venmans and P. Prangnell, "Leading the way with advanced aluminium solutions for aerospace structures," in *Aeronautics Days - AGEFORM*, Vienna (Austria), 2006.
- [8] I. Bordesoules, J. Ehrstrom, T. Warner, P. Lequeu and F. Eberl, "Trends in Developments of Aluminium Solutions for Aerospace Applications," in *European workshop on Short Distance Welding Concepts for Airframes - WELAIR*, Geesthacht, Hamburg (Germany), 2007.
- [9] "Total Materia - Aluminium Alloy Development for the Airbus A380," September 2009. [Online]. Available: <https://www.totalmateria.com/page.aspx?ID=CheckArticle&LN=ES&site=ktn&NM=227>. [Accessed 22 05 2018].
- [10] N. Eswara Prasad, A. A. Gokhale and R. Wanhill, *Aluminium-Lithium Alloys: Processing, Properties and Applications*, Oxford (UK): Elsevier - BH, 2014.
- [11] M. Knüwer, J. Schumacher, H. Ribes, F. Eberl and B. Bes, "2198 - Advanced Aluminium-Lithium Alloy for A350 Skin Sheet Application," in *17th AeroMat Conference and Exposition*, Seattle, Washington (USA), 2006.
- [12] K. H. Rendings, "Aluminium structures used in aerospace - status and prospects," *Materials Science Forum*, no. 242, pp. 11-24, 2001.
- [13] I. Rötzer, "Laser Beam Welding makes aircraft lighter," *Fraunhofer Magazine*, no. 1, pp. 36-37, 2005.
- [14] P. Mendez and T. Eagar, "New trends in welding in the aeronautic industry," in *2nd Conference of New Manufacturing Trends*, Bilbao (Spain), 2002.
- [15] H. Assler and J. Telgkamp, "Design of Aircraft Structures under Special Consideration of NDT," in *9th European Conference on NDT*, Berlin (Germany), 2006.
- [16] Project WEL-AIR, "Development of Short Distance Welding Concepts for Airframes," in *Aeronautics Days - Improving Cost Efficiency session*, Vienna (Austria), 2006.

- [17] M. Koçak and V. Uz, "Application of its fracture module to the stiffened Al alloy panels of airframe structures," in *European FITNET Fitness for service procedure - ESA/ESTEC*, Noordwijk (The Netherlands), 2009.
- [18] "One Aviation - Eclipse Jet," [Online]. Available: <http://oneaviation.aero/eclipse-jet.html>. [Accessed 22 05 2018].
- [19] B. Christner, "Development and testing of Friction Stir Welding (FSW) as a joining method for primary aircraft structure," in *23rd ICAS CONGRESS*, Toronto (Canada), 2002.
- [20] B. Christner, "A Friction Stir Welded Jet Aircraft: From Concept to Reality," in *11th International Symposium on Friction Stir Welding*, Cambridge (UK), 2016.
- [21] R. Aronson, "A new look at Aircraft Assembly," *Manufacturing Engineering*, vol. 132, no. 3, pp. 101-108, 2004.
- [22] F. Fernandez, "FSW applied on mid-size aircraft," in *8th International Symposium on Friction Stir Welding*, Timmendorfer Strand (Germany), 2010.
- [23] B. Christner, M. Hansen, M. Skinner and G. Sylva, "Friction Stir Welding system development for thin-gauge aerospace structures," in *4th International Symposium on Friction Stir Welding*, Park City (USA), 2003.
- [24] F. Marie and D. Allehaux, "Development of FSW for optimum run-out performance," in *6th International Symposium on Friction Stir Welding*, Toronto (Canada), 2006.
- [25] D. Allehaux, "Development of short distance WELding concepts for AIRframes (WEL-AIR), final report," AERONAUTICS and AEROSPACE Priority 4, CALL FP6-2002-Aero-1, Paris (France), 2007.
- [26] D. Lohwasser, "Application of Friction Stir Welding for Aircraft Industry," in *2nd International Symposium on Friction Stir Welding*, Gothenburg (Sweden), 2000.
- [27] D. Lohwasser, H. Ostersehlte and F. Zillekens, "First FSW application on Airbus Aircraft," in *8th International Symposium on Friction Stir Welding*, Timmendorfer Strand (Germany), 2010.
- [28] M. J. Booker, "Applying Friction Stir Welding to the Ariane 5 Main Motor Thrust Frame," in *2nd International Symposium on Friction Stir Welding*, Gothenburg (Sweden), 2000.
- [29] J. Freeman, G. Moore, B. Thomas and L. Kok, "Advances in FSW for Commercial Aircraft Applications," in *6th International Symposium on Friction Stir Welding*, Toronto (Canada), 2006.
- [30] R. Talwar, D. Bolser, R. Lederich and J. Baumann, "Friction Stir Welding of Airframe Structures," in *2nd International Symposium on Friction Stir Welding*, Gothenburg (Sweden), 2000.
- [31] W. Polt, "A little friction at Boeing," *Boeing Frontiers*, vol. 03, no. 5, 2004.
- [32] J. Dos Santos, U. Suhuddin, L. Bergmann, J. Carstensen, R. Brzostek y A. Barbini, «Rivetless aircraft structures: Possible solutions based on friction stir and derivative processes,» de *Proceedings of the 5th International Conference on Technical Advances in Friction Stir Welding and Processing (FSWP2017)*, Metz (France), 2017.
- [33] D. Lohwasser and Z. Chen, *Friction Stir Welding: From basics to applications*, CRC Press and Woodhead Publishing Limited, 2010.
- [34] Altran, "ecoTECH - Clean Sky 2," 16 January 2017. [Online]. Available: <https://www.cleansky2ecotech.eu/>. [Accessed 04 06 2018].
- [35] W. Thomas, E. Nicholas, J. Needham, M. Murch, P. Templesmith and C. Dawes, "Improvements relating to Friction Welding". UK Patent PCT/GB92/002203, 6 December 1991.

- [36] O. Midling, E. Morley and A. Sandvik, "Friction Stir Welding". UK Patent PCT/NO95/00005, 28 March 1994.
- [37] "Wikipedia - Friction Stir Welding," [Online]. Available: https://en.wikipedia.org/wiki/Friction_stir_welding. [Accessed 29 05 2018].
- [38] R. S. Mishra and Z. Ma, "Friction stir welding and processing," *Materials Science and Engineering R*, no. 50, pp. 1-78, 2005.
- [39] R. S. Mishra and M. W. Mahoney, Friction Stir Welding and Processing, Materials Park, Ohio (USA): ASM International, 2007.
- [40] B. Gibson, D. Lammlein, T. Prater, W. Longhurst, C. Cox, M. Ballun, K. Dharmaraj, G. Cook and A. Strauss, "Friction stir welding: Process, automation and control," *Journal of Manufacturing Processes*, no. 16, pp. 56-73, 2014.
- [41] ISO, *ISO25239: 2011; "Friction Stir Welding - Aluminium"*, Geneva (Switzerland), 2011.
- [42] P. Alvarez, G. Janeiro, A. A. M. da Silva, E. Aldanondo and A. Echeverria, "Material flow and mixing patterns during dissimilar FSW," *Science and Technology of Welding and Joining*, vol. 15, no. 8, pp. 648-653, 2010.
- [43] E. Aldanondo, P. Alvarez, E. Arruti and A. Echeverria, "Understanding material flow in FSW and its implications," in *Friction Stir Welding and Processing 2012 (FSWP2012)*, Saint Etienne (France), 2012.
- [44] E. Aldanondo, E. Arruti, G. Auzmendi, P. Alvarez and A. Echeverria, "Material flow phenomena in Friction Stir Spot Welding of butt joints," in *9th International Symposium on Friction Stir Welding*, Huntsville (USA), 2012.
- [45] W. Thomas, D. Staines, I. Norris and R. de Frias, "Friction Stir Welding - Tools and Developments," in *FSW Seminar at Instituto de Soldadura e Qualidade*, Porto (Portugal), 2002.
- [46] W. Thomas, K. Jhonson and C. Weisner, "Friction Stir Welding - recent developments in tool and process technologies," *Advanced Engineering Materials*, vol. 5, no. 7, pp. 485-490, 2003.
- [47] W. Arbegast, "Modeling friction stir joining as a metal working process," in *Hot Deformation of Aluminum Alloys*, Warrendale (USA), Z.Jin, Ed., TMS, 2003.
- [48] W. Arbegast, "Mechanisms of flow related defects in friction stir welds," in *XXXIII CONSOLDA - Congresso Nacional de Soldagem*, Caxias do Sul (Brazil), 2007.
- [49] L. Cederqvist and A. Reynolds, "Factors affecting the properties of friction stir welded aluminum lap joints," *Welding Journal*, pp. 281-287, 2001.
- [50] G. Buffa, G. Campanile, L. Fratini and A. Prisco, "Friction Stir Welding of lap joints: Influence of process parameters on the metallurgical and mechanical properties," *Materials Science and Engineering A*, no. 529, pp. 19-26, 2009.
- [51] L. Dubourg, A. Merati and M. Jahazi, "Process optimisation and mechanical properties of friction stir lap welds of 7075-T6 stringers on 2024-T3 skin," *Materials and Design*, no. 31, pp. 3324-3330, 2010.
- [52] M. Costa, D. Verdera, J. Costa, C. Leitao and D. Rodrigues, "Influence of pin geometry and process parameters on friction stir lap welding of AA5754-H22 thin sheets," *Journal of Materials Processing Technology*, no. 225, pp. 385-392, 2015.
- [53] M. Costa, D. Verdera, C. Leitao and D. Rodrigues, "Dissimilar friction stir lap welding of AA5754-H22/AA6082-T6 aluminium alloys: Influence of material properties and tool geometry on weld strength," *Materials and Design*, no. 87, pp. 721-731, 2015.
- [54] S. Ji, Z. Li, Z. Zhou and B. Wu, "Effect of Thread and Rotating Speed on Material Flow Behavior and Mechanical Properties of Friction Stir Lap Welding Joints," *Journal of Materials Engineering and Performance*, vol. 26, pp. 5085-5096, 2017.

- [55] S. Ji, Z. Liu and Z. Zhou, "Improving interface morphology and shear failure load of friction stir lap welding by changing material concentrated zone location," *The International Journal of Advanced Manufacturing Technology*, vol. 95, pp. 4013-4022, 2018.
- [56] Y. Huang, X. Meng, Z. Xu, Y. Xie, Y. Wang, L. Wan, Z. Lv and J. Cao, "Interface characteristic and tensile property of friction stir lap welding of dissimilar aircraft 2060-T8 and 2099-T83 Al-Li alloys," *International Journal of Advanced Manufacturing Technology*, vol. 94, pp. 1253-1261, 2018.
- [57] G. Sylva, *9th International Symposium on FSW*, Huntsville (USA): Private communication, 2012.
- [58] S. Fukada, M. Fujimoto, S. Yoshikawa, S. Haruna, K. Kamimuki and H. Okada, "Refill Friction Stir Welding for Aerospace application," in *10th International Conference on Trends in Welding Research*, Tokyo (Japan), 2016.
- [59] B. Gibson, M. Ballun, G. Cook and A. Strauss, "Friction stir sap joining of 2198 aluminium-lithium alloy with weaving and pulsing variants," *Journal of Manufacturing Processes*, vol. 18, pp. 12-22, 2015.
- [60] K. Doering, *Fatigue of Friction Stir Welded lap joints with sealants*, Missouri University of Science and Technology (USA): MSc Thesis, 2009.
- [61] J. Brown, *The effects of sealants and surface treatments on the faying surface of swept friction stir spot welds*, Wichita State University: MSc Thesis, 2006.
- [62] K. Erbslöh, C. Dalle Done and D. Lohwasser, "Friction Stir Welding of T-joints," *THERMEC 2003 - Materials Science Forum*, Vols. 426-432, pp. 2965-2970, 2003.
- [63] G. Biallas, U. Alfaro Mercado and H. W. Sauer, "Similar and dissimilar T-joints made from 2024-T3 cover sheet," in *8th International Symposium on FSW*, Timmendorfer Strand (Germany), 2010.
- [64] S. Tavares, P. Moreira, P. de Castro and F. de Oliveira, "Soldadura por Fricção Linear de Chapas em Ligações de Juntas em T". Portugal Patent 103867 B, 30 November 2009.
- [65] J. Martin, C. Stanhope and S. Gascoyne, "Novel techniques for corner joints using friction stir welding," in *140th Annual Meeting & Exhibition TMS2011 - FSW&P VI*, San Diego (USA), 2011.
- [66] T. Dursun and C. Soutis, "Recent developments in advanced aircraft aluminium alloys," *Materials and Design*, vol. 56, pp. 862-871, 2014.
- [67] Constellium, "AIRWARE brochure," 2013.
- [68] E. Starke Jr. and J. Staley, "Application of modern aluminium alloys to aircraft," *Prog. Aerosp. Sci.*, vol. 32, pp. 131-172, 1996.
- [69] E. Aldanondo, E. Arruti, P. Alvarez and A. Echeverria, "Friction Stir Welding of lap joints: Process parameters and joint properties," in *2nd International Conference on Technical Advances in Friction Stir Welding and Processing - FSWP2012*, Saint Etienne (France), 2012.
- [70] E. Aldanondo, E. Arruti, P. Alvarez and A. Echeverria, "Mechanical and microstructural properties of FSW lap joints," in *142nd Annual Meeting & Exhibition TMS2013 - Friction Stir Welding and Processing VII*, San Antonio (USA), 2013.
- [71] E. Arruti, J. Sarasa, E. Aldanondo and A. Echeverria, "The role of the tool design in properties of friction stir welded lap joints," in *11th International Symposium on FSW*, Cambridge (UK), 2016.
- [72] E. Aldanondo, E. Arruti, J. Sarasa and A. Echeverria, "Microstructural features in Friction Stir Welded lap joints," in *10th International Conference on Trends in Welding Research and 9th International Welding Symposium of Japan Welding Society*, Tokyo (Japan), 2016.

- [73] E. Aldanondo, E. Arruti and A. Echeverria, "Friction Stir Weld lap joint properties in aeronautic aluminium alloys," in *Friction Stir Welding and Processing X, in proceedings of the 148th Annual Meeting & Exhibition TMS2017*, San Diego (USA), 2017.
- [74] E. Aldanondo, E. Arruti, I. Quintana and J. Valer, "Developments in stringer-skin lap joints by FSW," in *12th International Symposium on FSW*, Chicoutimi-Quebec (Canada), 2018.
- [75] M. Balakrishnan, C. Leitao, E. Arruti, E. Aldanondo and D. M. Rodrigues, "Influence of pin imperfections on the tensile and fatigue behaviour of AA7075-T6 friction stir lap welds," *The International Journal of Advanced Manufacturing Technology*, pp. Published online - 23 May 2018, 2018.
- [76] E. Aldanondo, E. Arruti, A. Echeverria and I. Hurtado, "Friction stir welding of lap joints using new Al-Li alloys for stringer-skin joints," in *Friction stir welding and processing X*, Cham (Switzerland), The Minerals, Metals & Materials Series; Springer, 2019, pp. 77-88.
- [77] E. Aldanondo, J. Vivas, P. Álvarez y I. Hurtado, «Effect of tool geometry and welding parameters on friction stir welded lap joint formation with AA2099-T83 and AA2060-T8E30 aluminium alloys,» *Metals*, vol. 10, nº 872, 2020.
- [78] E. Aldanondo, J. Vivas, P. Álvarez, I. Hurtado y A. Karanika, «Friction stir welding of AA2099-T83 and AA2060-T8E30 aluminium alloys with new Cr-free surface treatments and sealant application,» *Metals*, vol. 11, nº 644, 2021.
- [79] E. Aldanondo, O. Zubiri, J. Vivas, P. Álvarez y I. Hurtado, «Fretting fatigue as a limiting factor on the durability of friction stir welded lap joints using AA2099-T83 and AA2060-T8E30 aluminium alloys,» *Journal of Manufacturing and Materials Processing*, vol. 6, nº 94, 2022.